



Swansea University  
Prifysgol Abertawe



## Swansea University E-Theses

---

# Near infrared curing of high performance coil coatings.

Gowenlock, Cathren

How to cite:

---

Gowenlock, Cathren (2014) *Near infrared curing of high performance coil coatings..* thesis, Swansea University.  
<http://cronfa.swan.ac.uk/Record/cronfa42537>

Use policy:

---

This item is brought to you by Swansea University. Any person downloading material is agreeing to abide by the terms of the repository licence: copies of full text items may be used or reproduced in any format or medium, without prior permission for personal research or study, educational or non-commercial purposes only. The copyright for any work remains with the original author unless otherwise specified. The full-text must not be sold in any format or medium without the formal permission of the copyright holder. Permission for multiple reproductions should be obtained from the original author.

Authors are personally responsible for adhering to copyright and publisher restrictions when uploading content to the repository.

Please link to the metadata record in the Swansea University repository, Cronfa (link given in the citation reference above.)

<http://www.swansea.ac.uk/library/researchsupport/ris-support/>



**Swansea University**  
**Prifysgol Abertawe**

Near Infrared Curing  
of High Performance Coil Coatings

**Cathren Gowenlock**

Thesis submitted to Swansea University in fulfilment  
of the requirements for the Degree of Engineering Doctorate

Steel Training Research and Innovation Partnership  
College of Engineering Materials Research Centre

**2014**

ProQuest Number: 10805286

All rights reserved

INFORMATION TO ALL USERS

The quality of this reproduction is dependent upon the quality of the copy submitted.

In the unlikely event that the author did not send a complete manuscript and there are missing pages, these will be noted. Also, if material had to be removed, a note will indicate the deletion.



ProQuest 10805286

Published by ProQuest LLC (2018). Copyright of the Dissertation is held by the Author.

All rights reserved.

This work is protected against unauthorized copying under Title 17, United States Code  
Microform Edition © ProQuest LLC.

ProQuest LLC.  
789 East Eisenhower Parkway  
P.O. Box 1346  
Ann Arbor, MI 48106 – 1346



**DECLARATION**

This work has not previously been accepted in substance for any degree and is not being concurrently submitted in candidature for any degree.

Signed ..... (candidate)

Date ..... 19/09/2014 .....

**STATEMENT 1**

This thesis is the result of my own investigations, except where otherwise stated. Where correction services have been used, the extent and nature of the correction is clearly marked in a footnote(s).

Other sources are acknowledged by footnotes giving explicit references. A bibliography is appended.

Signed ..... (candidate)

Date ..... 19/09/2014 .....

**STATEMENT 2**

I hereby give consent for my thesis, if accepted, to be available for photocopying and for inter-library loans **after expiry of a bar on access approved by the Swansea University.**

Signed ..... (candidate)

Date ..... 19/09/2014 .....

## Summary

This thesis has investigated Near Infrared (NIR) curing, a fast thermal curing technique for polyester coil coatings used in exterior building applications where fast line speeds are required. The aim has been to further understanding of the NIR cure mechanism.

UV/Vis/NIR spectroscopy and curing trials with two types of AdPhos NIR ovens were used to assess the influence of NIR absorbing pigment locus on cure. Firstly, carbon black was removed from red and brown coatings and this resulted in a wider cure window, but re-siting this pigment in the primer layer was unable to maintain coating colour due to top coat opacity. Then the addition of 1 wt.% NIR absorbing pigment to the backing coat was shown to increase top coat PMT by ca. 46°C, thus enabling line speed or oven power settings to be reduced.

The convection cure of white coatings with carbon black primers was investigated and a 5 wt.% loading was able to reduce top coat cure time by ca. 3s. In-situ scanning Kelvin probe (SKP) studies showed that rates of coating delamination by cathodic disbondment remained unchanged for primer carbon black loadings of up to 3.5 wt.%.

Silver coatings are particularly difficult to cure by NIR, so glass and mica coated flake were investigated as alternatives to aluminium flake, but resulted in coatings with hiding powers reduced by more than 75%. Further formulation suggestions for silver coatings were made, and emissivity and pigment morphology were suggested as potential factors in cure.

Finally, NIR pigment additions of up to 10 wt.% to transpired solar collector (TSC) coatings were investigated, and were found to have a much smaller influence on TSC steady state surface temperature than reducing wind speed. An outdoor study of TSC temperature profile revealed that this closely mirrored the incident solar irradiation profile.

## Acknowledgements

I would like to acknowledge the funding of Tata Steel Colors and the Welsh European Funding Office and the support of BASF Coatings for this research. I would also like to thank Tata Steel Colors and BASF Coatings for the use of their laboratories at IJmuiden and Deeside respectively.

I am very grateful for the supervision I have had throughout this project; to Dave Worsley for trusting my abilities to undertake a doctorate after over twenty years absence from STEM, to Jon Elvins for his day to day guidance and prompt hunting out of steel and paint samples whenever they were needed, to Rob Ireson for many helpful insights and chats, and to Paul Jones for ensuring that my project was industrially relevant.

I would like to thank Ian Mabbett for his help and support particularly at the beginning of this research when my learning curve felt particularly steep; and to Carol Glover for her guidance and help with the electrochemical side of this research.

Thanks also to the many people at Tata Steel who have had an input to this project. I would particularly like to thank Gijs Van Reeuwijk, Reinier Broekhuis and Jean-Paul Gravemaker. I've also had good support from Graham Swanston and Steve Corkish at BASF Coatings.

To my friends Ruth Hopkins and Ingrid Hallin – thank you. You have shared the doctorate journey with me and helped to keep me sane.

Finally I would like to say a big thank you to three generations of my family for their continual support. It is of great sadness to me that my mother did not live to see me complete my doctorate – I know she would have been proud. Most of all I would like to thank Rob – for supporting me in this later in life venture, and for his unending love and support.

# Contents

<b>Chapter 1</b>	<b>Introduction.....</b>	<b>1</b>
1.1	Introduction to Organically Coated Steel.....	2
1.1.1	The Coil Coating Process.....	5
1.2	Coil Coatings.....	8
1.2.1	Binder.....	8
1.2.2	Pigment.....	9
1.2.2.1	Colourant Pigments.....	9
1.2.2.2	Metallic Pigments and Effect Pigments.....	9
1.2.3	Solvent.....	15
1.2.4	Additives.....	16
1.3	Curing.....	18
1.3.1	Convection Curing.....	21
1.3.2	NIR Curing.....	23
1.3.2.1	Background to NIR Curing.....	23
1.3.2.2	NIR Cure Mechanism.....	28
1.3.3	Other Fast Curing Techniques.....	35
1.3.3.1	Induction Curing.....	35
1.3.3.2	UV Curing & Electron Beam Curing.....	35
1.3.3.3	Infrared Curing.....	38
1.4	Characterisation of Coatings.....	39
1.4.1	Analytical Techniques.....	39
1.4.2	Physical Tests of Coatings.....	42
1.4.2.1	MEK Rub Test.....	42
1.4.2.2	Viscosity.....	43
1.4.2.3	Colour.....	44
1.4.2.4	Gloss.....	44
1.4.2.5	Flexibility and Adhesion.....	45
1.5	Transpired Solar Collectors.....	46
1.6	Introduction to Solar Radiation.....	49
1.6.1	Terrestrial Solar Radiation.....	49
1.6.2	Interaction of Light with Matter.....	49
1.6.3	Total Solar Reflectance.....	50
1.6.4	Solar Reflectance Index.....	51
1.7	Conclusions and Aims.....	51



1.8	References .....	53
<b>Chapter 2</b>	<b>Experimental Techniques.....</b>	<b>61</b>
2.1	Coated Sample Preparation .....	62
2.1.1	Polyester Coating Formulation .....	62
2.1.1.1	Mill Base and Let Down Method .....	62
2.1.1.2	Pigment Paste and Converter Method .....	63
2.1.2	Production of Polyester Coated Samples .....	66
2.1.3	Model PVC Coating Formulation .....	69
2.1.4	Production of Free-standing Coating Films .....	69
2.1.4.1	Production of Polyester Free-standing Films.....	69
2.1.4.2	Production of Model PVC Free-standing Films .....	69
2.2	Measuring Cure .....	70
2.2.1	Convection Curing .....	75
2.3	NIR Curing .....	75
2.3.1	AdPhos NIR Lab Unit.....	76
2.3.2	AdPhos Technicum .....	79
2.4	UV-Vis-NIR Spectroscopy.....	81
2.4.1	Perkin Elmer Lambda 750S Spectrophotometer.....	84
2.4.2	Ocean Optics HR2000+ Spectrometer .....	85
2.5	Emittance.....	87
2.6	Total Solar Reflectance .....	88
2.7	References .....	89
<b>Chapter 3</b>	<b>The Effect of Black Pigment on the NIR Cure of Coloured Polyester Coatings.....</b>	<b>91</b>
3.1	Introduction .....	92
3.2	Experimental Techniques .....	95
3.2.1	Polyester Coating Formulation .....	95
3.2.2	NIR Curing Trials using an AdPhos Technicum NIR Oven.....	97
3.3	Results and Discussion.....	98
3.3.1	UV-Vis-NIR Spectroscopy .....	98
3.3.2	Curing Trials .....	104
3.3.3	NIR Transparent Black Pigments .....	109
3.4	Conclusions .....	111
3.5	References .....	112

<b>Chapter 4</b>	<b>The Effect of Carbon Black Tinted Primer on the</b>	
	<b>Convection Cure of a White Polyester Coating .....</b>	<b>113</b>
4.1	Introduction .....	114
4.2	Experimental Techniques .....	115
4.2.1	Preparation of Coatings.....	115
4.2.2	Convection Curing Trials.....	115
4.2.3	Scanning Kelvin Probe Technique.....	116
4.3	Results and Discussion.....	120
4.3.1	Spectroscopic Studies and Colour Measurement.....	120
4.3.2	Cure Trials.....	126
4.3.3	Interaction of IR Photons with the Coating System.....	130
4.3.4	Effect of Carbon Black Tinted Primer on Corrosion Performance of Galvanised Steel Substrate.....	131
4.4	Conclusions .....	138
4.5	References .....	139
<b>Chapter 5</b>	<b>The Effect of Backing Coat Absorbing Pigments on Top</b>	
	<b>Coat NIR Cure.....</b>	<b>142</b>
5.1	Introduction .....	143
5.2	Experimental Techniques .....	145
5.2.1	Polyester Coating Formulation .....	145
5.2.2	NIR Curing Trials using an AdPhos NIR Oven.....	145
5.2.2.1	Single Sided Curing Trials.....	145
5.2.2.2	Double Sided Curing Trials.....	146
5.3	Results and Discussion.....	148
5.3.1	Comparison of White and Grey Backing Coats using the AdPhos NIR Lab Unit and AdPhos Technicum .....	148
5.3.2	Effect of Additions of NIR Absorbing Pigment to the White Backing Coat on Top Coat Cure.....	154
5.4	Conclusions .....	163
5.5	References .....	165
<b>Chapter 6</b>	<b>The Effect of Modification of Silver Coloured Polyester</b>	
	<b>Coating Formulation on NIR Cure .....</b>	<b>166</b>
6.1	Introduction .....	167
6.2	Experimental Techniques.....	169
6.2.1	Polyester Coating Formulation .....	169

6.2.2	NIR Curing Trials using an AdPhos Technicum NIR Oven.....	172
6.3	Results and Discussion.....	173
6.3.1	Comparison of the Cure of Silver Polyester Coating Formulations Modified for NIR Cure .....	173
6.3.2	Glass Flake Substituted Silver Polyesters.....	182
6.3.3	Mica Substituted Silver Polyesters.....	192
6.4	Changes to Substrate .....	198
6.5	Conclusions .....	199
6.6	References .....	202
<b>Chapter 7 Investigation of Transpired Solar Collector Performance ...</b>		<b>203</b>
7.1	Introduction .....	204
7.2	Experimental Techniques.....	208
7.2.1	Preparation of NIR Pigmented Coating Panels.....	208
7.2.2	Outdoor Testing of Transpired Solar Collector Panel.....	208
7.3	Results and Discussion.....	211
7.3.1	Effect of NIR Absorbing Pigments on TSC Performance .....	211
7.3.2	Outdoor Testing of Transpired Solar Collector Panel.....	215
7.4	Conclusions .....	219
7.5	References .....	221
<b>Chapter 8 Conclusions and Future Work.....</b>		<b>223</b>
8.1	Conclusions and Future Work.....	224
8.2	References .....	228

# Nomenclature

Common abbreviations used in this thesis:

AFM: atomic force microscopy

CCD: charge coupled device

CIE L\*a\*b\*: International Commission on Illumination colour space

(French: *Commission Internationale de l'Eclairage*)

dft: dry film thickness

DMA: dynamic mechanical analysis

DSC: differential scanning calorimetry

DVL2: Dompel Verzink Lijn 2

EB: electron beam

GWG: Goosewing Grey

hc: convective coefficient

HDG: hot dip galvanised steel

HMMM : hexamethylmethoxy melamine

MEK: methyl ethyl ketone

MZ: MagiZinc

NIR: near infrared

OCS: organically coated steel

PMT: peak metal temperature

PVB: poly vinyl butyral

PVC: poly vinyl chloride

PVD: physical vapour deposition

PVDF: polyvinylidene fluoride

RAL: European colour matching system

SEM: scanning electron microscopy

SHE: standard hydrogen electrode

SKP: scanning Kelvin probe

SRI: Solar Reflectance Index

SSPA-FTIR: Step-scan photoacoustic Fourier Transform Infrared spectroscopy

SSST: steady state surface temperature

TGA: thermo gravimetric analysis

T<sub>g</sub>: glass transition temperature

THF: tetrahydrofuran

ToF-SIMS: time-of-flight secondary ion mass spectrometry

TSC: transpired solar collector

TSR: total solar reflectance

ULAM: ultra low angle microtomy

UTC: unglazed transpired collector

Vis: visible

UV: ultra violet

VOC: volatile organic compound

XPS: X-ray photoelectron spectroscopy

# **Chapter 1**

## **Introduction**

## 1.1 Introduction to Organically Coated Steel

Organically coated steel (OCS) is a galvanised mild steel strip product which has been coated with an organic coating system prior to its finished use. The origins of the OCS industry can be traced back to the 1930s when the Californian industrialist Joe Hunter came up with the idea of a continuous process for coating paint onto the metal used for making venetian blinds [1]. After the Second World War uses for OCS rapidly grew, and by the 1960's production of OCS by a continuous industrial process had been established in Europe. By 2010 the European pre-painted metal market in Europe was worth over €10 billion, with 81% of this market being on steel substrate [2]. Pre-finished OCS is now used across a range of products as shown in Figure 1.1, with the market being dominated by roofing and cladding materials for the construction industry.

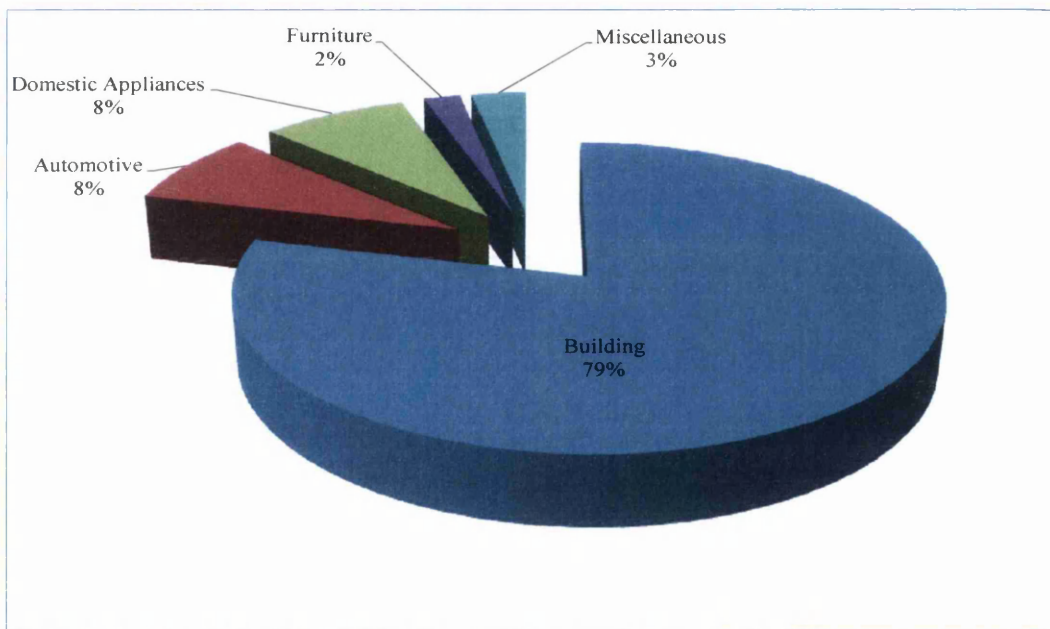


**Figure 1.1 – End Uses of Pre-Finished Steel Products (Europe 2010) - data taken from [3]**

Organically coated steel in the construction industry is primarily used in an external environment. Organic coatings therefore serve three functions; firstly they provide a barrier to elements in the environment such as oxygen and rain water that promote corrosion of the underlying steel substrate. In more aggressive environments such as coastal areas and industrial sites they will also act as a barrier to sea water and chemicals, such as sulphur dioxide and nitrous oxide.



Secondly, organic coatings have an aesthetic function as shown in Figure 1.2.



**Figure 1.2 – Old Trafford Football Stadium: an Organically Coated Steel Building**

*Image Copyright Steven Haslington. This work is licensed under the Creative Commons Attribution-Share Alike 2.0 Generic Licence.*

Finally, organic coatings have a functional role. For example, coatings incorporating infrared reflective pigments, so called ‘cool paints’, can be used to moderate the energy transfer in and out of buildings [4-6]. Anti-microbial coatings can aid the self cleaning of coating surfaces [7] and spectrally selective coatings with a high solar absorbance and low thermal emittance can aid energy harvesting in transpired solar collectors (TSCs) [8, 9].

In Europe, OCS is manufactured by steel companies who galvanise and apply an organic coating system to the steel in one continuous process known as coil coating. The resulting pre-finished OCS products are extremely robust, and hence companies such as Tata Steel are able to offer guarantees of up to 40 years [10].

Steel manufacturers are always looking to produce their products at increasingly competitive prices. In 2006, Tata Steel Colors (then Corus Colors) installed a coil coating line on the end of an existing galvanising line, Dompel Verzink Lijn 2 (DVL2) at their IJmuiden site in the Netherlands. In order to cure the coating coil coating lines have traditionally been dominated by gas fired convection ovens, but in this instance

Tata Steel chose to install a relatively new technology, a Near Infrared (NIR) oven. There were three reasons for this at the time; time, energy and space savings. NIR cure is essentially a fast thermal cure with reports of increased energy efficiency compared to convection ovens [11], and a cure time of less than 3 seconds for a 15-20  $\mu\text{m}$  coil top coat [12, 13]. This compares with ca. 30 seconds for the same thickness coating cured by a convection oven. The fast NIR cure time also means that NIR oven lengths are considerably smaller than convection oven lengths (10 m compared to 30 m).

As NIR curing was a relatively new technology with the only information about the cure mechanism at the time coming from the oven manufacturers, Tata Steel and BASF sponsored an Engineering Doctorate in 2006 to look at increasing the understanding of the effects of the NIR cure mechanism on the resulting coating properties of polyester coated steel [14]. Research by Knischka et al in 2009 suggested that the presence of NIR absorbing pigments in the top coat may be beneficial for NIR cure [15], however key findings from the 2006 Engineering Doctorate were that for 25 $\mu\text{m}$  polyester coated galvanised steel, coatings that did not absorb a lot of NIR radiation cured with a wider cure window, whilst coatings that absorbed a lot of NIR radiation had a smaller process window and a surface prone to defects [14]. This thesis is also sponsored by Tata Steel and BASF. The thesis aims to study the mechanisms involved in light absorption in NIR curing, and so to determine if there is an optimum position for NIR absorbing pigments within the coating system. A further aim is to investigate if NIR absorbing pigments can be used in coatings for transpired solar collectors.

### 1.1.1 The Coil Coating Process

Coil coating is a continuous roll to roll process which deposits an organic coating onto a substrate, frequently galvanised steel [16]. A typical coil coating line employing forced air convection ovens is shown in Figure 1.3.

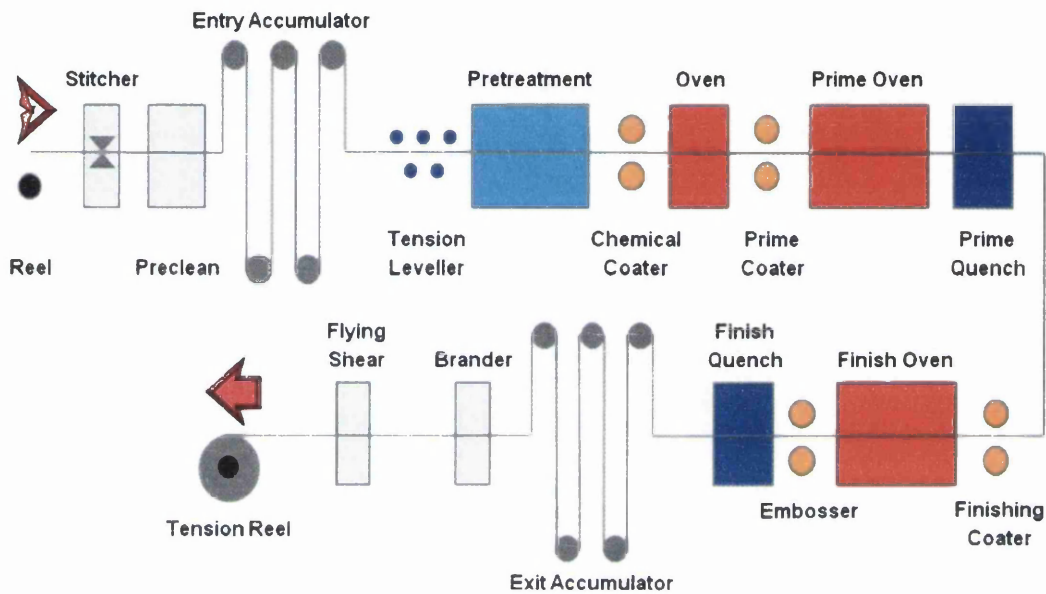
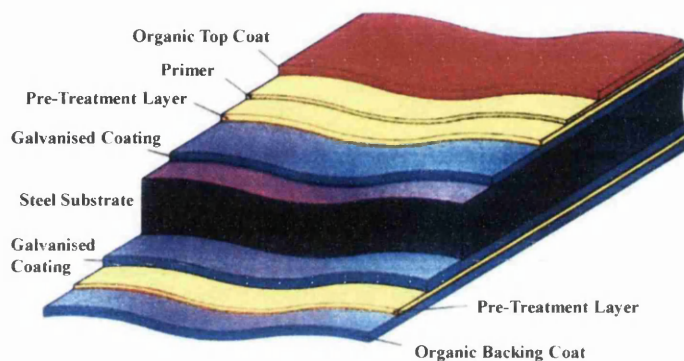


Figure 1.3 – A Typical Coil Coating Line

The first stage of the coil coating process is alkali cleaning of the galvanised steel strip followed by a water rinse to ensure that it is free from grease and particles. Entry and exit strip accumulators allow the line to operate continuously at high speeds, seven days a week and twenty four hours a day for maximum efficiency, with lines typically operating at speeds of between 60 – 170 m/min, with coil widths of up to 1850 mm and substrate thickness ranging from 0.3 – 2.0 mm.

A 1 $\mu$ m thick pretreatment layer, frequently chromate or phosphate, is then applied in the chemical coater to enhance corrosion resistance of the substrate, and to modify the surface to improve compatibility between the steel substrate and organic coating. After application the steel strip is dried in an oven to remove water content from the coating. Next, a primer coat (between 5-8  $\mu$ m thick) is applied to enhance corrosion resistance of the coated product and to provide good adhesion between the pretreatment layer and top coat. Primers are based on epoxy, polyester or acrylic resins with the addition of corrosion inhibitors. The primer coating is cured in the prime oven, the steel strip is quenched and then moves on for top coat application. Once the top coat

is applied, some coating products have an additional embossing stage to texture the surface of the top coat. On some production lines an additional laminate film is added; this might be an integral part of the coating system or as a temporary protective layer [17]. The steel strip is again quenched, and then re-coiled at the end of the process. The typical composition of a coil coated steel strip is shown in Figure 1.4.



**Figure 1.4 – Coating Layers of an Organically Coated Steel**

The main categories of top coat resins used in pre-finished steel for the construction market are polyester, PVC plastisol, polyurethane and polyvinylidene fluoride (PVDF), with top coat thicknesses ranging from 20 - 200  $\mu\text{m}$ . This thesis deals with polyester coil coated steels, which also form the largest market share. Note that the top coat and backing coat are applied simultaneously to the steel strip. Backing coats are generally thinner (ca. 8  $\mu\text{m}$ ) than top coats and usually applied directly on top of the pretreatment layer.

The polyester coil coated steel studied in this thesis differs from the usual coating layer structure shown in Figure 1.4. This is due to space constraints on the DVL2 line, that mean that the pretreatment layer and the primer layer have had to be combined and applied as a combined pretreatment primer layer. The coating layer structure of polyester coil coated steel produced on the DVL2 line is hence as shown in Figure 1.5.

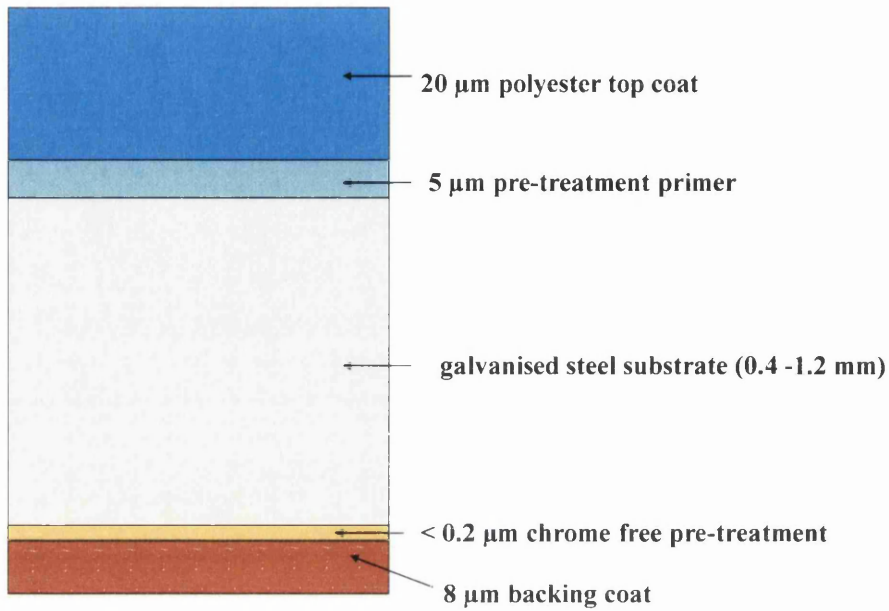


**Figure 1.5 – Schematic of the Layer Structure of a DVL2 Polyester Coil Coating Strip**

Coil coating lines can run at line speeds in excess of 150 m/min, so even with relatively long ovens the oven dwell time is approximately 30 seconds. Although capital costs for a coil coating line are high, transfer efficiency of the coating to the substrate is high due to the reverse roller coating process illustrated schematically in Figure 1.6, and volatile organic compound (VOC) emissions are low due to thermal after burning and re-use as fuel. [18].

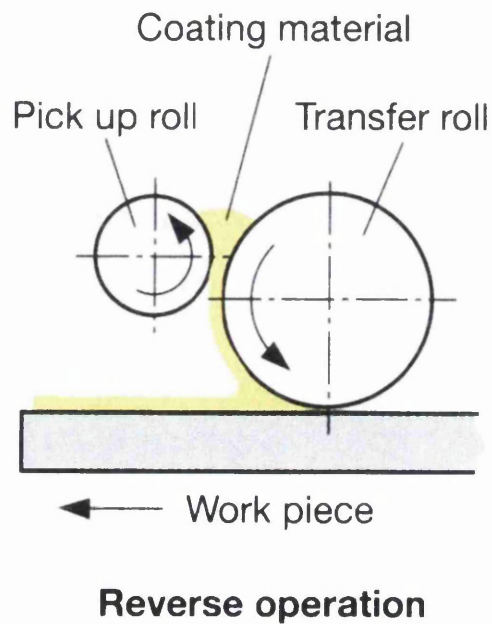


**Figure 1.6 – Schematic Illustration of Reverse Roller Coating – reproduced from [18]**

## 1.2 Coil Coatings

The term *coating* has multiple usage; it can refer to the material (liquid, paste or powder) applied to a substrate, the process of application, or the dry film that has resulted from that application. There also exist many different ways of classifying coatings such as by their service application (e.g., corrosion protection, self cleaning) or by their appearance (e.g., metallic effect, glossy) [19-21].

However, coil coatings are coatings that are applied as liquids and consist of a mixture of solid pigment particles and additives in a liquid vehicle. The vehicle is the total liquid portion of the coating, and consists of the binder and solvents [22].

### 1.2.1 Binder

In order to make the transition to a finished thin dry continuous film adhering to the surface of the substrate, the coating film needs to solidify by a film-forming process. This film-forming process requires the presence of a film-forming agent or binder. A binder is a polymer resin, which also serve the purpose of binding pigments to each other and to the substrate [23, 24].

The resins that are most commonly used in coatings on galvanised steel substrates in the construction industry are polyester, polyurethane, PVDF and PVC plastisol [25, 26], with polyester coatings forming over 50% of the market [27]. Coatings can further be classified as those based on thermoplastic or thermosetting polymers. Thermoplastic coatings such as PVDF and PVC plastisol undergo film formation by physical drying by the release of solvents, and exhibit plastic properties at elevated temperatures. On the over hand, thermosetting coatings such as polyesters and polyurethanes undergo film formation by a process which includes a polymer cross-linking reaction. At elevated temperatures many thermosetting coatings will degrade by decomposition [18, 28, 29].

## **1.2.2 Pigment**

Pigments are solid materials of fine particle size that are virtually insoluble in the coating resin. Their main purposes are to give colour and opacity to the coating, but they may also be added for functional reasons such as providing corrosion inhibition, UV protection or anti-microbial properties [30, 31].

### **1.2.2.1 Colourant Pigments**

Colourant pigments can be sub-divided into organic and inorganic pigments, there being far more organic pigments than inorganic pigments. Commonly used organic and inorganic pigments are given in Table 1.1 and Table 1.2. As organic pigments range in size from 0.01 – 0.1  $\mu\text{m}$  and are generally about ten times smaller than inorganic pigments, their smaller particle size means that they need to be effectively dispersed so that they end up evenly distributed within a coating.

### **1.2.2.2 Metallic Pigments and Effect Pigments**

Other important pigments are metallic pigments and effect pigments. These pigments have a different morphology from most other organic and inorganic pigments, having a plate-like lamellar structure [21].

Metallic coil coatings account for a significant volume of coil coating sales, and are pigmented using aluminium flake pigments. Metallic pigments are achromatic, with their metallic effect caused by reflection. The metallic lustre effect of metallic coil coatings is decreased when the proportion of light that is scattered at the edges and corners of the flakes is high. This means that larger flakes give a coating with a brighter more sparkling appearance. Smaller flakes on the other hand have greater opacity, a greyer appearance and give a coating with a smoother less sparkling finish.

**Table 1.1 - Organic Coil Coating Pigments - Adapted from [18]**

<b>Organic Pigments</b>	<b>Colour</b>
Azo pigments	Red/Yellow
Metal complex pigments	Blue/Green
Isoindolinones	Yellow/Orange/Red
Isoindolines	Yellow
Anthraquinones	Yellow/Orange/Red
Quinacridones	Red/Violet
Perylenes/Perinones	Red/Maroon
Dioxazines	Violet
Quinophthalones	Yellow
Diketopyrrolopyrrole	Red
Pyrazoloquinazolone	Red



**Table 1.2 - Inorganic Coil Coating Pigments - Adapted from [18]**

<b>Inorganic Pigments</b>	<b>Colour</b>
Titanium Dioxide	White
Carbon black	Black
Iron oxide	Red
Chromium oxide	Green
Mixed phase oxides	Yellow
Lead chromate/molybdate	Bright Red/Yellow
Bismuth vandate	Yellow

Observed colour with metallic coatings is affected by viewing angle. It can be seen from Figure 1.7 that if a coating is viewed from an angle near normal, the path length of light through the coating will be short as it is soon reflected back by an aluminium flake. If however it is viewed from a greater angle to normal, the light that will be observed will have followed a greater path length in the coating film by being reflected backwards and forwards and will appear darker. This difference in colour when viewing from different angles is known as colour flop.

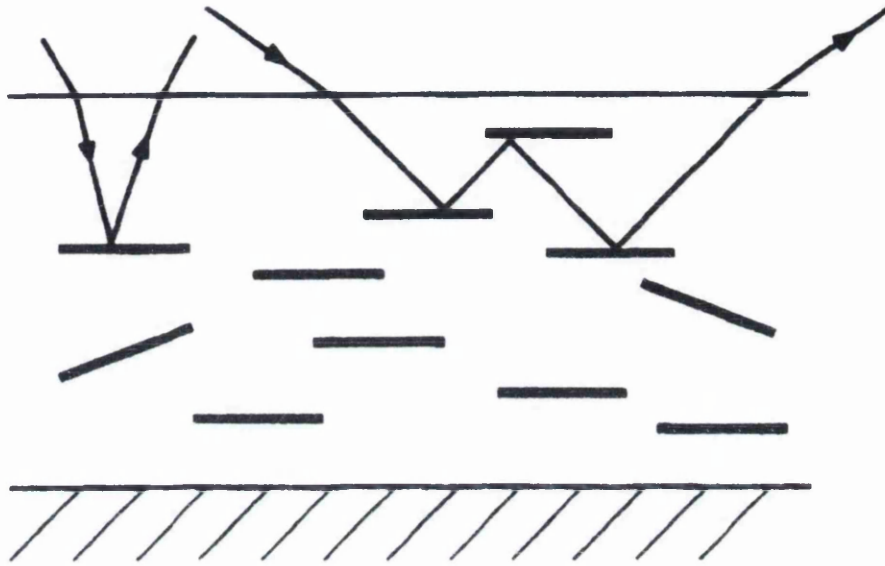


**Figure 1.7 – Colour Flop in an Aluminium Flake Coating - reproduced from [21]**

The metallic effect of coil coatings is also affected by differences in the aluminium flake shape, the flake size distribution, the smoothness of the flake surface and the flake orientation in relation to the coil coating surface. Flake orientation in relation to the coil coating surface is affected by application method and solvent content. Aluminium flake pigments used in coil coatings are generally around 5 - 45  $\mu\text{m}$  in diameter with thicknesses varying from 0.1 – 1  $\mu\text{m}$ .

Most aluminium pigments are milled into flake-like particles by a wet milling process in the presence of white spirit and a lubricating agent. Two types of pigment can be produced depending on the type of lubricant used; leafing and non-leafing pigments. Coil coatings employ non leafing pigments.

Leafing pigments are milled with a saturated fatty acid, typically stearic acid which creates a high surface tension on the pigment, and makes them resistant to wetting by the polymer binder. This results in the pigments rising to the surface of the wet film and remaining there after drying due to interfacial tension. This is shown schematically in Figure 1.8.

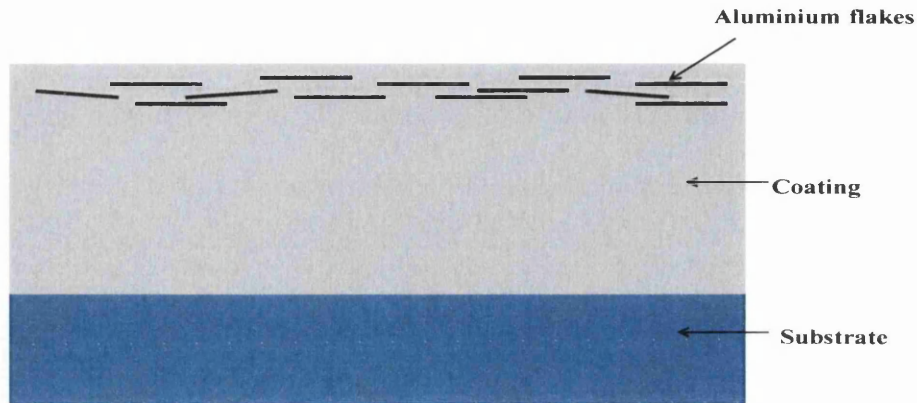


**Figure 1.8 – Schematic of Leafing Aluminium Pigment**

Non-leafing pigments are milled with unsaturated fatty acids, typically oleic acid. This lubricant is strongly polar and allows the pigment to wet readily and spread evenly throughout the wet coating. A uniform dispersion of pigment throughout the dry coating film is thus obtained, as shown schematically in Figure 1.9.

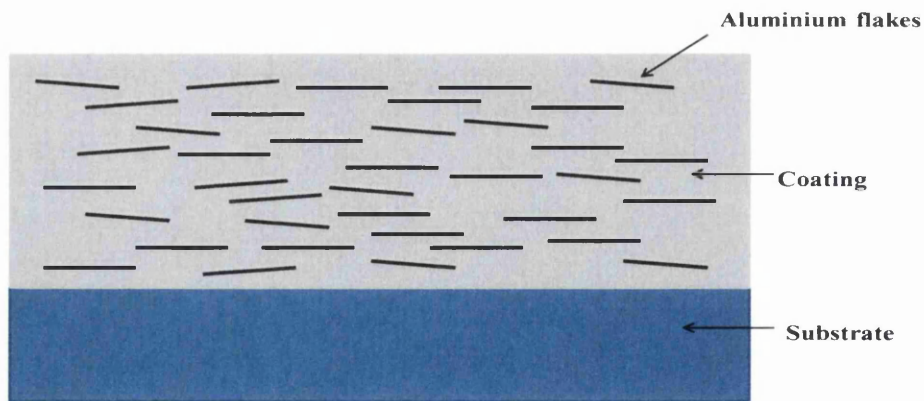


**Figure 1.9 - Schematic of Non Leafing Aluminium Pigment**

The first generation of aluminium flake grades that were produced were ‘cornflake’ pigments with irregular edges. This was followed by second generation

flakes known as ‘silver dollar’ pigments, which were thicker and smooth edged giving increased brightness and flop. Finally, there are physical vapour deposition (PVD) aluminium flakes (also known as Vacuum Metallized Pigments) which have even greater brightness and flop due to their thinness and mirror like surfaces. Cornflake morphologies are used in coil coatings. Scanning electron micrographs of the three grades are shown in Figure 1.10.

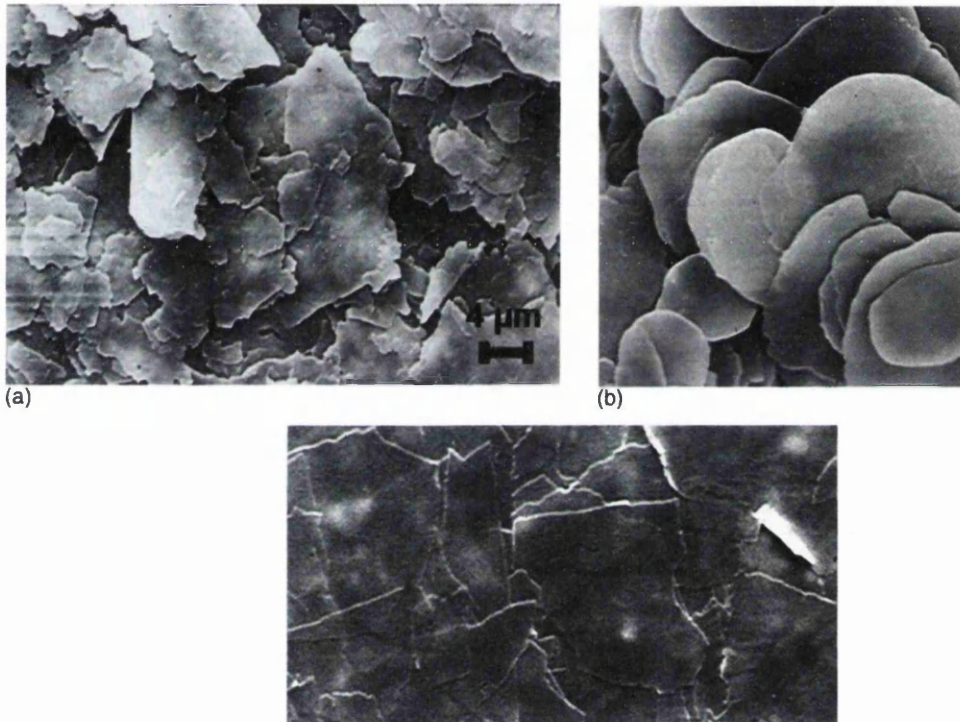


**Figure 1.10 – Scanning Electron Micrographs of Aluminium Pigments; (a) Cornflake Type, (b) Silver Dollar Type, (c) PVD Type - reproduced from [32]**

Another category of pigments that are used in coil coatings are effect pigments, also known as interference or pearlescent pigments. These pigments consist of platelets of substances such as natural or synthetic mica, silica, alumina or glass flake substrate, coated on all sides with thin layers (100 - 150 nm) of high refractive index substances such as  $\text{TiO}_2$  or  $\text{Fe}_2\text{O}_3$  [33]. The platelets are typically 5 - 100  $\mu\text{m}$  in diameter and 0.3 – 0.6  $\mu\text{m}$  thick. A cross-section through a  $\text{TiO}_2$  - mica pigment depicting the mica platelet and the outer  $\text{TiO}_2$  layer is shown in Figure 1.11. As light impinges on the pigment, some light is reflected at the  $\text{TiO}_2$  surface with the rest being refracted through this layer. The refracted light is then partially reflected at the  $\text{TiO}_2$ /mica surface and will end up leaving the pigment parallel to the light that was reflected at the  $\text{TiO}_2$  surface.

Depending on the thickness of the metal oxide layer, its refractive index, the transparency of the substrate and the angle with which light impinges on the pigment surface, colour will be produced by thin film interference [34]. As the thickness of the TiO<sub>2</sub> layer increases on a TiO<sub>2</sub> - mica pigment, the colour obtained changes from silver-white to yellow to red to blue to green.

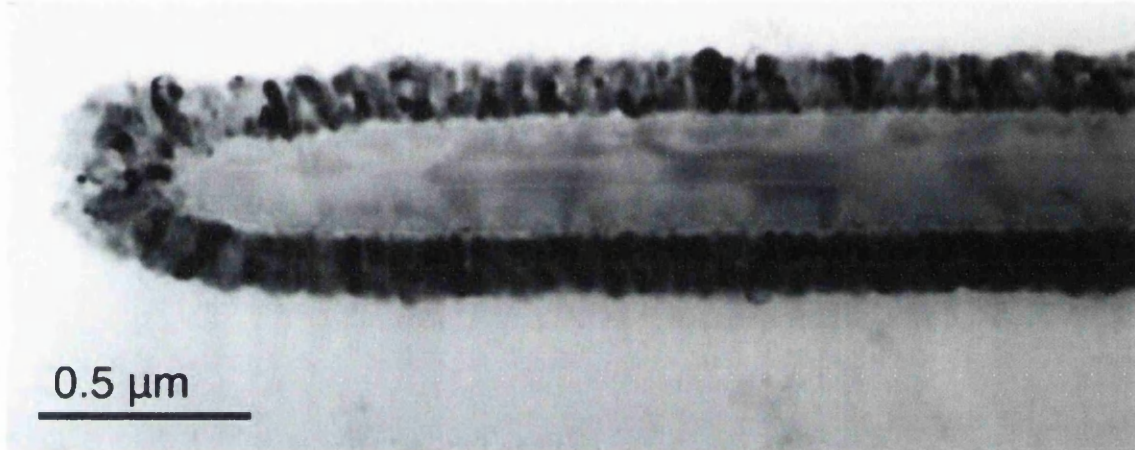


**Figure 1.11 – Cross Sectional Transmission Electron Micrograph of TiO<sub>2</sub>-Mica Pigment**  
*reproduced from [32]*

### 1.2.3 Solvent

The main purpose of solvents in the coating system is to dissolve the resin and to carry the pigments, whilst being volatile under the curing conditions for the coating. Solvents are also added for a variety of other reasons; to adjust the viscosity of the paint, to modify the evaporation rate or flash point of the coating vehicle, to influence the gloss and texture of the cured paint or to reduce cost. Modification of the evaporation rate, for example, may help to regulate the film forming process during curing by keeping the coating ‘open’ for longer. This will enable entrapped gaseous products to escape and prevent the formation of surface blisters on the coating [18-20]. This can be especially helpful for NIR cure as the cure is so rapid.

Thermal oxidation of solvents is used in the coil coating industry as a means of reducing volatile organic compounds (VOC) emissions with 97% of VOCs being captured and the recovered energy used to pre-heat incoming process air [27]. Solvents can also be added to the coating purely to adjust viscosity, and are then referred to as

diluents. Furthermore, if these diluents are chemically incorporated into the coalescing coating film during curing, they are referred to as reactive diluents. Reactive diluents from renewable sources have been used to lower the emissions of VOC in polyester/melamine coating systems [35].

Polyester coil coatings have a solvent content of between 30 and 45%, with common solvents being aliphatic hydrocarbon mixtures (e.g. solvent naphtha), high boiling point aromatic hydrocarbons, glycol ethers or esters, and high boiling point esters. Mixtures of solvents are often used. Solvents can be classified as active solvents, latent solvents and non-solvents. An active solvent will readily dissolve a solute at room temperature, whilst a latent solvent although not capable of dissolving a solute by itself will have its solvent power activated by the addition of a genuine solvent, or also by the addition of a non-solvent [18, 27].

#### **1.2.4 Additives**

Coil coatings need to be able to display a wide range of properties; for example they need enough flexibility to cope with fabrication without cracking or loss of adhesion, and to be able to withstand corrosion and degradation for 25 years or more. Although most of a coating formulation will consist of the binder, solvents and pigments, various additives are included in the formulation so that these properties can be met. A coating can therefore have some 15 - 20 different components, however additives usually account for less than 5% of the formulation [36].

An additive can modify the physical or chemical property of a coating. Additives have varying volatility; some are designed to stay in the coalescing coating film during curing whilst others are designed to escape from it [23, 37]. A list of the more common additives in coil coating systems and their effects are given in Table 1.3.

**Table 1.3 – Coil Coating Additives**

<b>Additive</b>	<b>Effect</b>
Defoamer	Foam (entrapped air) is introduced during the roller application of the coating. Act by lowering surface tension, causing bubbles to coalesce and burst.
Flow & leveling agent	Act by reducing the surface tension of the wet coating, thus increasing the coating's mobility after application and enabling leveling. Surface defects are hence minimised.
Catalyst	Act by increasing the rate of the cross-linking reaction between the cross-linking resin and the primary resin. In polyester-melamine coating systems, blocked acid catalysts are used.
Matting (flattening) agent	Act by increasing the level of micro-roughness of a coating surface and hence decreasing the gloss. Both inorganic (silica gel) and organic (polymethyl urea resins) matting agents are used.
Anti sagging agent (rheology modifier)	Act by increasing viscosity.
Slip aid	Wax that migrates to the surface during curing, coats the surface and improves slip characteristics. Important for the coil coating process as coils are rewound after coating and then post formed. PTFE modified polyethylene wax is used for coil coatings.
Wetting agent (dispersing agent)	Surfactants that lower surface and interfacial tension, hence improving dispersion of pigments and adhesion of the coating to the substrate.

### 1.3 Curing

This thesis is concerned with polyester coil coatings used in the construction industry. These coatings are based on branched or linear saturated polyester resins which are then cross-linked. The resins are first formed by the esterification of a di-/polyacid and a di-/polyol; the basic condensation reaction between a diacid and a diol is shown in Figure 1.12. Commonly used polyols are neopentyl glycol and trimethylolpropane, and more recently 2-methyl-1,3-propanediol (MPDiol glycol) [38]. Polyacids are usually used as a mixture of an aromatic and aliphatic diacid, such as isophthalic acid and adipic acid [21].

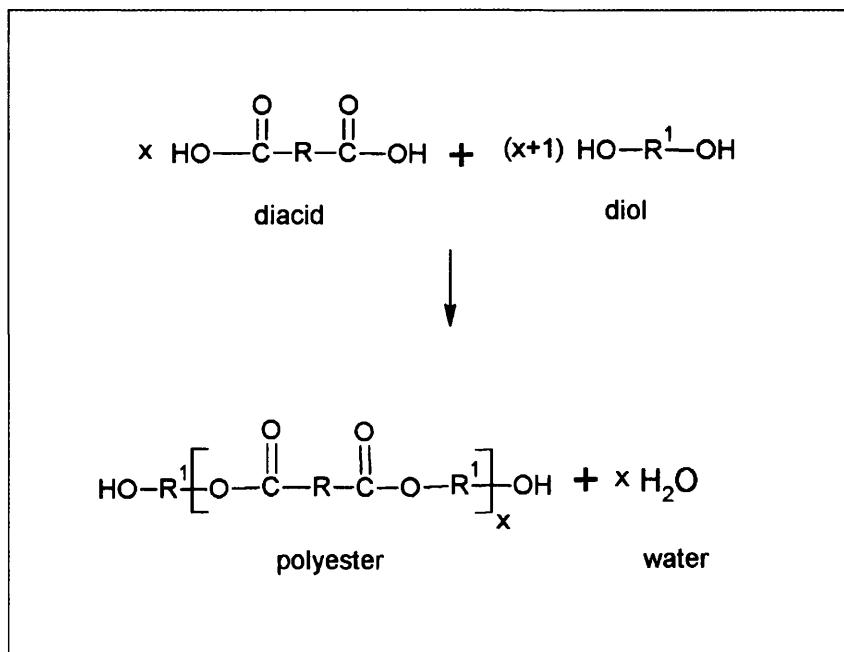


**Figure 1.12 – Formation of Polyester by a Condensation Reaction**

As an excess of the diol is used in the polyester formation, the resulting polyester is hydroxyl terminated. It is these hydroxyl functional groups on the polymer backbone which form reaction sites for a cross-linking agent. The relatively low molecular weight polyester resin that is produced is thus able to form a very high molecular weight polymer with a 3D infinite network [39]. Polyester cross-linking agents are melamine formaldehyde resins, predominantly based on hexamethoxymethyl melamine (HMMM) which is shown in Figure 1.13 [40]. The resin to cross-linker ratio



is usually between 70:30 and 90:10. The higher the melamine content, the harder and less flexible the resulting coating will be.

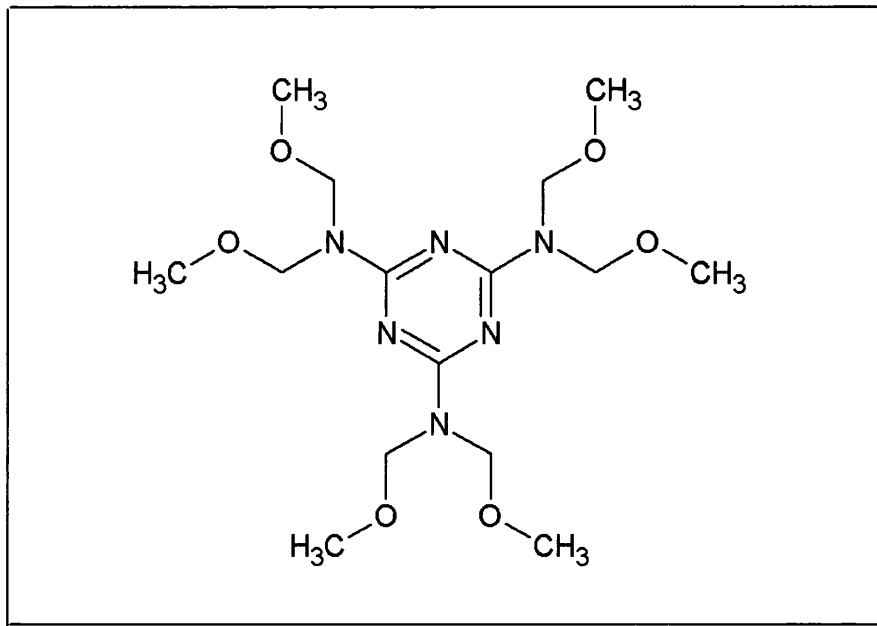


**Figure 1.13 - Hexamethoxymethyl Melamine (HMMM)**

A three dimensional thermoset polymer network is hence built up, with exterior durability, good flexibility and good adhesion properties. The reaction is catalysed by a blocked acid catalyst, commonly p-toluene sulfonic acid, and methanol is produced as a by product [41]. The cross- linking reaction is shown diagrammatically in Figure 1.14.

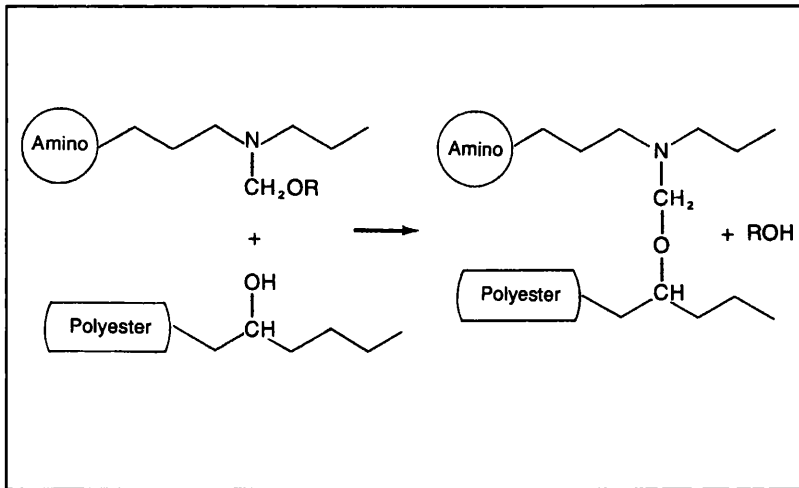


**Figure 1.14 – Polyester Resin Formation by Cross-linking Reaction between Polyester and Amino Formaldehyde Resin – reproduced from [39]**

Curing can be defined as a process of film formation taking place; i.e. the conversion of a coating from its applied liquid state to a dry solid form [42]. In polyester coil coatings, film formation is occurring from a solution of a cross-linking polymer system by a complex mechanism involving the two interdependent steps of solvent evaporation and cross-linking. These processes have been modelled mathematically; by quantifying the physical and chemical mechanisms involved, coating formulation and application conditions can be aided [43]. Models have shown that the final coating surface properties are dependent on the initial solvent content of the coating, the air velocity and the bulk air concentration of solvent [44].

In the early stages of the cure, solvent evaporation is independent of the presence of the polyester, with the rate of evaporation depending on the vapour pressure of the coating solvents, the ratio of the surface area to volume of the film and the rate of air flow. As the viscosity and glass transition temperature ( $T_g$ ) of the coating starts to increase, the rate of solvent loss will start to become controlled by the rate of diffusion of the solvents through the film [42]. These have been described as the first and second stages of solvent loss; in the first stage (vapour pressure controlled) evaporation rate has a first power dependence on wet film thickness. In the second phase (diffusion controlled) the evaporation rate depends on the inverse of the film thickness [21].

At the same time that solvent evaporation is taking place, chemical reaction will start to occur between the polyester and melamine formaldehyde cross-linking agent,

building up the molecular weight of the system. Methanol is a by-product of this reaction. A cross-linking reaction of this sort can be kinetically controlled if the diffusion rate is greater than the reaction rate, and diffusion controlled if the diffusion rate is slow compared to the kinetic reaction rate. In a polyester melamine system, the curing temperature is well in excess of the final  $T_g$  of the coating film. This means that free volume will be large and the rate of reaction will be kinetic controlled. The curing process is hence an extremely complex process, with the final film properties influenced by the viscosity time path followed by the coating during the cure.

The most common method used to cure polyester coil coatings is convection curing, with induction curing and near infrared (NIR) curing being more recent technologies.

### **1.3.1 Convection Curing**

Forced air convection heating using gas catenary or gas flotation ovens with air temperatures of at least 350°C has been the conventional method of curing coil coatings. This method of curing has been favoured by coil coaters as it provides a fairly wide process window and predictable results for a broad range of operating conditions [45].

Two important properties used in the coil coating industry to determine cure are the peak metal temperature (PMT) and the oven dwell time. PMT is defined as the temperature that a metal substrate has to reach in order to adequately cure (cross-link) the coating. Dwell time is defined as the time a coating spends within the oven. Typical polyester coil coatings have a PMT of between 216 and 232°C and take around 30 seconds to cure for a dry film thickness (DFT) of 20 -25µm [46].

During convection curing transfer of heat is by convection onto the surface of the coating and by conduction through the coating and metal. The solvent content of polyester coil coatings are typically 30 - 45% of aliphatic hydrocarbon mixtures, high boiling point aromatics, glycol ethers and esters and high boiling point esters. These solvents are transported by diffusion through the coating to the surface of the film where they will start to evaporate off. As the temperature of the strip continues to rise cross-linking of the polymer coating will be initiated.

A cure time of ca. 30 seconds is long enough for the physical process of solvent evaporation and the chemical process of cross-linking to be relatively well separated. If however process conditions are such that they are not well separated, a phenomenon known as solvent boil can occur. Here solvent evaporates by forcing its way through a surface film in an advanced stage of cross-linking, resulting in crater like defects. Other defects known as pin-holes can occur. During the cure process, a coating needs a low enough viscosity to flow back and cover over holes left by escaping solvent. If the viscosity becomes too high, this flow back will not occur and pin-holes will be left on the coating surface. Solvent boil and pin-holes are shown in Figure 1.15. Note that solvent boil defects show a raised profile, whilst pin-holes do not.

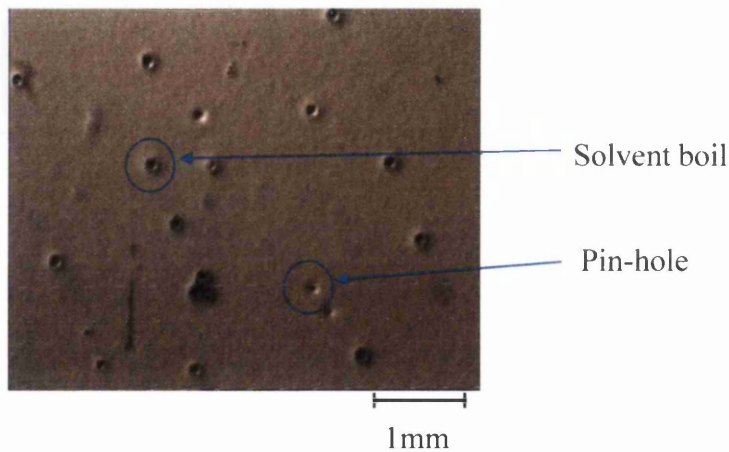


**Figure 1.15 – Polyester Coating Surface Showing Solvent Boil and Pin-hole Defects [47]**

## 1.3.2 NIR Curing

### 1.3.2.1 Background to NIR Curing

Near infrared radiation lies just above the visible region and just below the infrared region of the electromagnetic spectrum from 0.8 – 1.5  $\mu\text{m}$ , and is highlighted in Figure 1.16. When NIR radiation is absorbed by a molecule it causes vibrational motions of bonds in the molecule due to overtone and combination bands, rather than due to fundamental vibrations.

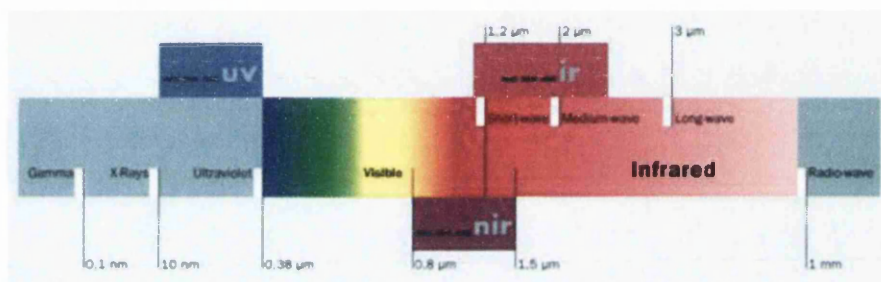


**Figure 1.16 - Electromagnetic Spectrum Showing the Near Infra Red Region**  
*reproduced from [48]*

In the coil coating industry, gas fired convection ovens have dominated the curing process for years, as electrical based infrared (IR) or induction curing were seen to be too costly. Convection curing requires very long oven lengths to achieve the thirty second cure time at typical line speeds at 100 – 120 m/min. Coil coaters have long been concerned with the space occupied by the curing ovens, the time taken to start and stop the coating line, the cure time and the line speed as all these affect the profitability of the coil coating process. A comparison of the ranges in oven dwell times for different curing technologies is given in Figure 1.17 and shows that NIR curing offers the shortest dwell time.

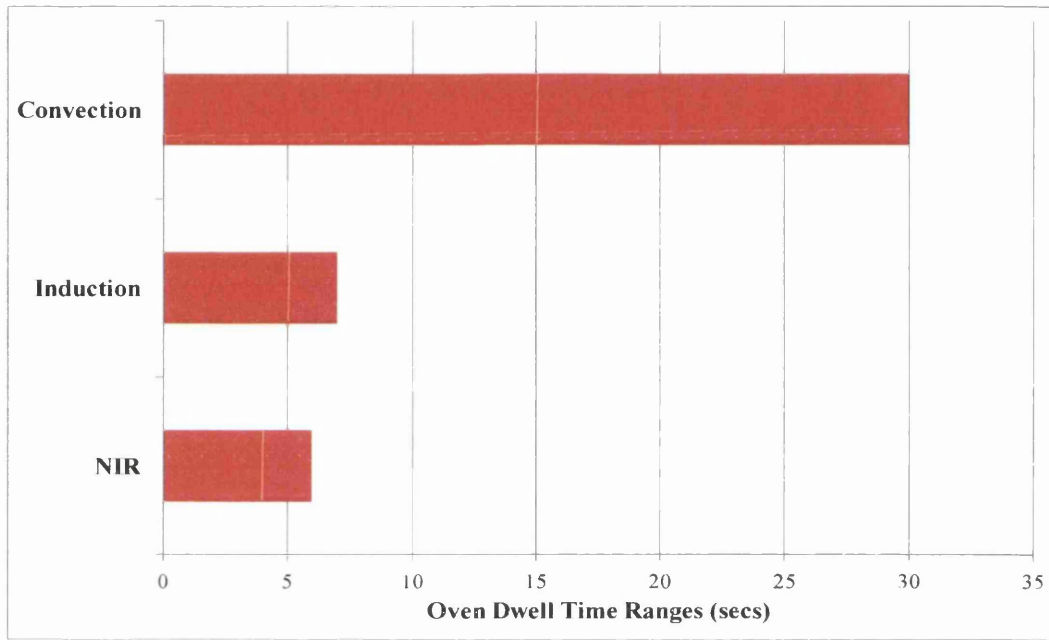


**Figure 1.17 – Comparison of Oven Dwell Times for 25µm Polyester Coil Coatings [49]**

As well as cure time, NIR curing offers benefits in terms of instantaneous on/off characteristics, short oven lengths and reduced energy operation costs [11]. NIR curing was developed from research by the European Space Program simulating the heat shock experienced by spacecraft re-entering the earth's atmosphere, and has been used industrially since the late 1990's. Tata Steel took the decision to invest in NIR curing in 2006 when expanding the capability of an existing galvanising line (DVL2) at their IJmuiden site in Holland. The aim was to create an integrated galvanising – coating line where space for the coating section of the line was limited. On a combined galvanising and coating line, the rate limiting step for thicker gauge substrate is the galvanising section of the line with the maximum line speed being ca. 100 m/min for 1.2 mm gauge. For thinner gauge substrate, the coating line could become the rate limiting step, as the galvanising section can run at ca. 170 m/min for 0.4 mm gauge [50]. Maximising the speed at which curing can take place is obviously beneficial cost wise. NIR curing has been reported by AdPhos as allowing coating lines to run at line speeds of up to 150 – 180 m/min [11]. NIR curing is also in use at coil coating lines at Shree Precoated Steels in India and at Dongbu Steel in Korea [51, 52].

NIR is a radiative curing technique, but unlike ultra violet (UV) or electron beam (EB) curing it is essentially a fast thermal cure. NIR curing offers energy

efficiency savings as heat is transferred directly into the coating by absorption of NIR radiation by the coating system, including absorption at the surface of the galvanised coating. In contrast, in convection curing heat transfer occurs by heated currents of air in the oven transferring heat at the surface of the coating and then transfer by conduction through the depth of the curing coating. NIR curing hence negates the need to preheat an entire oven and changes in oven settings can almost instantly change substrate temperatures [53].

The NIR emitters in the laboratory curing ovens used in this thesis are identical to those on the industrial DVL2 coil coating line. All these ovens are manufactured by AdPhos and use broad range tungsten halogen emitters. Black body theory can be used to predict the spectral distribution of radiation emitted from these emitters. A black body is defined as an object that absorbs all radiation incident on it regardless of wavelength or angle of incidence, and is also a perfect emitter of radiation. The Stefan-Boltzmann Law gives the total energy radiated from a black body per unit area and time over all wavelengths (Equation 1.1) [54].

**Equation 1.1**                      **Energy emitted =  $\sigma (T^4)$**

where

$$\sigma = \text{Stefan-Boltzmann Constant} = 5.670400 \times 10^{-8} \text{ W m}^{-2} \text{ K}^{-4}$$

$$T = \text{absolute temperature (K)}$$

Real materials such as the tungsten filament in a tungsten halogen emitter have a lower capacity to emit radiation compared to a black body. The emissivity,  $\epsilon$  of a material can therefore be defined as the relative ability of the material's surface to emit heat by radiation compared to a blackbody at the same temperature. A black body has an emissivity of one, and the total energy radiated from a real material per unit area and time over all wavelengths can be given by Equation 1.2.

**Equation 1.2**                      **Energy emitted =  $\epsilon\sigma (T^4)$**

A black body will emit specific wavelengths of radiation as a function of temperature, given by Planck's law of black body radiation given in Equation 1.3 [54].

**Equation 1.3**                       $M_e = (c/4)u_{e\lambda}$

where

$M_e$  = spectral radiant excittance per wavelength per  $m^2$

$u_{e\lambda} = 8\pi hc\lambda^{-5}(e^{hc/kT\lambda} - 1)^{-1}$  ( $Jm^{-3}$ )

T = absolute temperature (K)

$\lambda$  = wavelength (m)

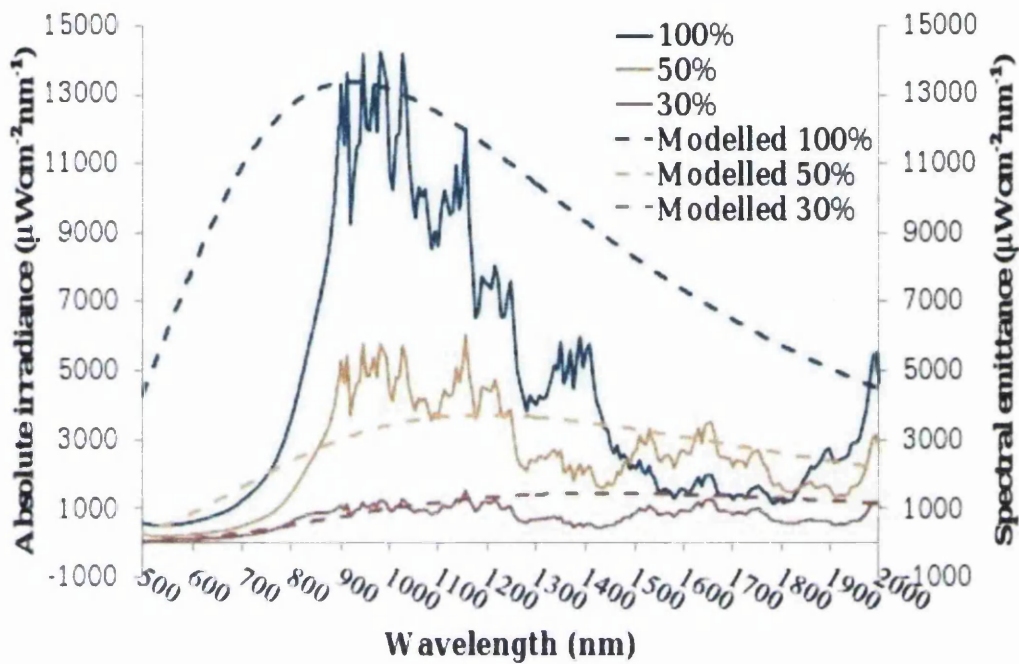
h = Planck's constant ( $6.626176 \times 10^{-34}$  Js)

c = velocity of light ( $2.99792458 \times 10^8$   $Ms^{-1}$ )

k = Boltzmann constant ( $1.380662 \times 10^{-23}$   $JK^{-1}$ )

Cherrington modelled the emitter output from the Adphos emitters using Planck's law and the colour temperature of the emitters corrected for the ratio of emitter input voltage to nominal voltage (supplied by the manufacturer Adphos). Emitter output was modelled at 100%, 50% and 30% emitter power settings and compared to empirical spectroscopic measurements of the emitters, and is shown in Figure 1.18. This figure shows that the theoretical peak wavelength for the emitter is close to the measured peak wavelength, with the exception of the 30% power setting. The measured absolute irradiance at the maximum wavelength is also close to the theoretical spectral emittance at the peak wavelength. The majority of the energy from the emitter is focussed between 800 – 1200 nm, but with some emission in the visible range as well [55].





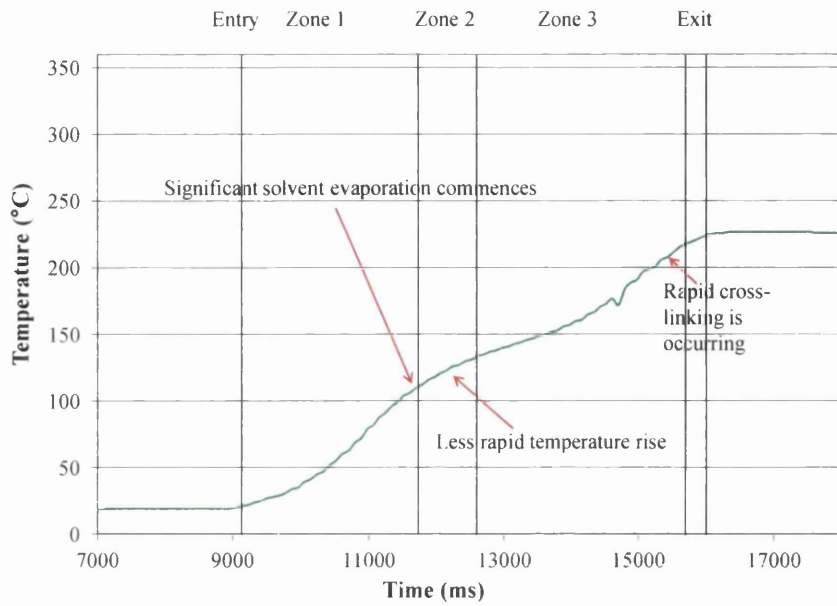
**Figure 1.18 – Comparison Between Measured and Modelled NIR Emitter Outputs**  
*reproduced from [55]*

Figure 1.18 shows that the NIR emitters are able to impart a very high radiation power density into a coating resulting in very short cure times. An energy density that is twice that of an induction curing system and four to six times that of an infrared curing system has been reported, with 15 -20 μm coil top coats curing in less than 3 seconds [12, 13].

Early reports in the literature suggested that NIR heating, as well as being used to cure coil coatings, could find use for heat treating metals, drying water and solvent based coatings, repairing micro-spot defects on car body coatings, plastic welding and curing powder coatings [12, 13, 52, 56]. More recently, NIR radiation has been suggested as a means of reducing some of the manufacturing steps in dye sensitised solar cell manufacture. Here it has been used to rapidly sinter titanium dioxide based photoanodes [57], reduce the processing time for silver inks used for current collection [58] and rapidly platinise counter electrodes [59]. It has also been suggested as a means of modifying the surface structure of tinplate and galvanised coatings on steel [14] [60] and has been used to cure resins in restorative dentistry applications [61].

### 1.3.2.2 NIR Cure Mechanism

NIR curing of polyester coil coatings takes place as a fast thermal cure involving the two stages of solvent evaporation and resin cross-linking. In convection curing the relatively longer oven dwell time of 30 seconds means that these two stages can be easily separated. NIR curing employs a much shorter oven dwell time, so in order to separate the two stages and reduce the risk of solvent boil occurring, NIR ovens are divided into three zones with the NIR emitter power tailored to provide a cure which is temperature profiled with time. An example of such a cure profile using a laboratory NIR oven is shown in Figure 1.19. The first zone of the oven increases the temperature of the steel strip to a point at which solvent evaporation begins to take place. Thermogravimetric analysis (TGA) can be used to determine the temperature at which solvents evaporate and the percentage of solvent in the formulation. Temperature rise in zone 2 is less rapid, which allows a lot of the solvent to evaporate. In this zone the substrate is being kept as long as possible at a temperature below the cross-linking initiation temperature, which is defined as the temperature at which the blocked acid catalyst unblocks. In zone 3, cross-linking occurs with polyester PMT being reached. Note that the small deflection in the zone 3 temperature profile can be attributed to the thermocouple wire used to measure the substrate temperature knocking against the wall of the oven. This temperature profiled cure contrasts with that used for a convection oven, where the temperature rises steadily to the PMT in one oven zone. A comparison of the two cure profiles using laboratory NIR ovens is shown in Figure 1.20. Once PMT has been reached the temperature needs to be decreased rapidly by a water quench which halts the cross-linking reaction. Quenching of the cross-linking reaction is required as an over cured coating can suffer from loss of gloss or flexibility.



**Figure 1.19 – Typical NIR Temperature Cure Profile for a 25µm Polyester Coil Coating**

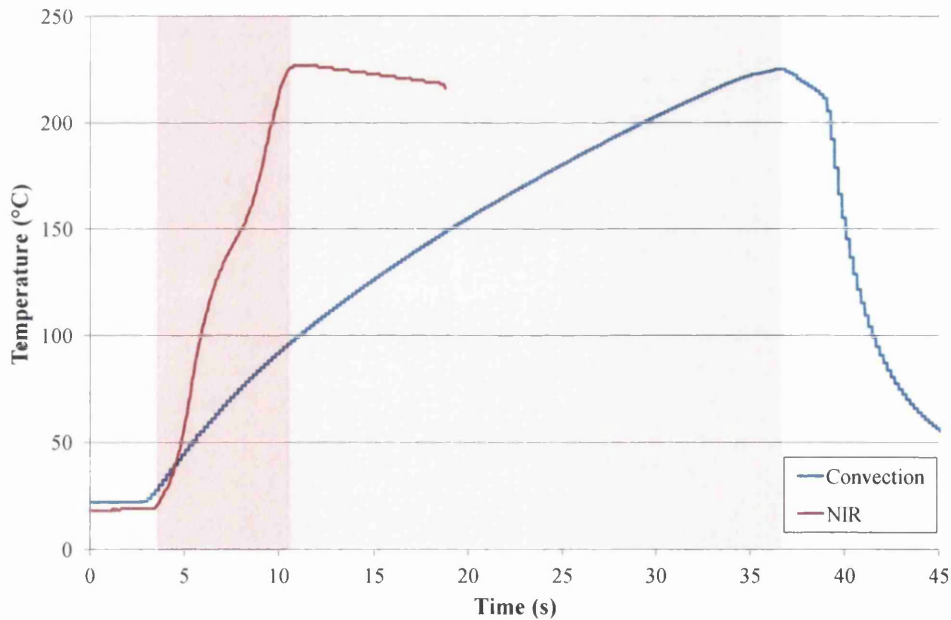


**Figure 1.20 – Comparison of Typical NIR & Convection Cure Profiles for 25 µm Polyester Coil Coatings**

A successfully cured coating is defined by its cure window, this being the range of temperature conditions over which the paint will cure and still meet its final performance criteria such as gloss, flexibility and weatherability. Coil coatings are

coated onto both the front side and the back side of the steel strip, with the backing coat having a smaller dry film thickness (dft) than the top coat. As the same oven conditions are curing both coatings, more industrial processing flexibility is available if this cure window is as wide as possible.

Coatings that have not reached a high enough temperature to ensure a sufficient enough amount of cross-linking has occurred will be soft. The lower cure window for a paint formulation is related to its resistance to solvents, and is commonly determined in the coil coating industry by the temperature above which a paint formulation passes the MEK rub test [62]. (See Section 1.4.2.1). The upper cure window can be defined as the temperature at which the onset of solvent boil first occurs. Polyester cure can also be determined by peak ratio measurement with Fourier transform infrared (FTIR) spectroscopy [63].

Of particular importance to NIR cure are the optical properties of the surface of the galvanising alloy immediately below the coating layers [53]. Although these alloys are highly reflective across the UV-visible-NIR region, it can be seen from the total reflectance spectra in Figure 1.21 that they show a peak at ca. 1000 nm associated with absorption by zinc. This peak is particularly pronounced for hot dip galvanised steel (HDG) and MagiZinc, the most commonly used substrates on Tata Steel's NIR line. As this peak is in the region of  $\lambda_{\text{max}}$  for the output from the NIR emitters, coatings with a high transparency to NIR could allow a proportion of NIR through the coating to allow substrate absorption to play a role in curing the top coat.

White, black and silver polyester coatings can be used to illustrate different scenarios of absorption, reflection and transmission of light occurring in a coating system, and how this affects cure. White polyester coil coatings get their colour from the  $\text{TiO}_2$  pigment in their formulation. The reflectance spectra of polyester coatings coated over HDG in Figure 1.22 show that for the white coating, the presence of  $\text{TiO}_2$  pigment means that the white coating reflects visible light well, but has more transparency in the NIR region. An absorption peak at ca. 1000 nm is also apparent, matching the zinc absorption peak in the HDG spectrum in Figure 1.21. This suggests the white coating has a degree of transparency in the NIR region, and this is confirmed by the Vis/NIR transmission spectrum of the white coating shown in Figure 1.23.

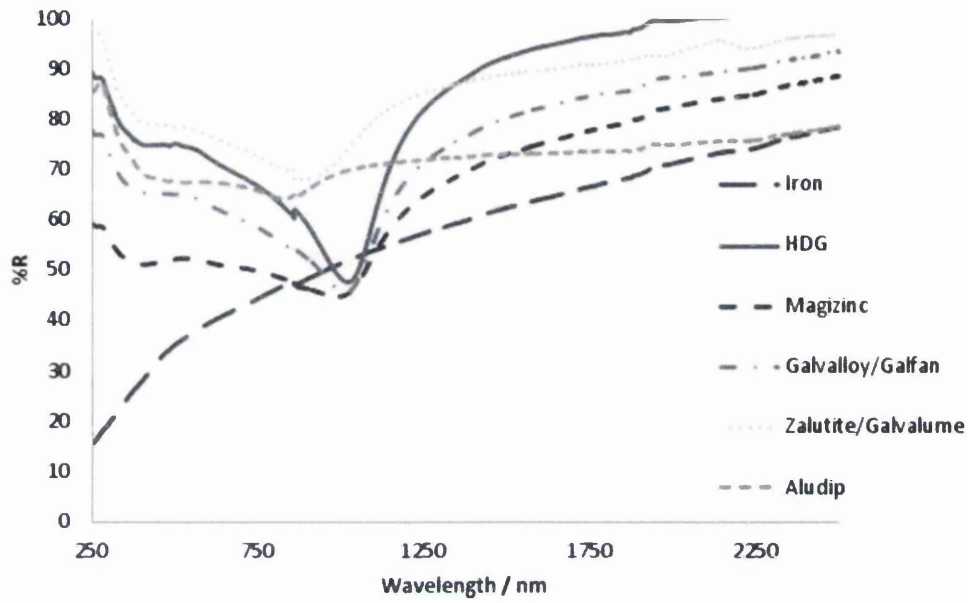


Figure 1.21 – UV-Vis-NIR Reflectance Spectra of Metallic Substrates

*reproduced from [53]*

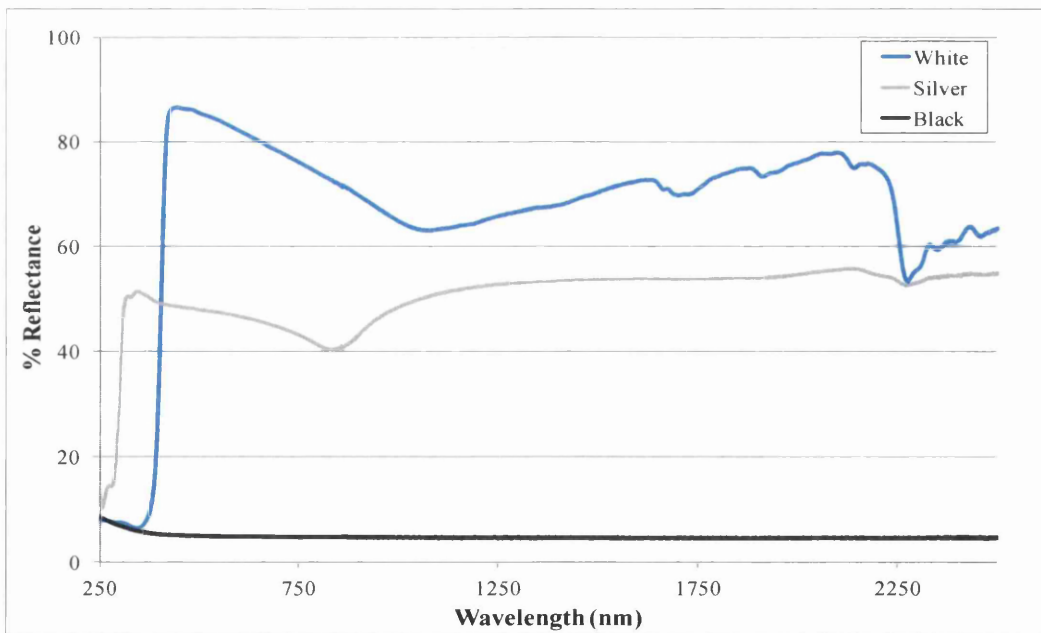
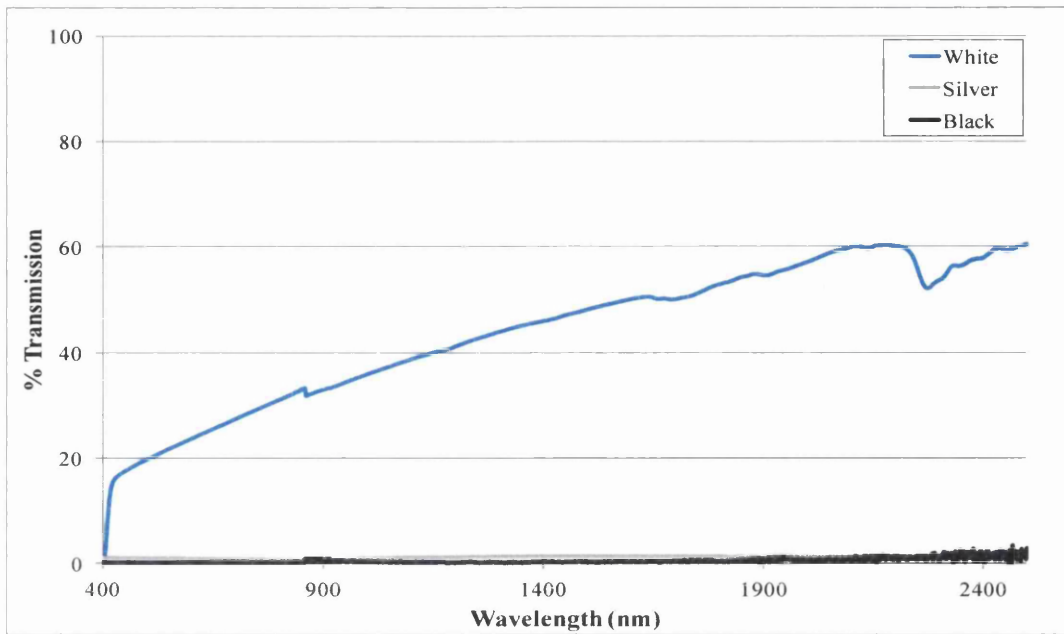


Figure 1.22 - UV-Vis-NIR Reflectance Spectra of White, Silver & Black Polyesters



**Figure 1.23 – Vis-NIR Transmission through Free Standing Films of White, Silver & Black Polyesters**

Black polyester coil coatings for exterior architectural applications are usually pigmented with carbon black pigment. As expected, the reflectance spectrum of the black coating in Figure 1.22 shows that there is strong absorption across all wavelengths with very little reflection of light. The transmission through a black coating in Figure 1.23 indicates that the entire light incident on the coating is absorbed in the coating itself.

Silver polyester coil coatings get their silver metallic appearance from aluminium flake. Here, the coating reflects ca. 50% of UV-Vis-NIR incident on it, with Figure 1.22 showing the absorption peak at ca. 800 nm characteristic of the aluminium flake. No absorption peak is seen at ca. 1000 nm, which suggests NIR radiation is not penetrating through to the substrate. The transmission spectrum for a silver coating in Figure 1.23 confirms that this is the case; silver coatings absorb all of the 50% of light that is not reflected at the surface of the coating.

These spectroscopic observations suggest that while white coatings will make use of substrate heating, in black and silver coatings heat transfer will start in the coating itself. Laboratory curing trials have shown that white coatings cure easily with a

wide cure window, whilst black and silver coatings are difficult to cure with a small cure window and are prone to solvent boil [53].

This difference in curing ability can be illustrated by considering how NIR is reflected, absorbed or transmitted in the coating system, and this is shown schematically in Figure 1.24. In case **A**, there is some penetration of the coating by radiation then absorption within the coating, whilst in case **A'** the penetration depth is greater before absorption. Case **B** shows penetration of radiation through the coating to the substrate surface and absorption there. Case **C** denotes reflection of radiation from the substrate surface and then absorption within the coating. In case **D**, radiation is reflected from the substrate surface but it is not absorbed as it makes its way back through the coating. Case **E** shows reflection of radiation at the coating surface. In reality all these mechanisms will also be present at other layers in the coating system such as at the pretreatment-primer layer, but for simplicity in these Figures only interactions with the top coat are considered. Coatings such as white polyesters which cure easily with a wide cure window make use of all of these mechanisms. The presence of mechanism **B** means that the coating is receiving heating from the bottom layer of the coating upwards, allowing solvent to more easily escape and minimising the chance of solvent boil occurring.

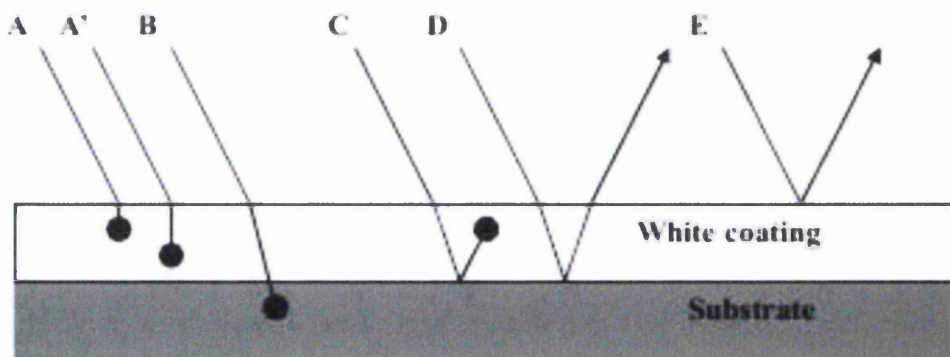


**Figure 1.24 – Different Ways that NIR can Interact with a Coating System and its Substrate**

*reproduced from [53]*

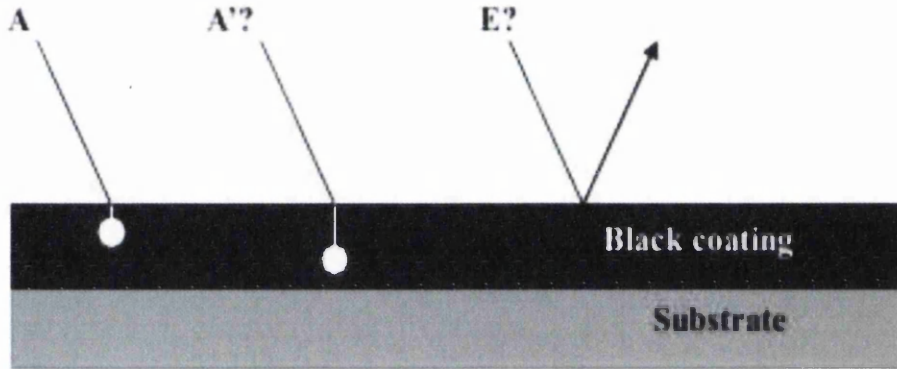


**Figure 1.25 – NIR Interacting with a Highly Absorbing Coating**

*reproduced from [53]*

The significant mechanisms at play in a darker more highly absorbing coating such as black polyester are shown in Figure 1.25. Here, most of the NIR absorption occurs in the top coat. Absorption at greater depth in the coating (case **A'**) and reflection from the surface of the coating (case **E**) will become questionable if the pigment loading is high enough. All absorption will then occur in the outer few microns of the coating. This means that solvent will have to force its way through the top few microns of coating where cross-linking is already advanced, predisposing the coating to solvent boil.

In summary, the presence of top coat NIR absorbers have been suggested as beneficial for some coating systems [15]. However, architectural polyester coil coatings on galvanised steel substrates have coating thicknesses and compositions that mean NIR cure is facilitated by a top coat largely transparent to NIR, but with a NIR absorbing substrate.



### **1.3.3 Other Fast Curing Techniques**

#### **1.3.3.1 Induction Curing**

In induction heating, an alternating current is passed through an electromagnetic coil which is mounted around a coated coil substrate. This is accompanied by an intense and rapidly changing magnetic field in the space within the electromagnetic coil, which induces eddy currents in the coil substrate and leads to Joule effect heating from resistance. Heating rates of hundreds of degrees per second can be reached, with heating commencing from the metal strip [64]. This means that induction curing produces a medium power density as opposed to the low power density of convection cure, but the power density is still half that of NIR cure. Typical oven lengths for induction curing are hence 2.5 m compared to an NIR oven length of 1.5 m [11].

#### **1.3.3.2 UV Curing & Electron Beam Curing**

UV curing and electron beam are both forms of radiation curing techniques which have become well established in the wood coating, printed circuit board and printing ink industries for acrylate and epoxy resins, with UV curing being by far the most popular of the two systems. They are, however, relatively new or emerging technologies in the coil coating industry and there has been considerable development effort by coil coaters and coating producers to develop these techniques [65]. The techniques are used to cure coating formulations that are liquid (containing polymer resin and reactive diluents) but with very little or no solvent content. This enables curing to be very fast, generally at near ambient temperature leading to the technologies being known as 'cold' curing techniques.

The main types of emitters used in UV curing are mercury arc lamps, microwave excited bulbs and excimer lamps, with the UV radiation being transmitted through air or nitrogen directly onto the coating.

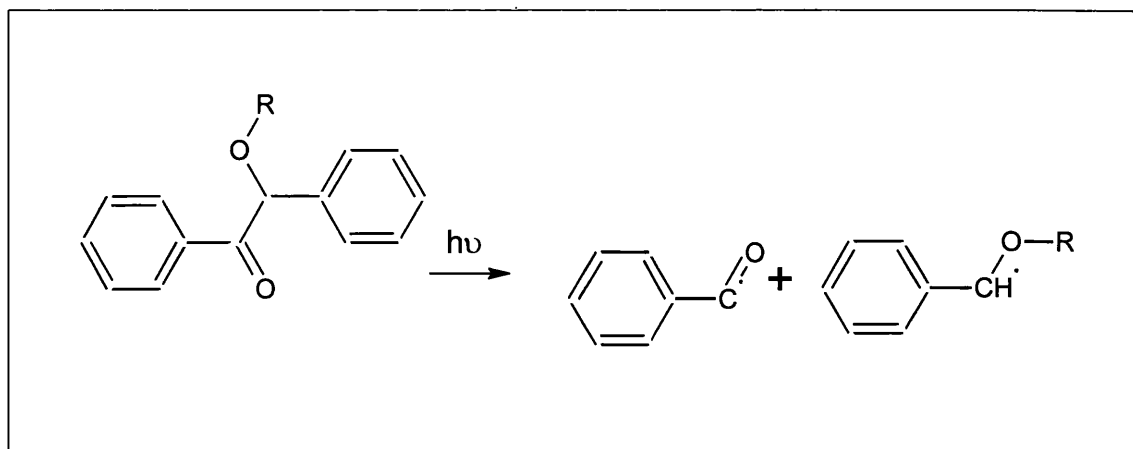


**Figure 1.26 – Unimolecular free radical UV Curing**

UV curing requires the presence of a photo initiator which forms an excited state by the absorption of an UV photon. Two types of polymerisation reaction are possible with UV curing; either free radical or cation initiated chain growth polymerisation. With free radical initiated UV curing, there are two types of photo initiator reaction. The first uses a unimolecular photo initiator whose excited state cleaves homolytically to form free radicals that initiate polymerisation. An example of this kind of photo initiator are benzoin ethers which are shown in Figure 1.26 [21].

The second type is a bimolecular photo initiated reaction. Here an excited state photo initiator abstracts hydrogen from a hydrogen donor to yield free radicals that initiate polymerisation. An example of this type of reaction is the use of benzophenones as a hydrogen abstracter with tertiary amines as the hydrogen donor, and is shown in Figure 1.27 [23]. Free radicals produced in this manner are used to polymerise acrylate resins (polyester acrylates, epoxy acrylates, urethane acrylates and polyether acrylates).

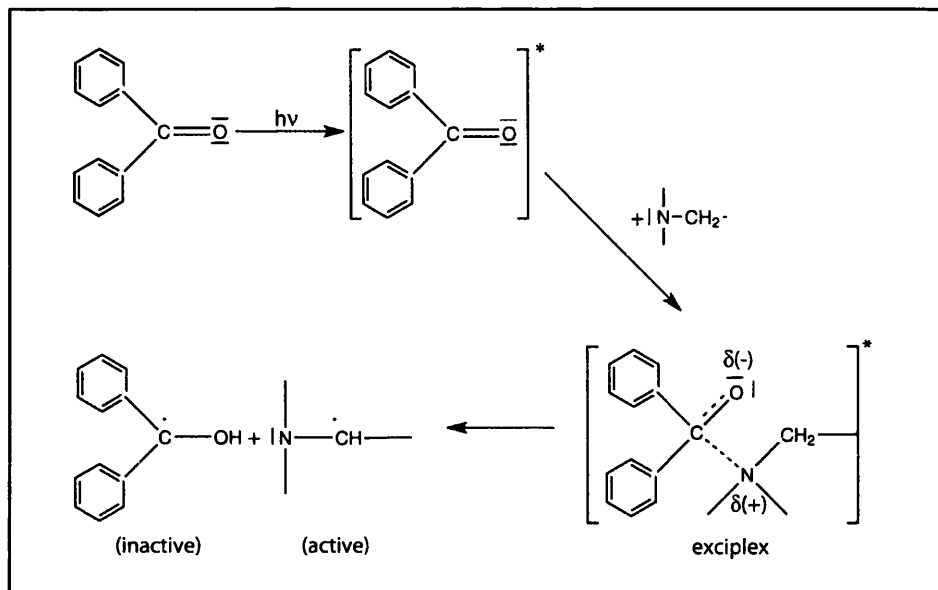


**Figure 1.27 – Bimolecular Photo Initiated UV Curing** reproduced from [23]

Photo initiators for cation initiated UV curing are typically onium salts of very strong acids which form protons by the type of reaction shown in Figure 1.28. The presence of protons then promotes the ring opening polymerisation of epoxy resins [66].

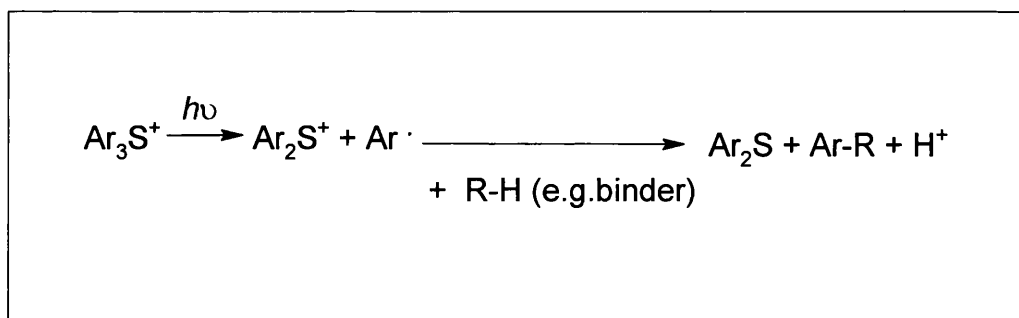


**Figure 1.28 – Cationic UV Curing by a Sulphonium Photo-initiator** - reproduced from [23]

Electron beam curing does not need a photo initiator, but involves direct interaction of high energy electrons (150 – 300keV) emitted from a hot cathode tube with the polymer resin, to form ionised molecules and radicals or radical ions thus

enabling the start of radical polymerisation. Other advantages over UV curing are that pigments do not interfere with the curing and curing is much faster, but capital cost of the equipment is higher, x-ray emission occurs with its associated shielding needs and an inert atmosphere is always required.

### **1.3.3.3 Infrared Curing**

Infrared curing works with the same physical principles as near infrared curing; the energy of radiation in this range of the electromagnetic spectrum is less than the bond dissociation energy of almost all chemical bonds, but is capable of making them vibrate which manifests itself as heat. Medium range infrared radiation with a maximum wavelength of 3.5 – 2.5  $\mu\text{m}$  produces a medium energy density cure. CH, OH and NH functional groups in the polymer resin will absorb radiation in this wavelength range, so that most radiation is absorbed at the surface of the coating and this limits the penetration depth of the radiation. This surface absorption means that if curing is too rapid there is a risk of escaping solvent becoming entrapped under a surface skin of cured coating, leading to surface defects in the coating. An infrared cure typically takes about 15 seconds for a coil coating, so is shorter than a convection cure but longer than a NIR cure.

## 1.4 Characterisation of Coatings

### 1.4.1 Analytical Techniques

A range of analytical techniques have been used to explore the topography and morphology of coatings.

Small quantities of aliphatic or partly fluorinated wax lubricants are commonly added to coil coatings to improve coil frictional behavior. Fischer et al used confocal Raman spectroscopy, optical light and Atomic Force microscopy (AFM) to investigate the effect of peak metal temperature and pigmentation on the morphology of polyester coatings modified with wax lubricant [67, 68].

Hexamethoxymethyl melamine (HMMM) is the cross-linking agent most commonly used in polyester coil coatings. During curing this cross-linking agent can self condense leading to regions of high cross-linking density within the coating, in a process known as melamine enrichment. This can modify the formability, stain resistance and weatherability of the coating, so it is therefore of great importance to coil coaters that this phenomenon is investigated. Zhang et al used confocal Raman spectroscopy to study the distribution of HMMM on the coating surface. Depth profiling showed that the melamine enrichment occurred not only at the surface but also through the depth of the coating and was not affected by the presence of pigment in the coating. Furthermore, the melamine enriched areas were also harder indicating that they had been formed by a self condensation reaction [69, 70].

Step-scan photoacoustic Fourier Transform Infrared spectroscopy (SSPA-FTIR) along with X-ray photoelectron spectroscopy (XPS), AFM, scanning electron microscopy (SEM) and colour and gloss changes have been used to investigate the surface and bulk changes in polyester melamine coil coatings. In particular the effect of pigment on degradation has been investigated. Pigments were shown to have a large effect on the appearance of the coating surface, with larger pigment particles and higher pigment loadings roughening the coating surface. Pigments affect the coating surface degradation; coatings with higher titanium dioxide content became more uneven at the surface after degradation due to the photo-activity of the titanium dioxide. [63, 71].

Step-scan phase modulation photoacoustic (SS-PM-PA) FTIR has also been used to look at the depth distribution of TiO<sub>2</sub> pigment within polyurethane coil coatings,

and verified by SEM cross-section imaging. TiO<sub>2</sub> pigment is shown to be heterogeneously distributed within the top coat, with the depth profile varying with increasing TiO<sub>2</sub> pigment content [72].

X-ray photoelectron spectroscopy (XPS) and time-of-flight secondary ion mass spectrometry (ToF-SIMS) are both surface analysis techniques that can be used to study the depth profile and the distribution of minor components within a coating and give information to help understand the processes occurring during application, curing and use of the coating. For example, XPS and ToF-SIMS have been used to investigate the segregation of siloxane based levelling agents in multilayer organic coating systems. Coil coatings are formulated with small quantities of additives to improve coating properties with some of these additives being added with the intention of them migrating to the coating surface; one such of these is a levelling agent. XPS and ToF-SIMS analysis of the surfaces of the coating components suggested that levelling agent had migrated from the primer surface, dissolved into the bulk of the top coat, then migrated through such that it was observed at the air/top coat surface. As depth of analysis with XPS is only about 5-8 nm, further information about the coating depth composition can be gained from XPS line scan along an ultra low angle microtomy (ULAM) taper of the coating system. The ULAM technique investigates compositional depth profile or 'buried' interface surfaces by fabricating an ultra-low angle taper through a multilayer coating system using a microtome knife. In this case, the silicon concentration profile through the depth of the top coat suggested that the levelling agent had migrated into the top coat during curing and prior to coating gelation [36, 73, 74].

ToF-SIMS with a bismuth cluster ion and a C<sub>60</sub> sputter/etch source has been used to depth profile a poly(vinylidene difluoride) (PVdF) /poly(methyl methacrylate) (PMMA) coil coating. This showed that the topcoat was comprised of three distinct layers; a thin outer surface layer of flow agent, an acrylic rich sub-surface layer and a bulk topcoat underneath [75]. ToF-SIMS has also been used to depth profile a range of other minor coating components; a PVdF coating cross-linked with HMMM was found to have the greatest concentration of the cross-linker at the surface of the coating [76]. Moreover, different cross-linkers have different abilities to segregate at the surface; HMMM is more concentrated on the surface of a coating than a tris-isocyanurate cross-linker [77]. A titanium dioxide pigmented polyester coating was found to have the lowest concentration of TiO<sub>2</sub> at the coating surface, with the TiO<sub>2</sub> concentration increasing with coating depth until a stable concentration was reached in the coating

bulk. The C<sub>60</sub> etch source used was assumed to have removed the silica/alumina coating shell from the TiO<sub>2</sub> particles [76]. A polyurethane coating with a <sup>35</sup>Cl/<sup>37</sup>Cl tagged acrylic based flow agent was shown to have a high surface concentration of flow agent and a depletion layer immediately below this [76].

Thermal analysis and spectroscopy techniques have been used to understand cure reactions. Polymeric coating materials undergo a dramatic change in their viscoelastic properties such as storage modulus, E', loss modulus, E'' and loss factor, tan δ during cure; the change in these with oven baking temperature can be used to monitor cure. Frey et al hence used dynamic mechanical analysis (DMA) to monitor the cure of OH functional polyacrylate thermosetting automotive clear coats. Already cured free films of coatings were characterised using tensile mode dynamic mechanical analysis, and uncured liquid coating samples by impregnating them onto a glass fibre braid carrier which had an inherent small temperature dependant moduli effect [78]. Korhonen et al used DMA and differential scanning calorimetry (DSC) to investigate the cure of polyester melamine coil coatings with different ratios of polyester resin to curing agent. Cured free standing coating films, liquid paint and cured coating on substrate were investigated, and a correlation between PMT and glass transition temperature (T<sub>g</sub>) was made [79, 80]. Buder-Stroiszniigg et al used DMA to investigate clear polyester coil coatings cross-linked with isocyanate based cross-linking agents, and found that similar thermomechanical and mechanical properties were obtained for coatings cured at industrial processing conditions and those cured at a much longer, lower oven baking temperature [81].

The effect of cure rate on mechanical properties of other thermosetting resins such as UV curable dimethacrylate dental resins has also been studied by Lovell et al using DMA and near IR spectroscopy. This showed that the glass transition temperature (T<sub>g</sub>) and storage modulus (E') were not affected by cure rate (varied by changing UV light intensity and cure temperature), but were strongly dependant on the final methacrylate double bond conversion. This was attributed to the high cross-linking density of the polymer resin [82].

Fourier transform infrared (FTIR) spectroscopy has been used to study cure reactions by monitoring the consumption of monomer with the decrease in a monomer functional group characteristic peak, relative to a reference peak as cure progresses. For example, de la Caba et al studied the cure reaction of an unsaturated polyester resin containing styrene, following the consumption of polyester C=C and styrene C=C bonds

with a C=O peak as an internal reference [83], whilst Grunden et al studied a similar resin system using fluorescence spectroscopy [84].

Escola et al studied the cure reaction of epoxy/amine and epoxy/amide coatings by near infrared (NIR) spectroscopy. The epoxy resin chain has oxirane rings at its ends, and the decrease in the intensity of a NIR band from the oxirane ring was measured against the band from a phenyl ring which was taken as an internal reference [85].

Barista et al studied the degradation of clear polyester melamine coatings with different resin structures using a FTIR spectroscopy photo-oxidation index. The photo-oxidation index was calculated by measuring the disappearance of the CH<sub>n</sub> band and the appearance of OH and NH bands during an accelerated weathering cycle, and was found to be consistent with gloss and optical microscopy results [86].

## **1.4.2 Physical Tests of Coatings**

A huge variety of quality control tests are available for use in the coatings industry to assess the performance of the product, including tests for impact resistance, viscosity, cure, gloss and colour, hardness, scratch resistance, boiling water resistance, flexibility and adhesion.

It is beyond the scope of this thesis to give details of all these tests; however some in common use in coil coating applications are described below.

### **1.4.2.1 MEK Rub Test**

The MEK rub test is the most used method of determining the degree of cure of a coating film in the coil coating industry. The test is based on the fact that as a coating becomes more cross-linked, its solubility in solvents decreases. The resistance of a coating film to the solvent methyl ethyl ketone (MEK) is determined by rubbing the cured surface of the coating with a cloth soaked with MEK until failure or breakthrough of the film occurs [62]. The rubs are counted as a double rub (one rub forward and one rub backward constitutes a double rub). A double rub result of 50 for a polyester coil coating is commonly taken as the minimum indication of adequate cure.



The MEK rub test is used widely in the coil coating industry because it provides a quick relative estimation of degree of cure and is the only method that has proved suitable for production conditions. It is however quite a subjective test, as it relies on constant force and speed being maintained by the operator. For this reason MEK rub test machines are available in an attempt to eliminate operator inconsistency. A 'false negative' result can also be obtained if the coating being tested has poor adhesion to the primer below; a low number of double rubs may be reported but this could be due to poor adhesion and not lack of cross-linking. Results should also be recorded from the middle of the rub area and not from the beginning or end as higher levels of force will be exerted here.

#### **1.4.2.2 Viscosity**

Viscosity is a measure of the resistance of a fluid to deform under shear stress, and is commonly perceived as thickness, or resistance to pouring. It is the parameter that provides the best indication of the behaviour of a liquid coating with regard to its application to a substrate.

Viscosity can be measured with a flow cup, a simple gravity device that measures the timed flow of a known volume of coating passing through an orifice located at the bottom of a shaped cup. As viscosity is temperature dependant, the temperature of the test conditions needs to be specified. Typical coating systems measured by this method are polyesters, polyurethanes and PVdFs. Zahn and Ford 4 are common makes of viscosity cups.

Another method is a Brookfield rotational viscometer, which employs a spindle submersed in the coating, rotating at a constant speed and measures viscosity by sensing the torque required to rotate the spindle. The torque is proportional to the viscous drag on the spindle, thus the sample's viscosity. Coatings with a higher viscosity such as PVC plastisol are measured by this technique.

### 1.4.2.3 Colour

The CIE  $L^*a^*b^*$  colour scale was introduced in 1976 to replace the CIE XYZ colour system, and provides a standard approximately uniform colour scale to enable colour values to be easily compared. It is used extensively in many industries including the coatings industry. CIE  $L^*a^*b^*$  colour space is shown in Figure 1.29 and is organised in cube form with the  $L^*$  axis running from 100 representing a perfect reflecting diffuser, to zero which represents black. The  $a^*$  and  $b^*$  axes have no specific numerical limits, with positive  $a^*$  representing red, negative  $a^*$  representing green, positive  $b^*$  representing yellow and negative  $b^*$  representing blue [87]. Colour can be measured by a colorimeter or a spectrophotometer.

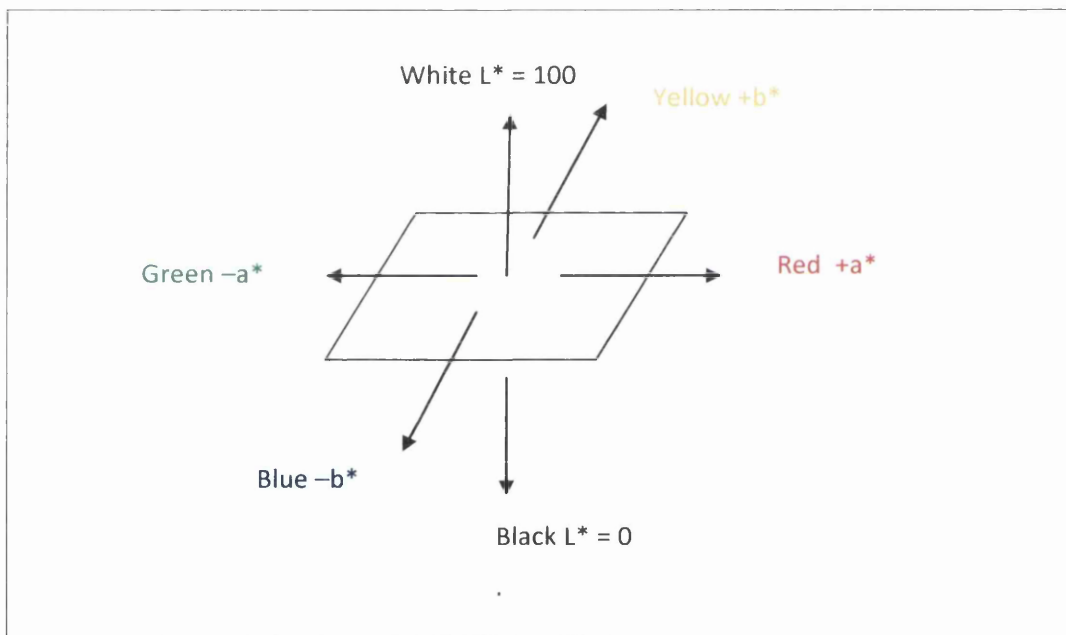


Figure 1.29 – CIE  $L^*a^*b^*$  Colour Space

### 1.4.2.4 Gloss

Gloss is an optical property of a surface, a measure of a surface's specular reflection of incident light at a specified incident angle based on refractive index. It is measured by a gloss meter with a polished black glass sample with a refractive index of 1.567 being used as a standard and assigned a gloss of 100 at all incident angles [88]. The angle at which gloss can be measured is usually taken at  $20^\circ$ ,  $60^\circ$  or  $85^\circ$  to the

normal of the surface of the coating. Smooth surfaces will reflect a high proportion of light falling on them and will have a high gloss value. Coating degradation can cause coating surfaces to pit, crack and roughen leading to a reduction in gloss which can be used to track degradation [25].

#### 1.4.2.5 Flexibility and Adhesion

Organically coated steels are subjected to stresses on fabrication into products by roll forming, brake bending and other deformation processes. These stresses can exceed the flexibility or adhesive strength of the coating and result in the coating fracturing and exposing the substrate, or in loss of adhesion to the substrate. It is therefore important to have a means of evaluating the ability of a coating system to withstand the stresses of fabrication.

The T-Bend test is commonly used in the coil coating industry to assess the flexibility of a coating. Organically coated metal is bent back on itself at  $180^\circ$  as in Figure 1.30, and the bend is assessed for cracking. If no cracks are formed at this point, the result is recorded as 0T. If the coat has opened up, the metal continues to be folded around itself, forming a less severe bend, the result this time for no cracking being 1T. The process is continued until the failure point is found.



**Figure 1.30 – T Bend Test - reproduced from [28]**

The cross hatch adhesion test is another common empirical test. A multi-cutter device is used to make a band of several parallel notches into the coating down to the substrate. Another band of cuts is then made at right angles, resulting in a grid of squares as shown in Figure 1.31. A strip of pressure sensitive adhesive tape is pressed over the cross hatched areas, and the adhesion assessed qualitatively by noting on an index scale of 0 to 4 how much coating is removed from the incisions.

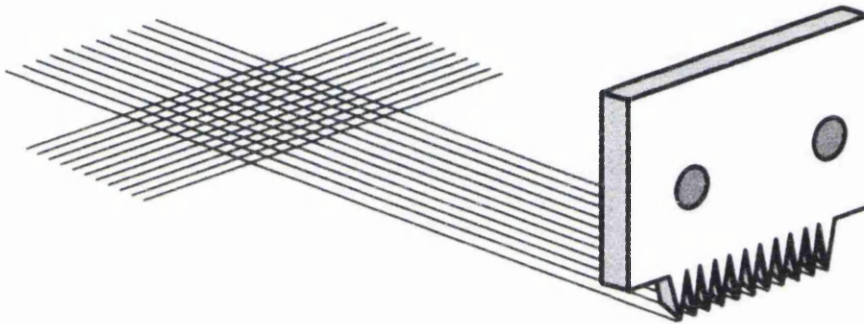


**Figure 1.31 - Cross Hatch Cuts Made for the Cross Hatch Adhesion Test**  
*reproduced from [18]*

A reverse impact test can be used to measure the resistance of a coat to cracking. In this test an organic coating is applied to a panel and cured, then a standard weight is dropped a distance to strike an indenter that deforms the coating and the substrate from its backside. Films generally fail by cracking, which is made more visible by the use of a magnifier or by a tape-pull test to determine the amount of coating removed.

Another adhesion test has been proposed by Van Ooij; the emersion of coated substrate in N-methyl pyrrolidone (NMP) which causes polymeric coatings to swell without dissolution and hence the coating film delaminates. Time taken to delaminate can be measured and is reproducible for a given coating system, and can be used to study interfacial changes [89].

## **1.5 Transpired Solar Collectors**

There is currently considerable concern about climate change caused by greenhouse gas emissions, and this has driven the need for sustainable construction with better energy performing buildings that will meet current environmental, political,

financial and architectural needs. The sun is a large source of potential energy; it is estimated 30 minutes of solar irradiation reaching the earth's surface is equivalent to the world's energy demand for one year [90]. Organically coated steel buildings can harness this energy by functionalising the building envelope by the use of renewable energy generating coatings enabling the building envelope to produce and export energy and thus cut CO<sub>2</sub> emissions. This leads to the idea of 'buildings as power stations' [91].

A transpired solar collector (TSC), sometimes also referred to in the literature as an unglazed transpired collector (UTC) is a solar air heating system which harnesses the power of the sun to provide solar thermal energy. Collectors of this type have been used for building ventilation air heating and more recently for crop drying [92, 93]. TSCs used for building ventilation air have the further advantage of capturing night time heat loss through the walls of the building to the atmosphere. During the day, air exiting the TSC will be cooler than indoor air temperature but greater than ambient; the TSC air will therefore have the effect of de-stratifying building air and reducing heat loss through the ceiling. An example of a building with a transpired solar collector façade is given in Figure 1.32.



**Figure 1.32 – Fire and Emergency Services Training Institute at Toronto Pearson International Airport, incorporating a Transpired Solar Collector Façade**  
*Image Copyright Conservat Engineering Inc. This work is licensed under the Creative Commons Attribution-Share Alike 3.0 Unported Licence.*

A schematic of the typical operation of a TSC is shown in Figure 1.33. A TSC consists of an additional skin of organically coated profiled strip steel installed ideally on the southerly facing elevation of a building envelope, the strip steel being uniformly covered across its entire face with thousands of tiny perforations, which are 1-2 mm in diameter. The void fraction, that is the amount of collector surface area in holes, is typically about 2%. Collectors can be fitted on as new build or can be retro-fitted.

Solar energy striking the surface of the collector is absorbed and heats the thermal boundary layer of air immediately in front of it. This heated layer of boundary air is then drawn by a ventilation fan through the perforations and into a 10 - 15 cm sealed cavity (plenum) between the collector and the original building elevation. From there it can be fed directly into the building as heated ventilation air, ducted to supplement the building's heating system or used to dry crops.

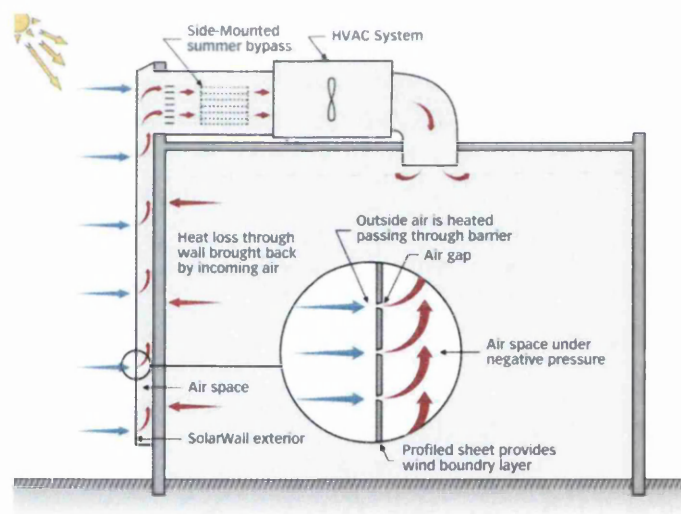


**Figure 1.33 – Schematic of Transpired Solar Collector Operation**

*Image Copyright Conservall Engineering Inc. This work is licensed under the Creative Commons Attribution-Share Alike 3.0 Unported Licence.*

Transpired solar collectors act as effective solar radiation-to-air heat exchangers where the overall heat balance can be modeled by considering convective and radiative heat losses [92, 94, 95]. High efficiencies (60-75%) can be reached, where efficiency is considered the ratio of the useful heat delivered by the solar collector to the total solar energy input on the collector surface [96]. The perforations in the collector increase the

convective heat transfer coefficient between the absorber surface and the air stream flowing through the collector. The continual drawing of air through the system by the ventilation fan means that the heated layer of boundary air is captured, and the convective heat loss to wind is therefore small [92].

## 1.6 Introduction to Solar Radiation

### 1.6.1 Terrestrial Solar Radiation

Solar radiation that reaches the ground is known as terrestrial solar radiation, comprising of 5% UV radiation, 45% visible radiation and 50% near infrared radiation as shown in Figure 1.34. Terrestrial solar radiation varies in wavelength from 280 to 4000 nm, with the majority being below 2500 nm.

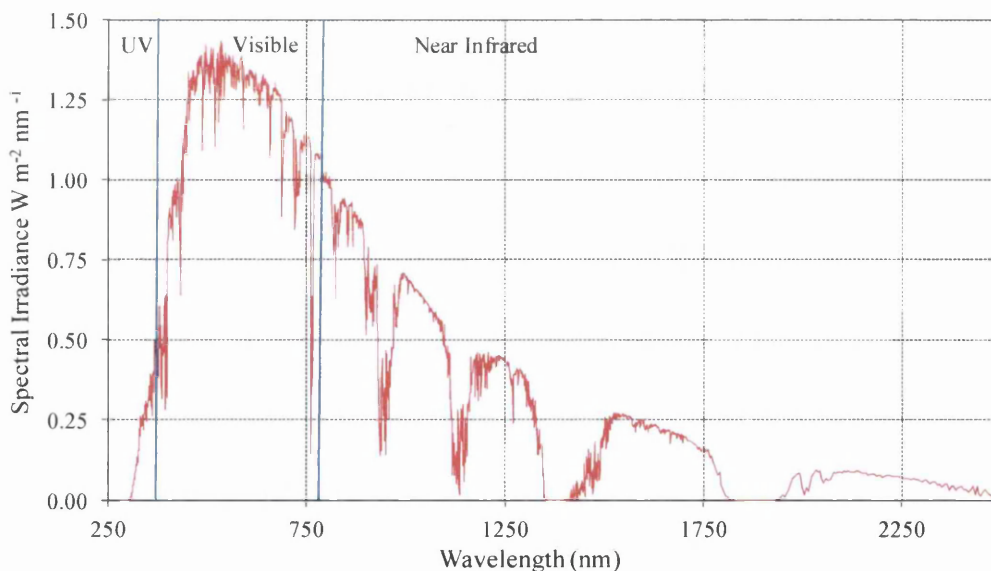


**Figure 1.34 - Terrestrial Solar Radiation**

### 1.6.2 Interaction of Light with Matter

When solar energy strikes a surface, one or more of the following can occur: reflection, absorption or transmission. Reflectance can be specular or diffuse (surface

scattered). Glossy surfaces have a large amount of specular reflectance, where the light is reflected at an angle opposite that of the incident angle. Matt surfaces have a large amount of diffuse reflectance, where incident light is reflected at varying angles from the surface [97].

Absorption of UV solar energy will promote some molecules within the coating to an excited state which leads to the production of free radicals and hence the breakdown of polymeric structures within the coating [25]. A coating should therefore be as transparent and reflecting to UV radiation as possible.

Visible light is absorbed by chromophores present in pigments in the coating, hence producing colour by reflected light, as chromophores will exhibit selective absorption in the visible region.

Near infrared solar energy will stimulate increased molecular vibrations or heat, this energy being partially re-emitted in the longer wavelength thermal infrared region.

### 1.6.3 Total Solar Reflectance

The amount of incident terrestrial solar energy reflected from a surface can be expressed as the total solar reflectance (TSR), given by Equation 1.4.

Equation 1.4 
$$\%TSR = \frac{\int (\%R \cdot I d\lambda)}{\int I d\lambda} \cdot 100$$

where

R = percent reflectance

I = solar irradiance

dλ = the wavelength interval of integration

Total solar reflectance is expressed as a percentage, with titanium dioxide white pigmented coatings typically having a total solar reflectance of 75% or greater, whilst black coatings based on carbon black pigmentation will have a total solar reflectance as low as 3.5%.



## 1.6.4 Solar Reflectance Index

A composite index that is able to numerically express a coating's overall ability to reject or retain heat is the Solar Reflectance Index (SRI), given by ASTM E1980-01 and expressed as Equation 1.5 [98].

**Equation 1.5** 
$$\text{SRI} = 123.97 - 141.35\chi + 9.655\chi^2$$

where

$$\chi = ((\alpha - 0.029\varepsilon)(8.797 + hc))/(9.5205 \varepsilon + hc)$$

$\alpha$  = solar absorbance (1 – TSR)

$\varepsilon$  = thermal emittance

$hc$  = convective coefficient,  $\text{Wm}^{-2}\text{K}^{-1}$

A standard white coating (TSR=0.80, emittance=0.90) is assigned a SRI of 100, whilst a standard black coating (TSR=0.05, emittance=0.90) a SRI of zero. A high SRI value denotes a surface which is able to reject heat, and the index is often used to rate 'cool roof' products which require a high TSR and a high thermal emittance [99, 100].

## 1.7 Conclusions and Aims

Carbon black pigment in the top coat reduces the process window size, so in Chapter 3 of this thesis UV-Vis-NIR spectroscopy and laboratory based cure trials were used to investigate whether moving the top coat carbon black pigment to the primer layer improves the NIR cure.

This led to an appreciation of the importance of locus of NIR absorbers in NIR cure. Carbon black pigmented primers can be used to reduce the power needed to NIR cure a top coat [46]. Chapter 4 investigates whether these power savings are also evident when a convection oven is used in a similar manner to cure a top coat. The effect of adding carbon black so close to the substrate surface could also provide sites for oxygen reduction, so the Scanning Kelvin Probe technique was used to assess the effect of carbon black additions on the corrosion performance of the coating system [46].

Locus of NIR absorbers was explored further in Chapter 5 by using UV-Vis-NIR spectroscopy to assess how top coat cure was affected by addition of NIR absorbers to the backing coat of the coating system.

Silver coloured coatings form an important part of the architectural OCS market, but like darker coloured coatings, have a very small NIR cure window. These coatings are pigmented with aluminium flake, so alternative pigments to aluminium flake were explored as a way of widening the process window.

Finally, another OCS product manufactured by Tata Steel, the transpired solar collector (TSC), was investigated. Here, the aim is for the organic coating surface to absorb sunlight radiation striking it. The outdoor performance of a TSC in UK weather conditions and the effect of additions of NIR absorbers to the TSC coating were investigated.

## 1.8 References

1. *90 Years with PCI : A Retrospective. In the 1930s Coil Coating Springs into View.* 1st May 2004, Paint & Coatings Industry.
2. ECCA, *Introduction to Coil Coating.* (cited 16th May 2013). Available from: [http://www.prepaintedmetalacademy.eu/prg/selfware.pl?id\\_sitemap=25&language=EN](http://www.prepaintedmetalacademy.eu/prg/selfware.pl?id_sitemap=25&language=EN).
3. ECCA, *Markets for Pre-Painted Steel.* (cited 16th May 2013). Available from: [http://www.prepaintedmetalacademy.eu/prg/selfware.pl?id\\_sitemap=201&language=EN](http://www.prepaintedmetalacademy.eu/prg/selfware.pl?id_sitemap=201&language=EN).
4. Wang, X., Kendrick, C., Ogden, R., and Maxted, J., *Dynamic thermal simulation of a retail shed with solar reflective coatings.* Applied Thermal Engineering, 2008. **28**(8–9): p. 1066-1073.
5. Smith, G.B., Gentle, A., Swift, P., Earp, A., and Mronga, N., *Coloured paints based on coated flakes of metal as the pigment, for enhanced solar reflectance and cooler interiors: description and theory.* Solar Energy Materials and Solar Cells, 2003. **79**(2): p. 163-177.
6. Smith, G.B., Gentle, A., Swift, P.D., Earp, A., and Mronga, N., *Coloured paints based on iron oxide and silicon oxide coated flakes of aluminium as the pigment, for energy efficient paint: optical and thermal experiments.* Solar Energy Materials and Solar Cells, 2003. **79**(2): p. 179-197.
7. Cai, R., Van, G.M., Aw, P.K., and Itoh, K., *Solar-driven self-cleaning coating for a painted surface.* Comptes Rendus Chimie, 2006. **9**(5–6): p. 829-835.
8. Orel, B., Spreizer, H., Vuk, A.S., Fir, M., Merlini, D., Vodlan, M., and Kohl, M., *Selective paint coatings for coloured solar absorbers: Polyurethane thickness insensitive spectrally selective (TISS) paints (Part II).* Solar Energy Materials and Solar Cells, 2007. **91**(2-3): p. 108-119.
9. Orel, B., Spreizer, H., Perse, L.S., Fir, M., Vuk, A.S., Merlini, D., Vodlan, M., and Kohl, M., *Silicone-based thickness insensitive spectrally selective (TISS) paints as selective paint coatings for coloured solar absorbers (Part I).* Solar Energy Materials and Solar Cells, 2007. **91**(2-3): p. 93-107.

10. Tata Steel, *Finding the Confidex® Guarantee Period for Colorcoat HPS200 Ultra®*. (cited 6th February 2014). Available from: [http://www.colorcoat-online.com/en/products/guarantees/confidex\\_guarantee/finding\\_confidex\\_ultra/](http://www.colorcoat-online.com/en/products/guarantees/confidex_guarantee/finding_confidex_ultra/).
11. Bar, K., *How to save energy costs with the NIR-technology in coil coating processes*. Steel Grips, 2006. **3**: p. 225-228.
12. Bar, K., *Ultra fast drying and curing technology*. 2005, Coil World.
13. Frederiksen, N., *Instant curing with near infrared technology*. 2007, Paint & Coatings Industry.
14. Mabbett, I., *Applications of Near Infrared Heating of Interest to the Coil Coating Industry*. 2011, Eng. D., Swansea University
15. Knischka, R., Lehmann, U., Stadler, U., Mamak, M., and Benkhoff, J., *Novel approaches in NIR curing technology*. Progress in Organic Coatings, 2009. **64**(2-3): p. 171-174.
16. Perruchot, C., Watts, J.F., Lowe, C., and Beamson, G., *Characterisation of the curing temperature effects on polyester systems by angle-resolved XPS (ARXPS)*. International Journal of Adhesion and Adhesives, 2003. **23**(2): p. 101-113.
17. Ireson, R. and Rousseau, J., *Gatekeeper report: Organic coatings on strip - curing processes*. 2012, Tata Steel Research Development & Technology.
18. Goldschmidt, A. and Streitberger, H.-J., *BASF Handbook on Basics of Coating Technology*. 2nd ed. 2007: Vicentz Network.
19. Boxhall, J. and Von-Fraunhofer, J.A., *Concise Paint Technology*. 1977: London: Elek Science
20. McMurray, N., *Paint Technology*, in *Coated Steel Products*. 2009, Materials Engineering, University of Swansea.
21. Wicks, Z.W., Jones, F.N., Pappas, S.P., and Wicks, D.A., *Organic Coatings Science and Technology*. 3rd ed. 2007: Wiley Interscience.
22. *Engineering & Design - Painting; New Construction & Maintenance*. 1995, U.S. Army Corps of Engineers.
23. Mischke, P., *Film Formation in Modern Paint Systems*. 2010: Vincentz Network.
24. Muller, B. and Poth, U., *Coatings Formulation*. 2nd ed. 2011: Vincentz Network.

25. Wray, J., *Next generation polyurethanes for enhanced durability pre-finished architectural steel products*. 2008, Eng. D., Materials Engineering, University of Wales Swansea
26. Robinson, A., *The Development of Organic Coatings for Strip Steels with Improved Resistance to Photodegradation By-Products*. 2005, Eng. D., Materials Engineering, University of Wales Swansea
27. *Guidance on VOC Substitution and Reduction for Activities Covered by the VOC Solvents Emissions Directive (Directive 1999/13/EC), Guidance 7: Coil coating*. 2009, AEA Energy & Environment, European Commission.
28. Gowenlock, C., *Radiation Curing of High Performance Coatings*. 2010, Eng. D. 1st Year Report, Materials Engineering, Swansea University
29. Osswald, T.A. and Menges, G., *Materials Science of Polymers for Engineers*. 1995: Munich: Hanser, Cincinnati: Hanser/Gardner.
30. Turner, G.P.A., *Paint Chemistry and Principles of Paint Technology*. 3rd ed. 1988: Chapman and Hall.
31. Yagci, M.B., Bolca, S., Heuts, J.P.A., Ming, W., and de With, G., *Self-stratifying antimicrobial polyurethane coatings*. *Progress in Organic Coatings*, 2011. **72**(3): p. 305-314.
32. Maile, F.J., Pfaff, G., and Reynders, P., *Effect pigments—past, present and future*. *Progress in Organic Coatings*, 2005. **54**(3): p. 150-163.
33. Mendon, S. and Thames, S., *Pigments - more than just a pretty color*. 25th September 2003, Paint & Coatings Industry.
34. Štengl, V., Šubrt, J., Bakardjieva, S., Kalendova, A., and Kalenda, P., *The preparation and characteristics of pigments based on mica coated with metal oxides*. *Dyes and Pigments*, 2003. **58**(3): p. 239-244.
35. Johansson, K. and Johansson, M., *The effect of fatty acid methyl esters on the curing performance and final properties of thermally cured solvent-borne coil coatings*. *Progress in Organic Coatings*, 2007. **59**(2): p. 146-151.
36. Hinder, S.J., Watts, J.F., and Lowe, C., *Surface and interface analysis of complex polymeric paint formulations*. *Surface and Interface Analysis*, 2006. **38**(4): p. 557-560.
37. Springate, R., Koleske, J.V., and Brezinski, D., *2010 Additives Handbook*, Paint & Coatings Industry.

38. Pourreau, D.B., Harris, S.H., Patel, S., Junker, L.J., Soon, T.C., and Sullivan, C.J., *Polyester Resins - Bang for the Buck*. 1999, Modern Paint & Coatings.
39. Oldring, P. and Hayward, G., *Resins for Surface Coatings, Vol. III*. 1987: SITA Technology.
40. Van Dijk, H., *The Chemistry and Application of Amino Cross-Linking Agents or Aminoplasts*. 1999: New York: Wiley.
41. Tracton, A.A., *Coatings Technology Handbook*. 3rd ed. 2005: CRC Press.
42. Marrion, A., *The Chemistry and Physics of Coatings*. 2004: Royal Society of Chemistry.
43. Kiil, S., *Quantification of simultaneous solvent evaporation and chemical curing in thermoset coatings*. Journal of Coatings Technology and Research, 2010. 7(5): p. 569-586.
44. Kiil, S., *Mathematical modelling of simultaneous solvent evaporation and chemical curing in thermoset coatings: a parameter study*. Progress in Organic Coatings, 2011. 70: p. 192-198.
45. Flores, J.R., *Evaluation of coated panels cured by convection and near infrared process*. 2005, Corus Research Development & Technology.
46. Mabbett, I., Elvins, J., Gowenlock, C., Glover, C., Jones, P., Williams, G., and Worsley, D., *Addition of carbon black NIR absorber to galvanised steel primer systems: influence on NIR cure of polyester melamine topcoats and corrosion protection characteristics*. Progress in Organic Coatings, 2014. 76: p. 1184-1190.
47. Mabbett, I., *The Use and Applications of the Perkin Elmer Lambda 750S UV/Vis/NIR Spectrophotometer of Relevance to Corrosion and Coatings Theme*. 2009, Eng. D. Technical Brief, Materials Engineering, Swansea University
48. Bar, K., *One two cured. Space technology provides ultimate cure*. 2006, Becker Industrial Coatings. p. 26-30.
49. Personal communication with Banabak, H., Tata Steel. December 2013
50. Personal communication with Penney, D., Swansea University. June 2011
51. Park, K.J., Lee, K.M., and Lee, Y.H., *NIR drying technology at Dongbu Steels's continuous coil coating line*. Steel Grips, 2007. 5(4): p. 250-252.
52. Ajmera, S.C. and Sivaramakrishnan, M.M., *The new colour coating line No. 2 at Shree Precoated Steels*. Steel Grips, 2006. 4(3): p. 175-180.

53. Mabbett, I., Elvins, J., Gowenlock, C., Jones, P., and Worsley, D., *Effects of highly absorbing pigments on near infrared cured polyester/melamine coil coatings*. Progress in Organic Coatings, 2013. **76**(9): p. 1184-1190.
54. Siegel, R. and Howell, J.R., *Thermal Radiation Heat Transfer*. 3rd ed: Hemisphere.
55. Cherrington, M., *Printing technologies for current collectors for dye-sensitized solar cells*. 2012, Eng. D., College of Engineering, Welsh Centre for Printing & Coating, Swansea University
56. Pelling, D., *NIR for powder coating*. 4th September 2008, Finishing.
57. Watson, T., Mabbett, I., Wang, H.X., Peter, L., and Worsley, D., *Ultrafast near infrared sintering of TiO<sub>2</sub> layers on metal substrates for dye-sensitized solar cells*. Progress in Photovoltaics, 2011. **19**(4): p. 482-486.
58. Cherrington, M., Claypole, T.C., Deganello, D., Mabbett, I., Watson, T., and Worsley, D., *Ultrafast near-infrared sintering of a slot-die coated nano-silver conducting ink*. Journal of Materials Chemistry, 2011. **21**(21): p. 7562-7564.
59. Charbonneau, C., Hooper, K., Carnie, M., Searle, J., Philip, B., Wragg, D., Watson, T., and Worsley, D., *Rapid radiative platinisation for dye-sensitised solar cell counter electrodes*. Progress in Photovoltaics, 2013.
60. Mabbett, I., Geary, S., Warren, D.J., Sullivan, J.H., Penney, D., Watson, T.M., and Worsley, D.A., *Near Infrared Heat Treatment to Flow Melt Tinplate Pore Formation and Characterization*. ECS Transactions, 2013. **50**(37): p. 155-164.
61. Stepuk, A., Mohn, D., Grass, R.N., Zehnder, M., Krämer, K.W., Pellé, F., Ferrier, A., and Stark, W.J., *Use of NIR light and upconversion phosphors in light-curable polymers*. Dental Materials, 2012. **28**(3): p. 304-311.
62. ASTM, *International Astm D5402 - 06 Standard Practice for Assessing the Solvent Resistance of Organic Coatings Using Solvent Rubs*. 2011.
63. Zhang, W.R., Lowe, C., and Smith, R., *Depth profiling of coil coating using step-scan photoacoustic FTIR*. Progress in Organic Coatings, 2009. **65**(4): p. 469-476.
64. Puente, J.M., Fernandez, S., Alonso, F., Arguelles, A., and Andres, L., *Fast curing for organic and inorganic coatings by high frequency induction*. Revue De Metallurgie-Cahiers D Informations Techniques, 2003. **100**(6): p. 653-657.
65. *Reference Document on Best Available Techniques on Surface Treatment using Organic Solvents*. 2007, European Commission.

66. Hay, J.N. and O'Gara, P., *Recent developments in thermoset curing methods*. Proc. IMechE J. Aerospace Engineering, 2006. **220**(Part G): p. 187-195.
67. Fischer, J., Wallner, G.M., Strauss, B., and Jandel, L., *Effect of curing conditions on the morphology of wax modified coil coatings*. Progress in Organic Coatings, 2009. **66**(4): p. 420-424.
68. Fischer, J., Wallner, G.M., Strauss, B., and Jandel, L., *Morphology of wax modified coil coatings without and with pigmentation*. Progress in Organic Coatings, 2010. **67**(1): p. 38-43.
69. Zhang, W.R., Smith, R., and Lowe, C., *Confocal Raman microscopy study of the melamine distribution in polyester-melamine coil coating*. Journal of Coatings Technology and Research, 2009. **6**(3): p. 315-328.
70. Zhang, W.R., Zhu, T.T., Smith, R., and Lowe, C., *An investigation on the melamine self-condensation in polyester/melamine organic coating*. Progress in Organic Coatings, 2010. **69**(4): p. 376-383.
71. Zhang, W.R., Hinder, S.J., Smith, R., Lowe, C., and Watts, J.F., *An investigation of the effect of pigment on the degradation of a naturally weathered polyester coating*. Journal of Coatings Technology and Research, 2011. **8**(3): p. 329-342.
72. Zhang, Y., Barber, A., Maxted, J., Lowe, C., Smith, R., and Li, T.Z., *The depth profiling of TiO<sub>2</sub> pigmented coil coatings using step scan phase modulation photoacoustic FTIR*. Progress in Organic Coatings, 2013. **76**(1): p. 131-136.
73. Hinder, S.J., Lowe, C., Maxted, J.T., and Watts, J.E., *Migration and segregation phenomena of a silicone additive in a multilayer organic coating*. Progress in Organic Coatings, 2005. **54**(2): p. 104-112.
74. Hinder, S.J., Lowe, C., Maxted, J.T., and Watts, J.F., *The morphology and topography of polymer surfaces and interfaces exposed by ultra-low-angle microtomy*. Journal of Materials Science, 2005. **40**(2): p. 285-293.
75. Hinder, S.J., Lowe, C., and Watts, J.F., *ToF-SIMS depth profiling of a complex polymeric coating employing a C-60 sputter source*. Surface and Interface Analysis, 2007. **39**(6): p. 467-475.
76. Hinder, S.J., Watts, J.F., Simmons, G.C., and Lowe, C., *An investigation of the distribution of minor components in complex polymeric paint formulations using ToF-SIMS depth profiling*. Surface and Interface Analysis, 2008. **40**(3-4): p. 436-440.



77. Marino, P., Lowe, C., Abel, M.L., and Watts, J.F., *Surface characterization of polyester resins formulated with different cross-linking agents*. Surface and Interface Analysis, 2008. **40**(3-4): p. 137-141.
78. Frey, T., GrosseBrinkhaus, K.H., and Rockrath, U., *Cure monitoring of thermoset coatings*. Progress in Organic Coatings, 1996. **27**(1-4): p. 59-66.
79. Korhonen, M., Starck, P., and Lofgren, B., *Characterization of coil coatings by thermal analysis*. Journal of Applied Polymer Science, 2003. **87**(12): p. 2016-2022.
80. Korhonen, M., Starck, P., Lofgren, B., Mikkila, P., and Hormi, O., *Study of polyester-based coil coatings by using thermal analysis methods*. Journal of Coatings Technology, 2003. **75**(937): p. 67-73.
81. Buder-Stroisnigg, M., Wallner, G.M., Strauss, B., Jandel, L., and Lang, R.W., *Flexible clear coats-Effect of curing conditions*. Progress in Organic Coatings, 2009. **65**(1): p. 44-48.
82. Lovell, L.G., Lu, H., Elliott, J.E., Stansbury, J.W., and Bowman, C.N., *The effect of cure rate on the mechanical properties of dental resins*. Dental Materials, 2001. **17**(6): p. 504-511.
83. de la Caba, K., Guerrero, P., Eceiza, A., and Mondragon, I., *Kinetic and rheological studies of two unsaturated polyester resins cured at different temperatures*. European Polymer Journal, 1997. **33**(1): p. 19-23.
84. Grunden, B.L. and Sung, C.S.P., *Cure characterization of unsaturated polyester resin by fluorescence spectroscopy*. Journal of Applied Polymer Science, 2004. **94**(6): p. 2446-2450.
85. Escola, M.A., Moina, C.A., Gomez, A.C.N., and Ybarra, G.O., *The determination of the degree of cure in epoxy paints by infrared spectroscopy*. Polymer Testing, 2005. **24**(5): p. 572-575.
86. Batista, M.A.J., Moraes, R.P., Barbosa, J.C.S., Oliveira, P.C., and Santos, A.M., *Effect of the polyester chemical structure on the stability of polyester-melamine coatings when exposed to accelerated weathering*. Progress in Organic Coatings, 2011. **71**(3): p. 265-273.
87. McLaren, K., *Development of CIE 1976 (LAB) uniform color space and color-difference formula*. Journal of the Society of Dyers and Colourists, 1976. **92**(9): p. 338-341.

88. Nadal, M.E. and Thompson, E.A., *New primary standard for specular gloss measurements*. Journal of Coatings Technology, 2000. **72**(911): p. 61-66.
89. Vanooij, W.J., Edwards, R.A., Sabata, A., and Zappia, J., *Testing the adhesion of paint films to metals by swelling in n-methyl pyrrolidone*. Journal of Adhesion Science and Technology, 1993. **7**(8): p. 897-917.
90. Kalogirou, S.A., *Solar thermal collectors and applications*. Progress in Energy and Combustion Science, 2004. **30**(3): p. 231-295.
91. Specific, *Buildings as power stations*. (cited 4th June 2013). Available from: <http://www.specific.eu.com/>.
92. Leon, M.A. and Kumar, S., *Mathematical modeling and thermal performance analysis of unglazed transpired solar collectors*. Solar Energy, 2007. **81**(1): p. 62-75.
93. *Buckingway Road, Swavesey, South Cambridgeshire Sustainability and Renewable Energy Plan*. 2008, DSA Engineering.
94. Kutscher, C.F., Christensen, C., and Barker, G., *Unglazed transpired solar collectors: heat loss theory*. ASME Journal of Solar Engineering, 1993. **115**(3): p. 182-188.
95. Kutscher, C., Christensen, C., and Barker, G., *Unglazed transpired solar collectors: an analytical model and test results*. ISES Solar World Congress, 1991. **2**: p. 1245-1250.
96. Brunger, A.P., *Low Cost, High Performance Solar Air-Heating Systems Using Perforated Absorbers*, in *IEA Report No. SHC.T14.Air.1*. 1999, IEA.
97. Tipler, P.A. and Mosca, G., *Physics for Scientists and Engineers*. 6th ed. 2008: W H Freeman.
98. ASTM, *International ASTM E1980-01 Standard Practice for Calculating Solar Reflective Index of Horizontal and Low Sloped Opaque Surfaces*. 1980.
99. Levinson, R., Akbari, H., Berdahl, P., Wood, K., Skilton, W., and Petersheim, J., *A novel technique for the production of cool colored concrete tile and asphalt shingle roofing products*. Solar Energy Materials and Solar Cells, 2010. **94**(6): p. 946-954.
100. Levinson, R., Berdahl, P., Akbari, H., Miller, W., Joedicke, I., Reilly, J., Suzuki, Y., and Vondran, M., *Methods of creating solar-reflective non white surfaces and their application to residential roofing materials*. Solar Energy Materials and Solar Cells, 2007. **91**(4): p. 304-314.

# **Chapter 2**

## **Experimental Techniques**

## **2.1 Coated Sample Preparation**

Polyester coatings were prepared for use in curing trials and spectroscopic studies at BASF laboratory facilities in Deeside. Formulations were supplied by BASF, and were based on near commercial formulations suitable for fast curing applications.

The polyester coatings were produced by the method used at the BASF laboratory, the pigment paste and converter method rather than by the two stage milling and let down method. Both methods are described in the next section.

Additionally, model Poly Vinyl Chloride (PVC) coatings were prepared. These coatings were simple air drying formulations consisting of only PVC resin and pigment, using tetrahydrofuran (THF) as a solvent. These formulations were used to produce free standing coating films that could be quickly used to assess the effect of individual pigments by spectroscopic analysis.

### **2.1.1 Polyester Coating Formulation**

#### **2.1.1.1 Mill Base and Let Down Method**

Firstly a mill base is produced, consisting of the pigments, some of the additives and a proportion of the resin and solvents. Ceramic mill beads are added to this mixture, which is then placed in a paint shaker to break up pigment particles agglomerations. A Fineness of Grind (Hegman) gauge is used to check pigment agglomerations have broken down to below 15  $\mu\text{m}$ . A Hegman gauge, shown in Figure 2.1, consists of a piece of steel with a wedge machined in it, with the varying depth of the wedge marked by the side of the wedge. A pool of coating is placed at the deepest end of the machined wedge and a steel blade is used to draw the coating down the length of the wedge towards the shallowest part of the wedge. The point at which the coating displays a streaky, grainy appearance marks the point of the coarsest ground pigment particles in the coating.

The mill beads are then removed by sieving and the remaining resin, solvent and additives are added in a process known as the let down. The formulation is mixed by further shaking and the viscosity and gloss are checked as described in Section 1.4.2.2 and Section 1.4.2.4.

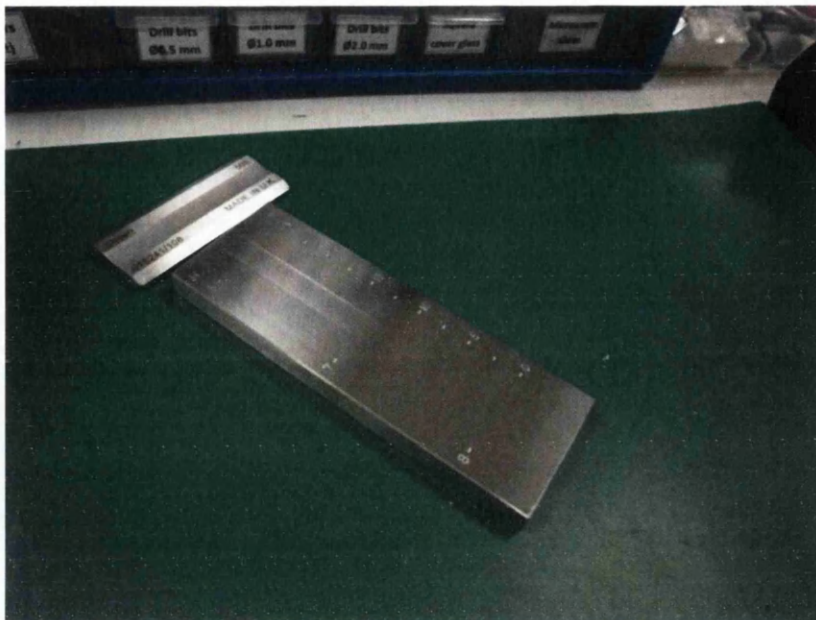


**Figure 2.1 – Hegman Gauge**

### **2.1.1.2 Pigment Paste and Converter Method**

The polyester coating formulations were supplied by BASF and produced using their laboratory facilities at Deeside. The coatings were based on a saturated polyester resin cross-linked with hexamethoxymethyl melamine (HMMM). Apart from the polymer resin, the coatings contained the standard constituents of any polymeric coating system; pigment, catalyst, solvent and small quantities of additives designed to improve the rheological and surface properties of the coating.

Pigment was added to the formulation as pigment pastes, consisting of ready milled pigments dispersed in solvent. The percentage by weight pigment content of each pigment paste is shown in Table 2.1. The Kronos 2310 and Carbon Black FW200 pigment pastes also contained Disperbyk 170, a wetting and dispersing additive.

Gloss converter and matt converter containing the resin, the cross-linker, some solvent, catalyst and all the additives were shaken with the appropriate amounts of pigment pastes in a Skandex paint shaker. Solvent was added until the viscosity specification of 65-70 seconds to empty a DINN 4 flow cup at 21°C was met, as described in Section 1.4.2.2. Gloss specification was 25 - 40% at an incident angle of 60° and was measured with an Erichsen gloss meter as described in Section 1.4.2.4.

Further matting agent or additional solvent were then added to ensure that both gloss and viscosity specifications were met.

Formulation guidelines for the coatings are shown in Table 2.2.

**Table 2.1 - Pigment Pastes used in Polyester Coating Formulations**

<b>Pigment code</b>	<b>Pigment name</b>	<b>Colour</b>	<b>Chemical type</b>	<b>Pigment (wt %)</b>	<b>Disperbyk 170 (wt %)</b>
M031	Kronos 2310	White	Titanium Dioxide	67.5	9.5
M994	Carbon black FW200	Black	Carbon Black	6.25	6.5
M158	Colortherm 10	Yellow	Iron Oxide	39.3	
M306	Bayferrox 130 BMP	Orange	Iron Oxide	37.8	
RX06-4226	Alu-Stapa Mobilux R 187 (Eckart)	Silver	Aluminium flake	65	

**Table 2.2 – Formulation Guidelines for Polyester Coatings**

	<b>White (wt %)</b>	<b>Black (wt %)</b>	<b>Brown (wt %)</b>	<b>Red (wt %)</b>	<b>Silver (wt %)</b>	<b>Clear (wt %)</b>
Converter gloss	19.7	21.16	21	22	86	31
Converter matt	36.28	38.95	41	40.5	0	61.32
M031	36.86		1.74	1.56		
M994		32.21	8.95	2.9		
M158			14.24	4.16		
M306			5.07	20.88		
RX06-4226					6	
Solvent Naphtha 180/210	3.58	3.84	4	4	6	3.84
Bring to viscosity specification with approximately						
Solvent Naphtha 180/210	3.58	3.84	4	4	2	3.84

### 2.1.2 Production of Polyester Coated Samples

Curing studies of coatings were carried out with panels of coated substrate where the coating had been applied by a wire wound draw bar according to ASTM D4147 [1]. These bars, also known as K-bars or Meyer bars, consist of a steel bar with steel wire wound round it to produce a regular series of grooves. The distance between these grooves determines the wet film thickness of the coating, and this in turn determines the dry film thickness of the cured coating. The substrate panel is first cleaned with methyl ethyl ketone (MEK) to remove any residual grease from its surface, and then placed on paper on a flat surface. An excess amount of coating is poured across one end of the panel and the draw down bar is placed across the coating layer and allowed to wet the wires of the bar. The bar is then drawn uniformly down the length of the panel towards the operator. This process requires some practice, needing a smooth and steady action to leave a uniform wet film behind on the substrate. Excess coating is carried over onto the surrounding paper. The wire wound draw down bar method is illustrated schematically in Figure 2.2.

Batches of panels of galvanised mild steel were obtained from Tata Steel and used as substrate. The gauge of each batch was in the range 0.5 to 0.7 mm, depending on availability from the production line. Several different galvanised coatings can be used with organically coated steel, but the galvanised substrates used for this research were the substrates used on Tata Steel's DVL2 NIR curing line, hot dip galvanised substrate (HDG) and MagiZinc (MZ). The compositions of these galvanised coatings are given in Table 2.3.

**Table 2.3 – Composition of Galvanised Coatings used in this Thesis**

<b>Substrate</b>	<b>Zinc (wt %)</b>	<b>Aluminium (wt %)</b>	<b>Magnesium (wt %)</b>
HDG	99.85	0.15	-
MZ	96 - 98	1 - 2	1 - 2

HDG, otherwise known by the Tata Steel brand name Galvatite®, can be regarded as the bench mark for galvanised coatings. Aluminium is added to increase



formability of the galvanised coating by the formation of a  $\text{Fe}_2(\text{Al}, \text{Zn})_5$  inter-metallic [2]. MZ is a more recent galvanised coating, and is the brand name of a hot dip zinc-magnesium-aluminium (ZMA) coating developed by Tata Steel Strip Products at their IJmuiden site. The presence of magnesium in the alloy produces a coating with superior corrosion resistance to HDG. MZ can hence be applied at reduced thickness to HDG, with associated cost savings [3].

Panels were de-burred before use, and were typically 200 x 100 mm when used with the AdPhos NIR Lab Unit, 296 x 210 mm or 148 x 210 mm with the AdPhos NIR Technicum and 148 x 210 mm with the Mathis convection oven. Sizes were chosen to fit the respective oven's sample holder.

A wire wound draw down bar designed to produce a wet film thickness of 60  $\mu\text{m}$  was found to give a dry film thickness of 20 - 22  $\mu\text{m}$  with a polyester coating. Dry film thicknesses were measured with an Elcometer 456 Coating Thickness Gauge or Bore Gauge.

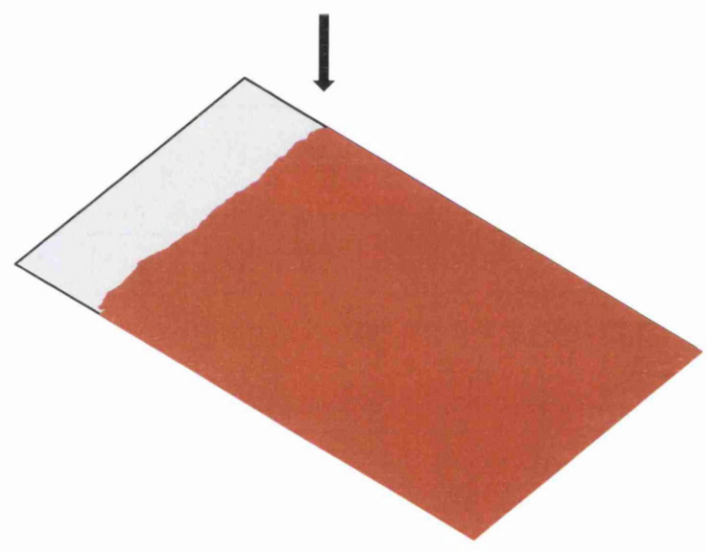
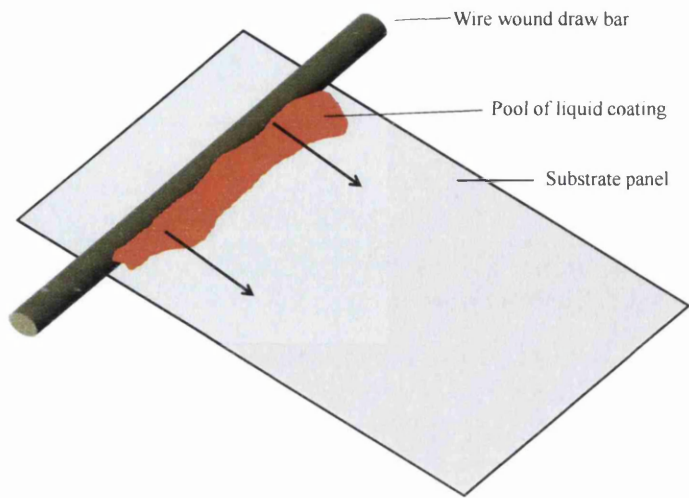


**Figure 2.2 – Polyester Bar Coating Method Showing Substrate Panel Before and After Draw Down**

### **2.1.3 Model PVC Coating Formulation**

The model PVC coatings were air drying coating systems consisting of PVC resin, tetrahydrofuran (THF) solvent and pigment. These coatings were used to produce free-standing coating films for use in the spectroscopic studies. Pigment paste or pigment powder was dispersed in THF solvent and stirred using a magnetic stirrer to ensure homogeneous pigment dispersion. Laboratory grade powdered PVC was then added to the stirring dispersion, and left to stir for a further 48 hours to ensure completion dissolution of the PVC and even dispersion of the pigment. Dispersions were made up in glass bottles with lids to avoid evaporation of the THF.

### **2.1.4 Production of Free-standing Coating Films**

Free standing films of both polyester coatings and model PVC coatings are used to produce coating transmission spectra in the UV/visible/NIR wavelength range. The method of free-standing film production differs for the two coatings as the former is an oven curing coating requiring a substrate Peak Metal Temperature (PMT) of 216 - 230°C, whilst the latter is a simple air drying coating.

#### **2.1.4.1 Production of Polyester Free-standing Films**

A wire wound draw down bar was used to draw down a polyester film on a PTFE bake-ware sheet, in a similar manner to that outlined in Section 2.1.2. The sample was cured for 50 seconds in a Mathis oven set to 240°C and quenched after curing on a magnetic chuck. The polyester coating film was then carefully peeled from the bake-ware sheet and the dry film thickness measured with a Mitutoyo Micrometer.

#### **2.1.4.2 Production of Model PVC Free-standing Films**

Two thicknesses of electrical insulating tape were taped down the length of 200 x 100 mm glass panels to act as a height guide for the coating thickness, resulting in a

dry film coating thickness of  $20\mu\text{m} \pm 2\mu\text{m}$ . A pool of PVC coating was then placed on the top of the panel and the coating drawn down the panel with a glass tube. This is illustrated schematically in Figure 2.3.

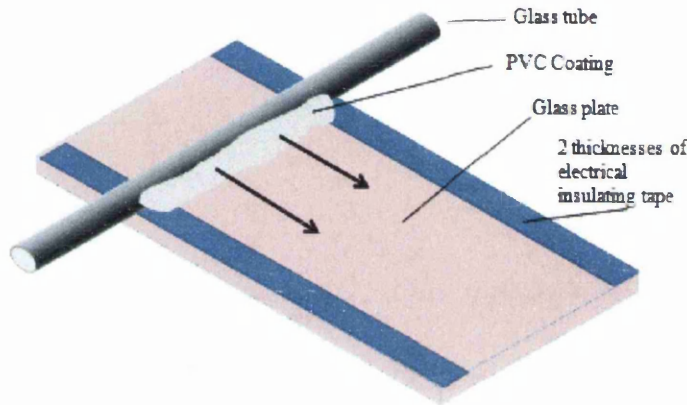


**Figure 2.3 – Draw Down Procedure for PVC Coatings**

The panels were left for 24 hours in a fume cupboard for the THF solvent to evaporate, after which the coating film was carefully peeled from the glass panel and the dry film thickness measured with a Mitutoyo Micrometer.

## **2.2 Measuring Cure**

A successfully cured polyester coating is defined by its cure window, this being the range of oven conditions over which the coating will cure and still meet its performance criteria of colour, gloss, flexibility and weatherability. Industrially, the convection cure of 20 - 25  $\mu\text{m}$  thick polyester melamine coil coatings is achieved on the production line with a PMT of between 216 and 232°C and an oven dwell time of ca. 30 seconds [4].

For the lab curing trials undertaken in this research, cure profile was logged using thermocouples and a data logger. Typical lab cure trial profiles for NIR and convection cure are shown in Figure 2.4. In these trials the convection oven had one

temperature zone, whilst the NIR lab oven had three temperature zones to enable separation of solvent evaporation and cross-linking.

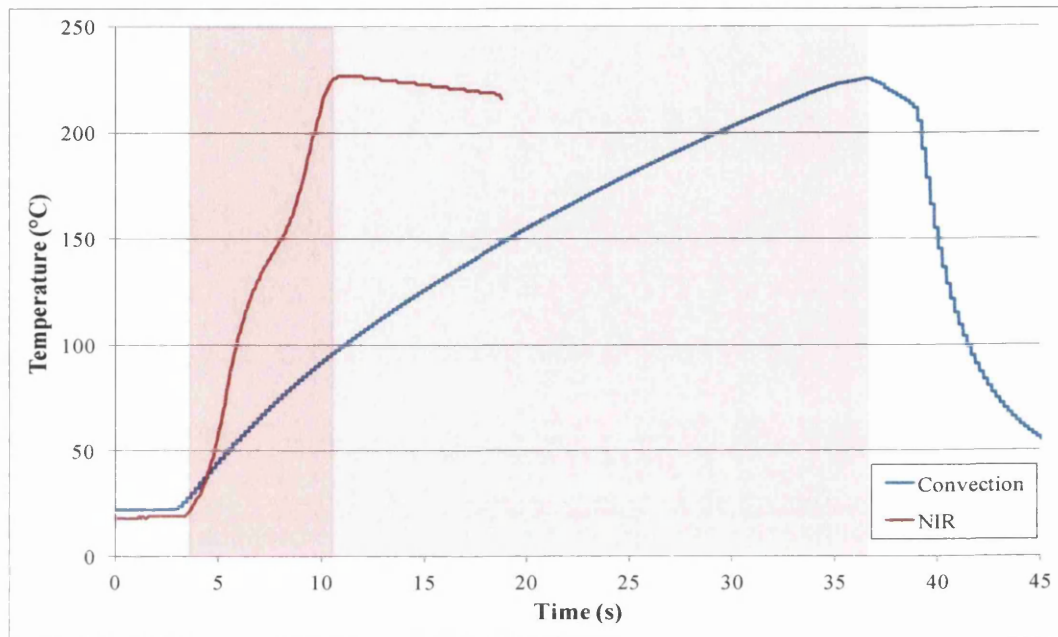


**Figure 2.4 – Typical Cure Profiles for NIR and Convection Oven Cures**

Thermocouples are a common way of sensing temperature and are based on the Seebeck effect, namely that an electric current flows in a closed circuit of two dissimilar metals when one of the two metal junctions is heated with respect to the other [5]. A simple circuit of this type is shown in Figure 2.5. The properties of the two metals and the temperature difference between the junctions affect the magnitude and direction of the current. A thermocouple circuit will hence generate a low voltage output that is proportional to the temperature difference between the hot and the cold junctions. If the voltage-temperature relationship of the two metals is known, temperature can be computed from measured voltage.

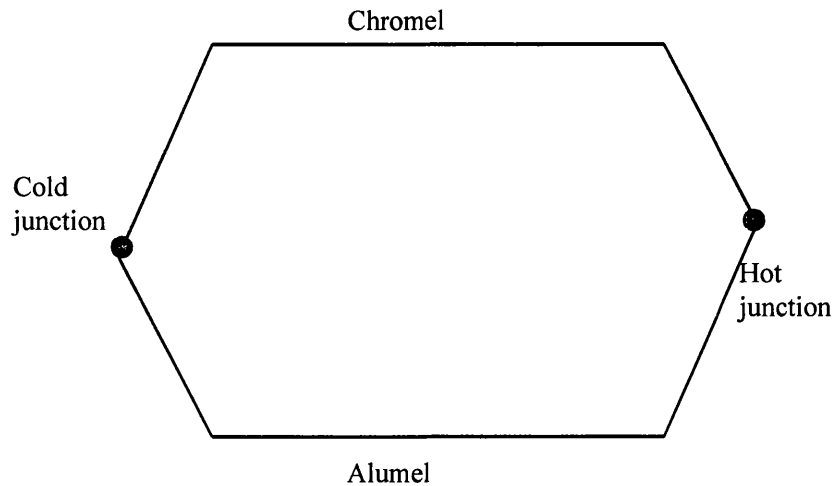


**Figure 2.5 – Thermocouple Circuit of Two Dissimilar Metal Alloys**

K type thermocouples are the most common type of thermocouples and having a temperature range of  $-270^{\circ}\text{C}$  to  $+1370^{\circ}\text{C}$  are well within the range needed to monitor polyester cure temperatures. They consist of two nickel alloy wires, chromel (90% nickel, 10% chromium) and alumel (95% nickel, 2% manganese, 2% aluminium, 1% silicon) and were welded together using a SR 50 capacitance discharge welder shown in Figure 2.6. The other end of the thermocouple wires are then connected to a thermocouple plug; the chromel wire forming the positive terminal and the alumel wire the negative terminal. The thermocouple can hence be connected to an Omega TC-08 data logger, shown in Figure 2.7, which measures and calibrates the generated potential difference, with readings being recorded every 10 milliseconds.



**Figure 2.6 - SR 50 Capacitance Discharge Welder used to Spot Weld Thermocouples**

Good thermal contact between the thermocouple and the substrate is ensured by abrading away the galvanised substrate layer with emery paper prior to spot welding. The spot weld was strengthened by placing a small piece of high temperature tape over the weld.

Infrared pyrometers are used on the industrial NIR line to measure the temperature of the coated strip steel. Previous work by Mabbett using an infrared pyrometer with the Adphos NIR Lab Unit to measure the temperature of a coated panel concluded that a pyrometer records a slightly higher temperature than a thermocouple attached to the steel substrate. He concluded that this suggests that the coating may be reaching a higher temperature than the steel substrate and that due to the short time involved in a NIR cure, the coating and metal substrate may not have had time to have fully equilibrated [6]. He advised that care must be taken when interpreting NIR cure temperature data as there are many sources of error. These include the absorption of NIR by the thermocouple wires at higher cure temperatures, leading to blackening of the wires. This blackening then increases NIR absorption even further. Other potential

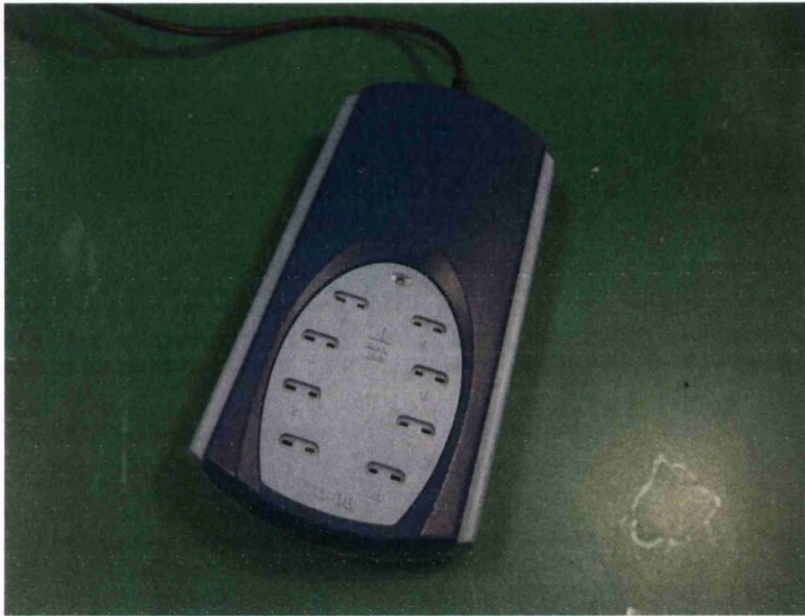


**Figure 2.7 - Omega TC-08 Data Logger used to Record Thermocouple Temperatures**

sources of error include the temperature profile across the substrate panel due to heat sink effects and the fragility of the thermocouple spot weld to the panel. He concludes that this marks a big change in what information can be derived from NIR cure PMT values [6]. PMT values have historically been used to measure convection cure where sufficient time has elapsed for thermal equilibrium between the steel substrate and the coating. In this situation PMT can be taken as the temperature a cross-linking polyester coating reaches during cure. With NIR cure, Mabbett concluded that PMT values can only be used to compare the relative robustness of cure of a coating system [6].

In this thesis the cure window of a coating system was defined as the range of NIR oven zone power settings and oven dwell times that would produce a cured coating. Coatings produced on an industrial NIR line will require as wide a cure window as possible in order to produce an industrially robust product. In this thesis the lower end of the cure window was determined by the MEK rub test described in Section 1.4.1.2, and the upper cure window limit by the temperature at which the onset of coating micro-blistering occurs.



### 2.2.1 Convection Curing

A Mathis convection oven as shown in Figure 2.8 was used to cure coatings by the conventional convection method. Samples were placed on the oven's wire mesh sample holder which took the samples automatically in and out of the oven for a pre-set cure time. The oven was set to 450°C to achieve a peak metal temperature (PMT) of 220 - 230°C for a 148 x 210 mm polyester coated substrate panel in 45 seconds. Samples were cooled on exit from the oven by quenching them in a bucket of water or placing them on a heat sink such as a magnetic chuck.



Figure 2.8 – Mathis Oven for Convection Cure of Polyester Coatings

### 2.3 NIR Curing

Industrial NIR cure on Tata Steel's DVL2 NIR curing line uses an AdPhos NIR oven. This company also supplies two laboratory NIR ovens, the NIR Lab Unit and the Technicum, which were used to perform laboratory based NIR curing trials. Both laboratory ovens are equipped with the same tungsten halogen emitters used in the industrial oven.

### **2.3.1 AdPhos NIR Lab Unit**

The NIR Lab Unit is shown in Figure 2.9 and consists of a substrate panel platform attached to a variable speed conveyor belt, which transports the substrate panel under the bank of six NIR lamps situated at the top of the oven and with a total oven power rating of 25.8 kW. Aluminium reflectors around the oven serve to focus the NIR radiation onto the substrate panel. The height between the upper and lower reflector panels can be varied, but for this research was set at 50 mm. This maximised the NIR radiation incident on the substrate panel, and was the smallest practicable gap that avoided the thermocouple wires catching on the reflector panels as they travelled through the oven. The distance from the NIR lamps to the substrate panel surface is variable from 50 mm to 100 mm, and for this research was kept constant at 70 mm.

The NIR Lab Unit is set up under extraction, which in our laboratory is provided by an extractor hood covering the whole unit. The extraction hood removes coating solvent fumes produced during the cure, but will also provide a level of convective heat transfer within the oven. For this reason, the extraction hood was always placed on the same setting (full) during curing trials.

Samples of 200 x 100 mm substrate were bar coated with polyester coating and placed on the substrate panel platform. The touch control panel was used to set the line speed (conveyor belt speed) in meters per minute, the power setting of the NIR lamp module as a percentage of full power, and to start movement of the substrate panel platform through the oven.

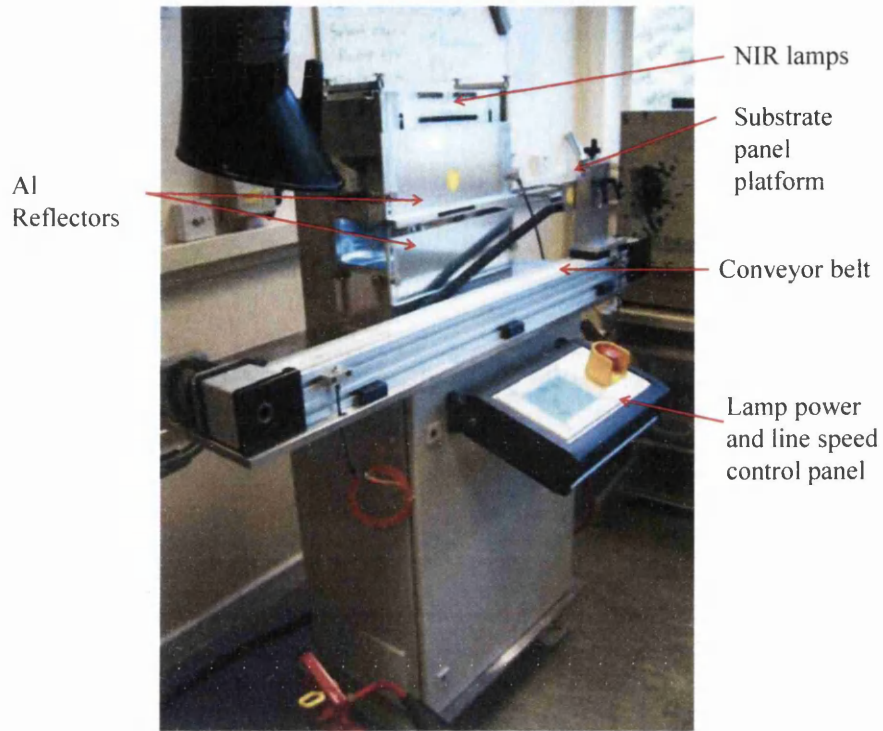


**Figure 2.9 – AdPhos NIR Lab Unit Oven [7]**

The substrate panel platform consists of a metal holder which supports the substrate panel around its edges. Previous work using a thermal imaging camera has shown that conduction occurs between the substrate panel and the substrate panel platform, and that the substrate panel platform acts as a heat sink [6]. This results in the sides of the substrate panel being cooler than the centre of the panel, as shown in the thermograph in Figure 2.10.

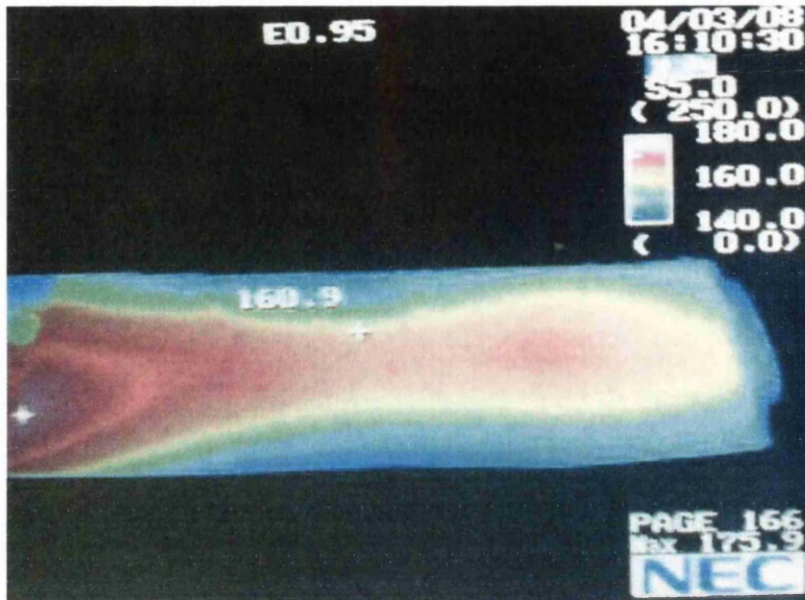


**Figure 2.10 – Thermograph of a Substrate Panel that has been Irradiated with an AdPhos NIR Lab Unit [6]**

The two stages of a NIR cure are firstly the removal of solvents, and secondly the cross-linking of the polyester resin. In the industrial AdPhos NIR oven, solvent removal and polyester resin cross-linking are separated out by using three temperature zones in the oven. As the NIR Lab Unit has only one NIR lamp zone, these three temperature zones are addressed within the NIR Lab Unit by the following process. First the sample is passed under the lamp module to remove the solvents (zone 1), a short period of time elapses as the conveyor belt changes direction and brings the sample back towards the lamp module (zone 2) and then the sample passes back under the lamp module again to achieve the peak metal temperature (zone 3).

The leading edge of the sample through the first pass of the lamp zone becomes the trailing edge of the sample as it passes back through the lamp zone again. This edge spends more time outside the lamp zone and therefore is cooler by the end of the cure time than the opposite edge [7], as shown by thermography and backed up by variations in MEK rub test results across the panel [6].

Temperature measurements of substrate panels were therefore taken by thermocouples welded to the centre of the panels, as areas close to the side of the panel will be suffering from heat sink effects.

Line speeds used in the curing trials were typically 12 m/min giving a dwell time of 7 seconds, and equivalent to a line speed on Tata Steel's DVL2 line of 110 m/min.

### 2.3.2 AdPhos Technicum

The AdPhos Technicum is shown in Figure 2.11 and has a similar operation to the AdPhos Lab Unit through the substrate panel platform, conveyor belt and control panel system. The Technicum is a closer simulation of the AdPhos NIR oven used on Tata Steel's DVL2 line, as like the DVL2 oven it has three oven zones with lamps in each zone situated above and below the path of the substrate panel. There are two banks of staggered lamps in each zone, as shown in Figure 2.12. Each bank has six lamps providing a total of 25.8 kW at full power, giving the Technicum a total power rating of 154.8 kW.

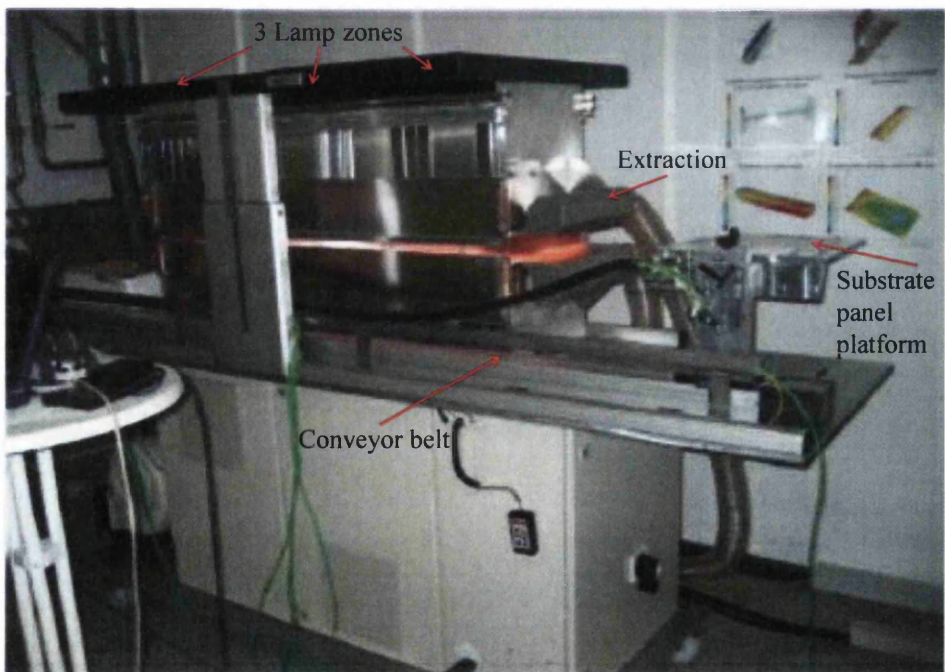
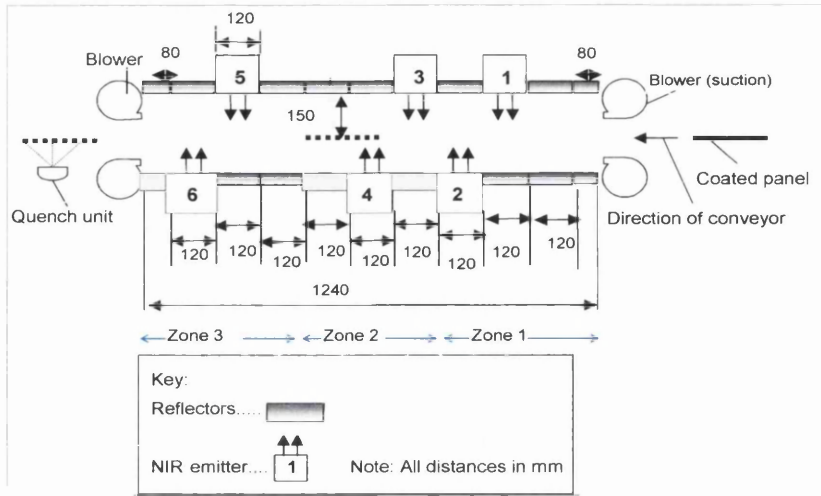


Figure 2.11 – AdPhos Technicum Oven



**Figure 2.12 - Schematic of AdPhos Technicum NIR Oven Showing the Position of the Three Oven Zones and the Staggered Lamps**

The Technicum, like the DVL2 oven, has forced convection from a blower/extraction system, which introduces blown air at the oven exit and extraction at the oven entrance.

In the Technicum, the gap between the upper and lower reflector panels was set to 50 mm, and the substrate panel platform was set to carry the substrate panel through the Technicum equidistant between the upper and lower NIR lamps.

NIR lamps in zone 1, lamp banks one and two, are set at a percentage of full power required for solvent evaporation. Zone 2 allows time for most of the solvent evaporation to complete and this usually requires lamp banks three and four to be set to zero. Lamp banks five and six in zone 3 are then set at power percentages that enable the peak metal temperature for cross-linking to be achieved. On exit from the oven, the substrate panel has its thermocouples removed and is promptly quenched in a water tray.

The slowest line speed used in the curing trials was 9 m/min, which is equivalent to a line speed on Tata Steel's DVL2 line of 110 m/min, a typical operating line speed. Highest line speeds used were 12 m/min to 15 m/min, equivalent to 150 m/min to 180 m/min and representing the highest target line speeds required from the DVL2 line.

## 2.4 UV-Vis-NIR Spectroscopy

UV-Visible spectrophotometry was originally developed as a technique that uses UV-Visible light to measure chemical concentrations. In this technique, the spectrometer is used in transmission mode with samples of dilute solutions that do not spread the spectrometer's light beam by scattering. The spectrometer's light beam comes from a tungsten lamp for the visible part of the spectrum and from a deuterium lamp for the ultra violet part. The light beam is dispersed into its constituent wavelengths in a monochromator and light of a narrow wavelength band width is passed through a cuvette of a sample containing UV/Visible absorbing chromophores.

The Beer Lambert law (Equation 2.1) is then used to determine the concentration of a specific analyte in a sample at a specific wavelength [8, 9].

$$A = \epsilon c l \quad \text{(Equation 2.1)}$$

Where  $\epsilon$  = molar absorptivity ( $M^{-1}cm^{-1}$ )

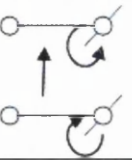
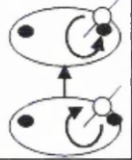
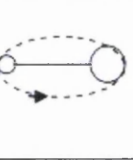
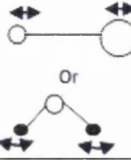


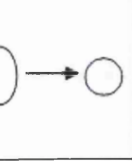
$c$  = analyte concentration (M)

$l$  = path length (cm)

$A$  = absorbance =  $\log T$

$T$  = transmittance

The absorption of a photon by a molecule increases the molecule's energy, with different regions of the electromagnetic spectrum being associated with stimulating different types of molecular excitation, as shown in Figure 2.13. UV-Visible absorptions are typically due to electronic excitations and tend to be broad in nature, whilst mid infrared absorptions stimulate molecular vibrations and produce sharper absorption bands. Infrared spectroscopy is an important tool in the characterisation of organic compounds. NIR absorptions can be due to electronic excitations or to combinations or overtones of molecular vibrations, with NIR spectroscopy having found uses in pharmaceutical analysis and medical diagnostics.

Change of spin		Change of orientation	Change of configuration	Change of electron distribution		Change of nuclear configuration
NMR	ESR	Microwave	Infrared	Visible and UV	X-ray	$\gamma$ -ray
						
$10^{-2}$	1	100	$10^4$	$10^5$	$10^8$	$10^9$
10m	100cm	1cm	100 $\mu$ m	1 $\mu$ m	10nm	100pm
$3 \times 10^6$	$3 \times 10^8$	$3 \times 10^{10}$	$3 \times 10^{12}$	$3 \times 10^{14}$	$3 \times 10^{16}$	$3 \times 10^{18}$
$10^{-5}$	$10^{-1}$	10	$10^3$	$10^5$	$10^7$	$10^9$
				Joules/mole	Energy	

**Figure 2.13 – The Electromagnetic Spectrum Showing the Different Electronic Excitations**

In addition to a spectrophotometer being used in transmission mode with dilute solutions, the instrument's scope can be extended further by the use of an integrating sphere. Here, the integrating sphere is used to measure the transmission and reflectance spectra of samples that scatter light. This makes an integrating sphere an ideal accessory for analysis of polyester coated steel, as both transmission through semi-opaque free standing polyester coating films and reflectance from the surface of polyester coated steel substrates can be tackled.

An integrating sphere consists of a completely spherical chamber with its interior wall coated with a highly diffuse reflecting surface, commonly Spectralon®, a Teflon® based material that reflects more than 99% of incident light falling on it. Integrating spheres range in size from 50 to 300 mm diameter [10-12].

In order to measure the transmittance of a turbid liquid or a semi-opaque material such as a free standing polyester coating film, the sample is placed directly in front of the integrating sphere, as shown in Figure 2.14 (a). The spectrometer's light beam passes through the sample, and then on into the integrating sphere. Light is captured by the integrating sphere that in a conventional sampling arrangement would otherwise have been lost through diffuse transmittance. Light entering the integrating sphere is scattered again and again until it reaches the detector which is built into the sphere.



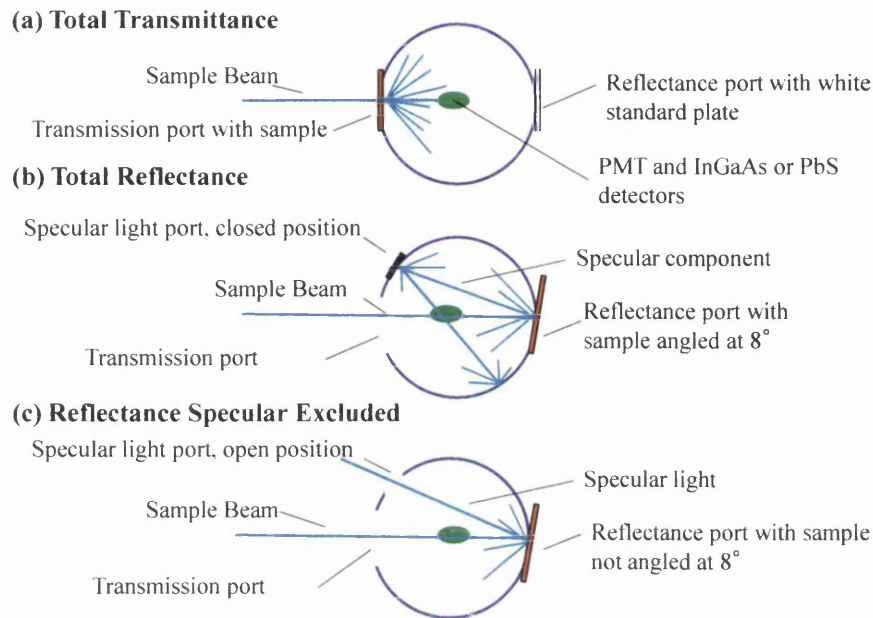


**Figure 2.14 – Schematics of Integrating Spheres, Showing the Sample Arrangement for (a) Total Transmittance (b) Total Reflectance (c) Reflectance Specular Excluded**

A reflectance measurement of an opaque sample, such as polyester coated steel substrate, is made by placing the sample at the back of the integrating sphere. Total reflectance can be measured, but this can also be separated into diffuse and specular components, by either including or excluding the specular component, as shown in Figure 2.14 (b) and (c).

In diffuse reflectance, light is scattered at all angles from a surface as with a matt surface, whilst in specular reflection, the light reflected from a surface has an angle of reflectance equal to the angle of incidence as with a mirror surface [13]. Polyester coated steel substrates will have surfaces which reflect both specular and diffuse components, so for this reason total reflectance is measured.

Specular reflectance can also be used to determine the thickness of thin films. The amount of light reflected from a thin film over a range of wavelengths is measured, and the thickness of the film computed from the wavelength separation of the interference bands of the wavelength scan. Films as thin as 0.1  $\mu\text{m}$  can be measured by this method [14].

### 2.4.1 Perkin Elmer Lambda 750S Spectrophotometer

The Lambda 750S spectrophotometer is a double beam, double monochromator instrument equipped with a 60 mm integrating sphere [15], and is shown in Figure 2.15. The instrument's detectors are a photomultiplier and a PbS detector, which allows detection over the UV-Vis-NIR wavelength range, 190 – 3300 nm. The photomultiplier detects in the UV-Vis region and the PbS detector in the NIR region, with detector changeover occurring at 860 nm. The spectrophotometer's light beam comes from two light sources, a deuterium lamp for the UV region (up to 319 nm) and a tungsten halogen lamp for the Vis-NIR region.

The Lambda 750S operates over a wavelength range that more than covers the region of maximum output from the AdPhos NIR lamps, which is from 800-1500 nm, as shown in Figure 1.18. This makes the spectrophotometer, along with its integrating sphere, an ideal tool for the investigation of the NIR cure of polyester coating systems.

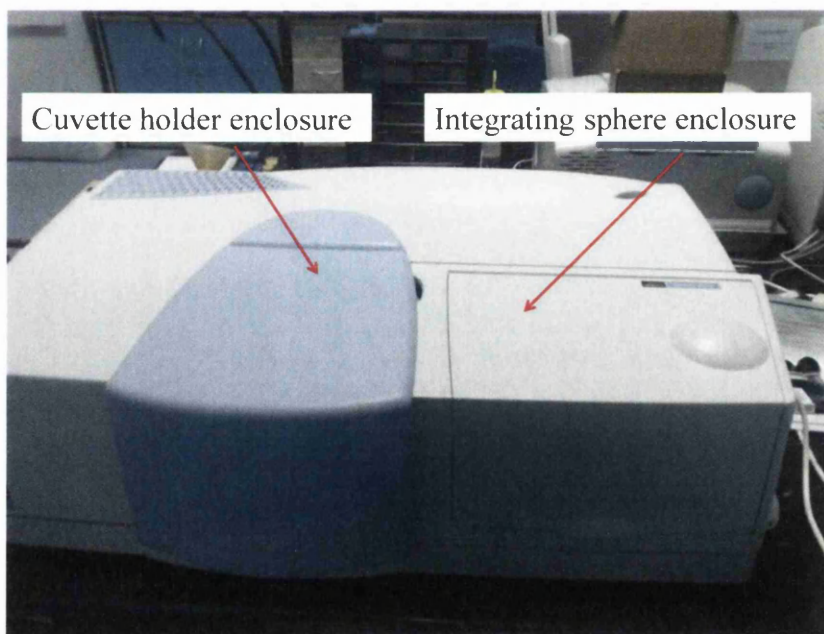


Figure 2.15 – Perkin Elmer Lambda 750S Spectrophotometer [6]

## 2.4.2 Ocean Optics HR2000+ Spectrometer

The HR2000+ spectrometer is a miniature modular UV-Vis-NIR spectrometer using an optical fibre patch sampling cable fitted with a cosine corrector. SpectraSuite, the spectrometer's operating software, controls the spectrometer via an USB lead and Notebook PC. The instrument is shown in Figure 2.16.



**Figure 2.16 – Ocean Optics HR2000+ Spectrometer**

The spectrometer can also be configured to make optical measurements in absorbance, transmission or reflection mode, but in this thesis was used to make absolute irradiance measurements of sunlight. The absolute spectral response of the spectrometer in the UV-Vis-NIR region was radiometrically calibrated using a DH-2000-CAL deuterium/tungsten halogen standard light source supplied by Ocean Optics [16]. Recalibration of the spectrometer is necessary if the optical fibre patch cable is detached from the SMA connector.

A schematic of the HR2000+ spectrometer is shown in Figure 2.17. Sampled light (sunlight) enters the spectrometer via an optical fibre cable attached to the SMA connector (1). A slit (2), a rectangular aperture directly behind the SMA connector, regulates how much light enters the spectrometer. Light then passes through a filter (3) which filters out unwanted wavelengths and onto a collimating mirror (4) which focuses the light onto the grating (5). The grating diffracts the light from the

collimating mirror and directs the diffracted light onto the focusing mirror (6). From here it passes to the detector (8). The detector is a charge coupled device (CCD) array with a spectral acquisition range from 220 to 1050 nm. The CCD converts the optical signal into a digital signal by each pixel on the CCD responding to the wavelength of light that hits it.

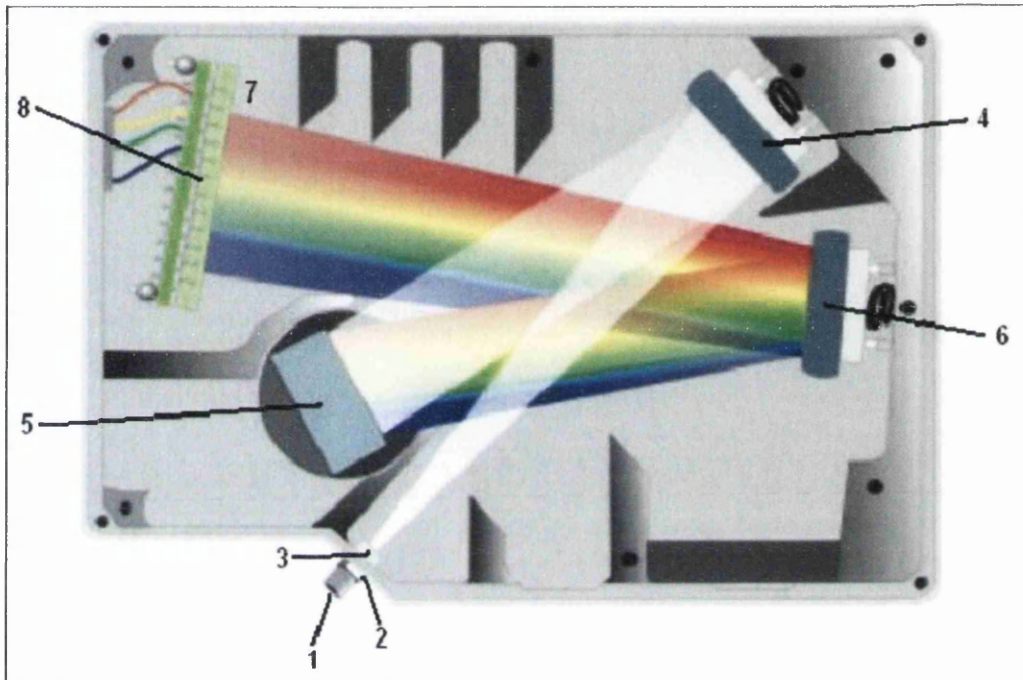
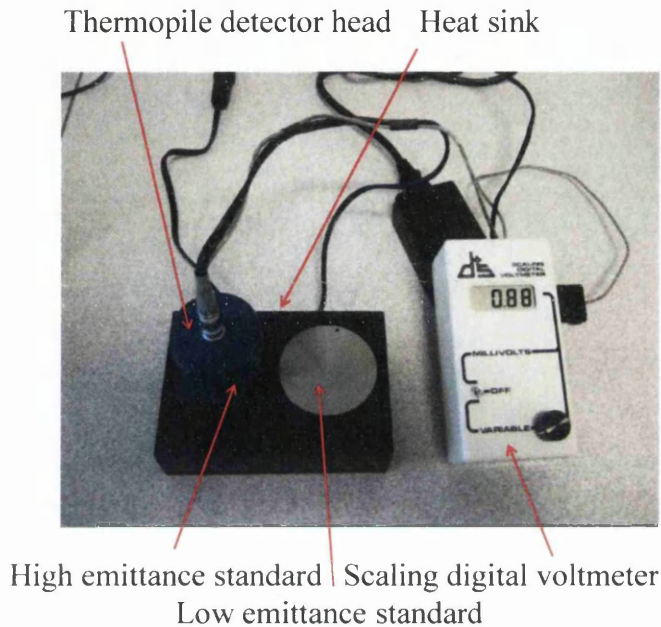


Figure 2.17 – Schematic of the HR2000+ Spectrometer Optical Bench - reproduced from [17]

- (1) SMA connector
- (2) Slit
- (3) Filter
- (4) Collimating Mirror
- (5) Grating
- (6) Focusing Mirror
- (7) L2 Detector Collection Lens
- (8) CCD Detector

## 2.5 Emittance

A Devices & Services AE1 Emissometer, shown in Figure 2.18 was used to make emittance measurements of cured polyester coated substrate panels.



**Figure 2.18 - Devices & Services AE1 Emissometer, showing the Calibration Procedure with Low Emittance and High Emittance Standards**

The emittance of a surface can be defined as the ratio of the radiation emitted by the surface to that from a black body at the same temperature [18]. The AE1 emissometer measures emittance with a thermopile detector head which responds to radiation heat transfer, producing a voltage output that is linear with emittance. Samples and reference materials are kept at the same temperature by placing them on a heat sink, using a few drops of water between the sample and heat sink to ensure good thermal contact.

The emissometer is first calibrated using standards of known emittance ( $\epsilon$ ); a black high emittance standard ( $\epsilon = 0.88$ ) and a silver low emittance standard ( $\epsilon = 0.05$ ).

## **2.6 Total Solar Reflectance**

The Lambda 750S spectrophotometer [19] and a spreadsheet tool based on ASTM E903-96/G159-98 [20-22] were used to measure Total Solar Reflectance (TSR) from the surface of coated substrate panels. Total raw reflectance from a coated substrate surface was measured in 5 nm increments from 300 to 2500 nm and solar weighting factors from ASTM G159-98 applied. These solar weighting factors reflect the solar spectral irradiance available to a surface at each wavelength. This is then used to calculate TSR.

TSR along with emittance values give a measure of how much a surface will heat up, and have been used extensively with ‘cool roof’ technology [23, 24]. For this reason they are also useful measures for transpired solar collectors.

## 2.7 References

1. ASTM, *International Astm D4147 - 99 e1 Standard Practice for Applying Coil Coatings Using The Wire-Wound Drawdown Bar*. 2007.
2. Elvins, J., *The Relationship Between the Microstructure and Corrosion Resistance of Galvan Coated Steels*. 2005, Eng. D., University of Wales Swansea
3. Mehraban, S., *Corrosion Mechanism, Inhibition and Mechanical properties of Zinc Magnesium Aluminium Alloy coated Galvanised Steel*. 2013, Eng. D., Swansea University
4. Mabbett, I., Elvins, J., Gowenlock, C., Glover, C., Jones, P., Williams, G., and Worsley, D., *Addition of carbon black NIR absorber to galvanised steel primer systems: influence on NIR cure of polyester melamine topcoats and corrosion protection characteristics*. *Progress in Organic Coatings*, 2014. **76**: p. 1184-1190.
5. Benedict, R.P., *Fundamentals of Temperature, Pressure & Flow Measurements*. 1969: John Wiley & Sons.
6. Mabbett, I., *Applications of Near Infrared Heating of Interest to the Coil Coating Industry*. 2011, Eng. D., Swansea University
7. Binns, O.C., *An investigation into the heat characteristics of the AdPhos NIR Lab Unit*. 2006, Corus Research Development & Technology.
8. Harris, D.C., *Quantitative Chemical Analysis*. 7th ed. 2007, New York: W. H. Freeman & Co.
9. Laidler, K.J. and Meiser, J.H., *Physical Chemistry*. 2nd ed. 1995: Houghton Mifflin.
10. *Application Note: Applications and Use of Integrating Spheres With the LAMBDA 650 and 850 UV/Vis and LAMBDA 950 UV/Vis/NIR Spectrophotometers*. 2004, Perkin Elmer.
11. *Application Note: Transmission Measurements Using Integrating Spheres For the LAMBDA 950/850/650 UV/Vis/NIR and UV/Vis Spectrophotometers*. 2004, Perkin Elmer.
12. *High Performance Lambda Spectroscopy Accessories*. 2010, Perkin Elmer.

13. Mabbett, I., *The Use and Applications of the Perkin Elmer Lambda 750S UV/Vis/NIR Spectrophotometer of Relevance to Corrosion and Coatings Theme*. 2009, Eng. D. Technical Brief, Materials Engineering, Swansea University
14. Hind, A.R. and Chomette, L., *Application Note: The determination of thin film thickness using reflectance spectroscopy*, March 2011, Agilent Technologies.
15. *The new LAMBDA™ 750 UV/Vis/NIR spectrophotometer from PerkinElmer*. 2007, Perkin Elmer.
16. Yeo, R., *How to Make Photometric & Colorimetric Measurements of Light Sources using an Ocean Optics Spectrometer and SpectraSuite Software*. 2009, Pro-Lite Technology LLP.
17. *HR2000+ High-speed Fiber Optic Spectrometer Installation and Operation Manual* Ocean Optics.
18. Siegel, R. and Howell, J.R., *Thermal Radiation Heat Transfer*. 3rd ed: Hemisphere.
19. Upstone, S., *Application Note: Measurement of Total Solar Reflectance of Paint Panels using Perkin Elmer UV/Vis/NIR Spectrophotometers and UV WinLab Software*. 2010, Perkin Elmer.
20. Peake, G.T., *Spreadsheet Template used to determine Total Solar Reflectance Values for Painted Panels*. Beckers. File last modified 7 August 2009, Microsoft Excel file.
21. ASTM, *International Astm E903 - 12 Standard Test Method for Solar Absorptance, Reflectance, and Transmittance of Materials Using Integrating Spheres*.
22. ASTM, *Astm International Standard G159-98 Standard Tables for References Solar Spectral Irradiance at Air Mass 1.5: Direct Normal and Hemispherical for a 37° Tilted Surface*. 1998.
23. Levinson, R., Akbari, H., Berdahl, P., Wood, K., Skilton, W., and Petersheim, J., *A novel technique for the production of cool colored concrete tile and asphalt shingle roofing products*. Solar Energy Materials and Solar Cells, 2010. **94**(6): p. 946-954.
24. Levinson, R., Berdahl, P., Akbari, H., Miller, W., Joedicke, I., Reilly, J., Suzuki, Y., and Vondran, M., *Methods of creating solar-reflective non white surfaces and their application to residential roofing materials*. Solar Energy Materials and Solar Cells, 2007. **91**(4): p. 304-314.



**Chapter 3**  
**The Effect of Black Pigment on the**  
**NIR Cure of Coloured Polyester**  
**Coatings**

### 3.1 Introduction

Industrial experience at Tata Steel's NIR curing line has shown that white coloured polyesters are the easiest to cure, having the widest cure window and being the least prone to solvent boil defects [1]. Tata Steel is keen to expand the range of colours produced on this line beyond white, and the aim of this chapter is to use spectroscopy and laboratory curing trials to investigate ways of improving the cure of coloured polyester coil coatings.

Polyester resin itself is largely transparent to NIR radiation as shown in Figure 3.1, so the varying ability of cure of different coloured polyester coatings can be attributed to the type of pigment present in the coating [2]. In Section 1.3.2.2 it was seen that white and black coatings can be used to illustrate different scenarios of absorption, reflection and transmission of NIR occurring in a coating system during NIR cure. A white coating pigmented solely with titanium dioxide, was seen to make use of substrate heating and had a high transparency to NIR. The coating was heated from the lower layers upwards, helping to minimise solvent boil. In contrast a black coating (pigmented solely with carbon black), had extremely little transparency to NIR and heat transfer started in the coating itself. This difference in locus of the initial NIR absorption predisposes black coatings to solvent boil. In a black coating all absorption is occurring in the top few microns of the coating, so solvent will have to force its way through the top layers of the coating that are already highly cross-linked [3].

In laboratory curing trials, the cure window can be defined by taking the lower limit of the cure window as the passing of a MEK 50 double rub test, and the upper limit as the outset of blistering. The wider the range of process parameters (line speed and NIR lamp power settings) over which a coating can be cured in laboratory curing trials will then give an indication of how easily the coating should cure industrially on a coil coating line. The different response of a range of coloured polyesters to changes in cure process parameters is given in Table 3.1, summarised by a curability scale. It can be seen that white polyesters have the greatest robustness to altering process parameters, black and silver polyesters the least robustness with other colours falling somewhere in between.

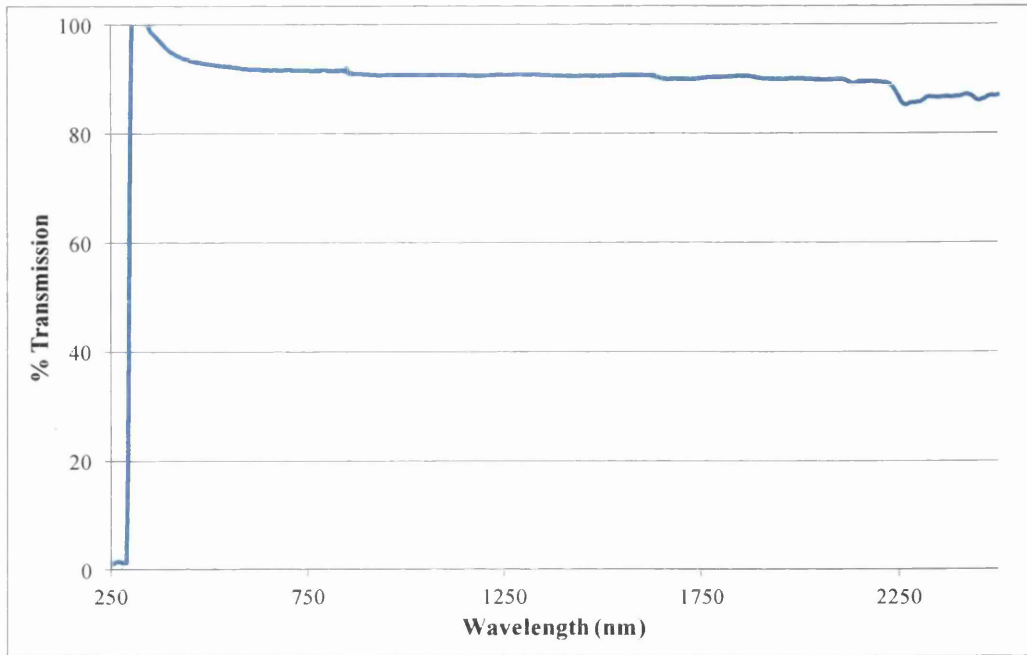


**Figure 3.1 – UV-Vis-NIR Transmission Spectrum of Free Standing Clear Polyester Coating adapted from [4]**

**Table 3.1 – How Well Coatings Cure and Their Robustness to Process Variability [3]**

Colour	Reflectance at 920 nm ( $\lambda_{max}$ emission at 100% power on NIR lamp (%))	Range of line speeds with successful cure (m /min)	Power settings with successful cure (%)	Curability Scale
White	69	9 -15	10	5
Red	18	9 -15	5	4
Brown	7	9 -15	2	3
Black	4	12	1	2
Silver	44	12	0	1

In the curability scale, 5 means cures well with a good process window and 4 means cures with a smaller process window. 3 means cures, but with very small process window. Here, any changes in parameters are problematic. 2 denotes cures, but with imperfections on the top coat and 1 denotes does not cure well at all [2].

The near commercial red and brown polyester coil coating formulations used in this thesis contained differing proportions of carbon black pigment to tint their colour and it is thought that the presence of this pigment contributes to these coatings absorption of NIR and therefore reduces the size of their cure windows. In this chapter the effect of lowering the position of carbon black in the coating system will be investigated with the aim being to widen cure window but also maintain colour. Red and brown top coats will have carbon black removed from their formulations and will be coated over a black tinted primer layer. It is proposed that the presence of carbon black in the primer layer rather than in the top coat should widen the NIR cure window and help to reduce solvent boil. The colour of carbon black-free top coats coated over a carbon black primer layer will be compared to standard formulation top coats coated over a standard primer layer, to see if colour has been maintained.

## 3.2 Experimental Techniques

### 3.2.1 Polyester Coating Formulation

Polyester coatings were made up by the pigment paste and converter method given in Section 2.1.1.2. The coatings were near commercial formulations slightly modified for NIR fast cure applications, and produced using the pigment pastes and formulations supplied by BASF in Table 3.2 and Table 3.3.

**Table 3.2 - Pigment Pastes for Polyester Coatings**

<b>Pigment code</b>	<b>Pigment name</b>	<b>Colour</b>	<b>Chemical type</b>	<b>Pigment (wt %)</b>
M031	Kronos 2310	White	Titanium Dioxide	67.5
M994	Carbon black FW 200	Black	Carbon Black	6.25
M158	Colortherm 10	Yellow	Iron Oxide	39.3
M306	Bayferrox130 BMP	Orange	Iron Oxide	37.8

**Table 3.3 - Polyester Coatings Formulations**

<b>Component</b>	<b>White (wt %)</b>	<b>Black (wt %)</b>	<b>Brown (wt %)</b>	<b>Brown without black (wt %)</b>	<b>Red (wt %)</b>	<b>Red without black (wt %)</b>
<b>Converter gloss</b>	19.7	21.16	21.0	21.0	22.0	22.0
<b>Converter matt</b>	38.28	38.95	41.0	41.0	40.5	40.5
<b>M031</b>	36.86		1.74	1.74	1.56	1.56
<b>M994</b>		32.21	8.95		2.9	
<b>M158</b>			14.24	14.24	4.16	4.16
<b>M306</b>			5.07	5.07	20.88	20.88
<b>Solvent naphtha 180/210</b>	3.58	3.84	4.0	12.95	4.0	6.9
	Bring to the viscosity specification with approximately:					
<b>Solvent naphtha 180/210</b>	3.58	3.84	4.0	4.0	4.0	4.0

The converter gloss and converter matt contain polyester resin, catalyst, some solvent and small amounts of any additives needed to increase the curing and casting capabilities of the coatings. These were shaken with the appropriate amounts of pigment pastes in a Skandex paint shaker, and then solvent was added until the viscosity specification was met. Viscosity was checked with a DINN 4 flow cup. The gloss of the coatings was checked with an Erichsen gloss meter, and matting agent or additional solvent added to ensure that both gloss and viscosity specifications were met. Standard white, black, brown and red coatings were formulated; in addition brown and red coatings with the M994 carbon black pigment omitted were also formulated.

The polyester top coats were coated over a primer layer, which in this case was Granocoat 2840, a combined pretreatment-primer supplied by Henkel. 5% carbon black (Special Black® 100) tinted pretreatment-primer was prepared by magnetic stirring for 24 hours.

### **3.2.2 NIR Curing Trials using an AdPhos Technicum NIR Oven**

Panels of 0.47 mm non pre-treated HDG substrate were cut to 150 x 200 mm and the rough edges removed with a deburring tool. The composition of HDG is given in Table 2.3. Panels were cleaned with MEK and top coat was applied with a wire bound coating bar to produce a dft of  $20 \pm 1 \mu\text{m}$ .

The temperatures of the panels were monitored during the cure process by an Omega TC08 data logger recording data from a K type thermocouple spot welded to the middle of the back of the panels. One piece of heat resistant tape was placed over the thermocouple spot weld to give extra strength to the spot weld.

### 3.3 Results and Discussion

#### 3.3.1 UV-Vis-NIR Spectroscopy

Standard pretreatment-primer and black tinted pretreatment-primer were over-coated with 20  $\mu\text{m}$  brown and red polyester top coats. Two versions of the top coats were used, the standard top coat formulation and the top coat with the carbon black left out of the formulation. The UV-Vis-NIR spectra in transmission and reflectance mode were recorded for these four coating systems and are consistent with there being a decrease in the NIR absorption of the coating system when carbon black pigment is removed from the formulation.

Figure 3.2 shows that NIR transmission through free standing films of polyester coatings increases when there is no carbon black present. There is a bigger increase in NIR transmission when carbon black is removed from the brown polyester compared to from the red polyester; this is consistent with there being a greater percentage of carbon black in the brown formulation.

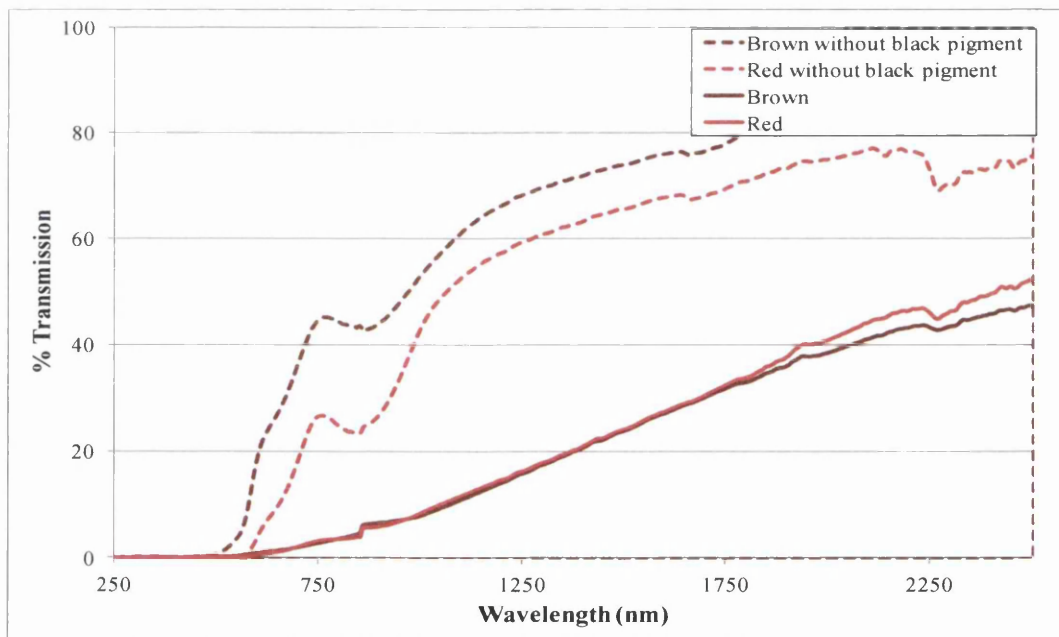
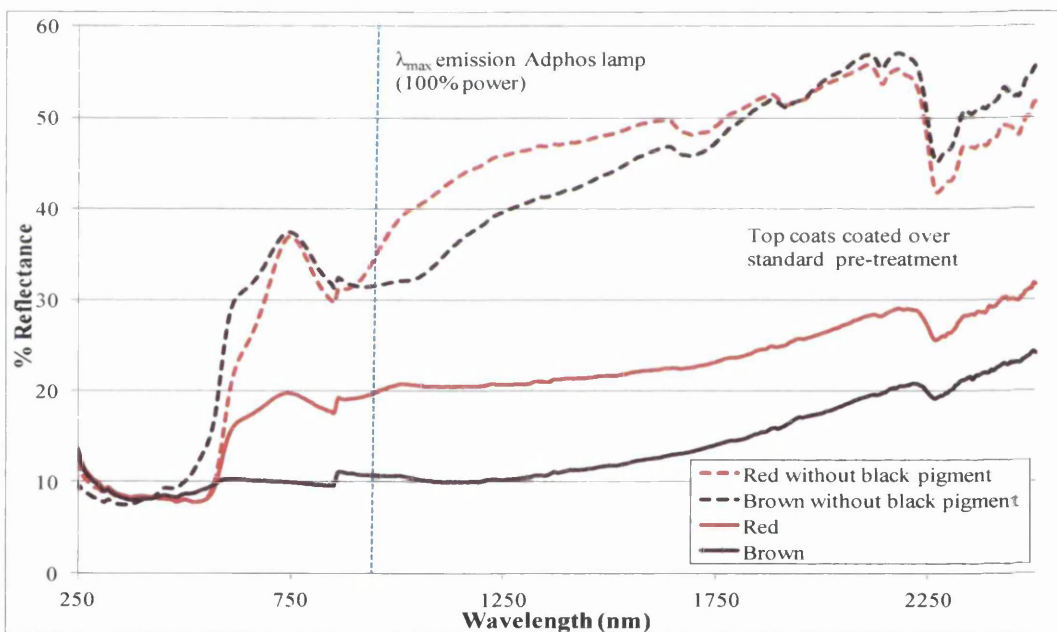


Figure 3.2 - UV-Vis-NIR Transmission Spectra of Free Standing Polyester Films



A decrease in coating NIR absorption due to carbon black removal is also confirmed by the reflectance spectra in Figure 3.3 which shows standard red and brown coatings, and also these coatings with the black pigment omitted. All four coatings are cured over a standard un-tinted pretreatment-primer. As NIR absorption in the top coats is reduced by carbon black removal, NIR reflectance in the coating systems increases due to reflectance from the HDG substrate. A dip in reflectance is now observable at ca. 1000 nm; the HDG reflectance spectra shown in Figure 3.4 suggests that this is probably due to absorption of NIR radiation by zinc in the HDG. This dip in reflectance is not seen when carbon black is present in the top coat, as the coating is then a lot less transparent to NIR radiation. Note also that the reflectance spectra of pretreatment-primer coated over HDG in Figure 3.4 indicates that the pretreatment-primer only reduces the reflectance of the HDG slightly.



**Figure 3.3 - UV-Vis-NIR Reflectance Spectra of Brown & Red Polyester Coatings with and without Carbon Black, coated over Standard Pretreatment-primer**

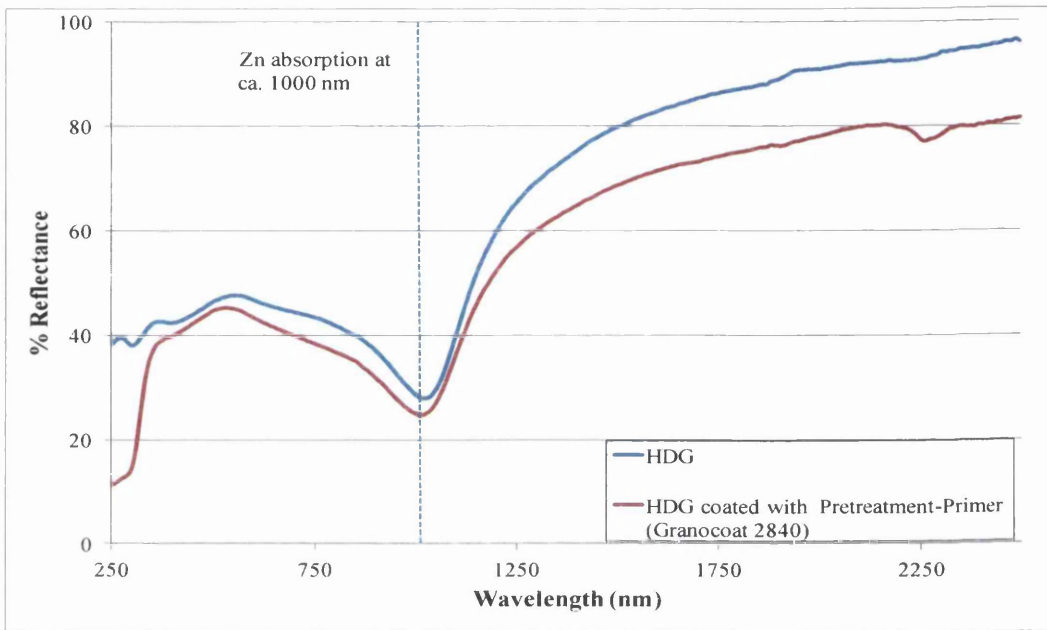


**Figure 3.4 - UV-Vis-NIR Reflectance Spectra of HDG**

The reflectance spectra shown in Figure 3.5 and Figure 3.6 compare the standard system of red and brown polyesters coated over standard un-tinted pretreatment-primers, with polyesters with the carbon black omitted coated over black tinted pretreatment-primer layers. These two coating systems hence represent a standard coating system, and one where the carbon black content of the top coat has been lowered to the primer layer. These two systems show a sizeable difference in reflectance in the visible region of the spectrum (highlighted as the light blue areas on Figure 3.5 and Figure 3.6), with the brown coating showing a greater difference than the red coating. This confirms the large Delta E\* values seen in Table 3.4 ( 27.78 for brown, 8.59 for red) and the colour differences seen in Figure 3.7 and Figure 3.8. The opacity of the top coats without carbon black is too high to allow tinting of the top coat colour with carbon black from the pretreatment-primer layer. There is therefore almost identical Delta E\* values when top coat with no black over standard primer is compared to top coat with no black over black primer, i.e. they are the same colour.

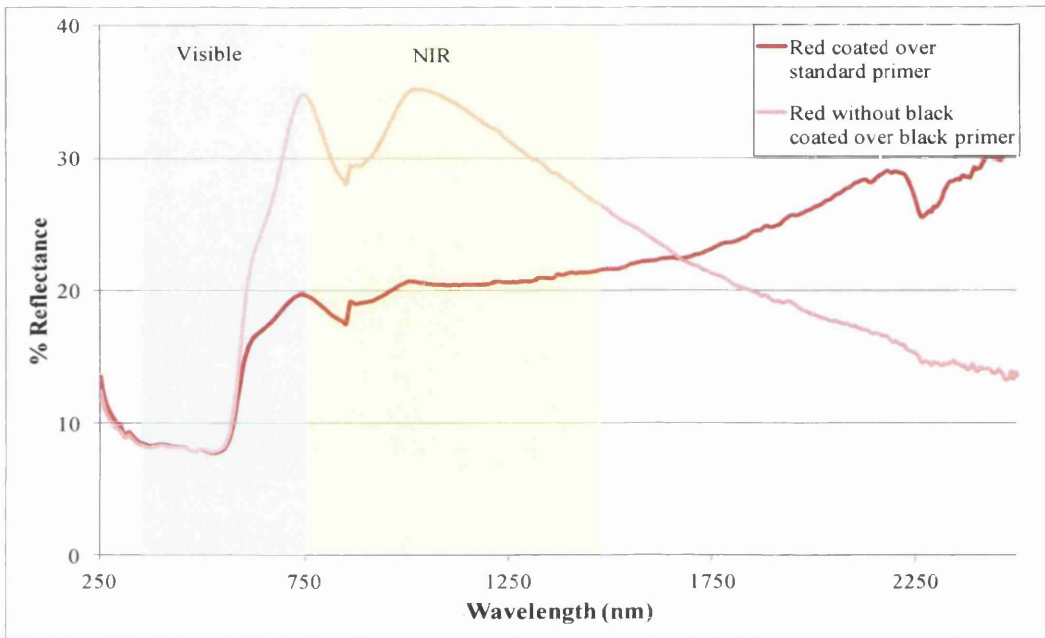


**Figure 3.5 - UV-Vis-NIR Reflectance Spectra of Red Polyester coated over Standard Pretreatment-primer, and Red Polyester without Carbon Black Pigment coated over Black Tinted Pretreatment-primer**

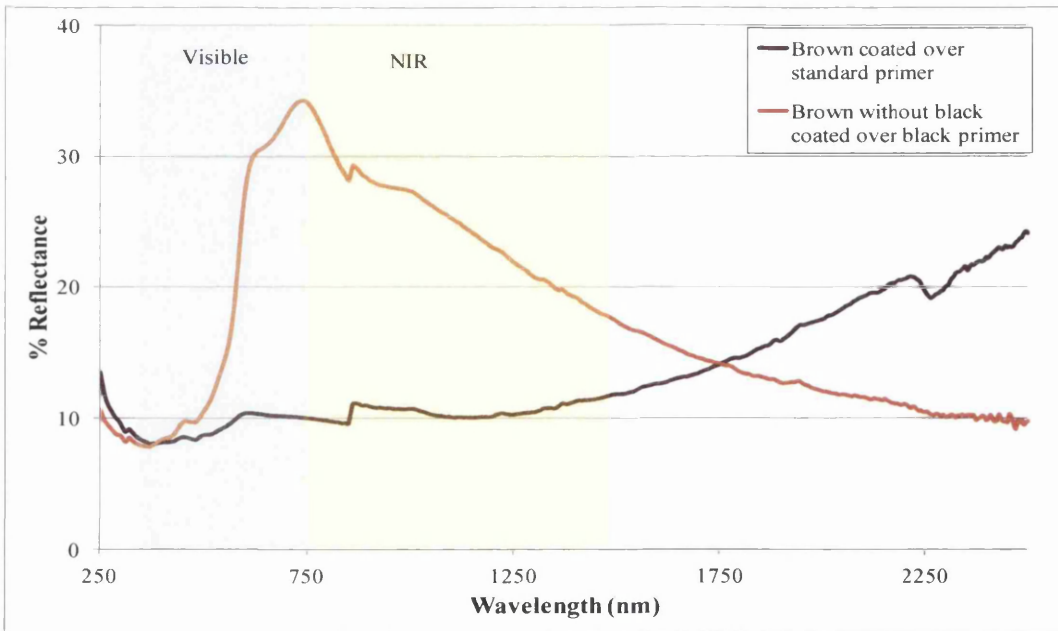


**Figure 3.6 - UV-Vis-NIR Reflectance Spectra of Brown Polyester coated over Standard Pretreatment-primer, and Brown Polyester without Carbon Black Pigment coated over Black Tinted Pretreatment-primer**

The NIR region in Figure 3.5 and Figure 3.6 are shown by the yellow shaded areas. The spectra in these figures show that the coating systems incorporating formulations with carbon black omitted from the top coat have a higher NIR reflectance than the standard formulations which have carbon black in the top coat; it would hence be expected that the cure windows for the formulations with carbon black omitted would be wider with lower PMTs being reached at the same NIR lamp power settings.

**Table 3.4 – DE\* (CIELAB 1976) for Brown & Red Coating Systems (Standard Top Coat Coated over Standard Primer is Reference)**

Sample	DE*	
	Brown coating	Red coating
Top coat without black pigment coated over standard primer	28.86	8.75
Top coat without black pigment coated over black primer	27.78	8.59
Standard top coat coated over black primer	0.80	0.97

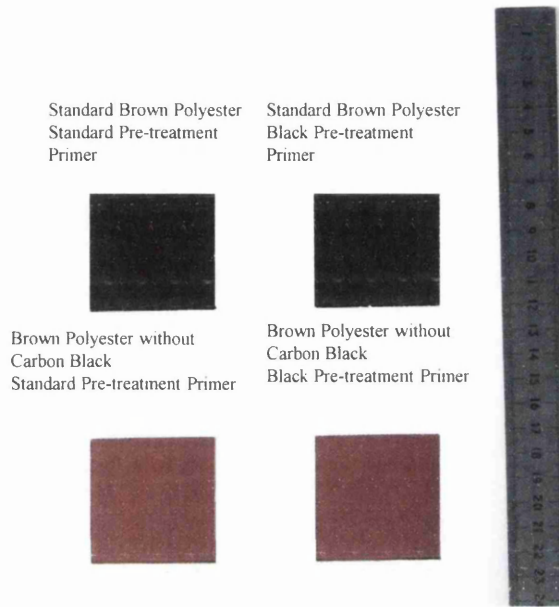


**Figure 3.7 - Brown Polyesters with and without Carbon Black Pigment cured over Standard and Black Pigmented Primed Substrate**

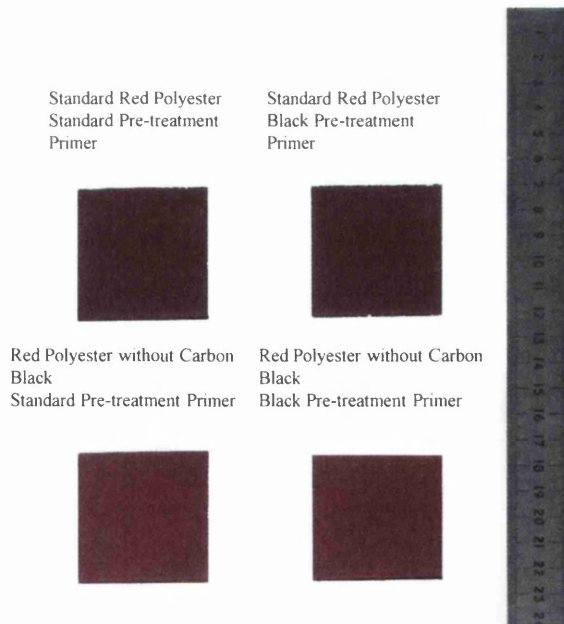


**Figure 3.8 – Red Polyesters with and without Carbon Black Pigment cured over Standard and Black Pigmented Primed Substrate**

### 3.3.2 Curing Trials

Curing trials of the red and brown formulations with and without carbon black were conducted with the Adphos Technicum oven to check the assumption that formulations without carbon black require less power to cure. Samples were coated onto 0.47 mm un-pretreated HDG and cured using the same NIR lamp powers and line speed. Five replications of samples were carried out. At the particular oven settings used ( line speed = 12 m/min; lamp powers set to 80%, 0% and 30% in oven zones 1, 2 and 3), the red and brown formulations with carbon black omitted reached lower peak metal temperatures, and typical cure profiles are shown in Figure 3.9 and Figure 3.10. Figure 3.11 shows that at these oven settings brown formulations reached on average a 19% lower peak metal temperature when carbon black was omitted from the formulation, whilst red coatings reached on average a 16% lower peak metal temperature.

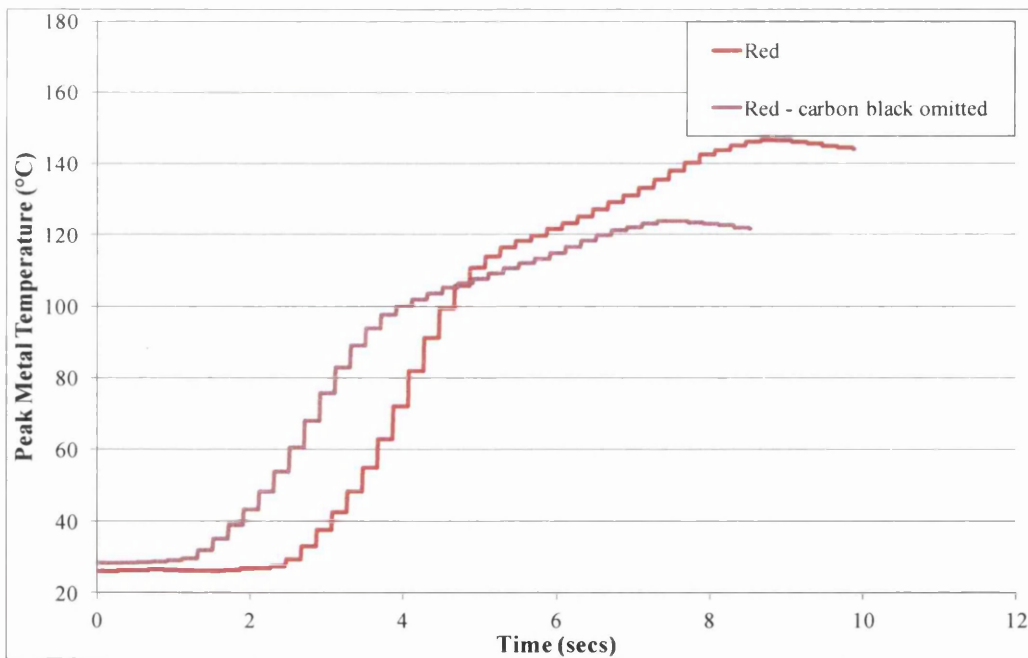


**Figure 3.9 – Typical Cure Profile of Red Polyester with and without Carbon Black at the same NIR Cure Conditions**

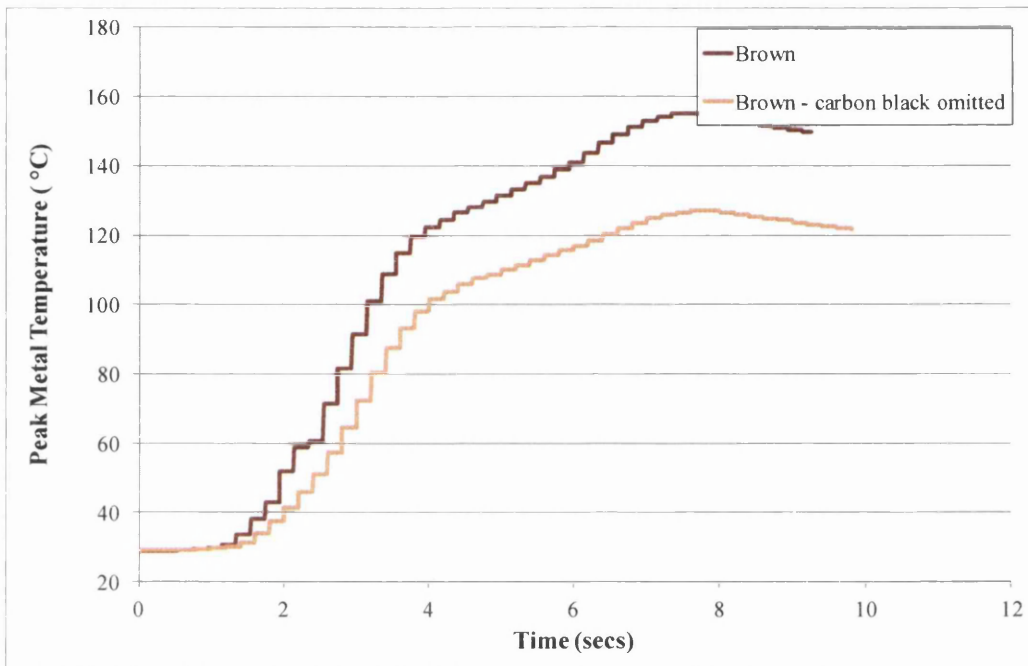


**Figure 3.10 – Typical Cure Profile of Brown Polyester with and without Carbon Black at the same NIR Oven Settings**

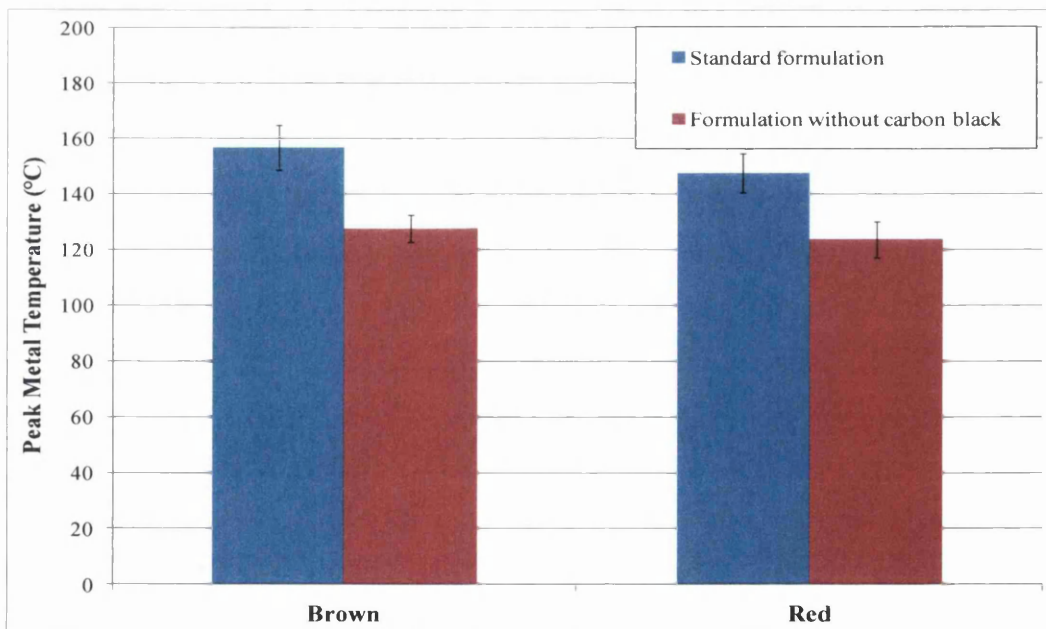


**Figure 3.11 - Peak Metal Temperatures reached for Brown and Red Formulations with and without Carbon Black, Cured at the same NIR Oven Settings**

The cure trial was then extended and the formulations cured over a range of different power settings and line speeds (9, 12 & 15 m/min). Samples which did not pass a 50 double rub MEK test were deemed to be under cured and below the lower cure limit, whilst samples that were blistered were deemed to be over cured and above the upper cure limit. The results are summarised in Table 3.5, and show that removing carbon black increases the chance of successful cure.

**Table 3.5 – Cure Trial Results for Polyesters with and without Carbon Black**

<b>Formulation</b>	<b>Total number of cure trials from experiments with different combinations of line speeds &amp; lamp power settings</b>	<b>Total number of successfully cured panels</b>	<b>Percentage of successfully cured panels (%)</b>
Brown coating	14	1	7
Brown coating with Carbon Black omitted	10	4	40
Red coating	9	1	11
Red coating with Carbon Black omitted	8	4	50

In contrast to the standard formulations with carbon black, the formulations without carbon black could be cured at all three line speeds. At a Technicum oven line speed of 15 m/min, which equates to a production line speed of 180 m/min, it was not possible to successfully cure the standard red and brown formulations with carbon black content included. There was evidence of both micro-blistering and pinholes in the cure of these coatings at 15 m/min, as shown in Figure 3.12 and Figure 3.13. Micro-blistering occurs when cross-linking has reached an advanced stage before sufficient solvent has escaped from the coating. The solvent then tries to force its way through the coating and will either create a micro-blister bubble (as in the examples in Figure 3.12 and Figure 3.13), or a volcano like hole in the coating with the edges of the hole being raised above the rest of the coating surface. Pinholes occur when the solvent is removed



too rapidly; usually the coating will flow back to fill these holes, but if the viscosity of the coating is too high or if the hole are large and there is not enough time for this to happen then a hole will result. This time the edges of the hole will not protrude above the rest of the coating surface.

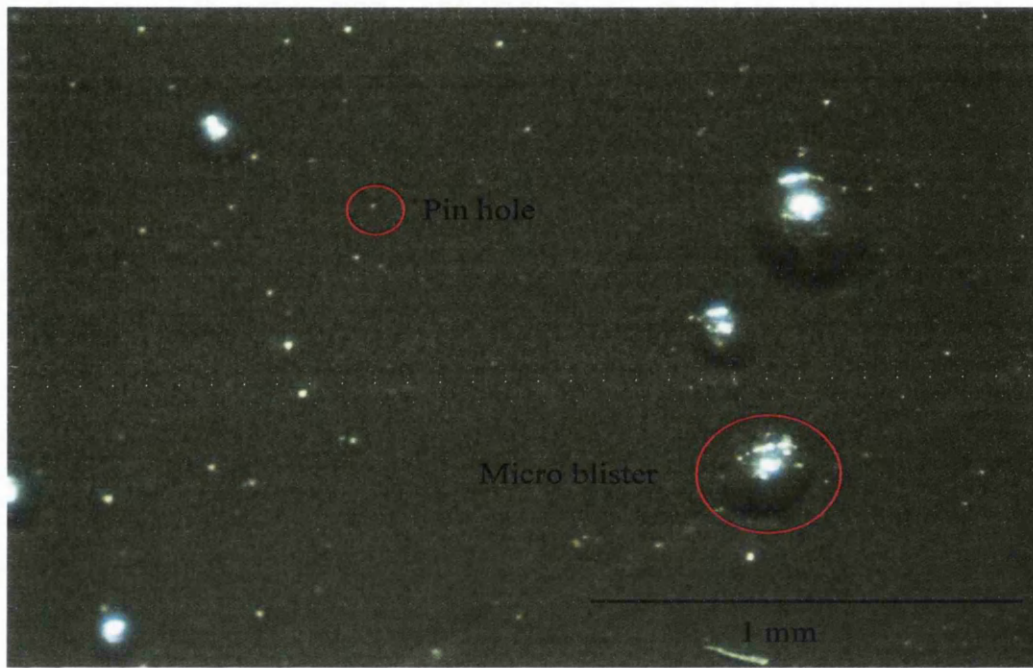


**Figure 3.12 – Brown Polyester with Carbon Black Showing Both Pinholes and Micro-blisters. (Line speed = 15m/min)**

It has been shown that micro-blistering can be countered by increasing the NIR power in zone 1 of the Technicum oven; this helps to remove most of the solvent before cross-linking occurs [2]. This would also have the effect of increasing the PMT, but this would then make pin holing worse. The remedial actions for micro-blistering and pin holing thus act against one another and from this it can be construed that the combination of micro-blistering and pinholes in the same sample is indicative of a very small or a non-existent cure window.

The red and brown formulations without carbon black successfully cured at 15 m/min. The increase in line speeds over which the formulations can be cured when carbon black is removed from the formulations is evidence of a wider range of process parameters on removing carbon black from the formulations.

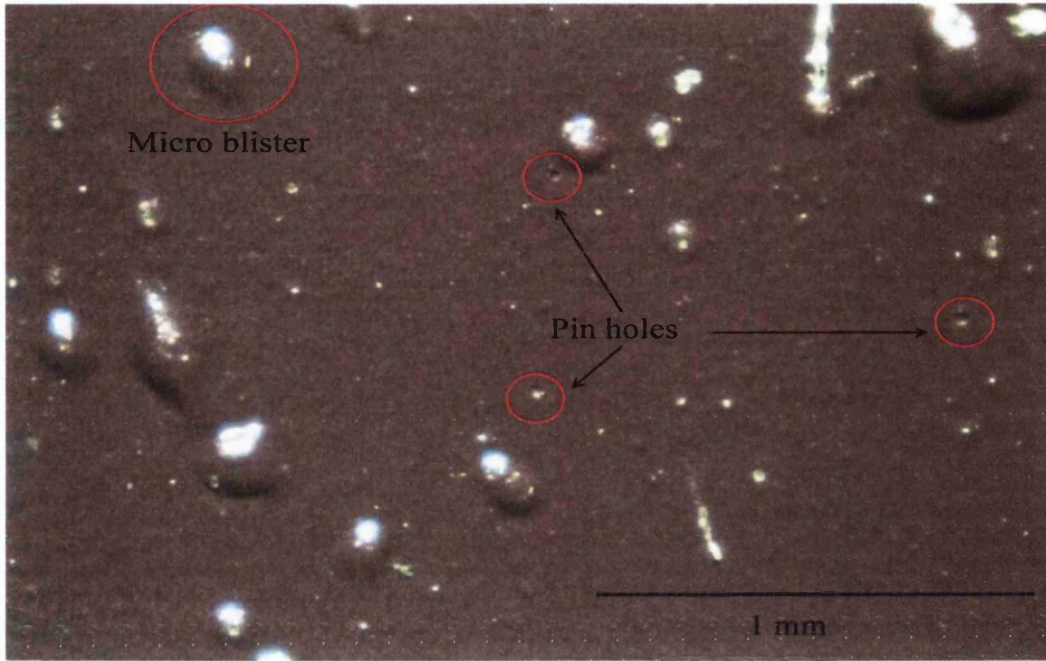


**Figure 3.13– Red Polyester with Carbon Black Showing Both Pinholes and Micro-blisters.  
(Line speed = 15m/min)**

### 3.3.3 NIR Transparent Black Pigments

NIR transparent black pigments may be suitable as an alternative pigment to carbon black in the red and brown polyester formulations. These pigments are marketed as 'cool' black pigments because they give the optical appearance of blackness whilst absorbing minimally in the near infrared. As NIR radiation accounts for 58% of sunlight, pigments of this type have found a role in coatings for the solar heat management of buildings [5].

PVC free standing films of the three near infrared transparent pigments were prepared and their transmission spectra are shown in Figure 3.14. Paliogen<sup>®</sup> and Sicomix<sup>®</sup> are commercially available BASF pigments. Paliogen<sup>®</sup> is an organic pigment based on perylene, whilst Sicomix<sup>®</sup> is a blend of organic and inorganic pigments. The Silberline pigment is currently under development and due to commercial sensitivity no further information on chemical composition was supplied by the manufacturer.

The Silberline and Paliogen<sup>®</sup> pigments show the highest transparency in the NIR and although not a true black colour (as indicated by their spectra in the visible region), they do provide a better colour than the Sicomix<sup>®</sup> pigment. Note that the oscillations in the Paliogen<sup>®</sup> spectra are an interference pattern resulting from the thin film nature of the sample; interference fringes of this type have an application in determining coated thin film thicknesses [6].

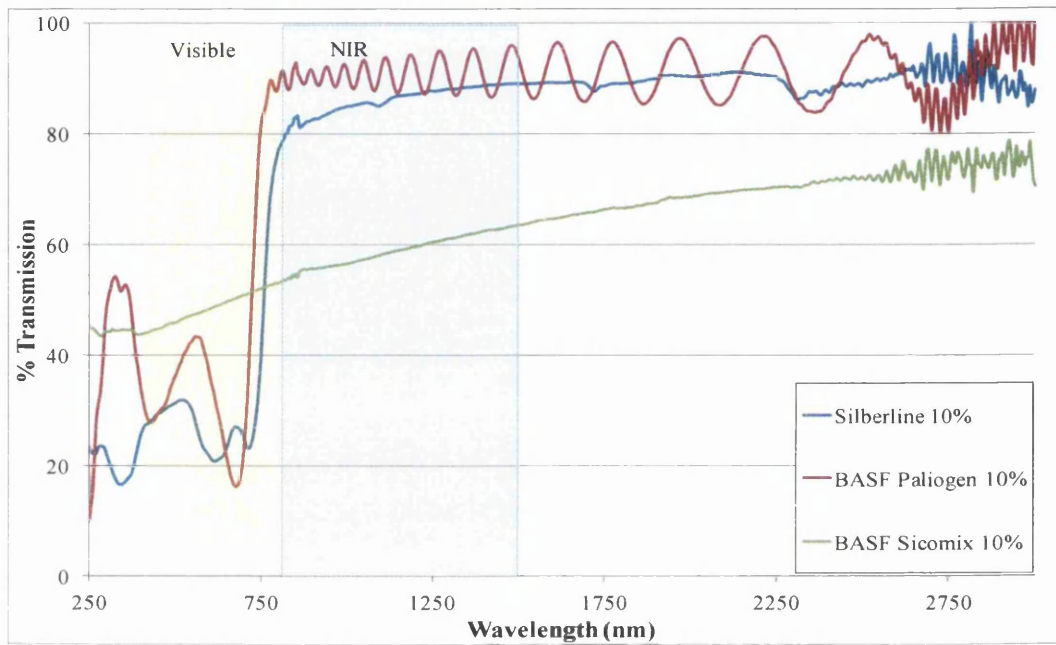


**Figure 3.14 - Transmission Spectra of Free Standing PVC NIR Transparent Black Pigment Films**

### 3.4 Conclusions

Previous work has shown that NIR curing can be optimised when the substrate absorbs most of the NIR radiation, with only a small proportion of NIR being absorbed by the top coat [3]. White coatings are hence the easiest coatings to cure and have a wide cure window, as their sole pigmenting agent titanium dioxide is a strong reflector of NIR and the coatings are relatively transparent to NIR. Black coatings however, are more difficult to cure and have a small cure window due to the presence of carbon black which is a strong absorber of NIR.

These experiments have shown that removing the carbon black content in red and brown polyesters widens the cure window making them easier to cure and less prone to solvent boil, but at the same time having a critical effect on colour. At the same NIR power settings and line speed, removal of carbon black reduces the peak metal temperature. Pigmenting the primer layer with carbon black in an attempt to provide the black tint in the polyester top coat colour is not successful, as the top coat is too opaque. We have however, tinted a primer layer with carbon black and used this layer to reduce the energy needed to NIR cure a white polyester top coat [4, 7]. The next chapter explores whether this energy benefit is also present with convection curing.

Further work could look at substituting the carbon black pigment in the polyester top coat with a near infrared transparent black pigment such as Paliogen<sup>®</sup> or Sicomix<sup>®</sup>. It would be anticipated that pigments of this nature would reduce the peak metal temperature reached and widen the cure window. Draw backs would be that the pigments are not a true black colour, so may not provide the hiding power and colour of carbon black thus making it difficult to reproduce the colour of the top coat. The NIR lamps used in NIR curing also have substantial spill over into the visible region of the spectrum, so the strong absorption of the NIR transparent black pigments in the visible region may compromise their ability to widen the cure window of the top coat. Furthermore, the cost of such pigments and their ability to produce coatings for exterior applications with robust weatherability may restrict their use.

### 3.5 References

1. Gowenlock, C., *Radiation Curing of High Performance Coatings*. 2010, Eng. D. 1st Year Report, Materials Engineering, Swansea University
2. Mabbett, I., *Applications of Near Infrared Heating of Interest to the Coil Coating Industry*. 2011, Eng. D., Swansea University
3. Mabbett, I., Elvins, J., Gowenlock, C., Jones, P., and Worsley, D., *Effects of highly absorbing pigments on near infrared cured polyester/melamine coil coatings*. *Progress in Organic Coatings*, 2013. **76**(9): p. 1184-1190.
4. Gowenlock, C.E., Mabbett, I., and Worsley, D.A., *Optimization of near infrared cured polyester/melamine coil coatings by the use of near infrared absorbing primers*. *GSTF Int J Eng Tech*, 2013. **2**(2): p. 47-50.
5. Huijnen, J. and van Ravenswaaij, B., *Solar-Reflective Colorants for Exterior Buildings and Facades*, November 2013, in *Paint & Coatings Industry*.
6. Hind, A.R. and Chomette, L., *Application Note: The determination of thin film thickness using reflectance spectroscopy*, March 2011, Agilent Technologies.
7. Mabbett, I., Elvins, J., Gowenlock, C., Glover, C., Jones, P., Williams, G., and Worsley, D., *Addition of carbon black NIR absorber to galvanised steel primer systems: influence on NIR cure of polyester melamine topcoats and corrosion protection characteristics*. *Progress in Organic Coatings*, 2014. **76**: p. 1184-1190.

**Chapter 4**  
**The Effect of Carbon Black Tinted  
Primer on the Convection Cure of a  
White Polyester Coating**

## 4.1 Introduction

Chapter 3 looked at the effect of carbon black, a strongly NIR absorbing pigment, and how its presence in coloured polyester coatings affects NIR cure. Key findings were that removing carbon black pigment content from coloured polyesters widens the NIR cure window, thus making them easier to cure and less prone to solvent boil. This however, was at the expense of maintaining top coat colour. Adding carbon black pigment to the primer layer in an attempt to replace the black tint in the polyester top coat colour did not reproduce the top coat colour because the top coat was too opaque.

Early reports in the literature suggested that NIR absorbers should be added to top coat formulations to improve the efficiency of NIR cure [1, 2], however more recently we have proposed that with 25  $\mu\text{m}$  polyester coil coatings, if the coating absorbs too strongly, most of the energy will be absorbed in the top few microns of the cross-linking coating. This will result in solvent boil, as film formation and cross-linking occur before full solvent removal [3, 4]. NIR curing is hence optimised when the polyester top coat is relatively transparent to NIR and with the substrate absorbing most of the radiation [3, 4].

We have also demonstrated that the benefits of absorption occurring in the bottom most layers of the coating system during NIR cure can be taken a stage further by tinting the primer layer of a 25  $\mu\text{m}$  white polyester coil coating system with a NIR absorbing material [5]. Here, an 18% lower PMT is observed when a standard primer is used rather than a 5% carbon black tinted primer. This leads to the opportunity of either reducing radiation intensity during cure or decreasing the oven dwell time.

The aim of this work was to establish whether the energy saving advantages of a tinted primer was also present for the convection cure of 25  $\mu\text{m}$  polyester coil coatings. Coatings of this type are conventionally cured in gas fired flotation ovens which achieve cure by convection currents. There will however be a certain amount of residual mid infrared radiation emitted from the hot walls of the oven, and the aim is to see whether this can be harnessed to reduce the oven settings needed to achieve cure.

Carbon black is however a good cathode material [6], so the effect on corrosion performance of adding carbon black to the primer will also be assessed using a scanning electrochemical technique, the in situ scanning Kelvin probe (SKP). SKP is a technique



that has been used extensively in delamination studies as it allows the temporal and spatial resolution of potential distributions below intact organic surfaces to be studied [7, 8]. The delamination kinetics of thin polyvinyl butyral (PVB) coatings containing a range of concentrations of carbon black additions and coated onto a galvanised steel substrate will be used for these experiments.

## **4.2 Experimental Techniques**

### **4.2.1 Preparation of Coatings**

The primer used in this work was Granocoat<sup>®</sup> 2840, a chromium free aqueous resin dispersion of combined pretreatment-primer, supplied by Henkel. This pretreatment-primer (hereafter referred to as 'primer') was used to formulate tinted primers by the addition of weighed quantities of Special Black<sup>®</sup> 100 carbon black to the primer, dispersed with the aid of a magnetic stirrer for 24 hours. Primers with carbon black content of 1.0%, 2.5%, 3.5% and 5.0% by weight were prepared and a Hegman gauge used to check pigment agglomerates were less than 15 microns in size.

The white polyester coating was prepared at BASF Deeside laboratories by the pigment paste and converter method given in Section 2.1.1, and was a near commercial formulation modified slightly for NIR fast cure applications. Pigment agglomerations were milled to below 15 microns and checked with a Hegman gauge. Specification was between 40-50% gloss at 60° and viscosity checked to take 65-70 s to drain a DINN 4 flow cup at 21°C. The formulation contained 34.54% w/w polyester resin, 24.87% w/w coating solvents, 25.21% w/w TiO<sub>2</sub> and 15.38% w/w other additives.

### **4.2.2 Convection Curing Trials**

Panels of 0.50 mm gauge, 210mm x 100mm HDG steel substrate were cleaned with MEK and primer applied to give a dft of  $5 \pm 1 \mu\text{m}$ . Panels were then over-coated with white polyester top coat to produce a dft of  $20 \pm 1 \mu\text{m}$ .

Cure profiles for the panels were measured using thermocouples and an Omega TC-08 data logger. Thermocouples were K-type, spot welded to the middle of the back of the substrate panels.

Convection cure trials were carried out using a Mathis D70 convection oven set to 355°C with an oven dwell time of 30 seconds.

### 4.2.3 Scanning Kelvin Probe Technique

Figure 4.1 shows the SKP apparatus. SKP design, operation and calibration have been described in detail in the literature [9-11].

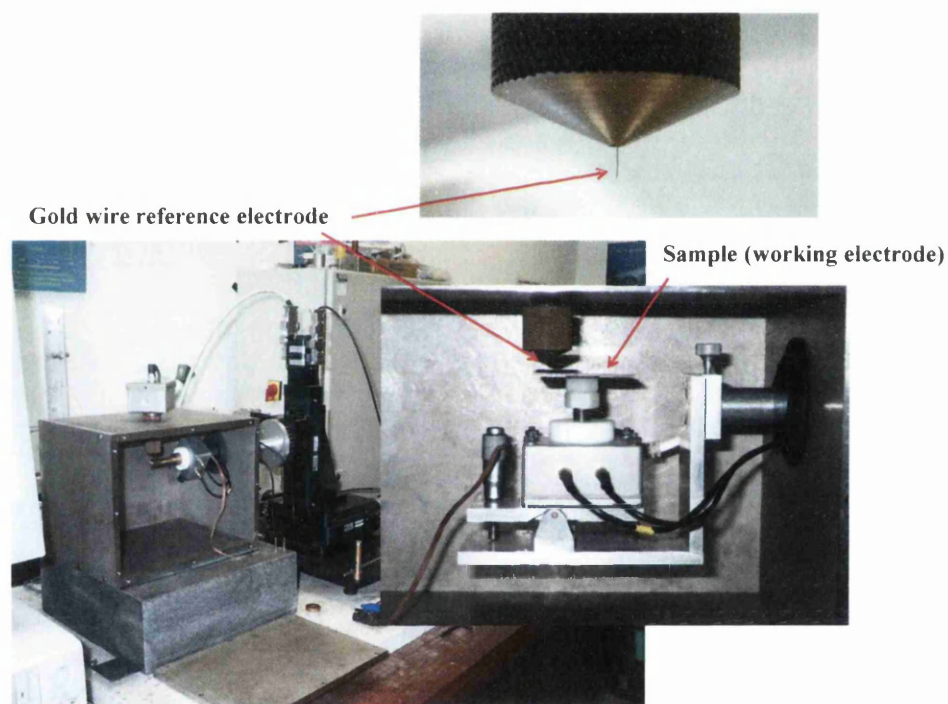
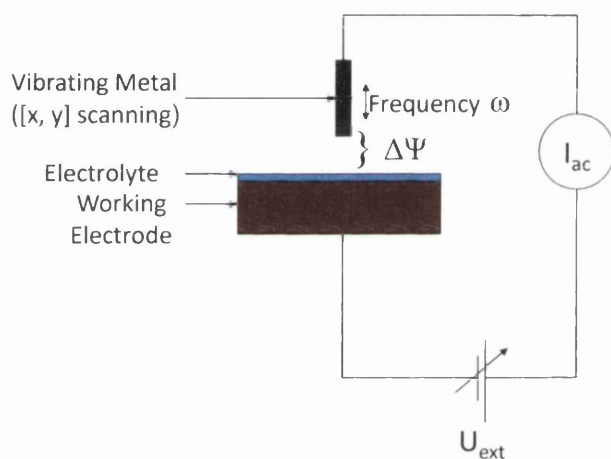


Figure 4.1 – Scanning Kelvin Probe Apparatus

A schematic of the SKP is shown in Figure 4.2. SKP works on a vibrating condenser method, whereby a gold probe (the reference electrode) oscillates perpendicular to the sample (the working electrode) at frequency  $\omega$ , separated by gap of 100 microns. The probe does not come into contact with the sample and is separated by a dielectric medium, air. The sample and probe are connected by an external circuit, and because of a difference in Fermi levels of the two materials, resultant current,  $I_{ac}$  flows. An external voltage,  $U_{ext}$  is switched into the circuit and the applied external voltage needed to null the current is noted; this is defined as the Volta potential,  $\Psi$ .



**Figure 4.2 – Schematic of Scanning Kelvin Probe Technique**

It has been shown, for a metal surface coated with an adherent and/or a delaminated PVB film, that:

$$E_{\text{corr}} = \Delta \Psi_{\text{Pol}}^{\text{Ref}} + A \text{ Volts vs. SHE} \quad \text{Equation 4.1}$$

where :

$E_{\text{corr}}$  = corrosion potential

$\Delta \Psi_{\text{Pol}}^{\text{Ref}}$  = Volta potential difference measured between the SKP reference probe (gold wire) and the polymer-air interface

A = constant.

The sample preparation procedure was based on methods given by Stratmann et al [7, 8, 12]. Polyvinyl butyral (PVB) solutions of MW 70,000 – 100,000 were prepared in 15.5% ethanol and the required amount of Special Black<sup>®</sup> 100 carbon black was added and mixed using a high shear mixer. Quantities of carbon black added ranged from 0.5 to 5 % by weight. An aqueous slurry of 5  $\mu\text{m}$  alumina was used to hand polish the sample surface to remove any contaminants and pre-existing oxide layer. Degreasing was carried out via an acetone rinse followed by air drying. PVB solution containing the appropriate amount of carbon black was bar cast onto a pre-cleaned sample and room-air dried. Carbon black was dispersed in PVB rather than the commercially available Granocoat<sup>®</sup> 2840 primer used in the curing studies, as this allowed the SKP experiments to be performed in a reasonable time frame and with an appropriate sample configuration.

The delamination experiments were carried out in an enclosed SKP chamber maintained at a constant 95% relative humidity and 25°C. Delamination was initiated each time using 0.86 M aqueous NaCl at pH 6.5. The SKP reference probe consisted of a gold wire of diameter 125  $\mu\text{m}$  vibrating vertically at 280 Hz and amplitude of 40  $\mu\text{m}$  at a distance of 100  $\mu\text{m}$  above the sample surface.  $E_{\text{corr}}$  data points were recorded at 20 per mm. The SKP reference probe was scanned over the coated surface along a 12 mm line normal to, and adjacent with, the defect-coating boundary, as shown in Figure 4.3. Scanning commenced immediately on the addition of electrolyte and thereafter at hourly intervals over a period of  $\geq 24\text{h}$ .

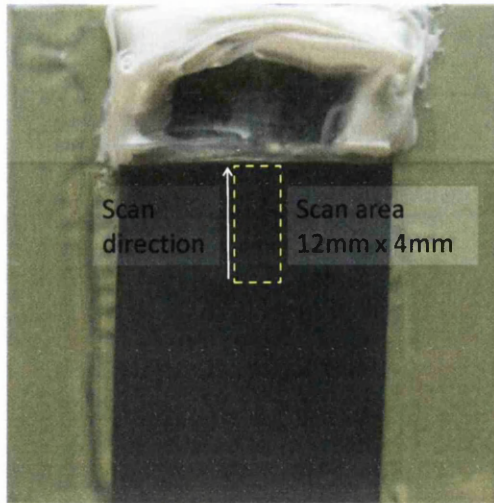


**Figure 4.3 – SKP Sample showing the Scan Area adjacent to the Defect-Coating Boundary**

## 4.3 Results and Discussion

### 4.3.1 Spectroscopic Studies and Colour Measurement

The carbon black content of the tinted primers was checked by using a Datacolour Spectraflash 600 Spectrophotometer to measure CIELAB Delta E\* values of primer coated substrate panels. Samples were measured in triplicate. This showed an increase of CIELAB Delta E\* with carbon black content, as given in Figure 4.4.

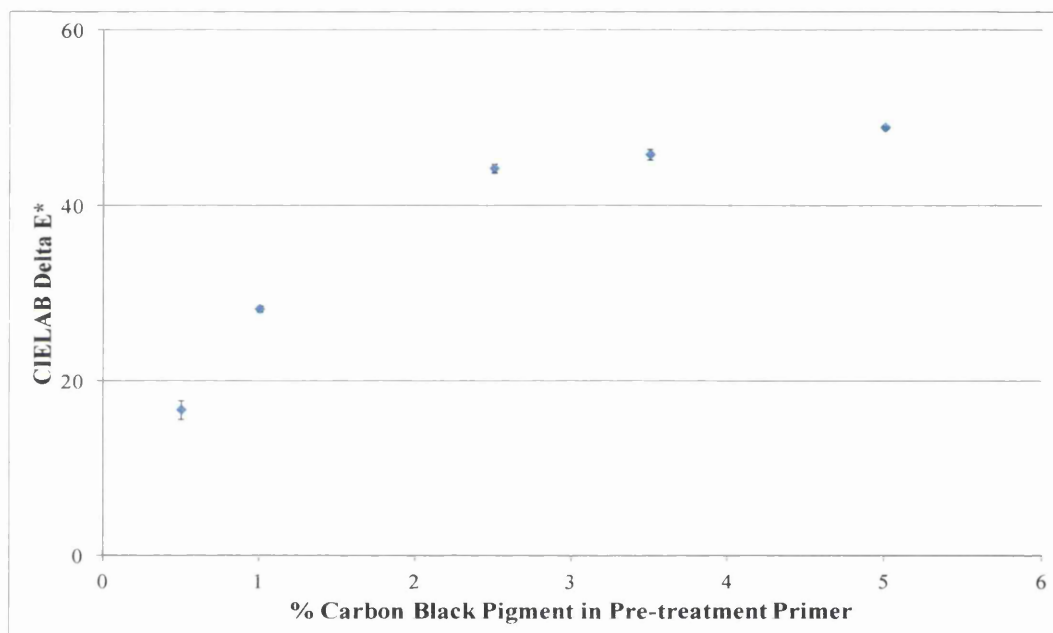


**Figure 4.4 – Relationship of Colour Difference to Carbon Black Content of Primer**

UV-Vis-NIR spectroscopy shows that the primer layer used in this work is largely transparent to IR radiation up to 2500 nm, as shown in Figure 4.5. Transmission through a 5 wt.% carbon black tinted primer layer is however almost negligible, as shown by the black spectrum in Figure 4.5, as carbon black absorbs strongly over all wavelengths of the visible region and IR region up to 2500 nm.

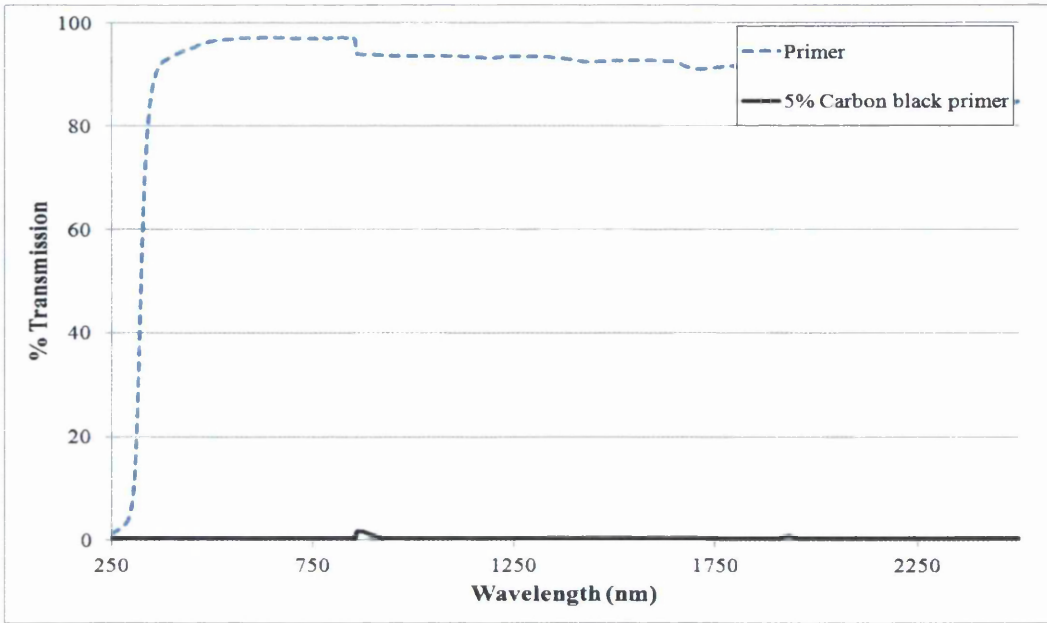


**Figure 4.5 – Comparison of UV-Vis-NIR Transmission Spectra of Free-Standing Primer Films**

The noticeable feature of the UV-Vis-NIR total reflectance spectra of HDG steel substrate shown by the blue dashed spectrum in Figure 4.6 is a peak associated with Zn absorption around 1000 nm [3]. When a primer layer is coated onto this HDG substrate only a modest decrease in absorption is seen in the reflectance, shown by the blue dotted spectra in Figure 4.6. This is consistent with the primer layer being highly transparent; a high proportion of the radiation is making its way through the primer to give the characteristic Zn absorption peak at ca. 1000 nm. A primer layer tinted with carbon black however, shows extremely low transparency at all IR wavelengths in the spectra absorbing most of the incident radiation as shown by the solid black spectrum in Figure 4.6.

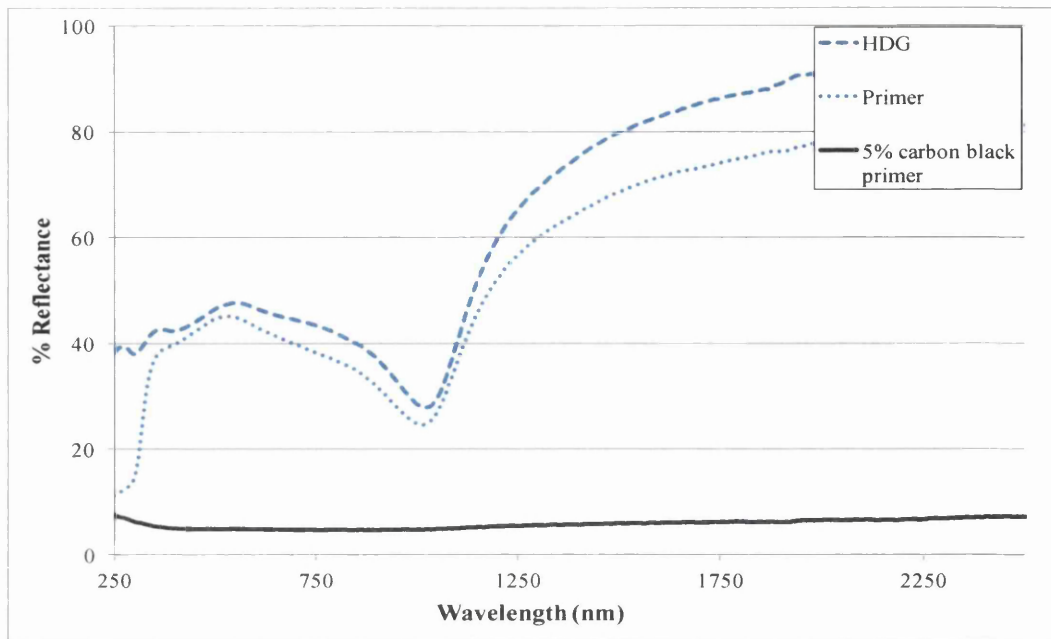


**Figure 4.6 – UV-Vis-NIR Reflectance Spectra of HDG Panels Coated with Primer**

Titanium dioxide reflectance dominates the visible region of the spectrum for a white polyester coating, as shown in Figure 4.7. It would therefore be expected that white polyesters coated over a standard primer or a black tinted primer would show a similar colour. CIELAB 1976 delta E\* values of white top coats with increasing percentages of carbon black in the underlying primer layer are shown in Figure 4.8. Samples are measured in triplicate. The coil coating industry commonly uses this colour difference measurement when an industrial specification for a colour match is needed. A delta E\* of 1.0 is commonly taken as barely perceptible to the human eye, and indicative of an adequate colour match in the industry. As a white top coat coated over even a 5 wt.% carbon black loaded primer has a delta E\* of less than 1.1, the effect on colour is negligible.



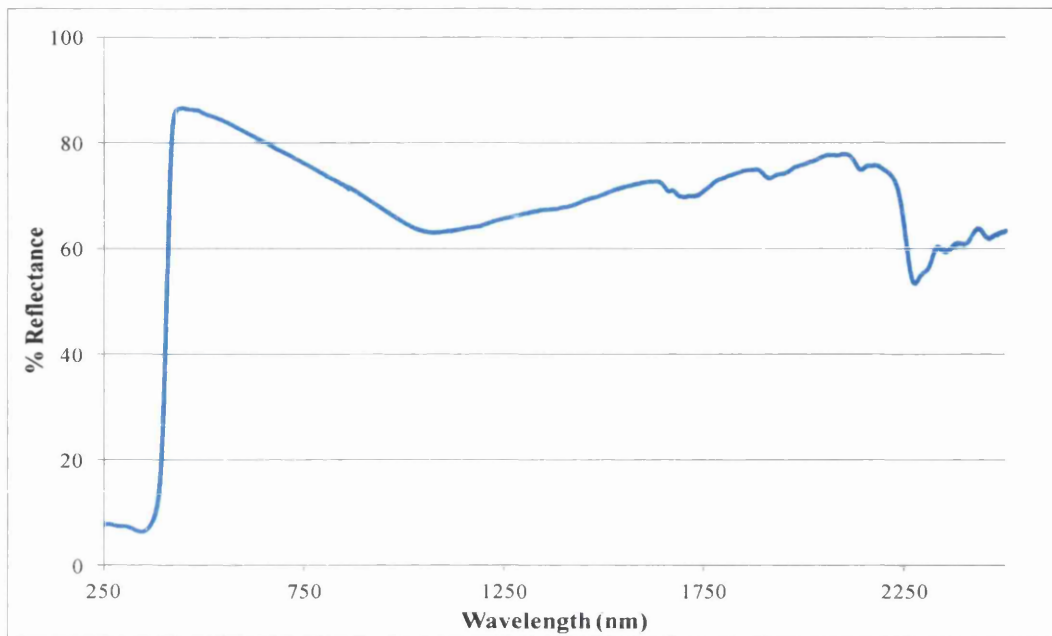


**Figure 4.7 - UV-Vis-NIR Reflectance Spectra of White Polyester Coating**

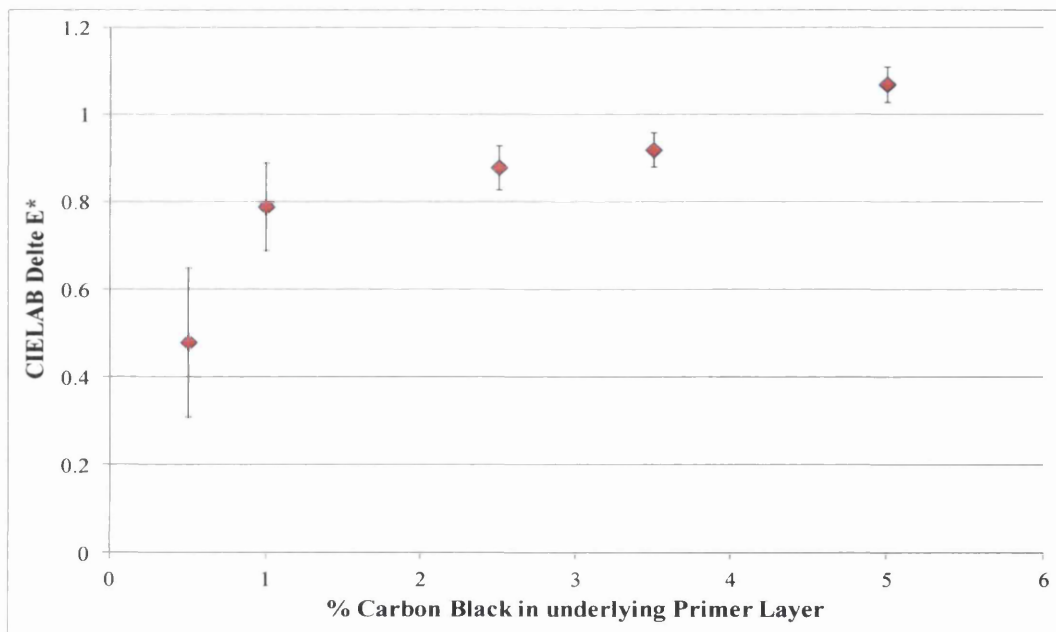


**Figure 4.8 – Variation of White Top Coat Panel Colour with Underlying Primer Carbon Black Content**

An increase in absorption of IR wavelengths in these panels should be seen when carbon black is present in the primer layer, as titanium dioxide pigment allows IR through the top coat [3]. The transmission spectra of free-standing coating films in Figure 4.9 show that the clear polyester film has a high degree of transparency to IR radiation up to 2500 nm. A white polyester coating (pigmented solely with titanium dioxide) and shown in the same Figure, still allows a sizeable proportion of IR radiation to pass through, with this increasing with increasing IR wavelength.

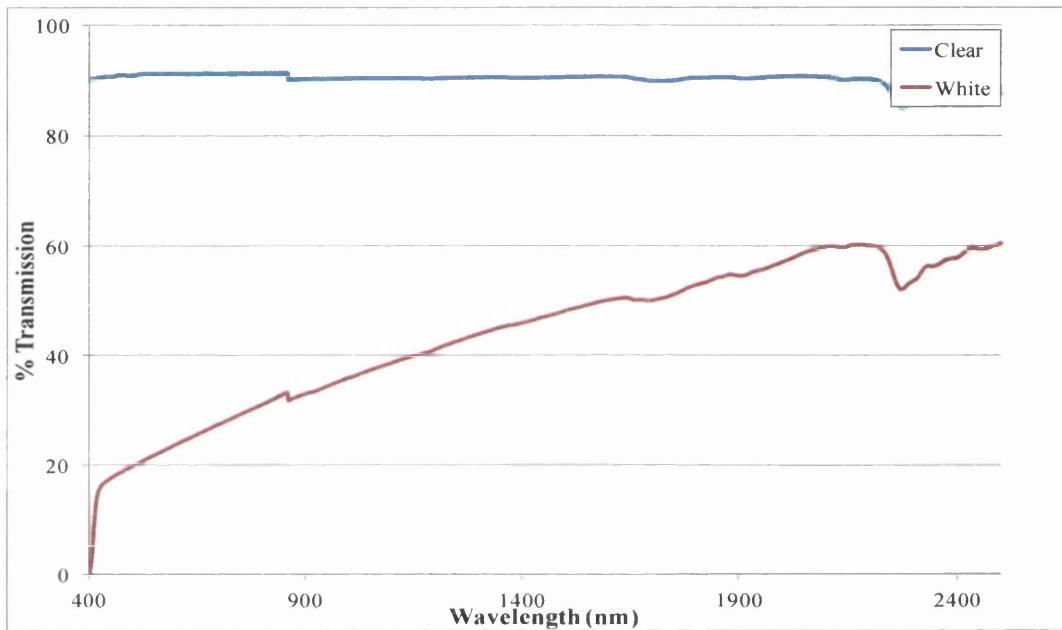


**Figure 4.9 – Comparison of Vis-NIR Transmission Spectra of Free-Standing Polyester Films**

The reflectance spectra of HDG substrate coated with a standard or a tinted primer and then over coated with a white polyester coating are shown in Figure 4.10. These show similar reflectance spectra in the visible region highlighted by the yellow area. In the IR region, the tinted primer samples show a decreasing reflectance or increasing absorption as carbon black content is increased. This indicates that some IR radiation is able to penetrate through the top coat and be absorbed by the increasing amount of carbon black in the primer underneath.

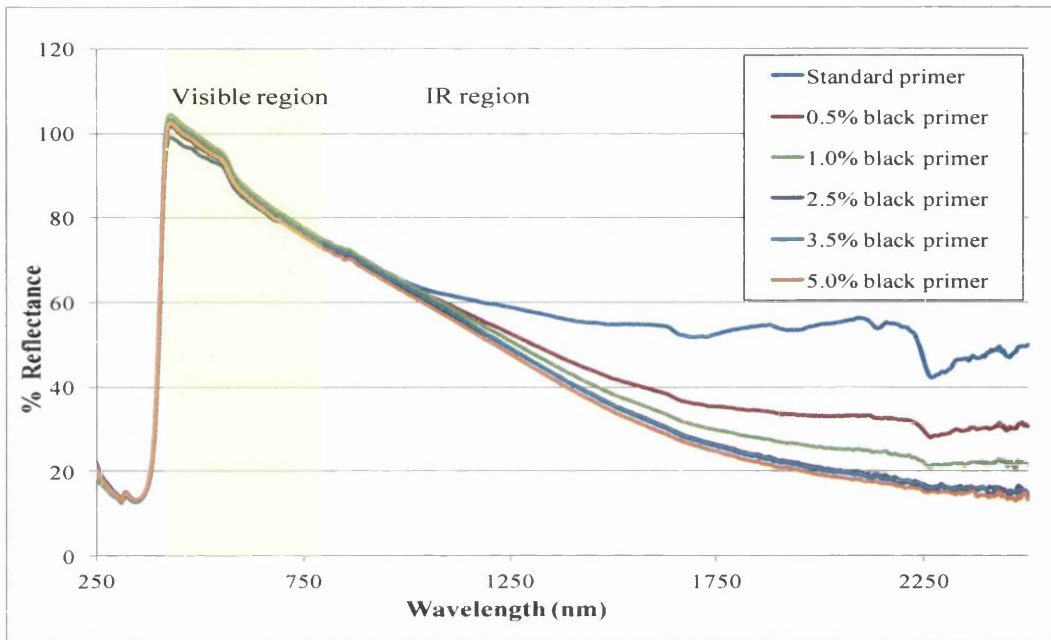


**Figure 4.10 – UV-Vis-NIR Reflectance Spectra of HDG Coated with Primer and 20 microns White Top Coat**

We have previously shown that this increase in absorption within the NIR range allows an increase of efficiency during NIR curing, with a 18% lower peak metal temperature (PMT) being reached when a standard primer is used rather than a 5% carbon black tinted primer [4, 13]. There may be sufficient IR radiation emitted from the refractory brick walls of a convection oven to enable a similar but smaller energy efficiency saving in a convection oven cure.

### 4.3.2 Cure Trials

Panels of coated substrate were initially cured in an AEW convection oven at the Tata Steel Tafarnaubach site, with the oven set to achieve a substrate PMT of 224 – 232 °C in 30 – 32 seconds. The cure temperature profile for a white polyester coating measured with a K-type thermocouple did not show an even temperature rise as expected; a typical cure profile is shown in Figure 4.11. Close examination of the cure process indicated that the shape of the cure profile correlated with the oven door being open and shut on the thermocouple wire. The refractory brick lining of the oven door would appear to be acting as a heat sink and lowering the temperature recorded.

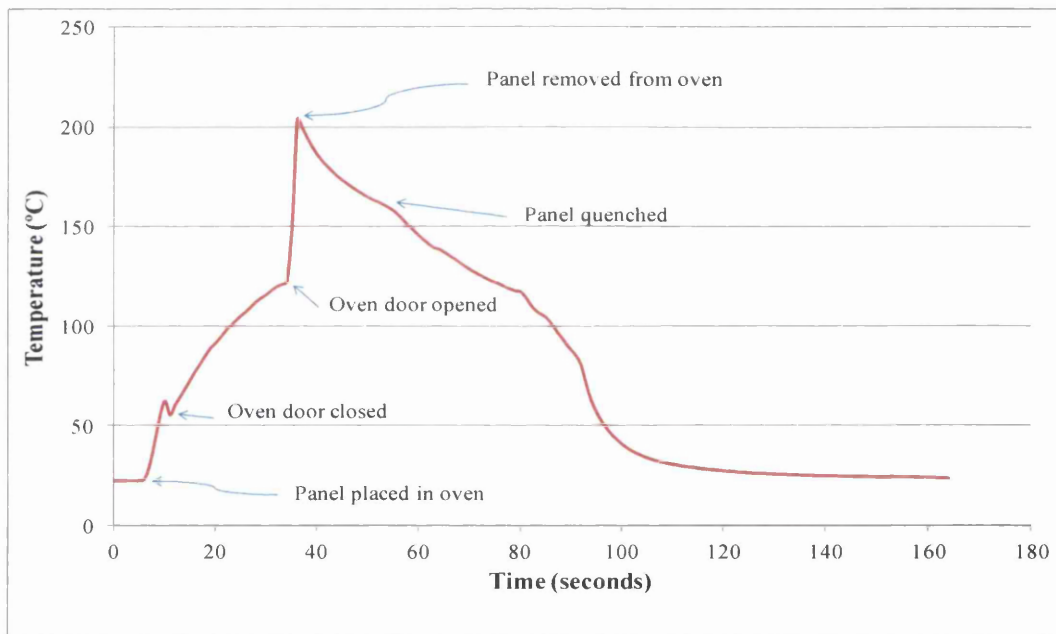


**Figure 4.11 – Temperature Profile using Thermocouple and AEW Oven**

The AEW oven was therefore not suitable for this work; work was carried out instead using a Mathis D70 convection oven at the BASF Deeside site, shown in Figure 4.12.



**Figure 4.12 – Mathis D70 Convection Oven with Timed Automated Entry and Exit**

The Mathis D70 oven has timed automated entry and exit of the sample into the oven on a wire tray, whilst the AEW oven entry and exit was performed manually with timing by a stop watch. The Mathis D70 oven will therefore reduce the error associated with timing of the PMT.

Despite the simple workings of a thermocouple, its performance must always be carefully checked. Performance can be affected by heat sink effects, by electrical shorting of the thermocouple wires and by blackening of the thermocouple junction [14].

Once spectroscopic studies had given some understanding of where different electromagnetic radiation wavelengths were interacting in the coating system, a cure trial was carried out in a convection oven to investigate the effect of primer tint on top coat PMT. Panels with a white top coat, coated over either a standard or carbon black tinted primer were cured in triplicate at the same oven temperature and dwell time. The plot of peak metal temperature versus the percentage of carbon black in the primer layer in Figure 4.13 shows that PMT increases with increasing carbon black content in the primer layer.

A 5% lower PMT was observed when a standard primer was used rather than a 5% wt. carbon black primer, as shown in Figure 4.14 and illustrated by the typical cure profiles of Figure 4.15. As a consequence, this method offers the opportunity to reduce oven temperature during convection cure to obtain the same PMT.

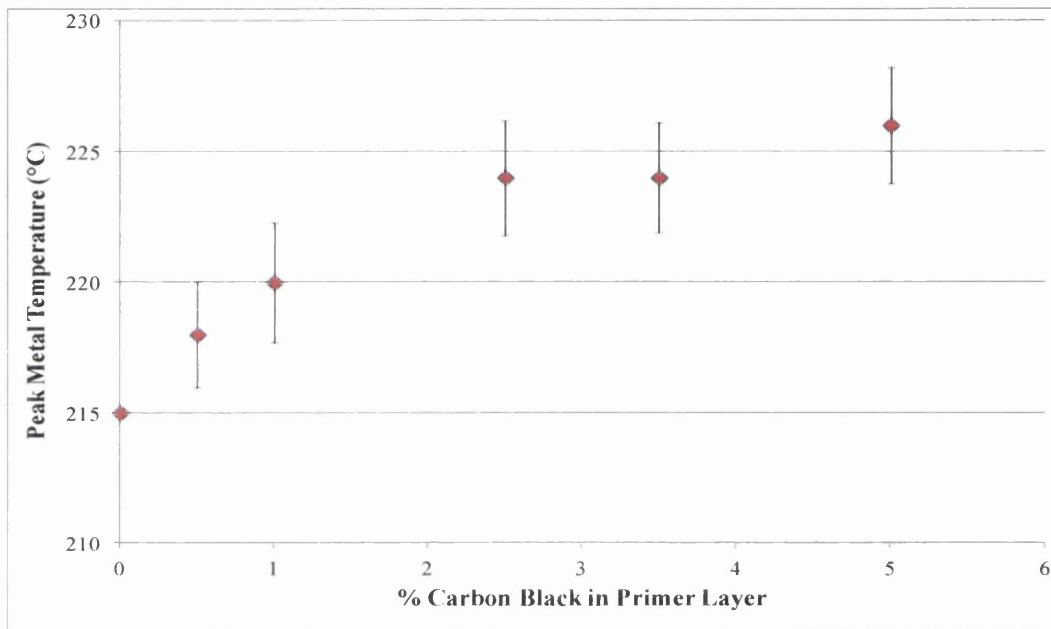


Figure 4.13 – Variation of White Top Coat PMT with Primer Tint

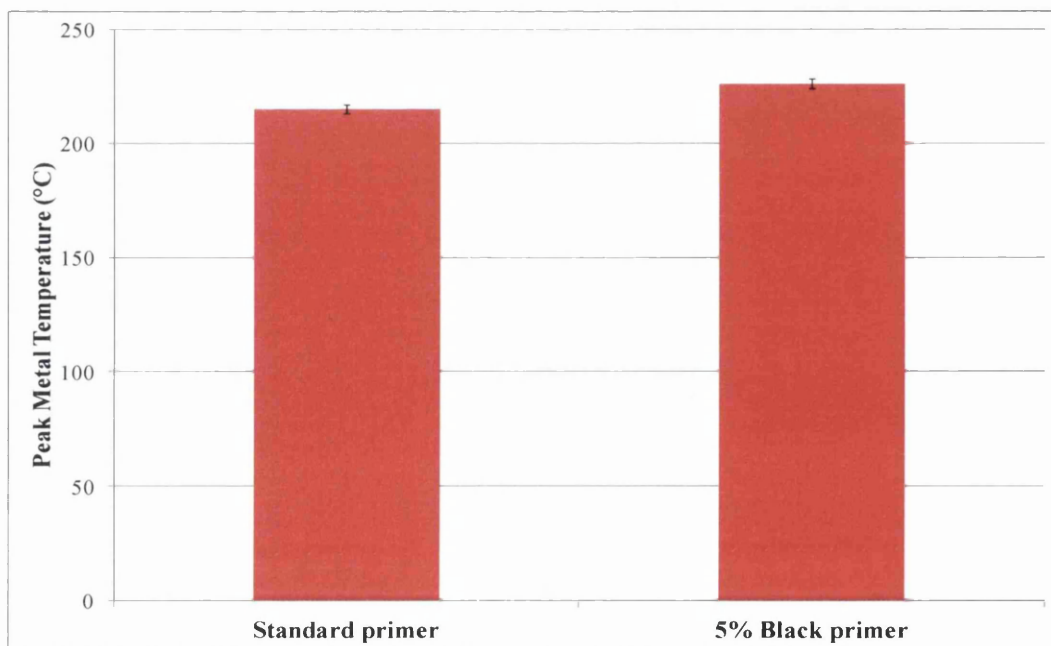
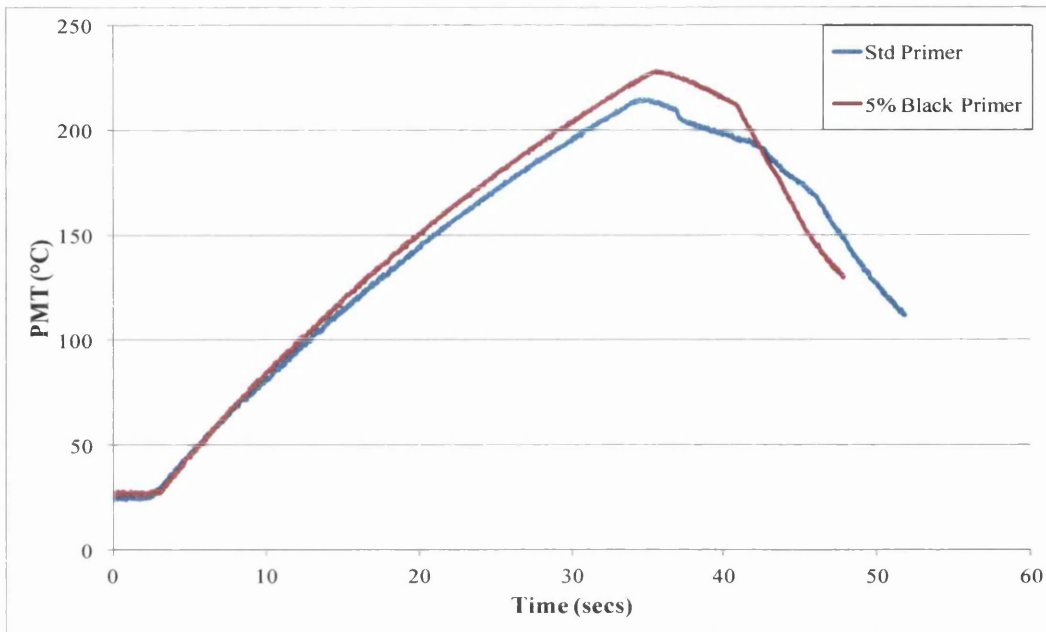
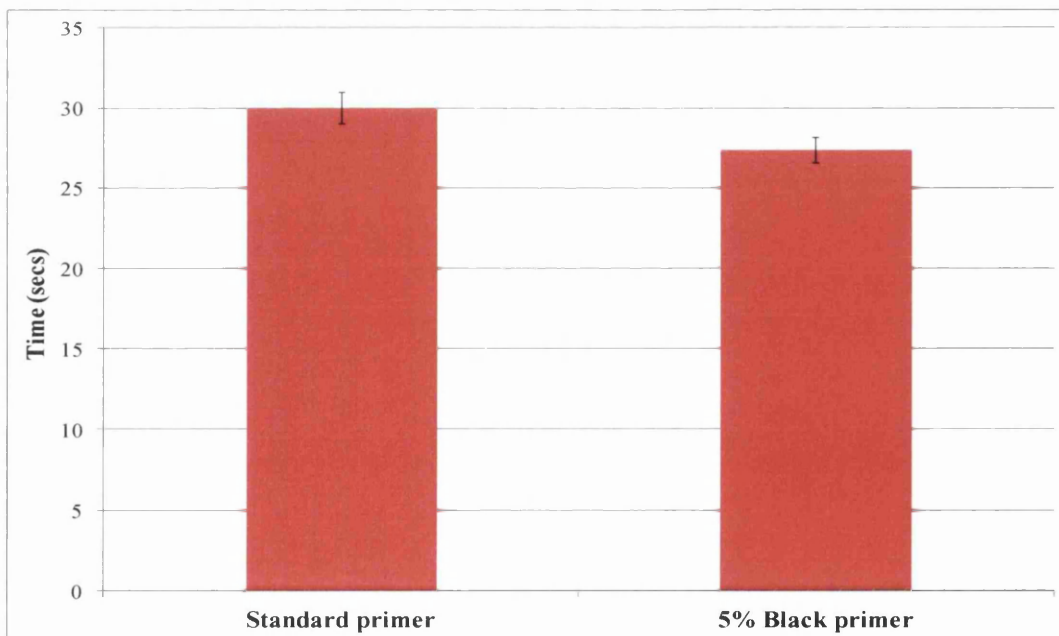


Figure 4.14 - PMTs Reached by Panels with Different Primers with Identical Convection Curing Conditions



**Figure 4.15 – Typical Cure Profiles of White Polyester with Standard and Tinted Primer**

A white top coat cured over a standard primer passed a 100 MEK double rub test after 30 seconds in a Mathis D70 convection oven set at 355°C. Figure 4.16 shows that a primer with 5 wt.% carbon black content reduces the time to reach PMT by ca. 3 seconds. Samples were carried out in triplicate.



**Figure 4.16 – Time for White Top Coat Under Coated with 5% Black Tinted Primer to Reach Same PMT as Un-tinted System**

### 4.3.3 Interaction of IR Photons with the Coating System

We have proposed mechanisms for NIR photon interactions with more highly absorbing coating systems and less strongly absorbing coating systems [3, 4]. Proposed mechanisms for photon interactions up to 2500 nm with a paint system incorporating a carbon black tinted primer are deduced from the spectral information in Figure 4.5 to Figure 4.10 and are given in Figure 4.17. Mechanisms A and A' show photon absorption by the top coat, with better depth penetration at A'. As white coatings are largely transparent to NIR and lower midrange infrared photons, mechanism B (absorption of photons by the primer layer) is likely to predominate. Mechanism C (photons reflected at the air/coating surface) will also be significant for a white top coat.

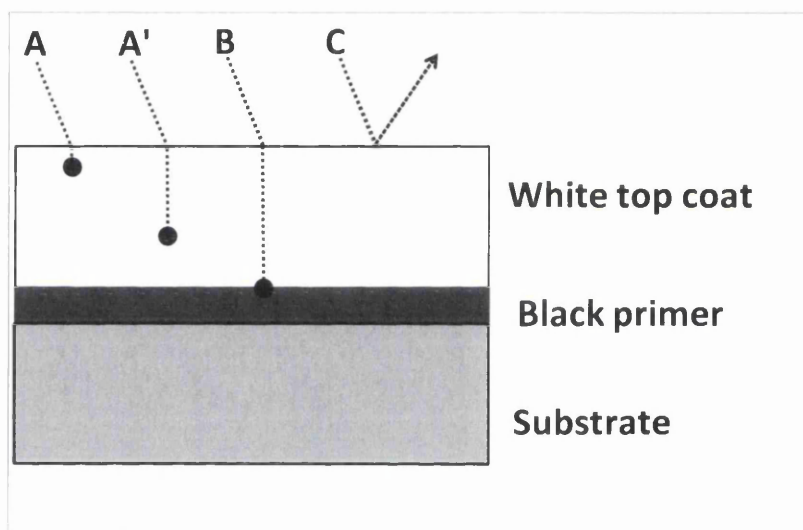


**Figure 4.17 – Proposed Mechanisms for Photon Interaction with Coating System**

Benefits of tinting the primer layer are that mechanism B will result in heating of the top coat by conduction from the primer, causing the bottom most layers of the top coat closest to the primer to heat up very quickly. This will drive solvents outwards from the region in which they have furthest to diffuse. Lower regions of the coating will cure before the upper regions; methanol, the resin cross-linking by-product will escape more easily and solvent boil will be minimised.

There is therefore scope for improved energy efficiency by increasing the amount of incident radiation absorbed without altering the colour properties of the coating. The increased IR absorbance of the primed surface allows for either increased line speeds or reduced oven power settings to reach a given PMT value.



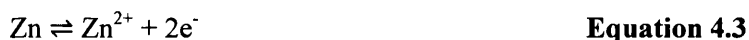
#### 4.3.4 Effect of Carbon Black Tinted Primer on Corrosion Performance of Galvanised Steel Substrate

The presence of carbon black in the primer layer improves the efficiency of the convection cure of a white polyester top coat, but there is a risk that this improvement may be counter balanced by a detrimental effect on the corrosion protection ability of the coating system. Due to the position of carbon in the galvanic series [6], carbon black pigment in the primer which is in electrical contact with zinc in the galvanised steel substrate could act as an under film cathode and accelerate coating delamination through a corrosion driven cathodic disbondment mechanism.

The cathodic disbondment mechanism is shown diagrammatically in Figure 4.18. In this mechanism, cathodic disbondment of the coating occurs in the vicinity of the delamination front due to oxygen reduction at a local cathode [8, 10], shown by the half reaction in Equation 4.2.



Anodic zinc dissolution is constrained to the coating defect region, and is shown by the half reaction in Equation 4.3.



A thin layer of electrolyte is able to make its way under the disbonding coating thus allowing the formation of an electrochemical cell.

The SKP is an ideal tool for studying the electrochemical delamination process at a coating substrate boundary, hence a SKP and model PVB coatings with and without carbon black additions were used to see the effect of carbon black being in contact with the hot dip galvanised steel substrate.

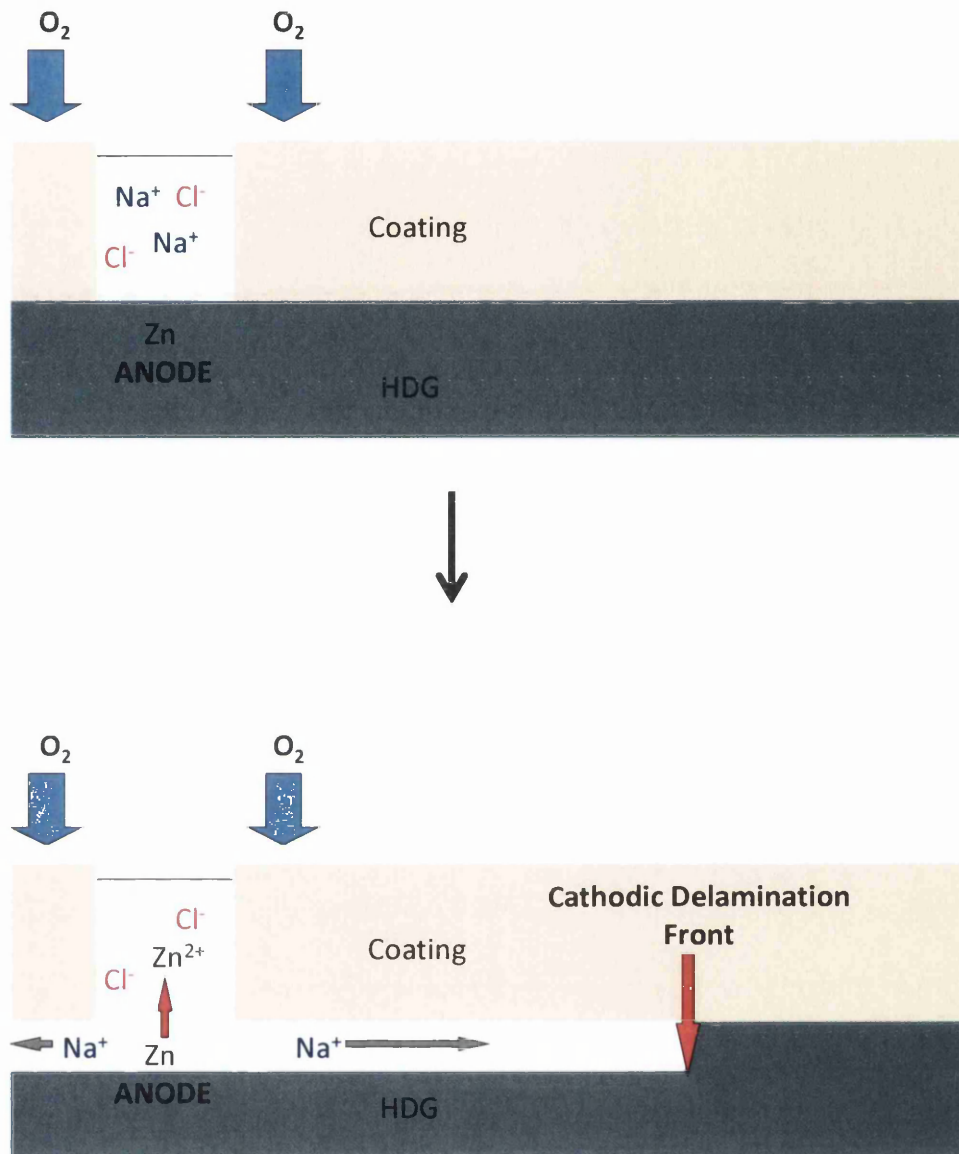
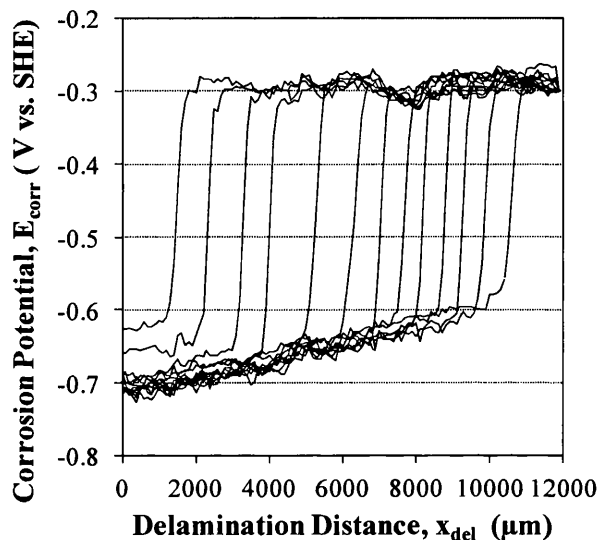


Figure 4.18 – Cathodic Disbondment under a Coating on Galvanised Steel

Firstly, a control delamination experiment was used to characterise the baseline kinetics of a delamination cell under a PVB coating with no carbon black addition on HDG. Figure 4.19 shows a typical time-dependant corrosion potential ( $E_{\text{corr}}$ ) vs. delamination distance ( $x_{\text{del}}$ ) profile established upon the addition of 5% wt/v NaCl (aq) to the sample defect.



**Figure 4.19 – Profiles of Time Dependant  $E_{\text{corr}}$  vs. Distance from an Artificial Coating Defect ( $x_{\text{del}}$ ) for a HDG Substrate Coated with Uninhibited PVB Measured Hourly from 0 min (left) to 840 min (right) where Delamination was Initiated with 5% wt/v Aqueous NaCl Solution and Experiments were Carried Out in 95% r.h.**

$E_{\text{corr}}$  values of the undelaminated region ( $E_{\text{intact}}$ ) in Figure 4.19 approximate to -0.3 V vs. SHE and indicate a passive zinc surface with the value for  $E_{\text{intact}}$  directly comparable to the potential for an uncoated galvanised surface in humid air. As time progresses, a change in electrochemical activity is observed, as the intact substrate-coating is replaced by substrate-electrolyte and electrolyte-polymer interfaces, as shown in Figure 4.18 [15]. This is indicative of a delamination front, and is shown by the characteristic steep potential drop of ca. 0.3 - 0.4 V vs. SHE, with the location of the delamination front being measured from the defect to the inflection midpoint of the profile.

Figure 4.19 also shows that by ca. 180 min after the addition of electrolyte, measured  $E_{\text{corr}}$  values in the region in direct proximity to the defect approximate the equilibrium potential of the reaction in Equation 4.2 i.e. ca. -0.76 V vs. SHE. The delamination front then moves progressively away from the defect, reaching a distance of ca. 11000  $\mu\text{m}$  over a period of 840 minutes.

Previous work has shown that the migrational mass transport of cations ( $\text{Na}^+$  ions in these experiments) from the defect region to the delamination front limits the ionic current linking the electrochemical half reactions, and hence the rate of delamination [15]. Therefore the ingress of  $\text{Na}^+$  ions, the loss of coating adhesion and the onset of oxygen reduction in Equation 4.2 can be seen to be associated with the steep potential drop of the delamination front in Figure 4.19. Here, the time elapsed since the introduction of electrolyte ( $t_{\text{del}}$ ) and the distance ( $x_{\text{del}}$ ) over which delamination has occurred are given by:

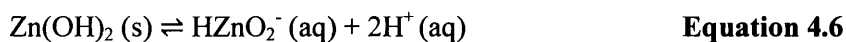
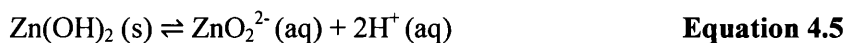
$$x_{\text{del}} = k_{\text{del}} (t_{\text{del}} - t_i)^{1/2} \quad \text{Equation 4.4}$$

where:

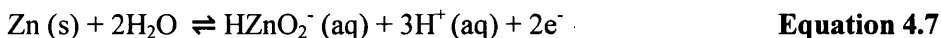
$t_i$  = time for delamination cell to become initiated following electrolyte addition

$k_{\text{del}}$  = delamination rate constant

The oxygen reduction in Equation 4.2 results in increased alkalinity at the delamination front, where previous research has shown values of pH 10-11 can be reached [16]. High alkalinity is favourable for disbondment as it aids polymer coating degradation. Eventually the high alkalinity will result in soluble zincate ( $\text{ZnO}_2^{2-}$ ) and bizincate ( $\text{HZnO}_2^-$ ) formation by the anodic equilibrium reactions in the underfilm area shown in Equations 4.5 and 4.6.



As the Zn(OH)<sub>2</sub> surface layer dissolves in the high pH environment of the under film region, the bare zinc that is revealed will have the ability to directly oxidise to bizincate by Equation 4.7 [8].



Delamination experiments were then carried out with a delamination cell under PVB coatings with carbon black additions on HDG. Additions of 0.5%, 3.5% and 5.0% wt. carbon black were made to a PVB coating and applied to a HDG substrate. At all addition percentages  $E_{\text{intact}}$  values were comparable to those in the control experiments indicating that the presence of carbon black in the coating has minimal effect on the steady-state delamination cell potentials.

PVB coatings with 0.5% and 3.5% carbon black additions gave time dependant  $E_{\text{corr}}$  delamination profiles that were similar to that of the control experiment shown in Figure 4.19 and displayed  $E_{\text{corr}}$  values of ca. -0.7 V vs. SHE at the defect boundary. There was, however a slight increase in the time ( $t_i$ ) taken for the delamination cell to become initiated following the addition of electrolyte, with 3.5% carbon black coatings showing an increase to 240 min.

A representative plot from an experiment with 5.0% carbon black coating content is shown in Figure 4.20. Here the first profile that shows the distinctive drop in potential representing the initiation of delamination was recorded at 600 min; this is an increase in the time taken for delamination to be established compared to the control. Also, the  $E_{\text{corr}}$  values recorded in close proximity to the defect region fall more slowly than the control and those with lower carbon black content, but they do eventually approach values associated with Equation 4.2 after ca. 900 min.

Most interestingly, 5% carbon black additions reduce the rate of delamination. This can be seen in a plot of  $x_{\text{del}}$  vs.  $(t_{\text{del}} - t_i)^{1/2}$  shown in Figure 4.21, where  $x_{\text{del}}$  is the distance over which delamination has occurred,  $t_{\text{del}}$  is the time elapsed since the application of electrolyte and  $t_i$  is time for delamination to become initiated following electrolyte addition.

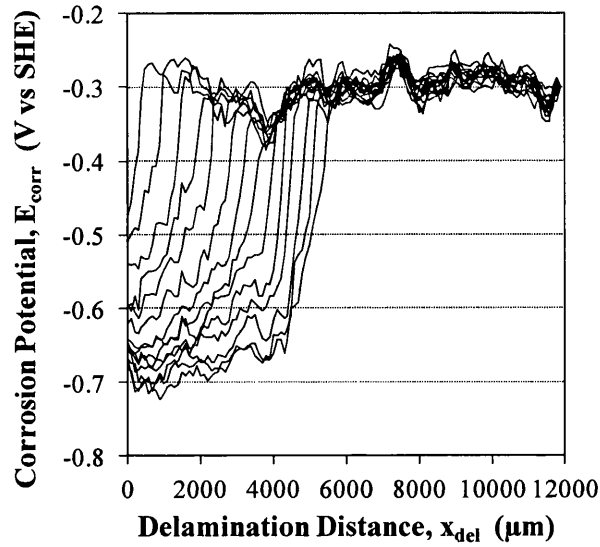


**Figure 4.20 - Profiles of Time Dependant  $E_{corr}$  vs. Distance from an Artificial Coating Defect ( $x_{del}$ ) for a HDG Substrate Coated with PVB Containing 5% Carbon Black, Measured Hourly from 600 Min (Left) to 1440 Min (Right)**

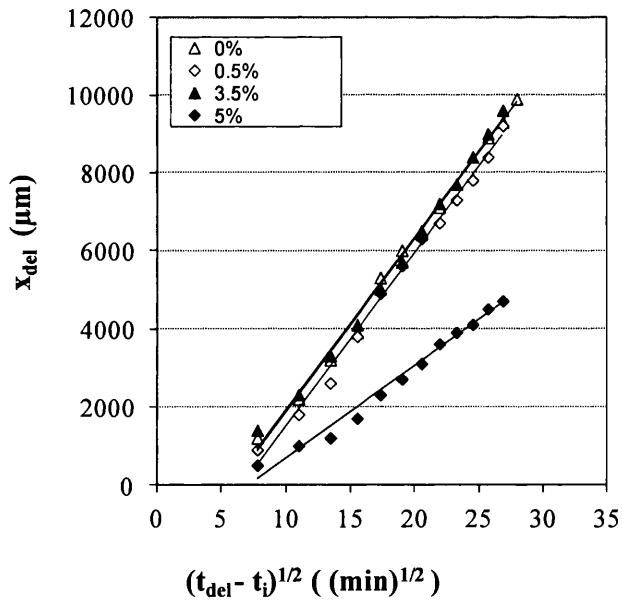


**Figure 4.21 – Plots of  $x_{del}$  vs.  $(t_{del} - t_i)^{1/2}$  for PVB Coated HDG Substrates where Additions of 0%, 0.5%, 3.5% and 5% Carbon Black have been made to the PVB Coating**

Values for the delamination rate constant  $k_{del}$  for 0%, 0.5% and 3.5% carbon black additions were 444, 442 and 440  $\mu\text{m min}^{-1/2}$  respectively. Additions of 5% carbon black however, gave a  $k_{del}$  value of 247  $\mu\text{m min}^{-1/2}$ , a reduction of ca. 44% compared to the control. These values are summarised in Table 4.1.

**Table 4.1 – Values of Parabolic Rate Constant and Time to Delamination Determined for PVB Coatings Containing Various Values of Carbon Black on HDG Substrates.**

Carbon black (%)	$t_i$ (min)	$k_{del}$ ( $\mu\text{m min}^{-1/2}$ )	$k_{del}$ change (%)
0	180	444	0
0.5	180	442	0.45
3.5	240	440	0.9
5.0	600	247	44.4

As all the plots in Figure 4.21 are linear, this suggests that rate control in the delamination cell is due to migration of under film  $\text{Na}^+$  ions from the external electrolyte to the delamination front when carbon black is present in the coating at any of the experimental levels [15, 17]. It also indicates that the oxygen reduction reaction occurring at the delamination front is not being blocked.

Leng has shown that high levels of water are present at the substrate-polymer coating boundary of unpigmented coatings when the coating has been exposed to high levels of humidity. This is because water is able to diffuse through the polymer layer to reach this boundary, and will hence provide an environment that will favour oxygen reduction. Delamination, however will not occur unless electrolyte has been able to ingress [15]. The increasing time for delamination ( $t_i$ ) to become established in these experiments may be due to the presence of carbon black in the PVB coating increasing the hydrophobicity of the coating and increasing the time taken for water to diffuse through the coating [18].

Five percent carbon black additions cause a reduction in delamination rate by ca. 44%. As water can rapidly permeate through a coating in a delamination cell [15], and the ingress of an electrolyte layer under a coating can occur as a highly swollen polymer gel [19], an explanation of the reduction in delamination rate could be that at 5% carbon black loading the path for  $\text{Na}^+$  ion migration has become longer. Another explanation

may be that the conductive nature of carbon means that the cathodic reduction of oxygen is displaced away from the metal/coating boundary into the coating, hence suppressing delamination [20].

#### **4.4 Conclusions**

We have shown that an increase in NIR curing efficiency or reduction in oven dwell time can be achieved when a NIR absorbing primer is used with the NIR cure of a white top coat [3, 4]. In this scenario energy emitted from NIR curing lamps where most of the radiation is focused between 800 – 1200 nm, is being absorbed in the coating system [21].

This chapter shows a smaller increase in efficiency is also seen when cure is carried out in a laboratory convection oven; in this case a 5% lower peak metal temperature (PMT) is reached when a standard primer is used rather than a 5% carbon black tinted primer, with the oven set at 355 °C [4, 13]. Alternatively, oven dwell time can be reduced by ca. 3 secs. In this case a carbon black tinted primer is allowing an increase in the absorption of residual mid infrared radiation emitted from the hot walls of the convection oven.

Industrial coil coating convection ovens can be run in excess of 400°C, such as at the former Tata Steel Tafarnaubach Works [22]. At these higher oven temperatures the increase in the non perfect black body emission from the oven walls is likely to result in an even greater percentage change in top coat PMT when a tinted primer is used. In this scenario it would be worth conducting an industrial line trial to assess the potential to reduce oven power settings. Polyester top coat ovens at Tata Steel Shotton Works, however, are commonly set to between 250 and 320 °C [23]. At these lower oven temperatures the potential to reduce oven power settings will be less.

Carbon black however can act as a cathode, so there is the possibility that its presence may drive cathodic disbondment reactions in the coating system. SKP disbondment studies with model PVB coatings were carried out to investigate this concern. The presence of carbon black was found to have little effect on the rate of cathodic disbondment; indeed at 5% loading there is evidence that carbon black may actually inhibit these reactions [13].



## 4.5 References

1. Knischka, R., Lehmann, U., Stadler, U., Mamak, M., and Benkhoff, J., *Novel approaches in NIR curing technology*. Progress in Organic Coatings, 2009. **64**(2-3): p. 171-174.
2. Bar, K., *How to save energy costs with the NIR-technology in coil coating processes*. Steel Grips, 2006. **3**: p. 225-228.
3. Mabbett, I., Elvins, J., Gowenlock, C., Jones, P., and Worsley, D., *Effects of highly absorbing pigments on near infrared cured polyester/melamine coil coatings*. Progress in Organic Coatings, 2013. **76**(9): p. 1184-1190.
4. Gowenlock, C.E., Mabbett, I., and Worsley, D.A., *Optimization of near infrared cured polyester/melamine coil coatings by the use of near infrared absorbing primers*. GSTF Int J Eng Tech, 2013. **2**(2): p. 47-50.
5. Mabbett, I., *Applications of Near Infrared Heating of Interest to the Coil Coating Industry*. 2011, Eng. D., Swansea University
6. Trethewey, K.R. and Chamberlain, J., *Corrosion for Science and Engineering*: 2 ed. 1995, Longman Scientific and Technical: Essex.
7. Fürbeth, W. and Stratmann, M., *The delamination of polymeric coatings from electrogalvanized steel – a mechanistic approach.: Part 3: delamination kinetics and influence of CO<sub>2</sub>*. Corrosion Science, 2001. **43**(2): p. 243-254.
8. Fürbeth, W. and Stratmann, M., *Scanning Kelvinprobe investigations on the delamination of polymeric coatings from metallic surfaces*. Progress in Organic Coatings, 2000. **39**(1): p. 23-29.
9. Williams, G., Geary, S., and McMurray, H.N., *Smart release corrosion inhibitor pigments based on organic ion-exchange resins*. Corrosion Science, 2012. **57**(0): p. 139-147.
10. Williams, G. and McMurray, H.N., *Chromate inhibition of corrosion-driven organic coating delamination studied using a scanning Kelvin probe technique*. Journal of the Electrochemical Society, 2001. **148** (10): p. B377-B385.
11. Williams, G., McMurray, H.N., and Worsley, D.A., *Latent fingerprint detection using a scanning Kelvin microprobe*. Journal of Forensic Sciences, 2001. **46**(5): p. 1085-1092.

12. Stratmann, M., Leng, A., Furbeth, W., Streckel, H., Gehmecker, H., and GrosseBrinkhaus, K.H., *The scanning Kelvin probe; A new technique for the in situ analysis of the delamination of organic coatings*. Progress in Organic Coatings, 1996. **27**(1-4): p. 261-267.
13. Mabbett, I., Elvins, J., Gowenlock, C., Glover, C., Jones, P., Williams, G., and Worsley, D., *Addition of carbon black NIR absorber to galvanised steel primer systems: influence on NIR cure of polyester melamine topcoats and corrosion protection characteristics*. Progress in Organic Coatings, 2014. **76**: p. 1184-1190.
14. Ireson, R. and Wullink, J., *Thermographical analysis of NIR heat treatments of coated steel panels using the AdPhos Technicum*. 2008, Corus Research, Development & Technology.
15. Leng, A., Streckel, H., and Stratmann, M., *The delamination of polymeric coatings from steel. Part 1: Calibration of the Kelvinprobe and basic delamination mechanism*. Corrosion Science, 1998. **41**(3): p. 547-578.
16. Leng, A., Streckel, H., and Stratmann, M., *The delamination of polymeric coatings from steel. Part 2: First stage of delamination, effect of type and concentration of cations on delamination, chemical analysis of the interface*. Corrosion Science, 1998. **41**(3): p. 579-597.
17. Leidheiser, H., Wang, W., and Igetoft, L., *The mechanism for the cathodic delamination of organic coatings from a metal surface*. Progress in Organic Coatings, 1983. **11**(1): p. 19-40.
18. Zhang, W.-g., Li, L., Yao, S.-w., and Zheng, G.-q., *Corrosion protection properties of lacquer coatings on steel modified by carbon black nanoparticles in NaCl solution*. Corrosion Science, 2007. **49**(2): p. 654-661.
19. Grundmeier, G., Reinartz, C., Rohwerder, M., and Stratmann, M., *Corrosion properties of chemically modified metal surfaces*. Electrochimica Acta, 1998. **43**(1-2): p. 165-174.
20. Lacroix, J.C., Camalet, J.L., Aeiayach, S., Chane-Ching, K.I., Petitjean, J., Chauveau, E., and Lacaze, P.C., *Aniline electropolymerization on mild steel and zinc in a two-step process*. Journal of Electroanalytical Chemistry, 2000. **481**(1): p. 76-81.

21. Cherrington, M., Claypole, T.C., Deganello, D., Mabbett, I., Watson, T., and Worsley, D., *Ultrafast near-infrared sintering of a slot-die coated nano-silver conducting ink*. Journal of Materials Chemistry, 2011. **21**(21): p. 7562-7564.
22. Personal communication with Potter, B., Tata Steel, Tafarnaubach Works. May 2012
23. Personal communication with Crinson, J., Tata Steel, Shotton Works. March 2014

**Chapter 5**  
**The Effect of Backing Coat**  
**Absorbing Pigments on Top Coat**  
**NIR Cure**

## 5.1 Introduction

We have shown that polyester coil coating top coats cure more easily with NIR if the top coat is relatively transparent to NIR radiation, with most of the absorption of the NIR occurring at the surface of the substrate underneath. In essence, this cures the coating from the bottom layer of the coating upwards and helps to avoid solvent boil. Hence a white coating with titanium dioxide pigment cures with a wider cure window and with less problems with solvent boil than a black coating pigmented with carbon black [1].

Moreover this principle can be extended to show that pigmenting the primer layer with a 5% NIR absorbing pigment such as carbon black, results in an 18% higher top coat PMT during NIR cure compared to using a standard primer. In Chapter 4 it was shown that in convection cure a 5% higher PMT results [2, 3].

A schematic of the layer structure of Tata Steel's 25  $\mu\text{m}$  polyester coil coating system on a galvanised steel substrate is shown in Figure 5.1. The aim of this chapter was to investigate whether NIR absorbing pigments could be added anywhere else in this coating system to obtain NIR curing energy savings.

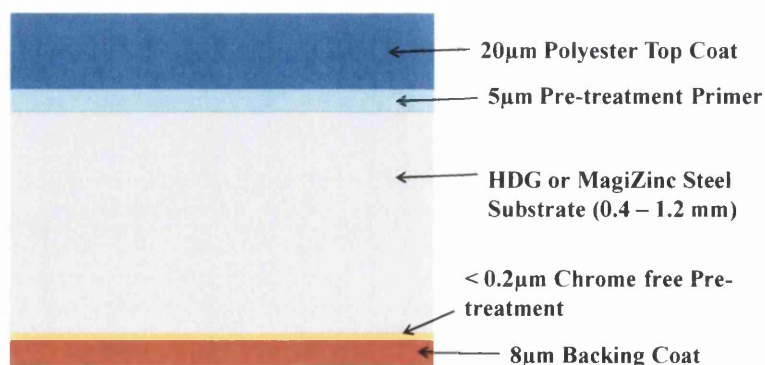


**Figure 5.1 - Schematic of the Layer Structure of Tata Steel's 25  $\mu\text{m}$  Polyester Coil Coating Galvanised Steel Substrate**

Knischka et al added a ceramic NIR absorbing pigment with a high level of transparency in the visible region to an 80 µm dft polyester coil coating top coat applied onto primed aluminium or glass pane substrates. A 0.05% w/w pigment loading was reported to lead to more than a doubling of the NIR cure line speed when added to a 45.0 % w/w titanium dioxide pigmented top coat [4]. However, in more recent research we suggest that NIR pigment additions to a top coat may increase the chance of surface blistering and reduce the size of the cure window [1]. This is likely to be particularly true at greater dry film thicknesses where the solvent has a further distance to travel before escaping.

In view of this it was decided to investigate the addition of NIR absorbing pigments to the backing coat of the coil coating system. As shown in Figure 5.1, the backing coat is only 40% of the thickness of the top coat and therefore solvents escaping from the backing coat during cure will have a shorter distance to diffuse through the coating depth compared to with a top coat. This will mean that there should be a much lower chance of a backing coat blistering when NIR absorbing pigments are added to the coating compared to a top coat. The quality of the surface finish of a backing coat and the colour specifications will also be less critical compared to that for a top coat. The beneficial principle of heating the top coat from the bottom layer of the coating upwards is also maintained, thus helping to minimise blistering in the top coat.

The backing coat used in Tata Steel's DVL2 coil coating product is either white or grey in colour, with products manufactured with a white backing coat forming the larger part of the sales volume. A NIR absorbing pigment with a high level of transparency in the visible region is therefore needed, particularly to maintain the colour of the white backing coat. Various NIR absorbing pigments were supplied by BASF and Merck for this investigation.

## 5.2 Experimental Techniques

### 5.2.1 Polyester Coating Formulation

White and grey polyester backing coats were Akzo Nobel commercial formulations supplied via Tata Steel IJmuiden, as used at their DVL2 NIR curing production line. Three sets of the white polyester backing coats pigmented with either Iriotec 8840, IR202 or IR203 pigment were prepared with a range of percentages of pigment up to 1% w/w using a high shear mixer at 1400 rpm. Even dispersion of the fine pigment powder in the paint was aided by first mixing the pigment powder to a paste with a little of the liquid coating. A Fineness of Grind (Hegman) gauge was used to check pigment agglomerates were less than 15µm in size.

White and RAL 9006 silver polyester coatings were made up by the pigment paste and converter method given in Section 2.1.1.

### 5.2.2 NIR Curing Trials using an AdPhos NIR Oven

#### 5.2.2.1 Single Sided Curing Trials

Panels of 0.56 µm MZ substrate (composition given in Table 2.3) were drawn down with white or grey polyester backing coat as described in Section 2.1.2. Samples were carried out in triplicate. Details of the samples are given in Table 5.1.

**Table 5.1 – Coated Samples for NIR Curing**

<b>AdPhos Oven</b>	<b>Panel Size (mm)</b>	<b>Backing Coat dft (µm)</b>
Technicum	200 x 300	10±1
Lab Unit	100 x 200	14±1

### 5.2.2.2 Double Sided Curing Trials

Additional MZ panels were drawn down with backing coat and cured as above. A chrome free pretreatment-primer layer (Henkel Granocoat 2840) was drawn down on the other side of the panel to give a dft of 5-7  $\mu\text{m}$  after curing for 60 s in a convection oven at 90°C.

This primer layer was then over coated with a silver polyester top coat (Beckers RAL 9006 NIR formulation) to give a dft of 15-17  $\mu\text{m}$  when cured using the AdPhos Technicum NIR Oven. The thermocouple was spot welded to the top side of the panel, with the experimental configuration shown in Figure 5.2.

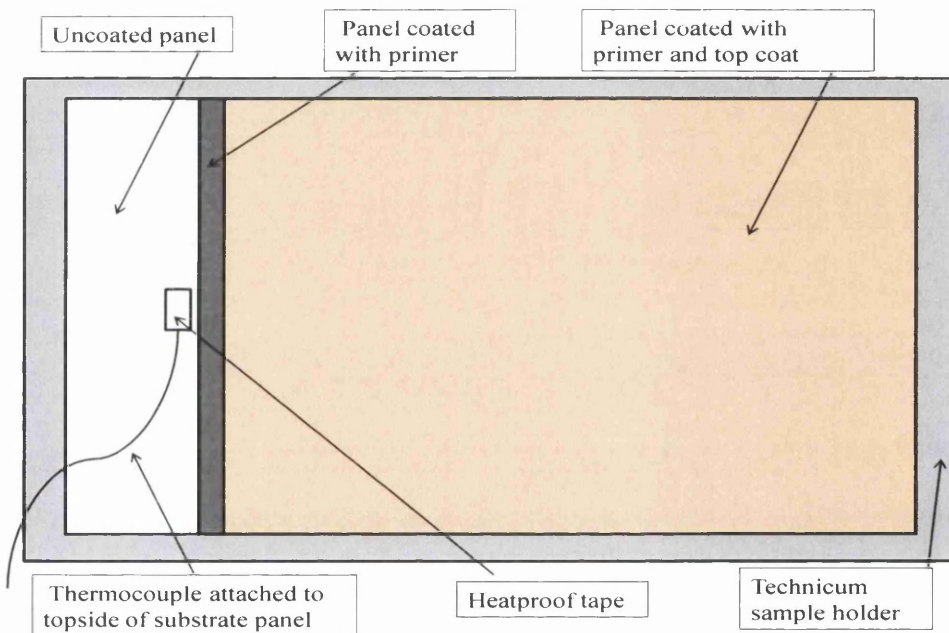


**Figure 5.2 - Schematic Showing Coated Panel in Technicum Sample Holder (Under Side of Panel Coated with Backing Coat)**

The final set of Technicum experiments involved panels with a double draw down of backing coat pre-cured in a convection oven at 370°C. Half of the back of the panel was coated with non-pigmented white backing coat and the other half coated with pigmented backing coat (either 0.5 or 1.0% wt. IR202), as shown in Figure 5.3. The aim of this experiment was to make a direct comparison within one panel of the PMT reached by a top coat on either side of the panel.



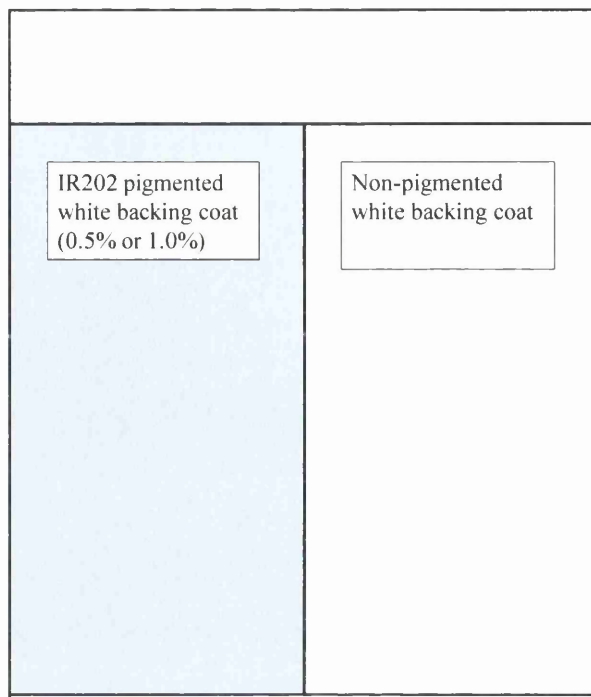


**Figure 5.3 - Schematic showing Back of Substrate Panel with a Double Draw Down of White Backing Coat**

White polyester top coat (formulation given in Section 2.1.1.2) was draw down on the front side of the panels to give a dft of 17-18  $\mu\text{m}$ . With a line speed of 9 m/min, lamp settings were optimised for white top coat cure at 65%, 0% and 75% power in zones 1, 2 and 3 respectively. Twelve replicates of samples were run.

The temperatures of the panels were monitored during the cure process by data loggers recording data from K type thermocouples spot welded to the front of the panel, close to the top coat and is shown in Figure 5.4. The Technicum's data logger only has one data channel so additional data was acquired using a Grant Instruments Squirrel data logger. The Squirrel data logger collected data from the pigmented and non-pigmented side of the panel, whilst the Technicum's data logger collected data from the pigmented side. One piece of heat resistant tape was placed over each thermocouple spot weld and also over the thermocouple wires near to the panel edge, to give extra strength to the spot weld.

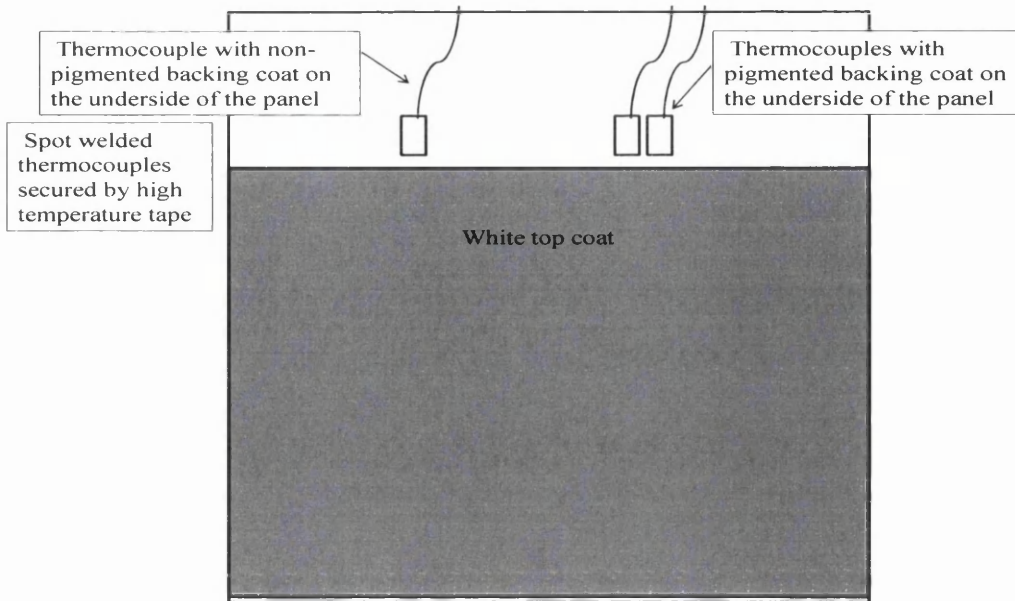


**Figure 5.4 - Schematic Showing Front of Substrate Panel Drawn Down with White Top Coat**

## 5.3 Results and Discussion

### 5.3.1 Comparison of White and Grey Backing Coats using the AdPhos NIR Lab Unit and AdPhos Technicum

Initial experiments involved the investigation of white and grey backing coats on the back of MZ substrate panels, to see how the backing coat affected the temperature reached by the uncoated top coat side of the panel during NIR cure. UV-Vis-NIR reflectance spectra of an uncoated MZ panel and panels coated with white backing coat or grey backing coat are shown in Figure 5.5. The panel coated with grey backing coat has the lowest reflectance (highest absorption) in the NIR region, and if used as a backing coat during NIR cure could be expected to have a greater ability to increase the PMT reached by the top coat compared to the white backing coat. Note that the step change in reflectance at ca. 860 nm in all spectra can be attributed to a changeover in the spectrophotometer's detector.

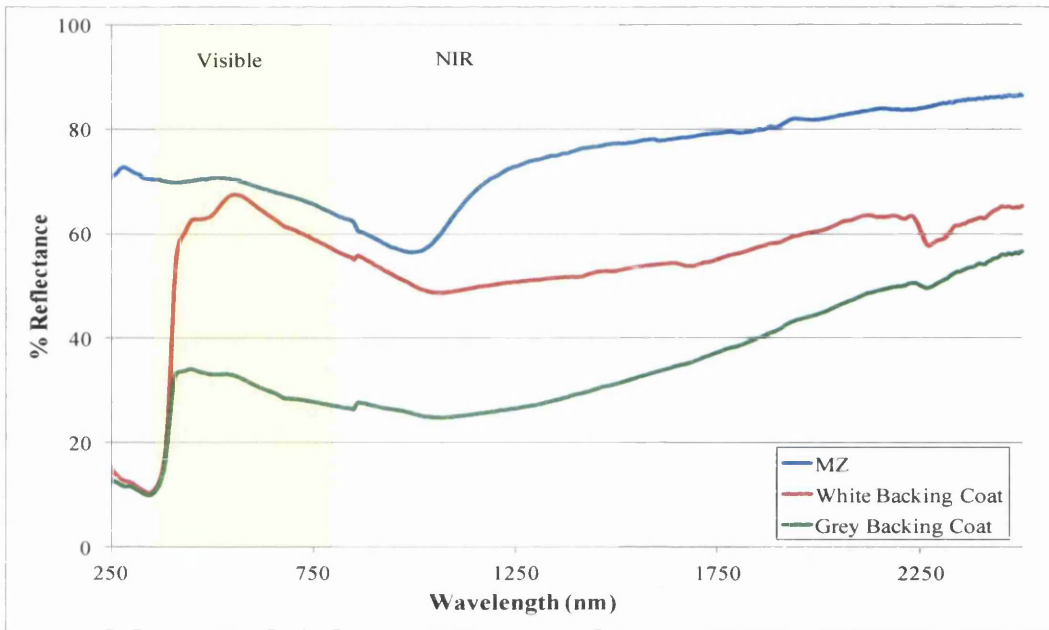


**Figure 5.5 - UV-Vis-NIR Reflectance Spectra of MZ, White Backing Coat and Grey Backing Coat**

A set of curing experiments were carried out in an ‘upside down’ configuration on both the AdPhos NIR Lab Unit and the AdPhos Technicum. Panels of either bare MZ, or MZ panels coated with white or grey backing coat were irradiated with the top set of lamps only and the temperature of the underside of the panel measured with a spot welded thermocouple. As the experiments were ‘upside down’ experiments the topside of the panel (irradiated side) represented the backing coat of the coating system, and the temperature recorded by the thermocouple represented the temperature that a top coat would be able to reach when different backing coats are used. The white and the grey backing coats were coated at a dft of  $15 \pm 1 \mu\text{m}$  for both oven cures. The temperatures reached by the top coat side of the substrate are shown in Figure 5.6; both curing ovens show a trend of increasing temperature on the topside of the panel on changing from uncoated MZ on the back of a panel, to coating with a white backing coat, to coating with a grey backing coat. A direct comparison of PMT cannot be made between the same backing system cured with the two different ovens due to the different lamp zone configurations and extraction systems of the two ovens, and different NIR lamp power settings and substrate panel sizes being used. The lamp power settings and coating thickness for each coating cured on the same oven were the same. However,

both sets of experiments show broadly the same relative increases in temperature comparing substrate panels with backing coat to bare substrate panels, as shown in Table 5.2. This is consistent with the reflectance spectra.

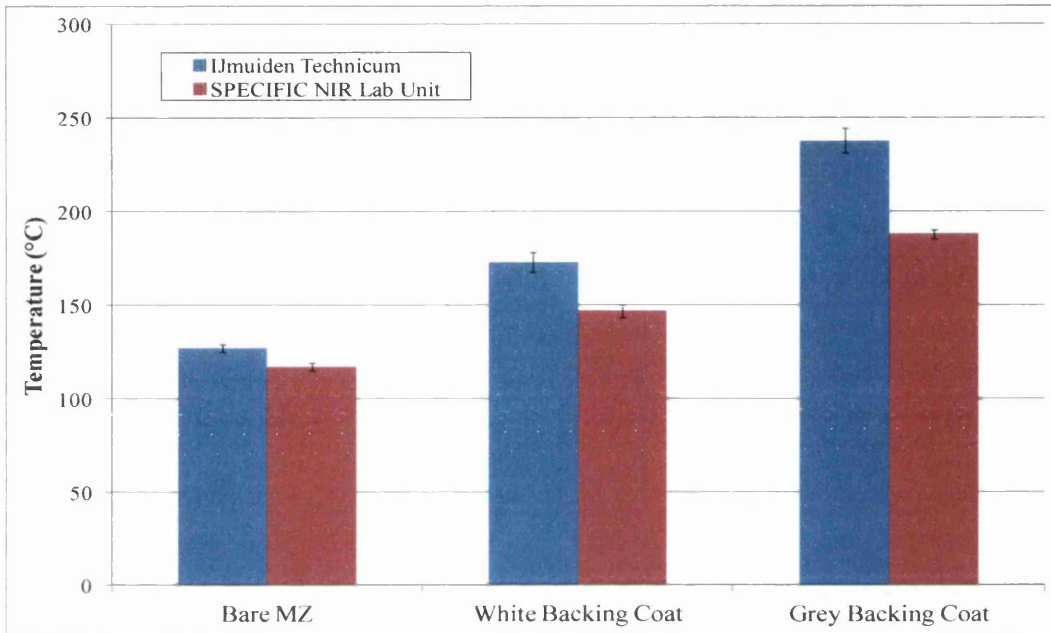


**Figure 5.6 – Temperature Reached during NIR Cure by the Top Coat Side of Substrate Panels, with Three Different Backing Systems**

**Table 5.2 – Comparison of Relative Temperature Increases during NIR Cure with Different NIR Ovens**

<b>Curing Oven</b>	<b>% temperature increase with white backing coat compared to bare MZ</b>	<b>% temperature increase with grey backing coat compared to bare MZ</b>
Technicum	36	87
Lab Unit	26	61

A RAL 9006 silver metallic coloured top coat was then cured from the back with a grey backing coat using the AdPhos Technicum, and reached a temperature 55°C higher than the same top coat cured at the same line speed and lamp settings with a white backing coat as shown in Figure 5.7. Moreover, the RAL 9006 top coat with the

grey backing coat had become over cured exhibiting fine micro-blistering. This experiment shows that a backing coat with reasonable absorption in the NIR, such as the grey backing coat, is able to significantly influence the PMT reached by a top coat during cure. This equates to the cure time of the silver metallic coloured top coat being reduced by ca. 34% when a grey backing coat is used rather than a white backing coat.

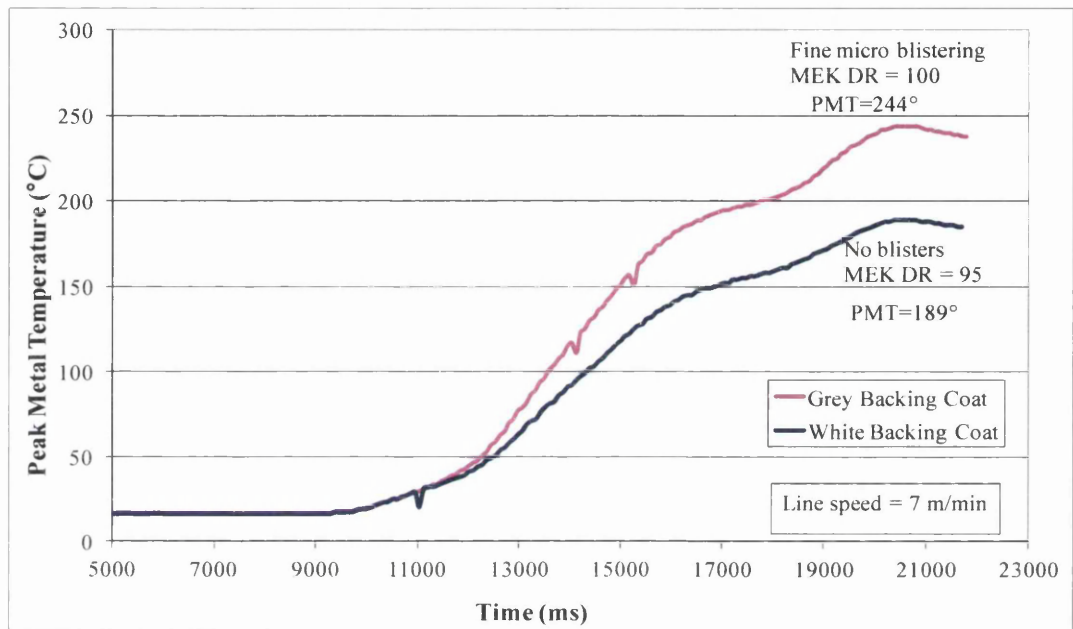


**Figure 5.7 - RAL 9006 Top Coat Cured from the Back with White and Grey Backing Coats using the Same NIR Lamp Power Settings and Line Speed**

Similar experiments were carried out using the AdPhos NIR Lab Unit. This time no thermocouples were attached, but a visual comparison of the panels was made, curing the panels at the same line speed and lamp power settings. The panel with the grey backing coat gave the most heavily blistered top coat, followed by the bare MZ panel and then the white backing coat panel, as shown in Figure 5.8 and Figure 5.9.

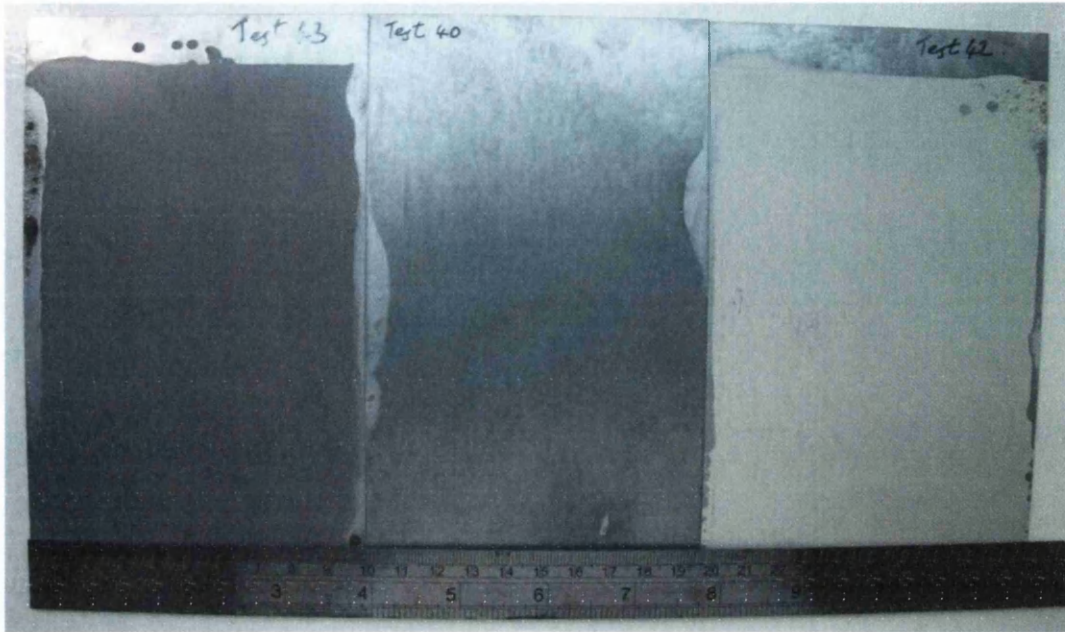


**Figure 5.8 – Underside of Substrate Panels, Cured with Same NIR Settings  
Grey Backing Coat (Left), Bare MZ (Middle) and White Backing Coat (Right)**



**Figure 5.9 – Corresponding Substrate Panel Topside (from  
Figure 5.8), Cured with Same NIR Settings  
with Silver Top Coat**

**Note the Increasing Level of Blistering on moving from Right to Left**

The heavier blistering of the top coat cured with a bare MZ underside surface compared to that with a white backing coat could be attributed to the relatively low emissivity of a metal surface such as MZ [5].

A comparison was made between RAL 9006 silver top coats cured from the back of the panel and is shown in Figure 5.10. In this set of experiments a white backing coat was used. The amount of NIR irradiation supplied was the same (NIR lamps in all three zones set to 100% with a line speed of 7 m/min), but the thickness of the top coat was varied.

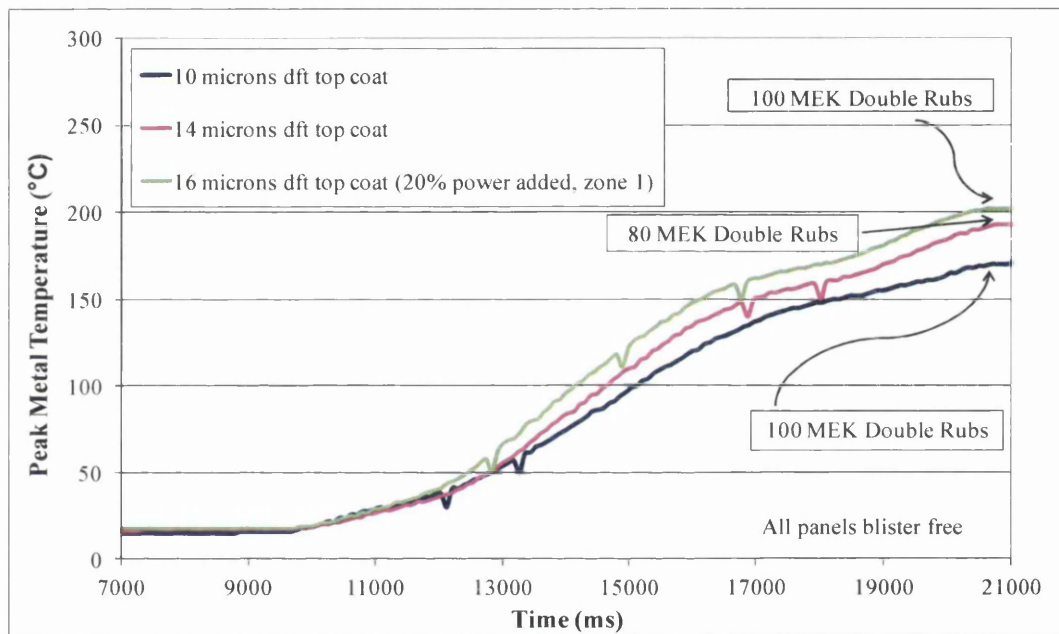


**Figure 5.10 – Typical Cure Profiles for Silver Top Coat Cured from the Back of the Panel with a White Backing Coat**

These experiments show that the cure is sensitive to the thickness of the top coat. The effect of increasing the thickness of the coating from 10  $\mu\text{m}$  to 14  $\mu\text{m}$  reduces the number of MEK double rubs achieved from 100 down to 80. The state of the cure was then restored back to 100 double rubs by adding an additional small amount of power (20%) from the front of the panel in zone 1 of the Technicum. All panels in these experiments were blister free. Increasing the thickness of the coating will increase the amount of aluminium flake present in the coating, hence increasing the PMT reached. There will also be more solvent present, which will have a greater distance to diffuse through the thicker coating to evaporate at the coating surface.

### **5.3.2 Effect of Additions of NIR Absorbing Pigment to the White Backing Coat on Top Coat Cure**

Three different NIR absorbing pigments were investigated; Iriotec 8840 (Merck) and IR202 and IR203 (BASF). Iriotec 8840 is a copper hydroxide phosphate, formula  $\text{Cu}_3(\text{PO}_4)_2 \cdot \text{Cu}(\text{OH})_2$  and is marketed as a laser marking additive for polymers using fibre, YAG and vanadate lasers operating in the 1060 - 1070 nm region of the electromagnetic spectrum [6]. This wavelength range is close to the maximum wavelength of emission for the Adphos emitters, 980 nm. IR202 and IR203 are developmental doped metal oxide pigments, produced by BASF as NIR absorbing pigments to aid NIR cure.

The white backing coat used on Tata Steel's DVL2 production line was prepared with various additions of Iriotec 8840, IR202 or IR203 pigment ranging from 0.1 – 1.0 % wt. As the BASF pigments were developmental pigments, no information was available about their formula or density so pigment additions were made on a percentage weight basis.

UV-Vis-NIR reflectance spectra of the Iriotec 8840 cured coating panels are given in Figure 5.11 and show that at these percentage weight additions Iriotec 8840 produces a negligible change in the NIR absorption of the white backing coat. The IR202 and IR203 pigments, however, have a greater effect on the NIR absorption of the coating at the same weight percentages as shown in the UV-Vis-NIR reflectance spectra in Figure 5.12. IR202 pigment produces the greatest increase in the NIR absorption of the coating, as shown in Figure 5.13.



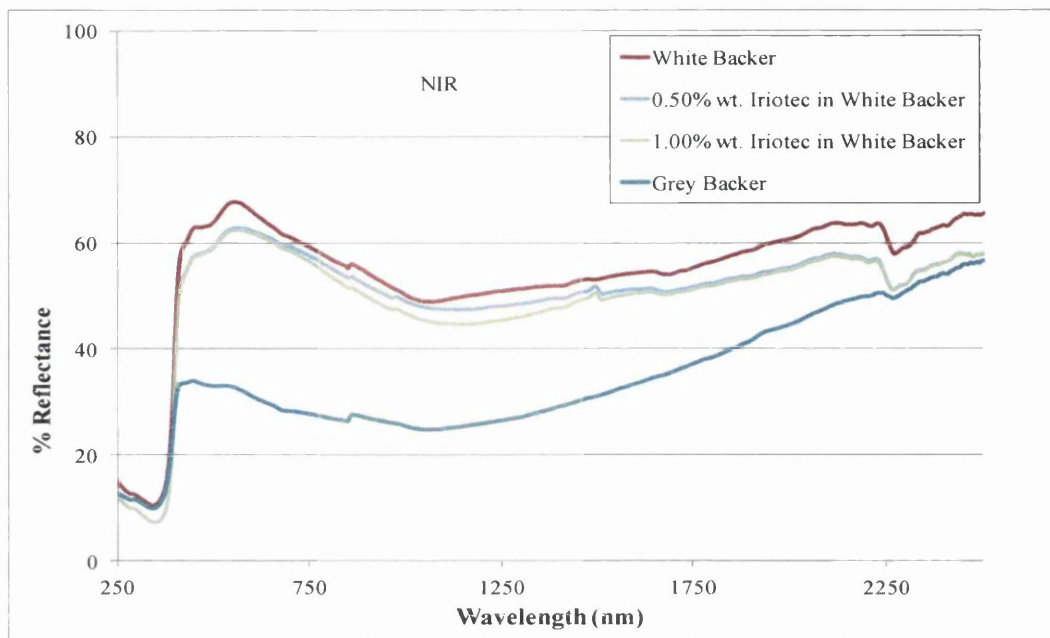


Figure 5.11 - UV-Vis-NIR Reflectance Spectra of Cured Backing Coat Panels with Various Additions of Iriotec 8840 Pigment

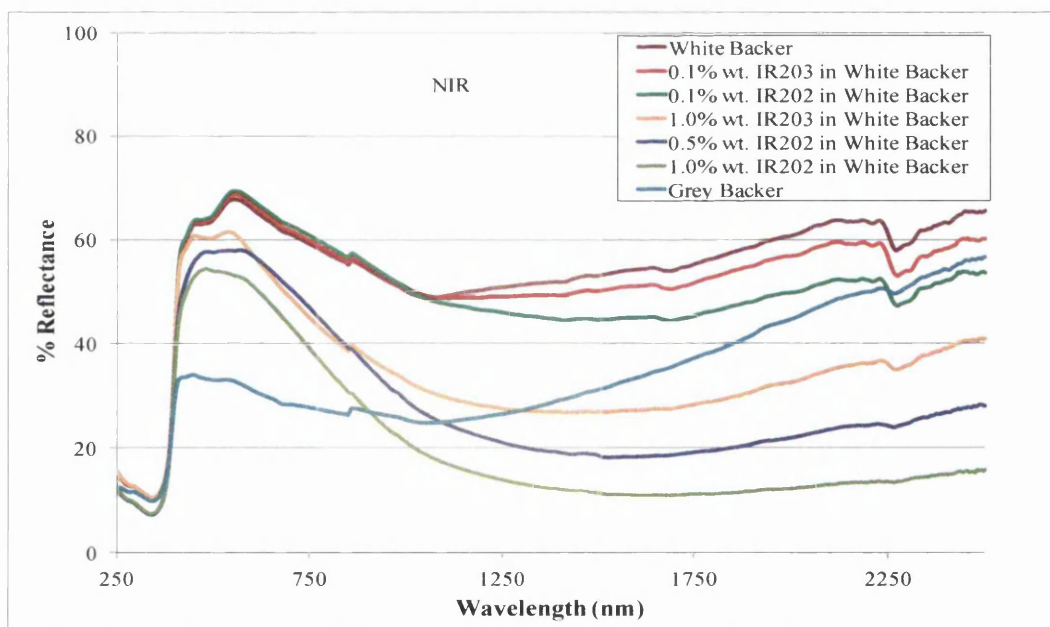
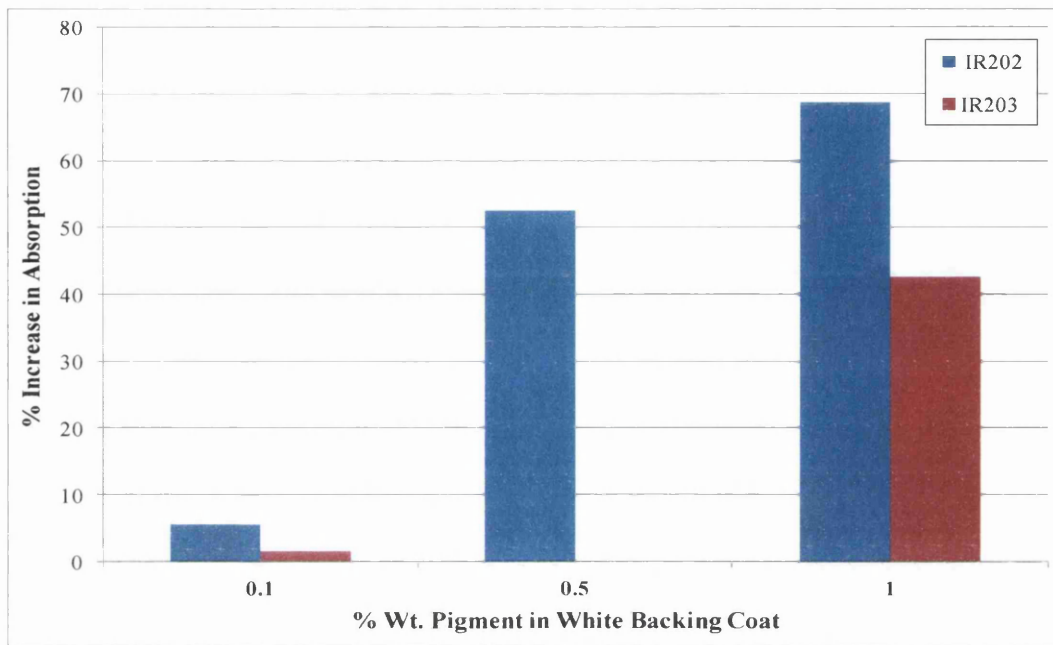
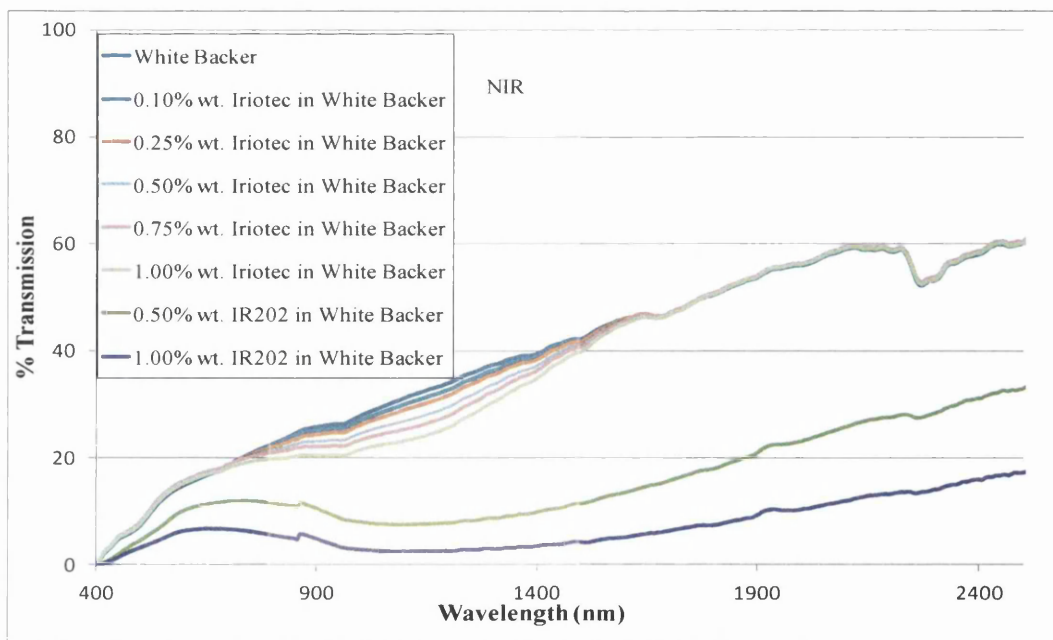


Figure 5.12 - UV-Vis-NIR Reflectance Spectra of Cured Backing Coat Panels with Various Additions of IR202 & IR203 Pigments



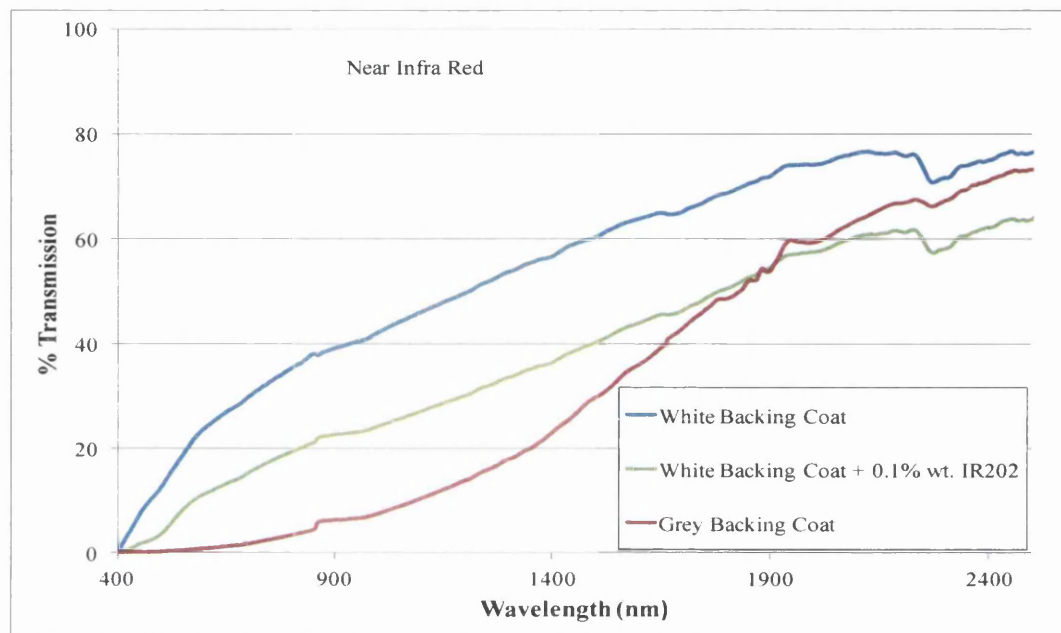
**Figure 5.13 – Percentage Increase in the NIR Absorption of a White Backing Coat with % Wt. Additions of IR202 & IR203 Pigments**

The addition of IR202 to the white backing coating results in a coating with a much lower transparency in the NIR compared to a coating pigmented with Iriotec 8840; however IR202 additions also reduces coating transmission in the visible and IR regions, as shown in the UV-Vis-NIR transmission spectra in Figure 5.14.



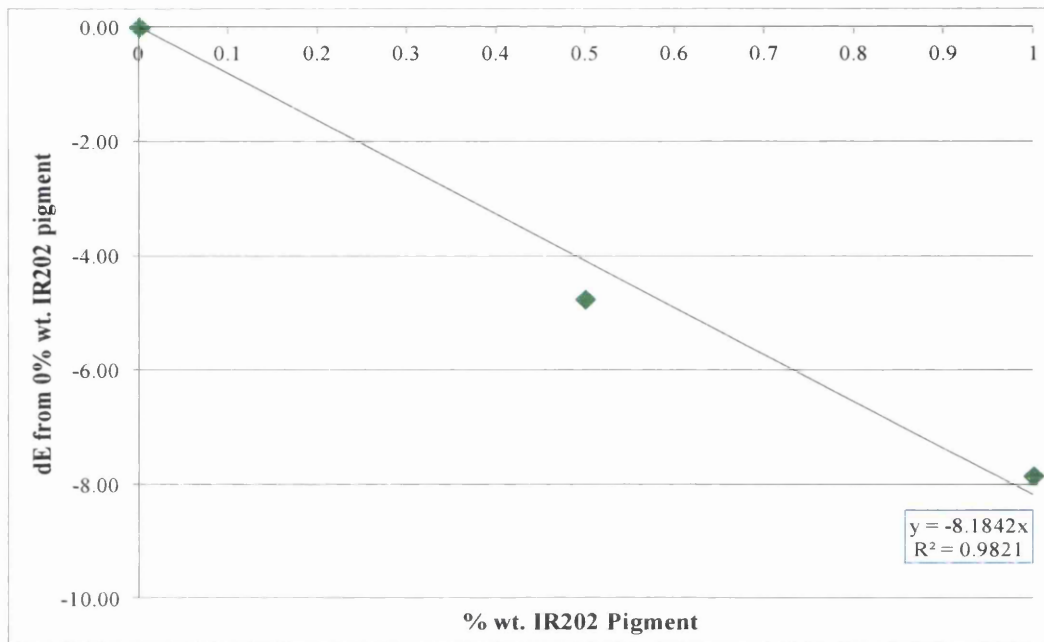
**Figure 5.14 - UV-Vis-NIR Transmission Spectra of Free-standing Films of White Backing Coat with Various Additions of NIR Absorbing Pigments**

Figure 5.15 shows that the addition of only 0.1% w/w IR202 pigment to a white backing coat has the effect of reducing the NIR transmission of the white coating to a level which is about equidistant between that of an un-pigmented white backing coating and a grey backing coating.



**Figure 5.15 - UV-Vis-NIR Transmission Spectra of Free-standing Films of White Backing Coats and Grey Backing Coat**

Figure 5.12 shows that in the visible region (wavelength 380 – 780 nm), additions of 0.1% wt. IR202 or IR 203 pigment produce very little change to the white backing coat reflectance spectrum. However, at a 1.0% wt. loading reflection is noticeably reduced. This is reflected in the Delta E\* colour difference chart shown in Figure 5.16; with a Delta E\* of ca. 1.0 a 0.1% wt. pigment loading of IR202 has a negligible effect on the colour of the white backing coat.



**Figure 5.16 - Change in White Backing Coat Colour with NIR Absorbing Pigment (IR202) Content**

The conclusion from these transmission and reflectance spectra results is that the IR202 pigment is likely to have the greatest potential of the three NIR pigments to increase the PMT reached by a top coat when used as a pigment addition in the backing coat, due to its greatest ability to absorb in the NIR region. IR202 pigment will have negligible effect on the colour of a white backing coat at 0.1% w/w addition.

A quick initial test of the likely effect on white top coat PMT, when NIR absorbing pigment is added to a white backing coat coated on the underside of the substrate panel was carried out using an AdPhos NIR Lab Unit. The temperature of the top coat side of the MZ substrate panel was measured by a thermocouple, with a white backing coat with increasing percentages of NIR absorbing pigments IR 202 and IR 203 coated on the underside. The results of these solo experiments are given in Figure 5.17 and show an increase in top coat PMT as the percentage of pigment in the backing coat is increased. IR202 gave a 42% increase in PMT at 1% weight addition, whilst IR203 gave a 28% increase.

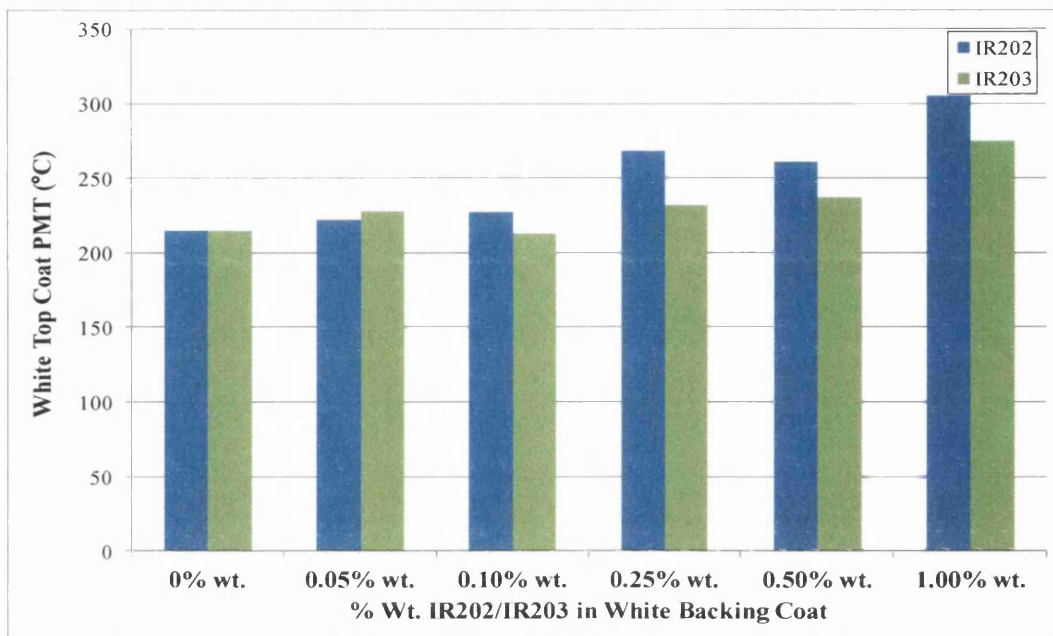


**Figure 5.17 - PMT reached by a White Top Coat with Increasing Weight Percentages of NIR Absorbing Pigment in the Backing Coat, using AdPhos NIR Lab Unit Oven**

As the IR 202 additions have the greater effect on raising top coat PMT, this pigment was investigated further by curing trials performed with the AdPhos Technicum oven.

The next set of experiments used a double draw down of IR202 pigmented and non-pigmented backing coat, so that two top coat PMT values could be recorded for each curing trial; one for a top coat cured with a non-pigmented backing coat on the underside and one with an IR202 pigmented baking coat on the underside. The double draw down will reduce variability in the recorded PMT caused by between run variability in backing coat and top coat thicknesses and Technicum Oven starting temperatures, all which can influence PMT. Schematics of the experimental set up are shown in Figure 5.3 and Figure 5.4.

Figure 5.18 shows that the temperature differential between the two sides of the panel remains constant following the immediate exit of the panel from the NIR oven. This would suggest that the PMT readings are not cross influencing each other by conduction through the substrate panel.

Previous work has shown that the Technicum Oven does not produce a uniform temperature profile across a substrate panel, most likely caused by uneven airflow

within the Technicum during the heating process [7]. Two thermocouples were hence spot welded close to one another on the pigmented side of the panel to assess the variability of temperature across the panel.

A further check on the repeatability of the recorded PMT values was made by re-running already cured panels through the Technicum again, with thermocouples left in place. From 12 sets of data for dry reruns of wet paint systems, the modal average of the difference was +3°C with a standard deviation of 8.9. This slight increase in PMT for a dry paint system is consistent with that found by previous research and could be accounted for by the energy required to evaporate solvents from the wet paint system [7].

The double draws down experiments were carried out with 0.5% and 1.0% wt. additions of IR202 to the white backing coat. First, oven line speed and lamp power settings were adjusted so that the white top coat passed a 100 MEK rub test and was blister free. The average PMT recorded for the white top coat was 186°C, below the PMT range specified for the convection cure of a polyester (216 - 230°C), but the top coat was checked again by a MEK 100 rub test and deemed to be cured. Previous research has observed similar low PMTs during NIR cure [1, 8], which were confirmed to be cured by FTIR peak ratio measurement [3]. The short time of NIR cure means that there is not much time for the coating and metal substrate to equilibrate and hence PMT values for NIR cure must be used with caution. It is likely the top coat is reaching a higher temperature than that recorded for the metal substrate. The white top coat increases in PMT by ca. 34°C when cured with 0.5% wt. addition IR202 and by ca. 46°C when cured with 1.0% wt. addition, at the same oven power settings and line speed and summarised in Figure 5.19. These differences in PMT show that there is potential for a white top coat to be cured at lower NIR lamp power settings when IR202 pigment is added to the backing coat, compared to no IR202 pigment being present. Expressed alternatively, the cure time of a white top coat reduces from ca. 9 to 7 seconds when 1% wt. IR202 is added to the backing coat, equivalent to an increase in line speed of ca. 23%. This is summarised in Table 5.3.

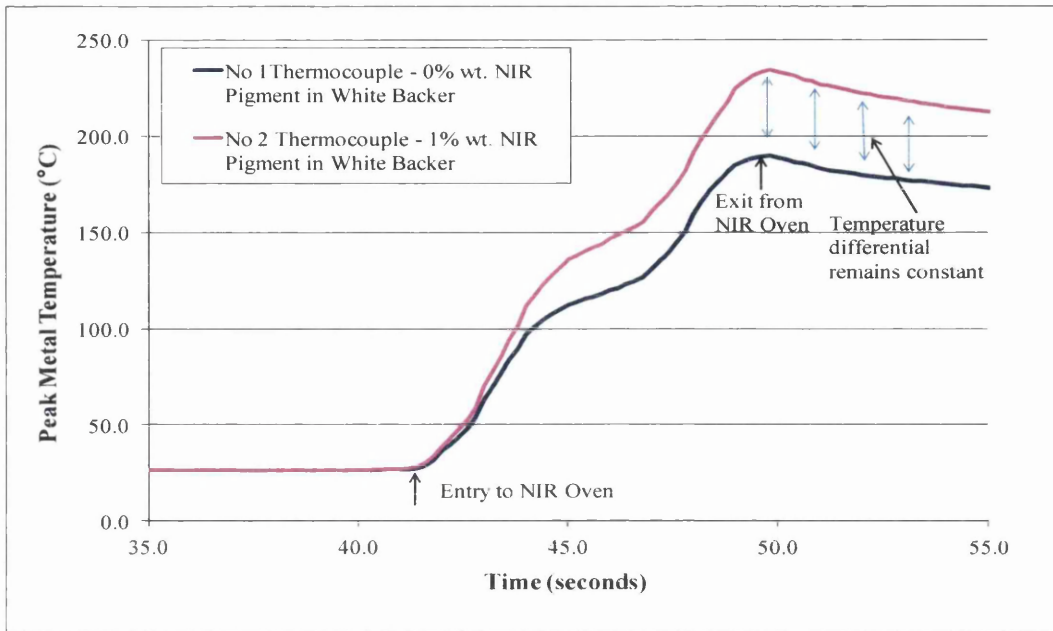


**Figure 5.18 - Temperature Profile of Top Coat PMT Showing Differential between Pigmented and Non Pigmented Side of the Panel**

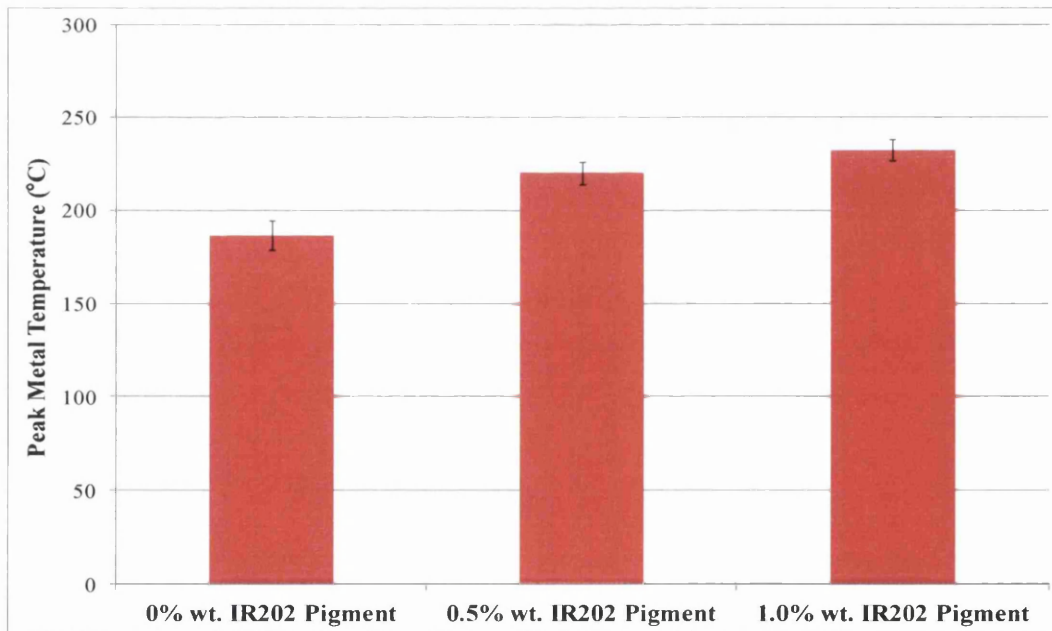


**Figure 5.19 – Difference in White Top Coat PMT with Different Percentage Weights of NIR Pigment in the Backing Coat, using a Double Draw Down of Backing Coat**

**Table 5.3 – Cure Time for White Top Coats with 0% and 1.0% wt. IR202 Pigment in the Backing Coat**

Sample	White Top Coat Cure Time (secs)
0% wt. IR202 in backing coat	9.2
1.0% wt. IR202 in backing coat	7.1

Further evidence of the increased temperature reached by a white top coat cured with a NIR absorbing pigmented backing coat is observation of yellow discolouration in the white top coat on that side of the cured panel, and is shown in a schematic in Figure 5.20. The yellow discolouration gives a DE\* (CIE 1994) of  $1.6 \pm 0.1$ .

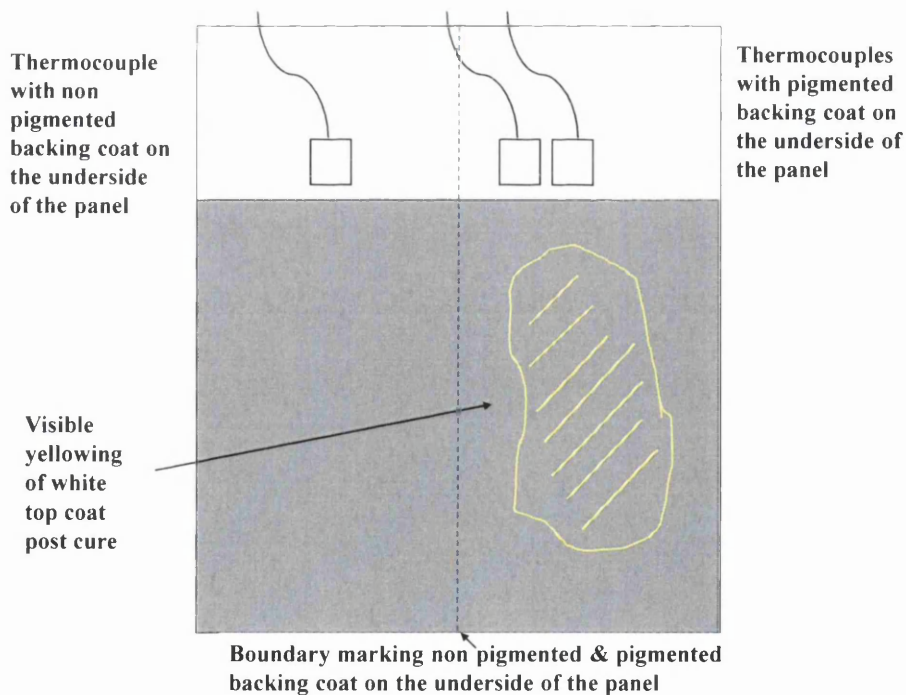


**Figure 5.20 - Visible Yellowing of White Top Coat Cured over the IR202 Pigmented Backing Coat**

Two measurements can be compared as percentage loading of NIR pigment in the backing coat is increased: top coat PMT and backing coat NIR absorption. Figure



5.21 shows a comparison of this sort for the Technicum experiments given in Figure 5.19. Only a limited number of data points are available here, but future work could investigate a ladder of pigment loadings to see if the NIR absorption of the backing coat could be used to predict top coat PMT. This would allow the amount of pigment added to the backing coat to be optimised, also taking into account pigment cost and NIR oven energy saving costs. More meaningful results would be obtained from this experiment with pigment loading expressed as a pigment volume concentration (PVC). The PVC is the volume percent of pigment in the dry film, with a volume relationship controlling many of the physical and optical properties of coatings [9].

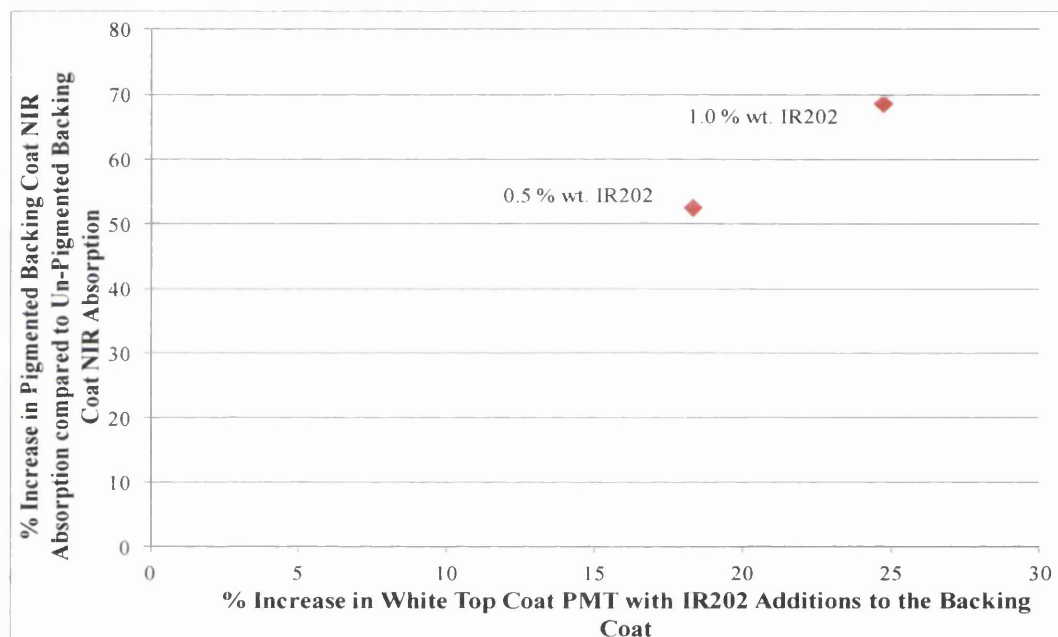


**Figure 5.21 – Effect of Backing Coat NIR Pigment Loading on Backing Coat NIR Absorption (780-1500 nm) and Top Coat PMT**

## 5.4 Conclusions

We have previously shown that NIR curing efficiency can be increased when a NIR absorbing primer is used with the NIR cure of a white top coat [1], and this chapter has shown that the principle of heating a top coat from the bottom upwards to minimise solvent boil can be extended further by moving the locus of high absorption of NIR in the coating system from the primer layer to the backing coat.

Backing coats in coil coating systems are thinner (8 -10  $\mu\text{m}$  dft) than top coats (20  $\mu\text{m}$  dft). It therefore made sense to add NIR absorbing pigments to the thinner

backing coat rather than the thicker top coat. This is because if the NIR absorbing pigments were added to the thicker top coat coating, the greater heating of the surface layers of the coating caused by the addition of the pigments could cause the surface layer to reach polyester cross-linking temperatures before the solvent in the lower layers of the coating has had time to escape. A thinner coat will have less solvent to remove, so this can be achieved in a shorter space of time and hence reduce the risk of solvent boil.

The results showed that a silver coloured polyester top coat could be cured by NIR with a line speed ca. 34% faster when a grey backing coat is used rather than when a white backing coat is used, due to the greater absorption of NIR by the grey backing coat. There is potential to translate these laboratory based increases in line speed to Tata Steel's NIR DVLA coil coating line where both grey and white backing coats are used with the line's coil coating system. Further work in the form of an industrial line trial would need to be carried out to assess the exact magnitude of the change in line speed possible, as the industrial NIR oven has a greater forced air flow than the AdPhos laboratory oven. An alternative to increasing line speed would be to reduce the power settings of the industrial oven. Further work could assess these reduced power settings in a laboratory oven, followed by an industrial line trial.

In a similar way, NIR absorbing pigment additions to the backing coat were also able to increase the PMT reached by the top coat. UV-Vis-NIR spectroscopy was used to identify the most promising pigment, IR202, which at 1% wt. addition to a white backing coat increased the temperature reached by a white top coat cured by an Adphos Technicum oven by 46°C, compared to a non pigmented backing coat cured under identical oven conditions. This increase in PMT equated to the potential to increase the line speed by ca. 23% when 1% wt. IR202 was added to the backing coat.

The IR202 pigment did however reduce visible reflectance more than the Iriotec 8840 pigment at the same pigment loading, with additions of more than ca. 0.1% w/w IR202 to the white backing coat being sufficient to fail an industrial quality control colour inspection ( $\Delta E^* > 1$ ). An assessment will have to be made of how much change in backing coat colour can be tolerated by customers. Further work to assess pigment impact on coating durability by means of accelerated weathering tests will also need to be carried out.

## 5.5 References

1. Mabbett, I., Elvins, J., Gowenlock, C., Jones, P., and Worsley, D., *Effects of highly absorbing pigments on near infrared cured polyester/melamine coil coatings*. Progress in Organic Coatings, 2013. **76**(9): p. 1184-1190.
2. Gowenlock, C.E., Mabbett, I., and Worsley, D.A., *Optimization of near infrared cured polyester/melamine coil coatings by the use of near infrared absorbing primers*. GSTF Int J Eng Tech, 2013. **2**(2): p. 47-50.
3. Mabbett, I., Elvins, J., Gowenlock, C., Glover, C., Jones, P., Williams, G., and Worsley, D., *Addition of carbon black NIR absorber to galvanised steel primer systems: influence on NIR cure of polyester melamine topcoats and corrosion protection characteristics*. Progress in Organic Coatings, 2014. **76**: p. 1184-1190.
4. Knischka, R., Lehmann, U., Stadler, U., Mamak, M., and Benkhoff, J., *Novel approaches in NIR curing technology*. Progress in Organic Coatings, 2009. **64**(2-3): p. 171-174.
5. Omega, *Emissivity of Common Materials*. (cited 21st March 2014). Available from: <http://www.omega.com/literature/transactions/volume1/emissivitya.html>.
6. Zheng, H.Y. and Lim, G.C., *Laser-effected darkening in TPEs with TiO<sub>2</sub> additives*. Optics and Lasers in Engineering, 2004. **41**(5): p. 791-800.
7. Ireson, R. and Wullink, J., *Thermographical analysis of NIR heat treatments of coated steel panels using the AdPhos Technicum*. 2008, Corus Research, Development & Technology.
8. Mabbett, I., *Applications of Near Infrared Heating of Interest to the Coil Coating Industry*. 2011, Eng. D., Swansea University
9. Perera, D.Y., *Effect of pigmentation on organic coating characteristics*. Progress in Organic Coatings, 2004. **50**(4): p. 247-262.

**Chapter 6**  
**The Effect of Modification of Silver**  
**Coloured Polyester Coating**  
**Formulation on NIR Cure**

## 6.1 Introduction

Organically coil coated steel is used extensively in the construction industry, with architects calling for a range of colours as illustrated in Figure 6.1.



**Figure 6.1 – Sustainable Building Envelope Centre, Tata Steel Incorporating a Range of Coloured Coil Coated Steel [1]**

In the polyester coil coated market, white polyesters account for a third of the sales volume, metallic silver grey colours a further third, and with other colours making up the final third sales volume [2]. Silver metallics hence form a significant proportion of the market, however previous work has shown that these colours are the most difficult to cure with a NIR oven [3].

Mabbett investigated silver metallic polyester coatings with aluminium flake as the sole pigmenting agent. UV-Vis-NIR spectroscopy studies showed that transmission through an aluminium flake polyester free standing coating film remained at less than 5% across the whole UV-Vis-NIR region, whilst reflectance from the coating surface was ca. 50% with a drop in reflectance in the region of 800 nm attributed to absorption by the aluminium flake [3]. Silver polyesters of this type could not be cured using the AdPhos NIR Lab Unit; curing trials resulted in panels that were blistered but were also under cured as they did not pass a MEK double rub test. This is indicative of a very small cure window where the coating solvents have not had sufficient time to escape

before cross-linking commences. In response to this the paint manufacturer was able to supply a formulation with the highest boiling point solvent omitted from the formulation and a cross-linking catalyst which unblocked at a higher temperature. These changes gave a less blistered but still under cured product with the AdPhos NIR Lab Unit, although a less blistered but cured product was achieved with the more sophisticated AdPhos Technicum [3].

Conclusions from Mabbett's research were that during NIR cure, although a lot of NIR radiation is likely to be reflected at the surface of an aluminium flake pigmented coating, a lot of the remaining NIR is being absorbed in the top layers of the coating by the aluminium flake and leading to blistering [3]. Although formulations with a lower boiling blend of solvents and a slower catalyst have improved NIR cure, it is unlikely that these changes alone will enable silver polyesters to be NIR cured on an industrial line where a reasonable sized cure window is needed.

The aim of this work was hence to investigate whether the NIR cure of silver polyester coatings can be further improved by replacing the aluminium flake with alternative pigments that absorb less strongly in the NIR region, but which maintain the visual appearance of the silver coating.

The starting point for this work was to compare the NIR cure of silver polyester coatings (RAL 9006) supplied by two competing paint manufacturers (Manufacturer A and Manufacturer B). The coatings investigated were the manufacturers' optimised formulations for NIR cure. Modifications were the incorporation of a lower boiling point solvent blend and a slower catalyst, although due to commercial sensitivity exact details of the formulation modifications were not disclosed by the manufacturers.

This was then followed by investigations of the replacement of the aluminium flake in the coating formulation by less absorbing coated glass flake and coated mica flake.

## 6.2 Experimental Techniques

### 6.2.1 Polyester Coating Formulation

Polyester coatings were made up by the pigment paste and converter method given in Section 2.1.1 and using the pigments given in Table 6.1. The coatings formulations are given in Table 6.2 and Table 6.3. The converter gloss shown in Table 6.3 contained polyester resin, catalyst, some solvent and small amounts of any additives needed to increase the curing and casting capabilities of the coatings.

**Table 6.1 – Pigments for Polyester Coatings**

<b>Pigment name</b>	<b>Manufacturer</b>	<b>Chemical type</b>	<b>Description</b>
STAPA® Mobilux R187	Eckart	Aluminium flake	Aluminium flake paste 65% Aluminium flake 35% volatiles d10 = 11 µm; d90 = 45 µm
Phoenix® PX 3001	Eckart	Coated Mica flake	Free flowing powder Mica coated with Rutile TiO <sub>2</sub> & SnO <sub>2</sub> 5 – 25 µm particle size
Luxan C001	Eckart	Coated Glass flake	Free flowing powder Glass flake coated with TiO <sub>2</sub> & SnO <sub>2</sub> 15 – 60 µm particle size

**Table 6.2 - Mica Flake Polyester Coatings Formulations**

	<b>Al coating</b>	<b>Al/Mica coating</b>	<b>Mica coating</b>
% wt. Flake in coating	4.55% Al	2.28% Al 3.5% Mica	7% Mica
% wt. Synolac 9605 S 65 (polyester resin)	50	50	50
% wt. Luwipal 066 LF (cross linking agent)	5.5	5.5	5.5
% wt. Crayvallac Flow 200 (flow agent)	0.6	0.6	0.6
% wt. Dynapol 1203 (catalyst)	1	1	1
% wt. NIR solvent blend (66.7% solvent naphtha 180/210, 33.3% solvent naphtha 160/180)	34.4	34.4	34.4
% wt. Pergopak M4 (matting agent)	1.5	1.5	1.5
% wt. STAPA® Mobilux R187 (Aluminium pigment)	7	3.5	0
% wt. Phoenix® PX 3001 (Mica pigment)	0	3.5	7



**Table 6.3 - Glass Flake Polyester Coatings Formulations**

	<b>Al coating</b>	<b>Glass Flake coating (1)</b>	<b>Glass Flake/ Al coating</b>	<b>Glass Flake coating (2)</b>	<b>Glass Flake coating (3)</b>
% wt. Flake in coating	3.9 % Al	3.9% Glass Flake	3.9% Glass Flake + 0.5% Al Flake	10% Glass Flake	20% Glass Flake
% wt. Converter gloss	86	86	86	80	70
% wt. STAPA® Mobilux R187 (Al pigment)	6	0	0.8	0	0
% wt. Solvent naphtha 180/210	8	10.1	9.3	10	10
% wt. Luxan C001 (Glass flake)	0	3.9	3.9	10	20

## **6.2.2 NIR Curing Trials using an AdPhos Technicum NIR Oven**

Manufacturers A and B supplied RAL 9006 polyesters with formulations modified for NIR cure. Panels were cured using an AdPhos Technicum NIR oven at Tata Steel's IJmuiden site. Substrate panel size was 210 x 300 mm 0.58 mm HDG primed with Henkel Granocoat 2840 pretreatment-primer.

Mica and glass flake substituted silver metallic polyesters (dft  $19 \pm 1$   $\mu\text{m}$ ) were cured using an AdPhos Technicum NIR Oven at BASF's Deeside site. Substrate panel size was 150 x 200 mm 0.47 mm unprimed MZ. Samples were carried out in duplicate.

## **6.3 Results and Discussion**

### **6.3.1 Comparison of the Cure of Silver Polyester Coating Formulations Modified for NIR Cure**

A Technicum NIR oven line speed of 10.5 m/min (equivalent to an industrial line speed of 123 m/min on Tata Steel's DVL2 industrial line) and a dry film thickness of 20  $\mu\text{m}$  were chosen as an initial starting point for this investigation as they represent typical industrial conditions. The aim was, for a given line speed and coating thickness, to compare the relative cure windows of two paint manufacturers' RAL 9006 silver polyester coating were the formulations had been optimised for NIR cure. Optimisation of the formulations involved omission of higher boiling point solvents from the solvent blend and higher temperature cross-linking catalysts, but further details than this were not provided by the paint manufacturers due to commercial sensitivity.

Cure window is defined by the lower and upper cure limits. The lower cure limit can be defined as occurring at oven power settings which enable a coating to cure and pass a 100 double rub MEK test. The upper cure limit can be defined as occurring at oven power settings where the coating first becomes over cured and blistered.

The Adphos Technicum NIR oven has three power zones, zone 1, 2 and 3, as shown in Figure 6.2.

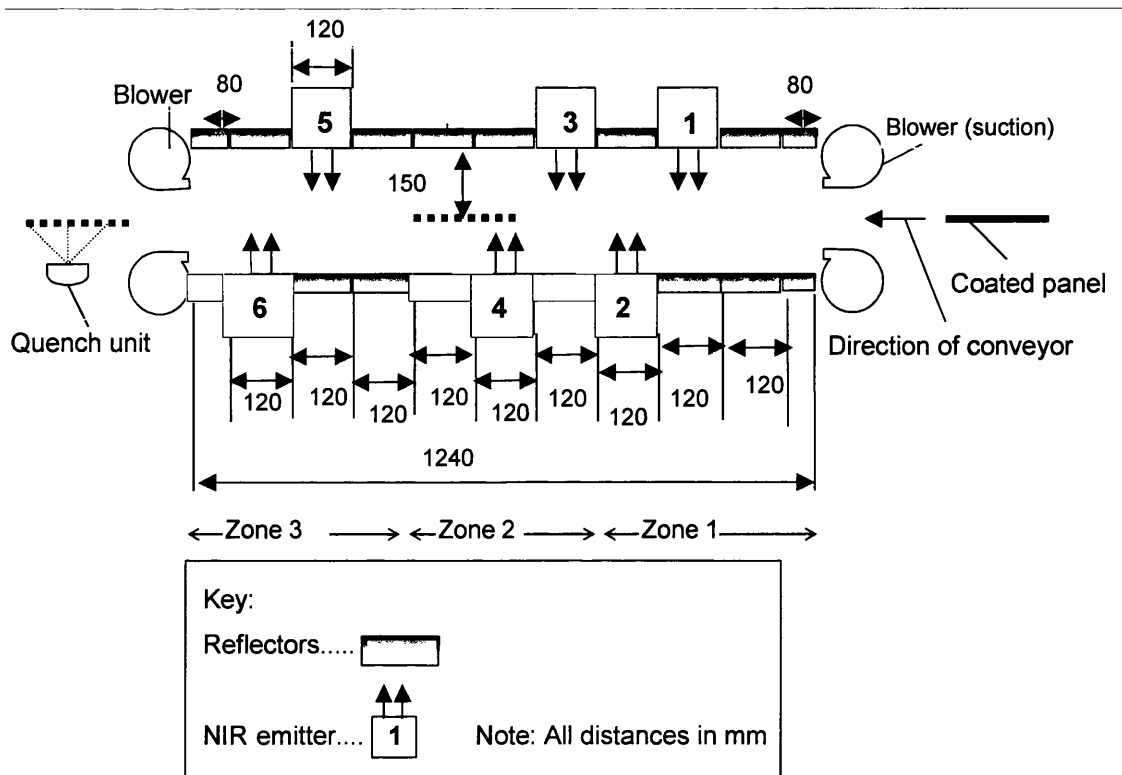


**Figure 6.2– Schematic of AdPhos Technicum NIR Oven Showing the Position of the Three Oven Zones**

Zone 1 corresponds to the zone where the majority of the first stage of the NIR cure mechanism is happening; the removal of solvent from the system. The temperature then rises at a slower rate in zone 2 to allow solvent evaporation to complete before cross-linking starts. This can often be achieved by setting the zone 2 NIR lamps (lamps 3 and 4 in Figure 6.2) to 0% power. Lamp powers are then set to allow a higher temperature in zone 3 to achieve cross-linking of the polyester. Profiling of the temperature of the NIR cure in this way allows the two stages of the cure mechanism to be distinct and helps to reduce the occurrence of solvent boil, where solvent is still being removed through an already cross-linked coating creating blisters.

The initial starting point for the curing trials with a 20  $\mu\text{m}$  dft coating gave an under cured coating with a dense covering of fine blisters with the power settings in zones 1, 2 & 3 set at 100%, 50% and 30%. The PMT reached was only 172°C and the coating failed a double rub MEK test. A higher power is therefore needed in zone 3 to

increase the PMT. The problem with increasing zone 3 power in a coating which already shows a combination of blistering and under curing, is that blistering is likely to get worse if zone 3 power is increased. Under these cure conditions the coating is showing the sign of there being no separation of the upper and lower cure limits.

A decision was therefore taken to investigate the conditions for a cure window using a thinner coating of 19  $\mu\text{m}$  dft. Previous work has shown that cure windows are wider on thinner coatings as there is less solvent present and the solvent has a shorter distance to diffuse to the surface and be removed [3].

The difficulties associated with the NIR cure of RAL 9006 silver polyester (Manufacturer A) of 19  $\mu\text{m}$  dft are summarized in Figure 6.3 and Table 6.4.

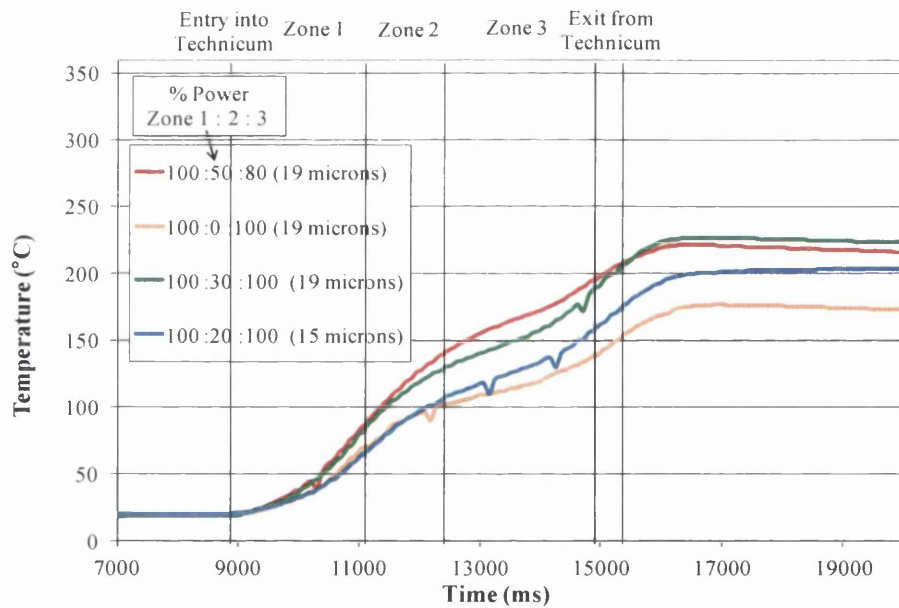


**Figure 6.3 – NIR Curing profiles of RAL 9006 Polyester (Manufacturer A)**

**Table 6.4 – Comparison of Cure Conditions of Manufacturer A’s RAL 9006 Polyester**

Profile	Coating Thickness( $\mu\text{m}$ )	% Power Zones 1:2:3	100 MEK DR Test	PMT ( $^{\circ}\text{C}$ )
<b>Red</b>	19	100 50 80	Pass	222
<b>Blue</b>	19	100 0 100	Fail	177
<b>Green</b>	19	100 30 100	Pass	227
<b>Amber</b>	15	100 20 100	Fail	204

The red cure profile in Figure 6.3 produced an over cured coating above the upper cure limit, because although a MEK double rub test was passed as shown in Table 6.4, the coating surface also had a considerable number of blister as shown in Figure 6.4. Closer inspection of the red cure profile in Figure 6.3 shows a fairly steep temperature gradient in zone 2, and this could be contributing to the cross-linking process starting too early during the cure. Action needs to be taken to further separate the two stages of the cure mechanism; solvent removal and polyester cross-linking. To this end the power in zone 2 was dropped from 50% to 0% and the power in zone 3 increased slightly from 80% to 100% with the aim of reducing the temperature gradient in zone 2 whilst still maintaining the final PMT reached.

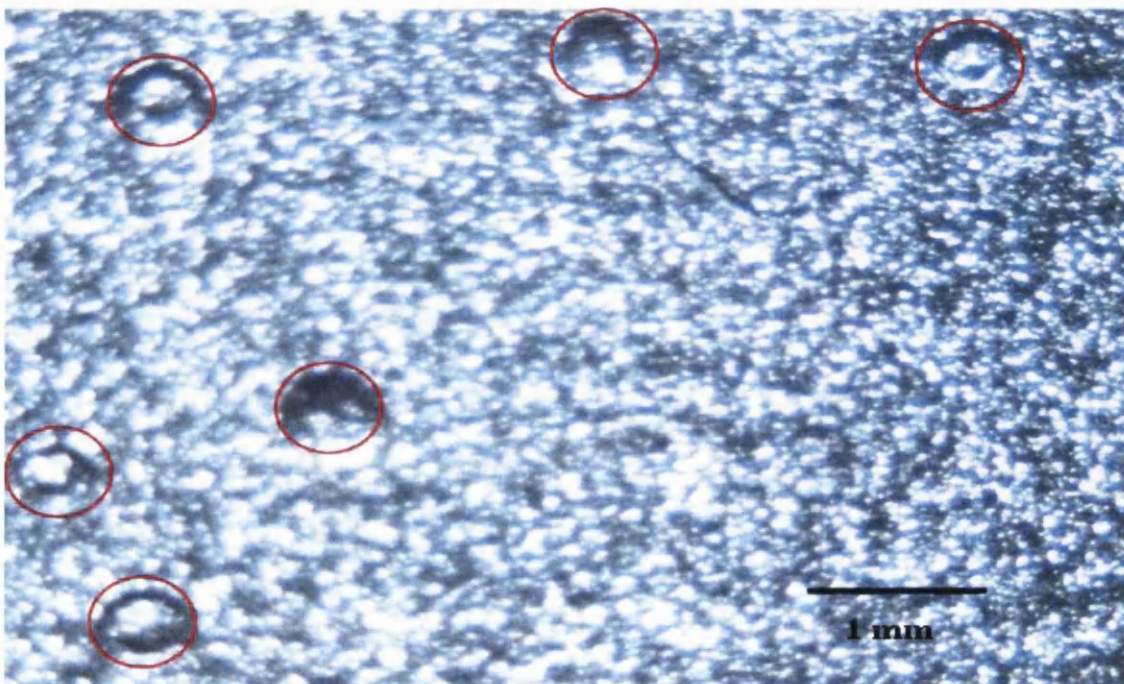


**Figure 6.4 – Cured Coating Produced from the Red Cure profile in Figure 6.3**

The resulting cure profile is the blue profile in Figure 6.3, which shows that the temperature gradient in zone 2 has indeed dropped, but so too has the PMT reached by the end of zone 3, by some 45°C. The coating is now under cured as evidenced by the failed MEK rub test in Table 6.4, although the size and number of surface blisters has decreased, as shown in Figure 6.5. Figure 6.3 also shows that the temperature of the blue cure profile is very low at the end of zone 1, suggesting insufficient solvent has been removed from the coating at this stage.

Modifications to the three zone lamp settings of the blue profile now need to be made to increase the PMT. As the lamps are currently set at 100%, 0% and 100% power, the only means of increasing PMT is to put some power back in to zone 2 as zone 3 is already set at 100% power. Zone 2 is hence increased from 0% to 30% with the resulting profile for this modification being the green profile in Figure 6.3. PMT has increased as planned, but the quantity and size of defects has increased significantly too, as shown in Figure 6.6. The temperature gradient of zone 2 has increased and also the temperature reached by the end of zone 1.

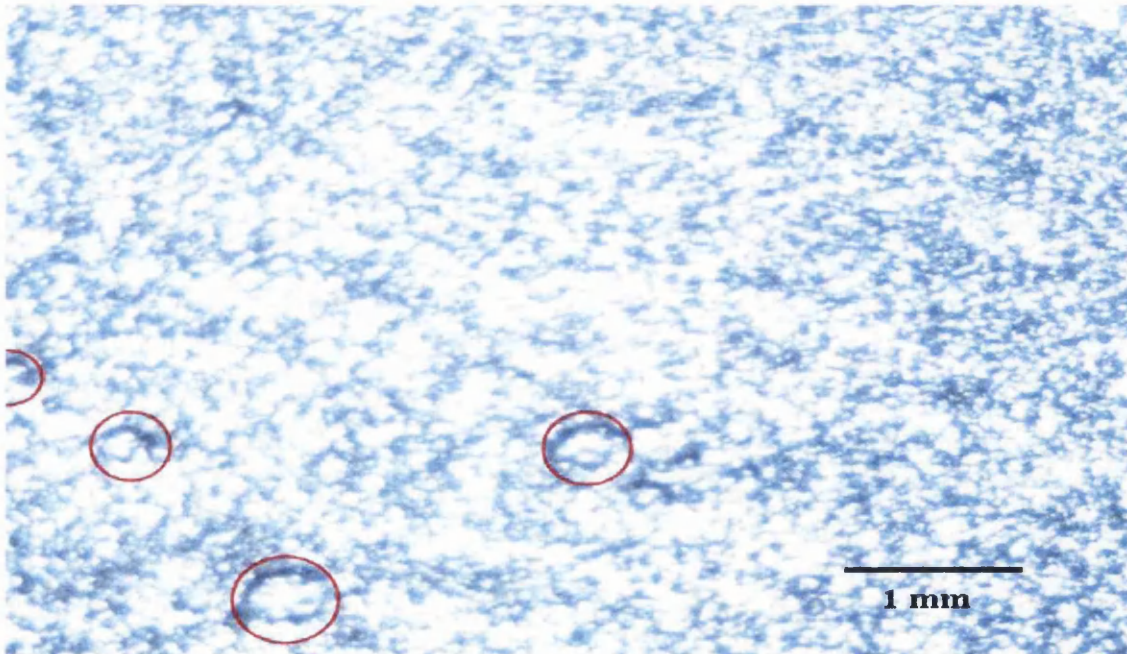


**Figure 6.5 - Cured Coating Produced from the Blue Cure profile in Figure 6.3 showing a Decrease in the Size and Number of Blisters Compared to Figure 6.4**

These three cure trials illustrate the difficulty of achieving a cure with aluminium flake pigmented polyester coatings. The curing process produces coatings that are blistered regardless of whether they pass a MEK double rub test or not; this suggests that the top most layer of the coating is reaching a higher temperature than the layer underneath. Cross-linking occurs rapidly in the top most layers, leaving solvent in the layers underneath with inadequate time to escape. Attempts to reduce the temperature reached by the top most layer results in the underlying layers not reaching a sufficiently high temperature to fully cross-link.

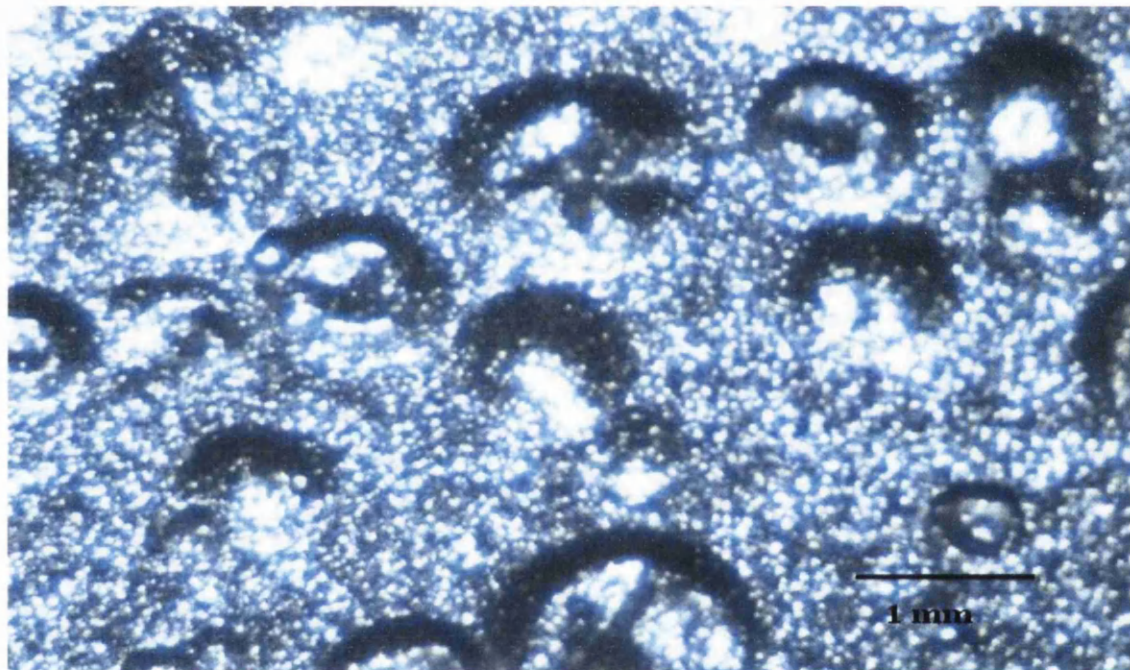


**Figure 6.6 - Cured Coating Produced from the Green Cure profile in Figure 6.3 Showing an Increase in the Size and Number of Blisters Compared to Figure 6.5**

A final curing trial investigated the cure of a thinner coating. This time the dry film thickness was reduced to 15  $\mu\text{m}$ . Fifteen microns is the very lowest top coat thickness that coil coaters deem as acceptable for an architectural polyester coil coating; standard coating build is a twenty five microns coating system comprising five microns pretreatment-primer and twenty microns top coat. There is scope to increase pretreatment-primer thickness to eight microns, which would then give a total coating build of twenty three microns. The amber profile in Figure 6.3 and associated figures in Table 6.4 show that the coating fails a MEK double rub test, but is still blistered, as shown in Figure 6.7.



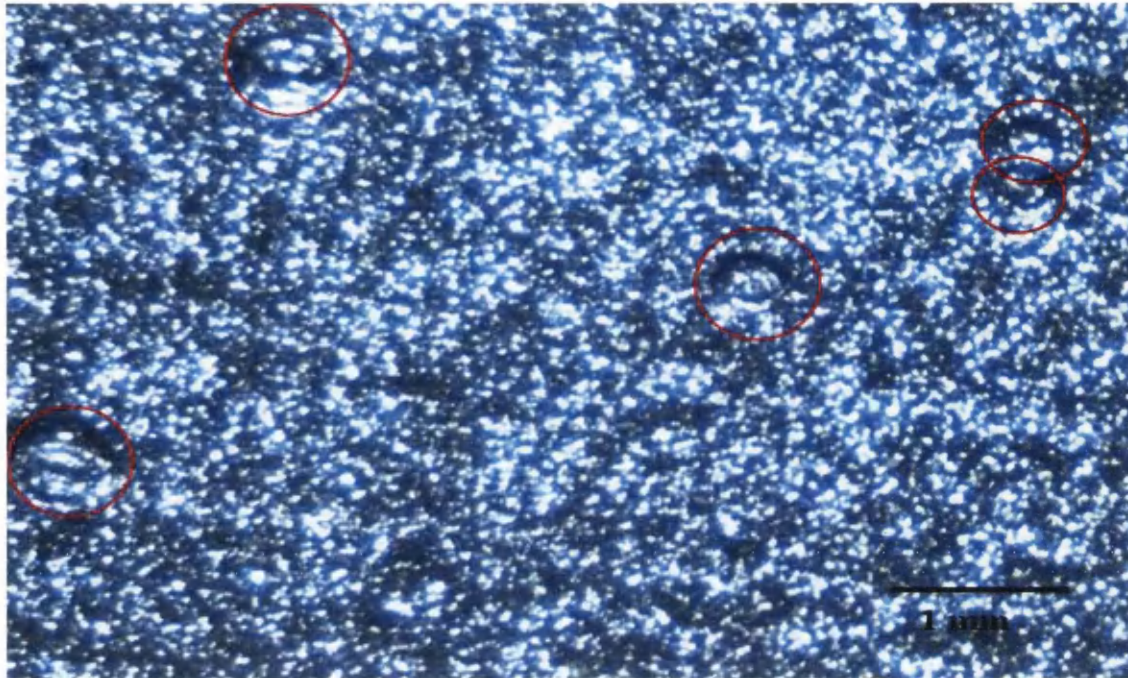


**Figure 6.7 – Cured Coating Produced from the Amber Cure profile in Figure 6.3**

A direct comparison was then made between the NIR cure of Manufacturer A and Manufacturer B's RAL 9006 silver polyester coating. These formulations represented each manufacturer's best attempts to modify the formulation for NIR cure by changing the solvent blend and catalyst. The two competing formulations were drawn down on the same substrate panel and cured using the cure conditions for the amber profile in Table 6.4. Examples of this direct comparison are given in Figure 6.8, Figure 6.9 and Figure 6.10. Manufacturer A and Manufacturer B's coatings failed a MEK double rub test and blistered, but the extent and size of blistering with Manufacturer A was substantially greater.

These initial experiments have indicated that modifications to the solvent blend and catalyst of aluminium flake pigmented polyesters are unlikely to produce coatings with the capability of having an adequate NIR cure window on the industrial line, although manufacturer B's formulation is getting close to an acceptable finish. It should also be born in mind that these experiments were conducted at a line speed equivalent to an industrial line speed of just over 120 m/min, whilst Tata Steel's NIR coil coating line, DVL2 has the capability of operating at speeds of up to 180 m/min. Further

modifications to the formulation are required, so the next step of this work was to try replacing the aluminium flake with a less absorbing pigment that would have the capability of producing the same visual effect as aluminium flake. The two pigments chosen for investigation were metal oxide coated mica pigment and metal oxide coated borosilicate flake (glass flake) pigment; both of these are special effect pigments used to create pearl luster coatings. Metal oxide coated synthetic mica pigments have been used in automotive coatings since the mid 1980's and metal oxide coated glass flake pigment since 2002 [4-6].

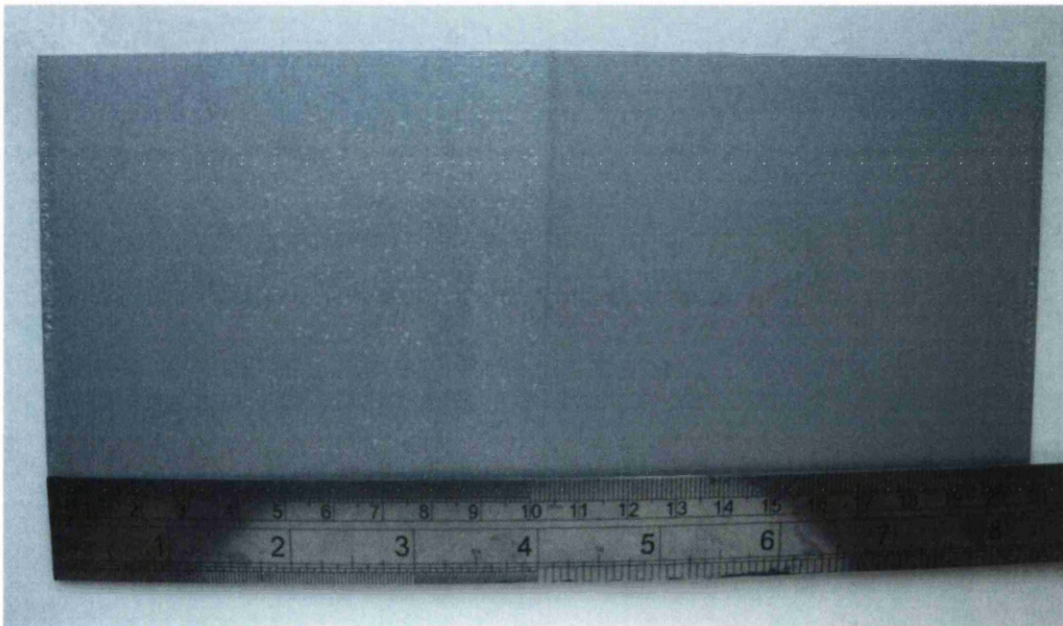


**Figure 6.8 – Direct comparison of NIR Cure of RAL 9006 Silver Polyester; Manufacturer A on Left, Manufacturer B on Right**

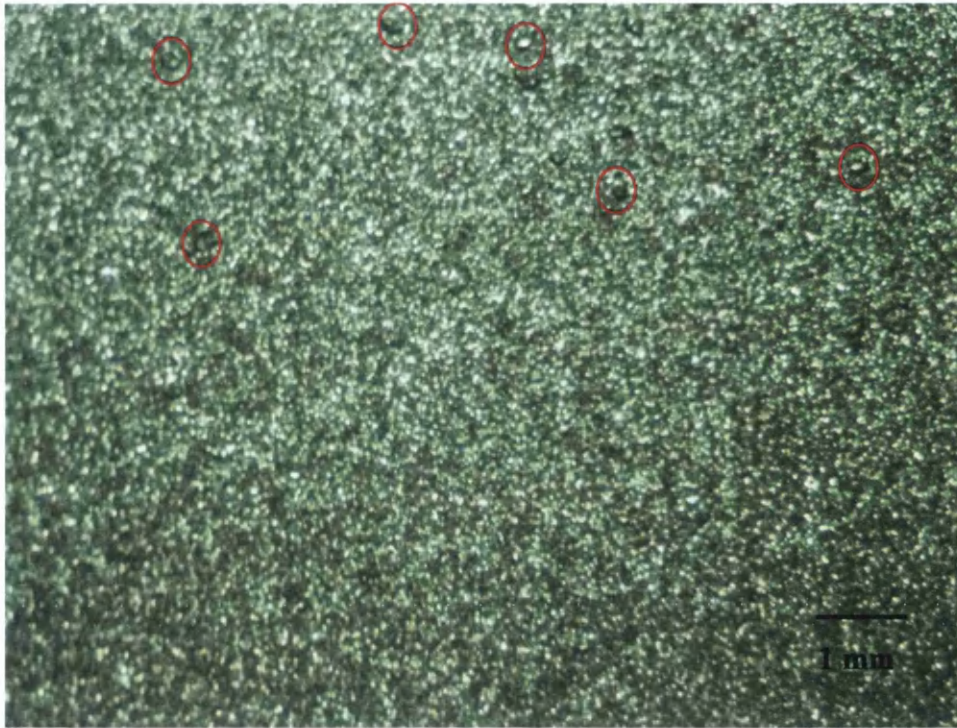


**Figure 6.9 - NIR Cure of RAL 9006 Silver Polyester (Manufacturer B) with Blister Defects Circled in Red**

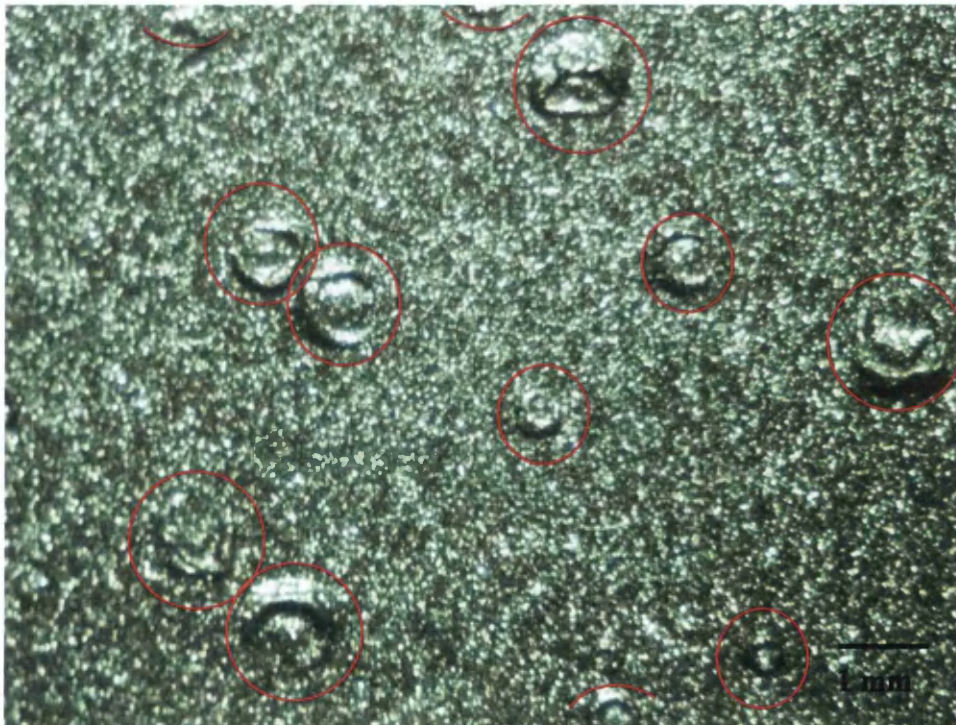


**Figure 6.10 - NIR Cure of RAL 9006 Silver Polyester (Manufacturer A) with Blister Defects Circled in Red**

### 6.3.2 Glass Flake Substituted Silver Polyesters

The metal oxide coated glass flake pigment used in this work was a borosilicate glass flake coated with  $\text{TiO}_2$  &  $\text{SnO}_2$ , with a particle size range of 15 – 60  $\mu\text{m}$ . (Eckart Luxan® C001), herein referred to as glass flake.

Polyester is largely transparent across the UV-Vis-NIR region as shown in Figure 6.11, whilst aluminium flake pigmented coatings exhibit a low level of transparency across this region. This fits with the observation in Section 6.3.1 that aluminium flake coatings are difficult to cure with a small cure window, as most of the absorption of radiation during a NIR cure can be assumed to occur in the top most layers of the coating hence increasing the risk of surface blistering.

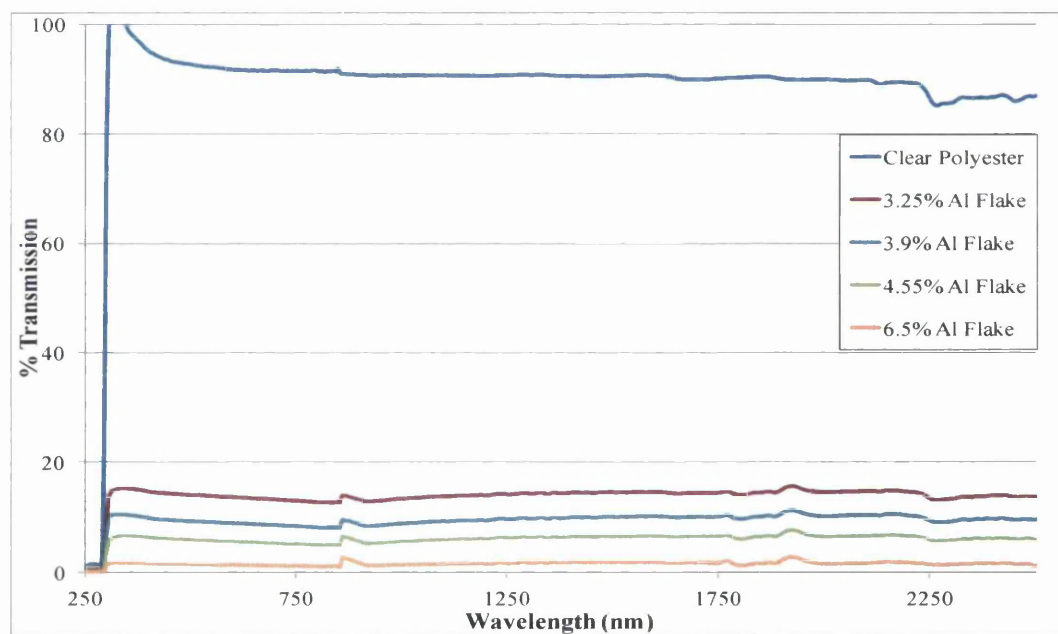


**Figure 6.11 - UV-Vis-NIR Transmission Spectra of Aluminium Flake Pigmented Polyester Free-standing Coating Films**

The difference in transparency of aluminium flake and glass flake pigmented coatings was investigated and the UV-Vis-NIR transmission spectra are shown in Figure 6.12.

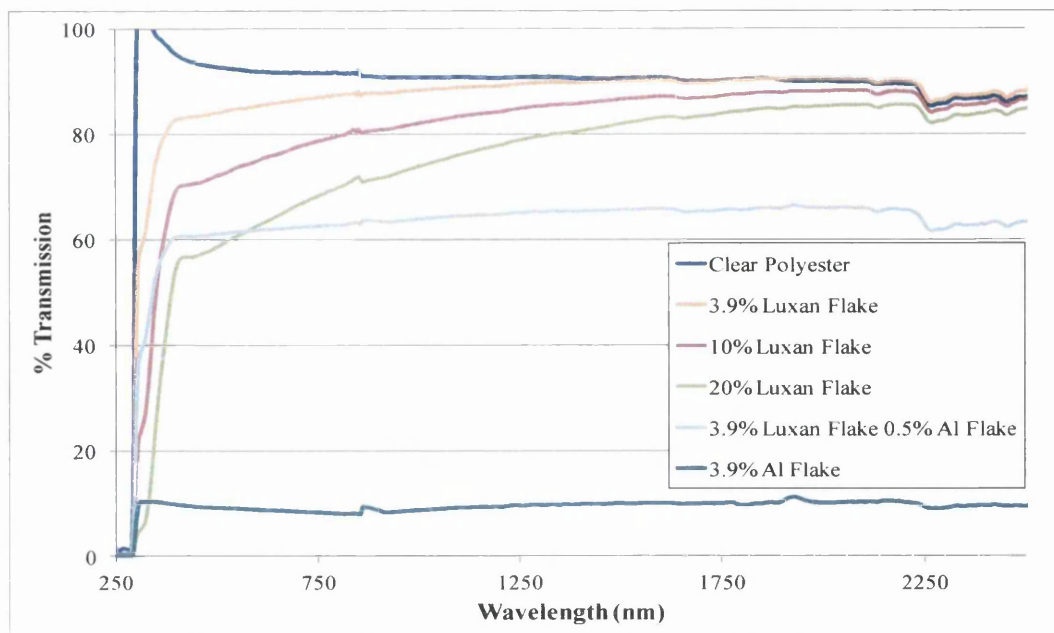


**Figure 6.12 - UV-Vis-NIR Transmission Spectra of Polyester Free-standing Coating Films**

As expected, transmission through coatings pigmented solely with glass flake is high compared to the low transparency of the aluminium flake coating. Comparing the same percentage weights of flake (3.9%), the aluminium flake coating has a transmission of ca. 10% across the UV-Vis-NIR wavelengths whilst the glass flake coating has a transmission of ca. 90% in the NIR dropping to ca. 85% in the visible wavelength range. This suggests that during NIR cure, radiation is able to penetrate through the glass flake coating to heat the coating from the bottom of the coating upwards and hence minimise surface blistering.

The spectra further suggest that the glass flake coatings will have a low hiding power, so a glass flake coating was therefore prepared that had a small percentage (0.5%) of aluminium flake added with the aim of increasing hiding power.

The hiding power of a coating is commonly defined in the coatings industry as the ability of a coating to obscure a background of contrasting standard black and white colours. Polyester coatings pigmented with either 3.9% aluminium flake or 3.9% glass flake were drawn down over a Zehntner hiding power test chart to produce coatings of dry film thickness of  $20 \pm 1 \mu\text{m}$  and are shown in Figure 6.13. The superior hiding power of the aluminium flake pigmented coating can be clearly seen. Figure 6.14 shows the visual effect of the addition of 0.5% aluminium flake to the 3.9% glass flake

coating, producing a marginally better hiding power than a 10% loading of glass flake. Even at 20% loading the glass flake coating has very little hiding power.

The visual hiding power endpoint where no visual distinction can be made between coatings coated over standard black and white backgrounds can be measured photometrically and is defined as a contrast ratio greater than 0.98, as given in Equation 6.1 [7].

$$CR = \frac{R_B}{R_W} > 0.98 \quad \text{Equation 6.1}$$

Where : CR = contrast ratio

$R_B$  = CIE-Y reflectance from coating over black background

$R_W$  = CIE-Y reflectance from coating over white background

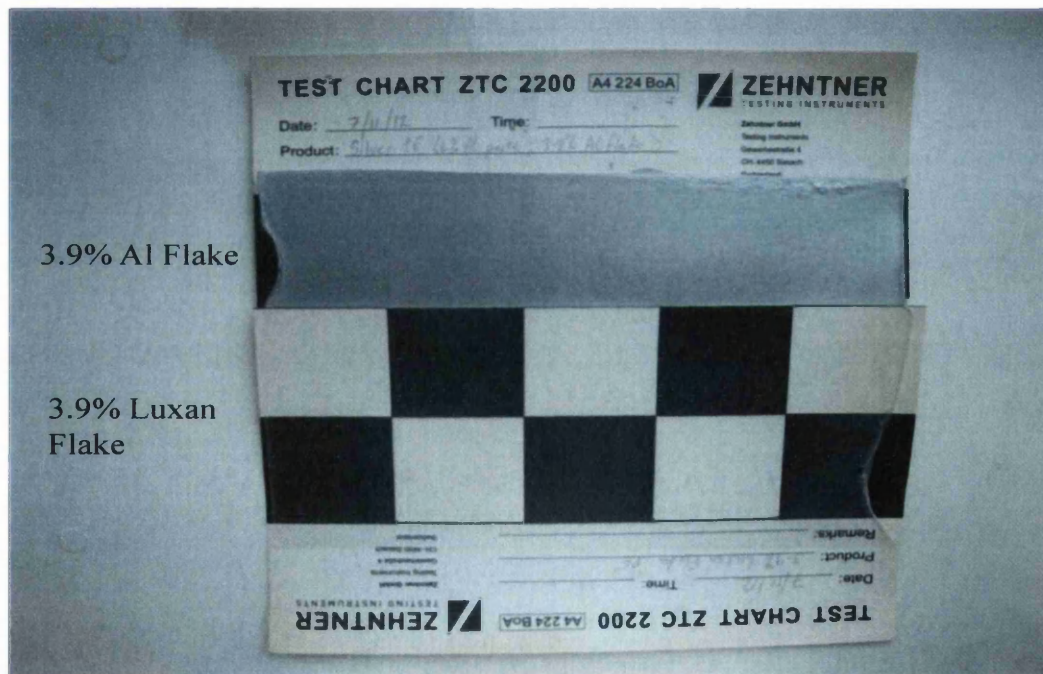
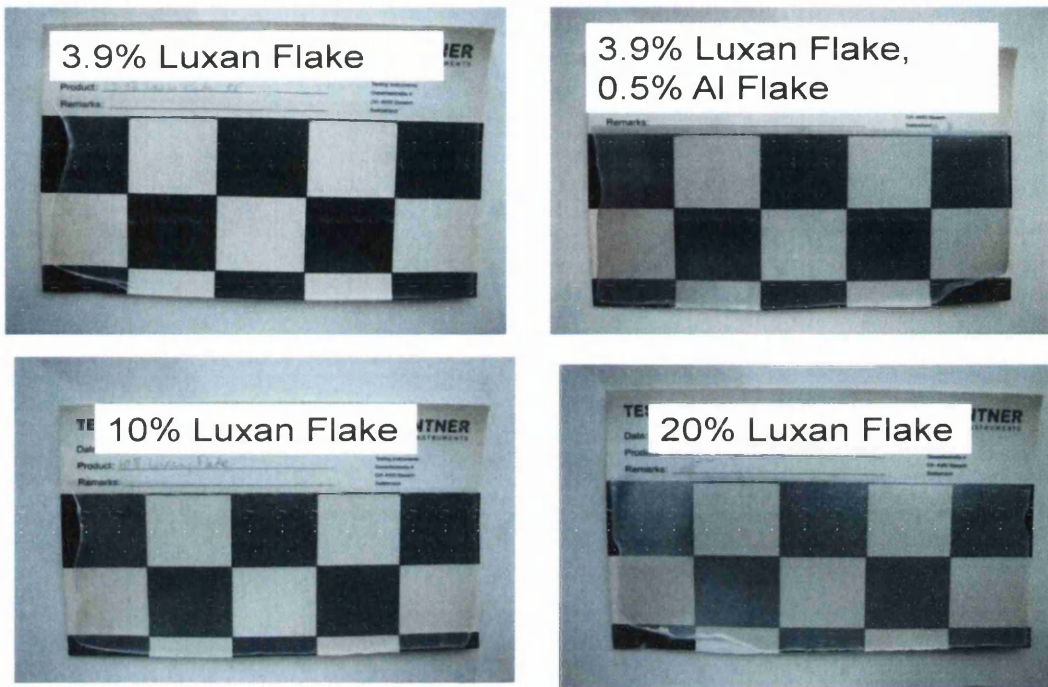
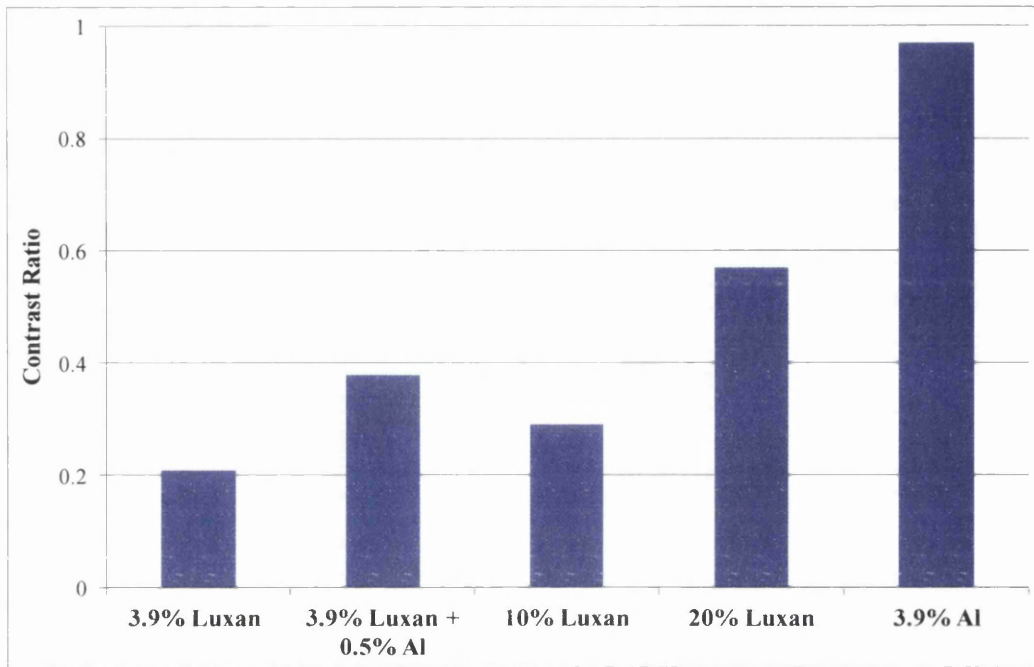


Figure 6.13 – Opacity Chart Showing the Visual Difference in Opacity between an Aluminium Flake and Glass Flake Pigmented Polyester Coating



**Figure 6.14 - Opacity Chart Showing the Visual Difference in Opacity between Polyester Coatings Loaded with Differing Percentages of Glass Flake**

Contrast ratios for the 3.9% aluminium flake and the various glass flake pigmented coatings are shown in Figure 6.15 and are confirmed by the visual results of the hiding power test charts shown in Figure 6.14. It can be seen that aluminium flake provides a hiding power over 4.5 times that of glass flake.



**Figure 6.15 – Contrast Ratios of Aluminium and Glass Flake Pigmented Polyesters**

The reflectance spectra of the aluminium and glass flake coatings give further clues to the likely interaction of the coatings with radiation during a NIR cure and are shown in Figure 6.16. There is a greater similarity between the spectra in the visible region compared to the NIR region; in the NIR the 3.9% aluminium flake coating has the greatest reflectance. Radiation that is not reflected must be either transmitted or absorbed, and as the aluminium flake coating shows low transmission, a lot of the NIR radiation not reflected must be being absorbed. The reflection minimum at ca. 800 nm can be attributed to aluminium absorption [3]. This again supports the idea that most of the absorption of radiation during NIR cure is happening in the top layers of the coating, increasing the chance of surface blistering.

The 3.9% and 10% glass flake coatings show a lower NIR reflectance than the aluminium flake coating that troughs at ca.1000 nm, the region of maximum zinc absorption, suggesting that in agreement with the transmission spectra, NIR radiation is penetrating through the coating to the galvanised layer underneath and being absorbed by the zinc there. This should help to minimise surface blistering by heating the coating from the bottom of the coating upwards.

The coating containing 3.9% glass flake and 0.5% aluminium flake shows a broadened reflectance trough in the NIR, suggesting that during NIR cure absorption is



occurring due to both aluminium flake in the coating and zinc at the galvanised substrate surface.

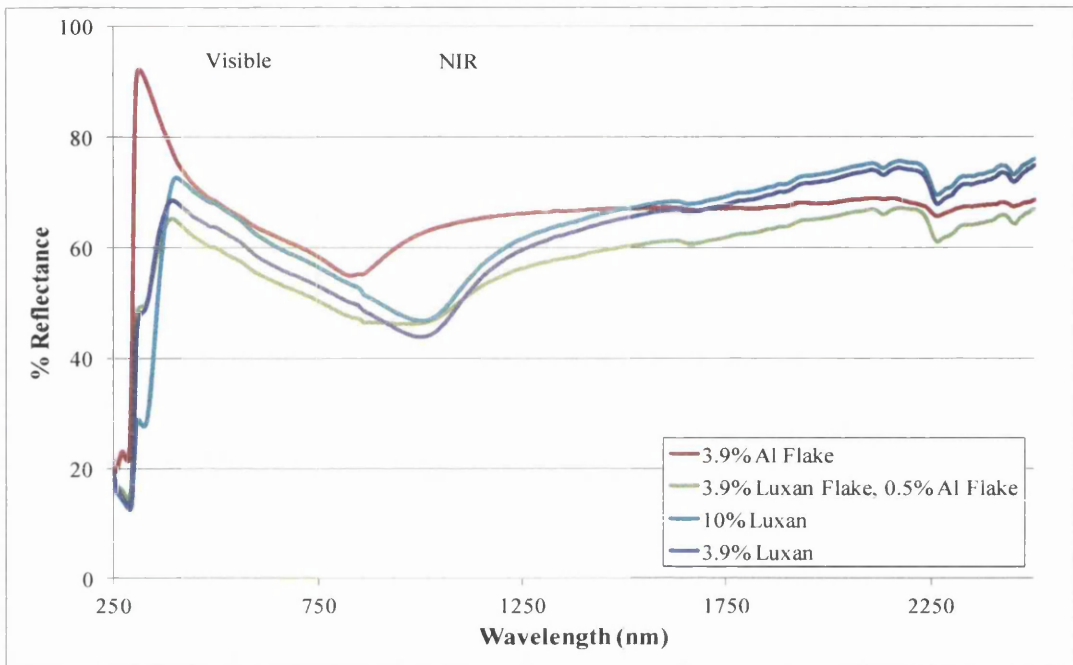


**Figure 6.16 - UV-Vis-NIR Reflectance Spectra of Aluminium and Glass Flake Polyester Coated Panels**

The colour difference between the glass flake coatings and the 3.9 % aluminium flake coating shown in Figure 6.17, Figure 6.18 and Figure 6.19 were measured using a spectrophotometer with 8° diffuse sphere geometry and are shown in Table 6.5. However these results do not give meaningful colour differences in agreement with visual perception, as a spectrophotometer with 8° diffuse sphere geometry illuminates a sample with diffuse light from all angles meaning that colour measurement is the measurement at an average of all angles. Metallic and interference coatings show differences in luminosity and chroma with viewing angle so a multi-angle goniospectrophotometer with a 45° angle of incoming light and measurement of reflected light at 15°, 25°, 45°, 75° and 110° from the angle of reflection is needed to measure colour difference [8].

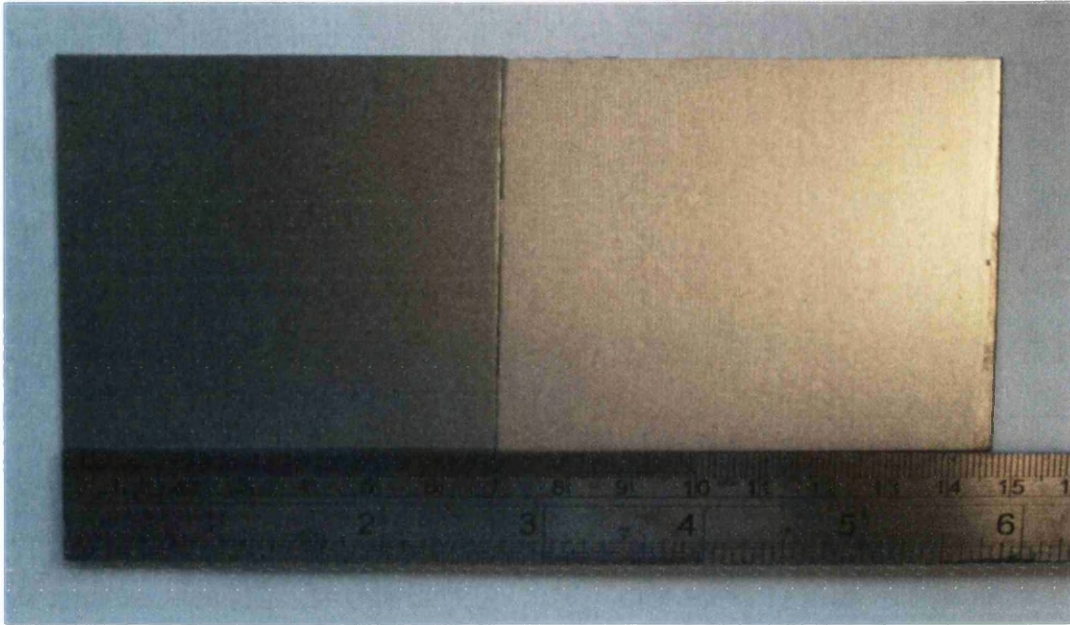


**Figure 6.17 – 3.9% Glass Flake Polyester Coating (left); 3.9% Aluminium Flake Polyester Coating (right)**

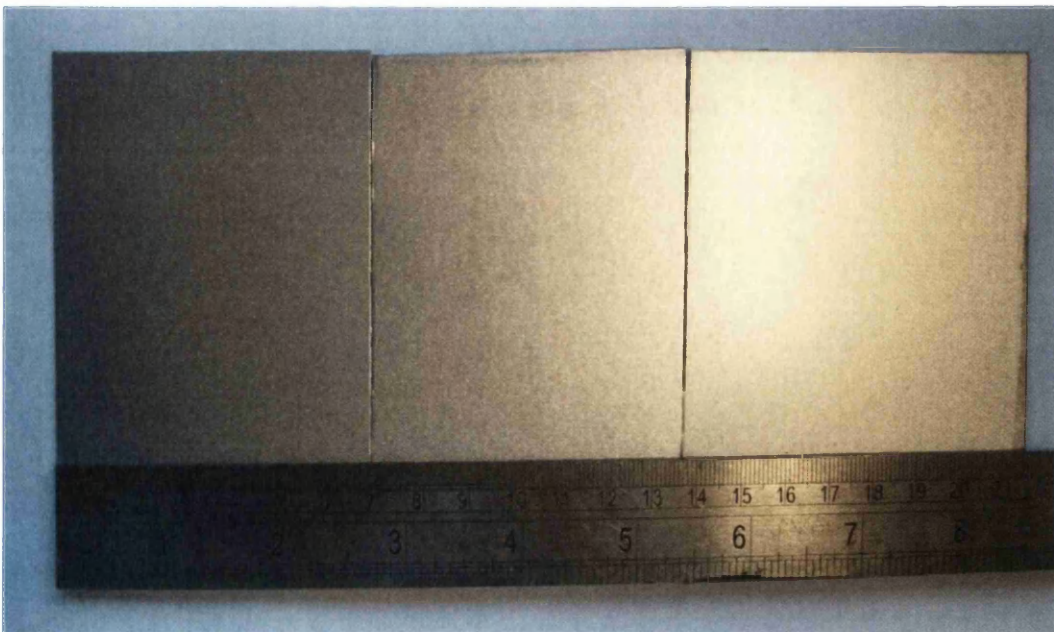


**Figure 6.18 - 3.9% Glass Flake Polyester Coating (left); 10% Glass Flake Polyester Coating (middle); 20% Glass Flake Polyester Coating (right)**

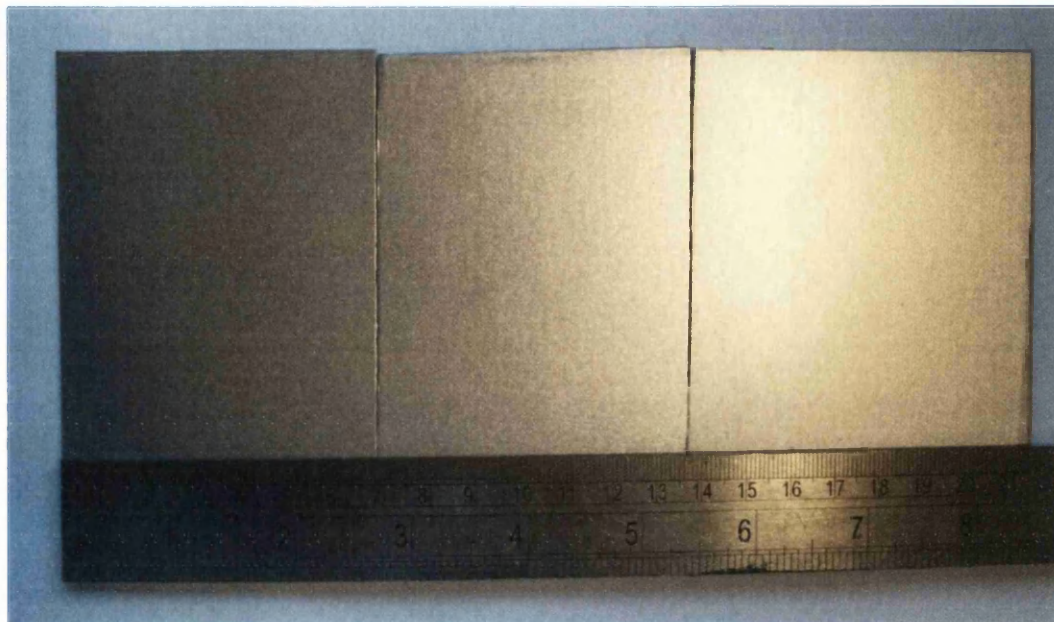


**Figure 6.19 - 3.9% Glass Flake Polyester Coating (left); 3.9% Glass Flake/0.5% Aluminium Flake Polyester Coating (middle); 3.9% Aluminium Flake Polyester Coating (right)**

**Table 6.5 - Colour Difference Between Glass Flake Polyesters Using d8 Instrument Geometry (Reference Coating: 3.9% wt. Aluminium Flake Polyester)**

Sample	Ill	Geom	dE*
<b>3.9% wt. Glass Flake Polyester</b> (Eckart Luxan C001)	D65	d8	3.02
<b>3.9% wt. Glass Flake / 0.5% Aluminium Flake Polyester</b> (Eckart Luxan C001; Eckart STAPA® Mobilux R187)	D65	d8	4.12
<b>10% wt. Glass Flake Polyester</b> Eckart Luxan C001)	D65	d8	1.10
<b>20% wt. Glass Flake Polyester</b> (Eckart Luxan C001)	D65	d8	1.96

NIR cure trials were then carried out to assess the PMT reached by the 3.9 % wt. aluminium flake, 3.9 % wt. glass flake, and 3.9 % wt. glass flake + 0.5 % wt. aluminium flake coatings at the same line speed and power settings. Figure 6.20 shows typical cure profiles for the 3.9 % wt. aluminium flake and 3.9 % wt. glass flake coatings, with higher PMTs being reached at the end of each oven zone by the aluminium flake coating. The aluminium flake coating reached a PMT 25°C higher than the glass flake coating as shown in Figure 6.21 with the PMT of the mixed flake coating being between the two. Once cured, the aluminium flake coating was densely covered with large blisters with surface browning in places; the mixed flake coating had a much sparser coating of finer blisters, whilst the glass flake coating was blister free, as shown in Figure 6.22.

The PMT values were those recorded for the back of the substrate panels, and are lower than the typical PMT range (216 - 230°C) specified for a polyester convection cure. The short cure time means that coating and metal substrate have not had time to equilibrate; the coatings are clearly reaching higher temperatures than the substrate as the aluminium flake coatings are browned on the surface.

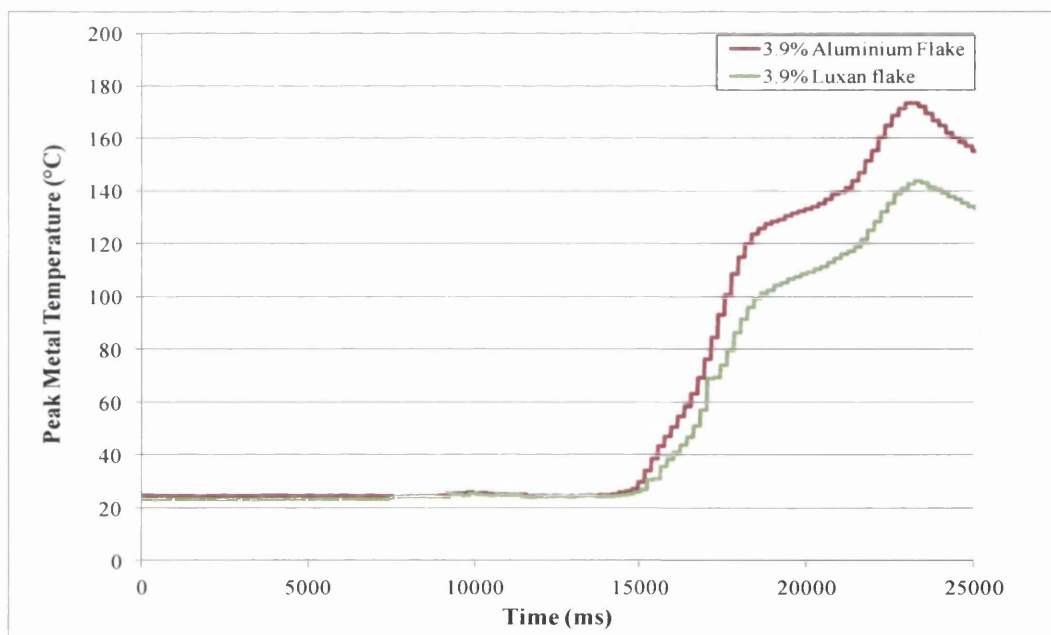


**Figure 6.20 – NIR Temperature Cure Profile for Aluminium Flake and Glass Flake Coatings Cured at the Same NIR Oven Settings**

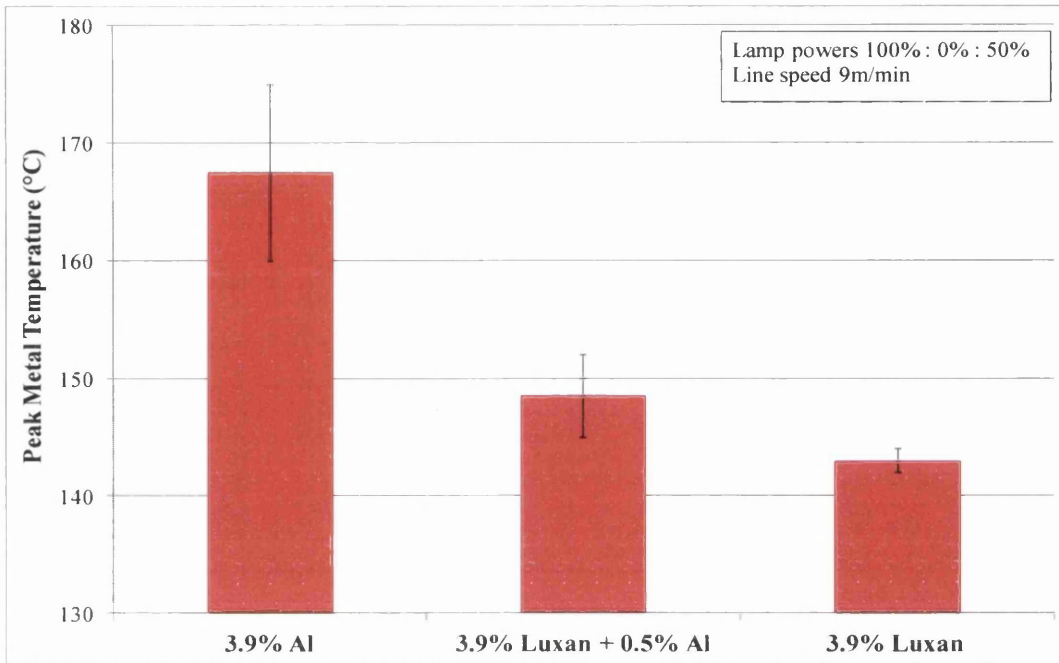


**Figure 6.21 – Comparison of PMTs reached by Aluminium Flake and Glass Flake Coatings under Identical Cure Conditions**

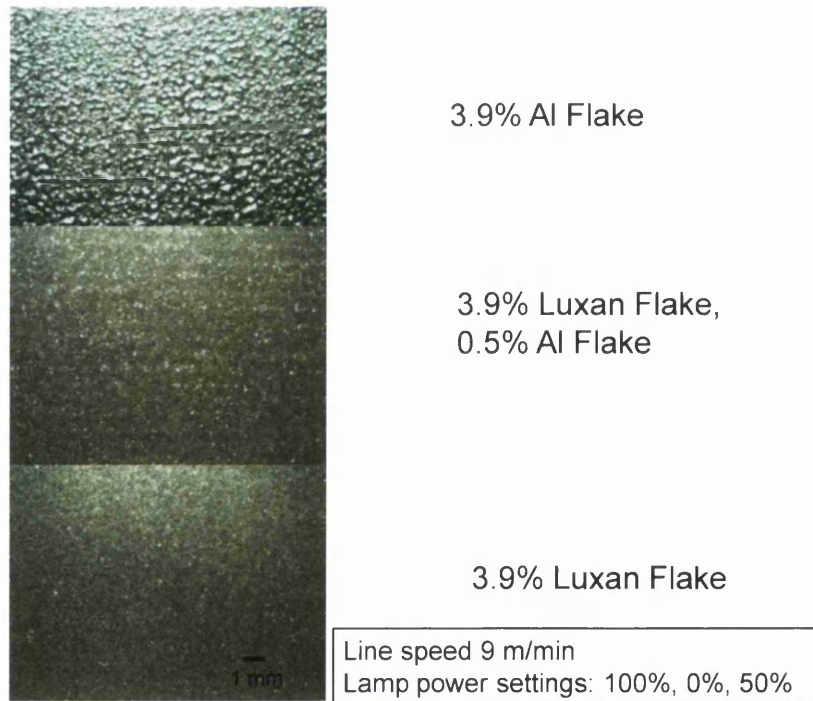


**Figure 6.22 – Comparison of Surface Finish of Aluminium Flake and Glass Flake Coatings Under Identical Cure Conditions Showing Aluminium Flake with Dense Blistering, Mixed Flake Coating with Sparser Fine Blisters and Blister Free Glass Flake Coating**

### 6.3.3 Mica Substituted Silver Polyesters

The metal oxide coated synthetic mica pigment used in this work was a mica platelet coated with rutile  $\text{TiO}_2$  &  $\text{SnO}_2$  with a particle size range of 5- 25  $\mu\text{m}$  (Eckart Phoenix® PX 3001), herein referred to as mica pigment.

Figure 6.23 shows the transmission spectra of free-standing films of simple model mica PVC coatings and these confirm that the pigment has a high degree of transparency through the visible and NIR range, with transmission only beginning to tail off below ca. 410 nm.

A comparison was then made of the transmission through free-standing films of standard formulation silver polyester coating pigmented with 7% aluminium pigment, and polyester coatings where part and all of the aluminium pigment had been substituted with mica pigment. This is shown in Figure 6.24. Again, the transmission through the polyester coating solely pigmented with mica is high in the NIR region.

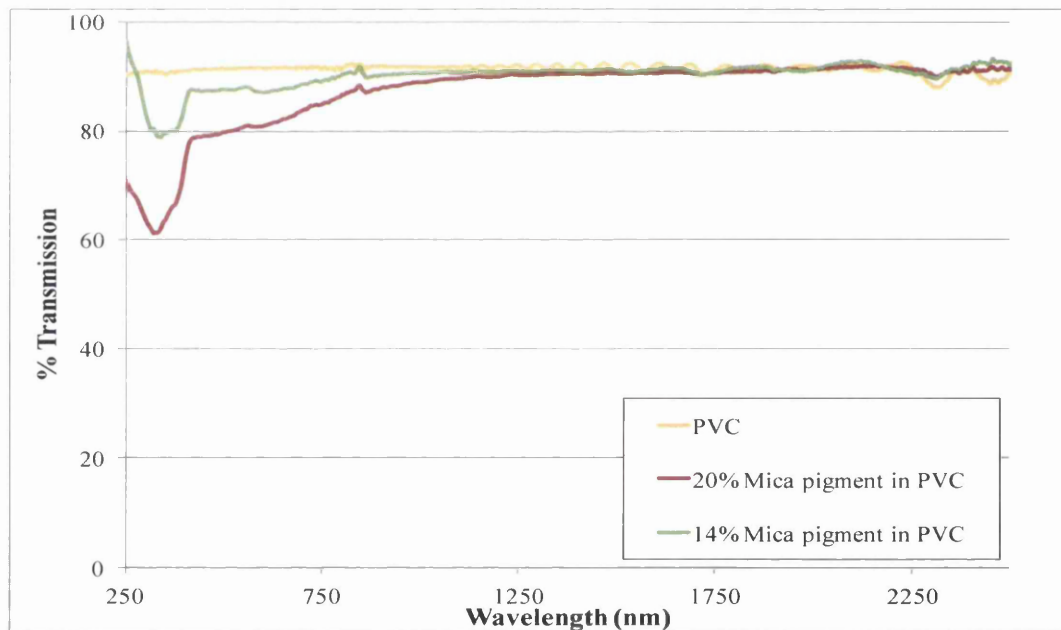


**Figure 6.23 – UV-Vis-NIR Transmission Spectra of Mica Pigment PVC Free-standing Coating Films**

This contrasts with the polyester coating solely pigmented with aluminium pigment which has less than 10% transmission across the UV-Vis-NIR region. The coating pigmented with a mix of aluminium and mica pigment has a transparency in between that of the 100% aluminium and mica pigment coatings, but at 35% across the UV-Vis-NIR region it is much closer to the transmission exhibited by the 100% aluminium pigmented coating despite being loaded more heavily with mica.

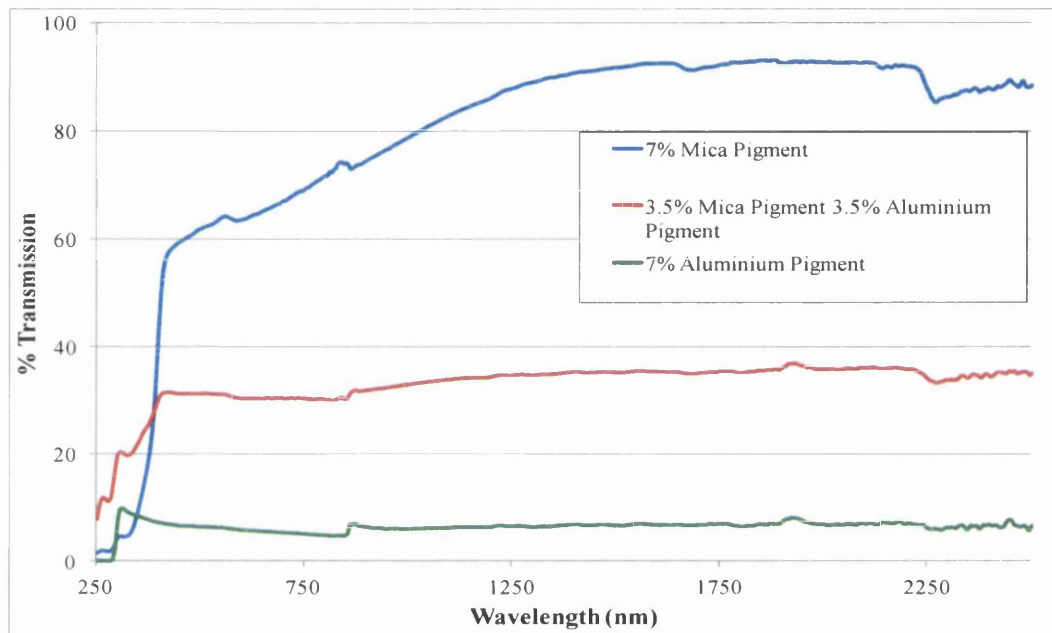


**Figure 6.24 - UV-Vis-NIR Transmission Spectra of Polyester Free-standing Coating Films**

The reflectance spectra of cured coated substrate panels of these three coatings show similar results to the glass flake pigmented coatings in Section 6.3.2 and are given in Figure 6.25. Here the 100% aluminium pigment coating and the coating with a mix of aluminium and mica pigment exhibit similar spectra; a dip in reflectance at ca. 800 nm attributable to absorption by aluminium and a relatively high reflectance in the NIR region. Once all of the aluminium has been removed from the coating, a different pattern of NIR reflectance is seen for the coating pigmented solely with mica; a marked drop at ca. 1000 nm which is also evident in the spectra of the primed substrate due to zinc absorption. Like glass flake pigmented coatings, mica coatings have a high degree of transparency in the NIR but a low hiding power. Figure 6.26 shows the low hiding power of the 7% mica pigment coating with the green chromated primer layer clearly showing through the top coat.

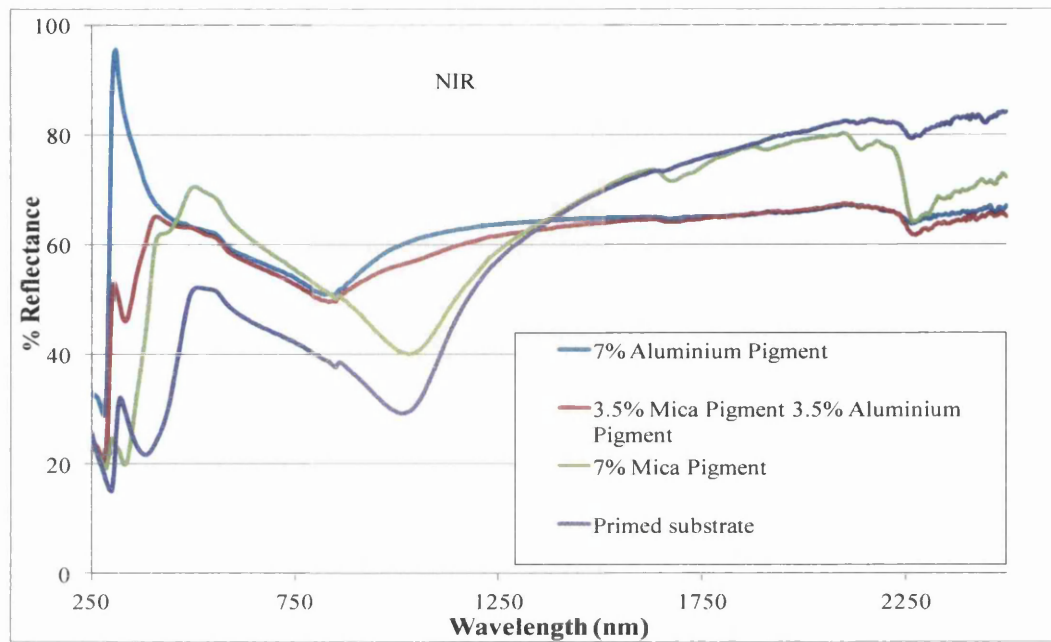


**Figure 6.25 - UV-Vis-NIR Reflectance Spectra of Polyester Coated Panels**

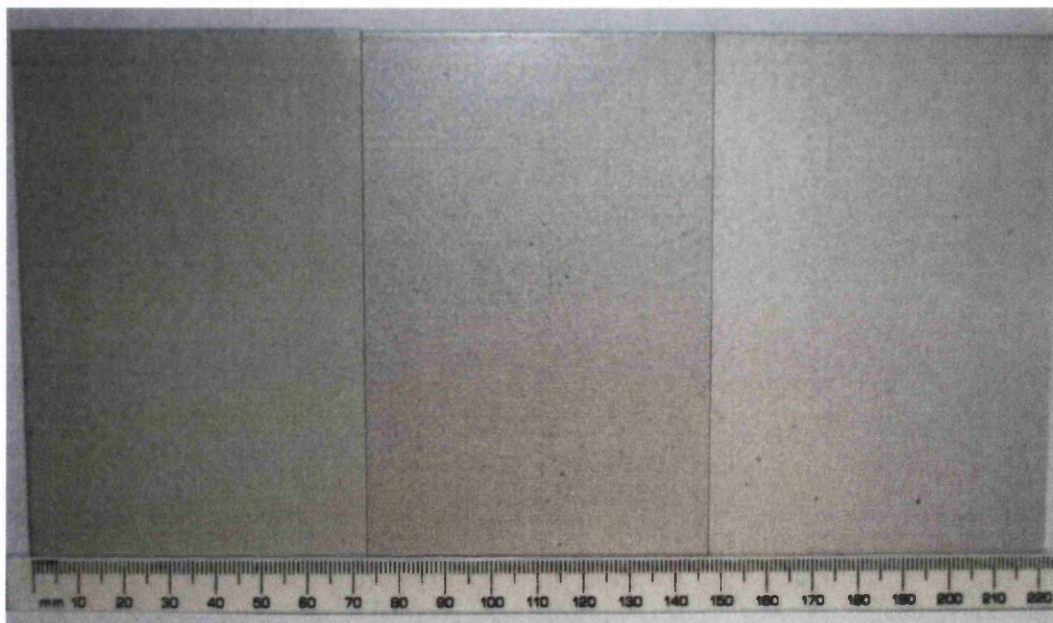


**Figure 6.26 – Comparison of 7% Mica Pigment Coating (Left); 3.5% Aluminium Pigment/3.5% Mica Pigment Coating (Middle); 7% Aluminium Pigment Coating (Right) Showing the Green Chromated Primer Showing through the 7% Mica Pigment Coating**



NIR cure trials comparing the PMT reached by the aluminium and mica pigment coatings were carried out using the same NIR oven settings and the PMTs reached are shown in Figure 6.27. An increase in PMT was observed at both NIR lamp settings on moving from the mica pigment coating to the mixed pigment coating to the aluminium pigment coating; this is consistent with the spectroscopy results. This is mirrored in the surface finish at both lamp settings shown in Figure 6.28 and Figure 6.29; the surface becomes more extensively blistered and even browned when aluminium pigment is present.

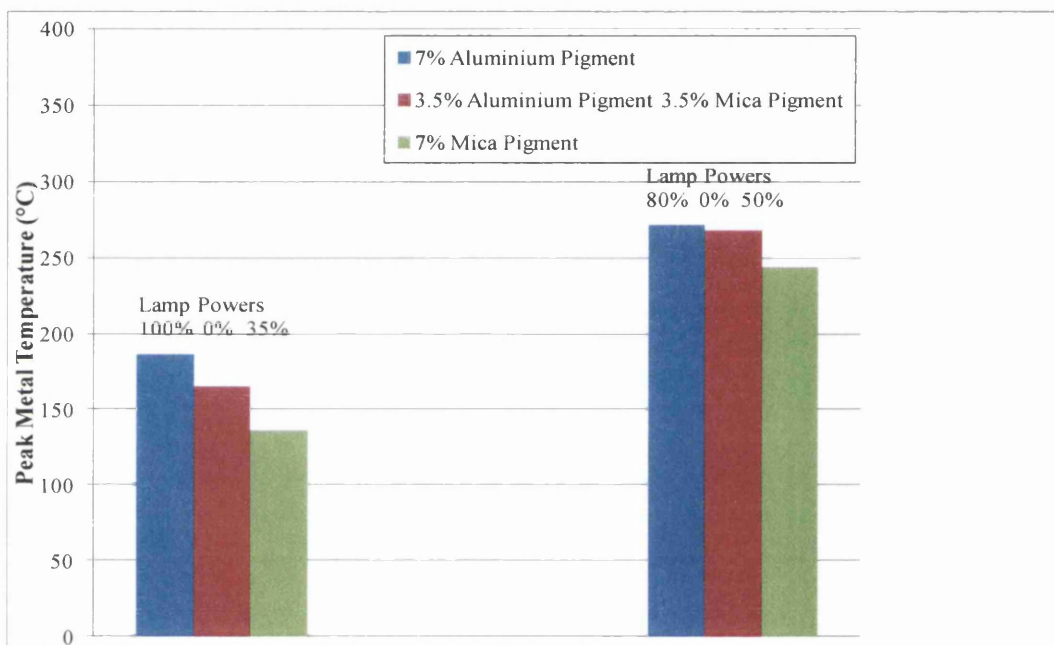


**Figure 6.27 – Comparison of PMTs Reached by Aluminium Pigment and Mica Pigment Coatings using Two Different NIR Lamp Power Settings**

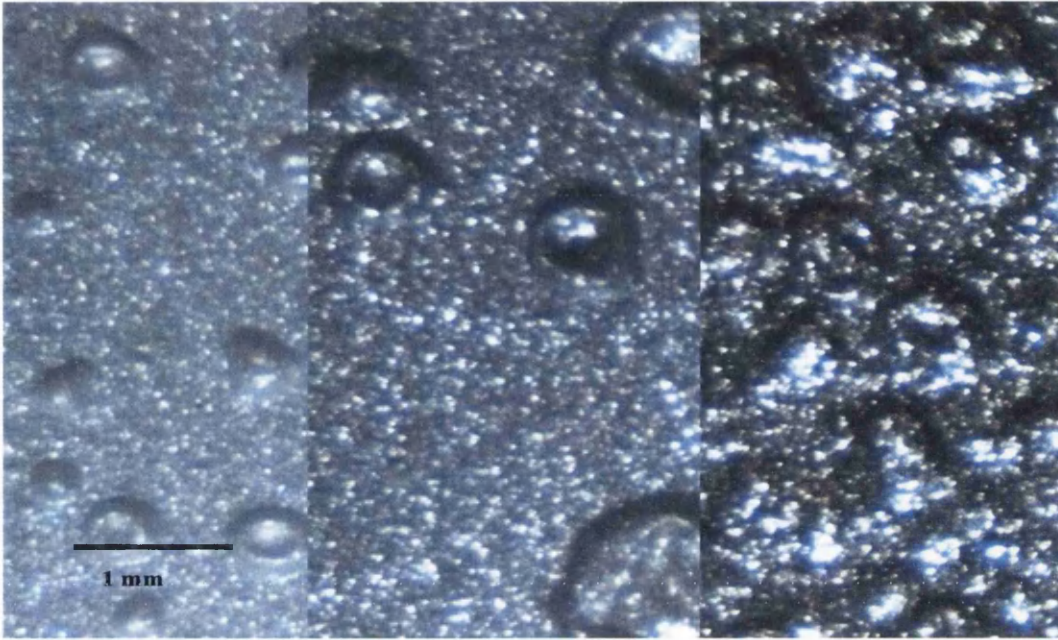


**Figure 6.28 - Comparison of Surface Finish: 7% Mica Pigment Coating (Left); 3.5% Aluminium Pigment/3.5% Mica Pigment Coating (Middle); 7% Aluminium Pigment Coating (Right) with 100% 0% 35% Lamp Power Settings**

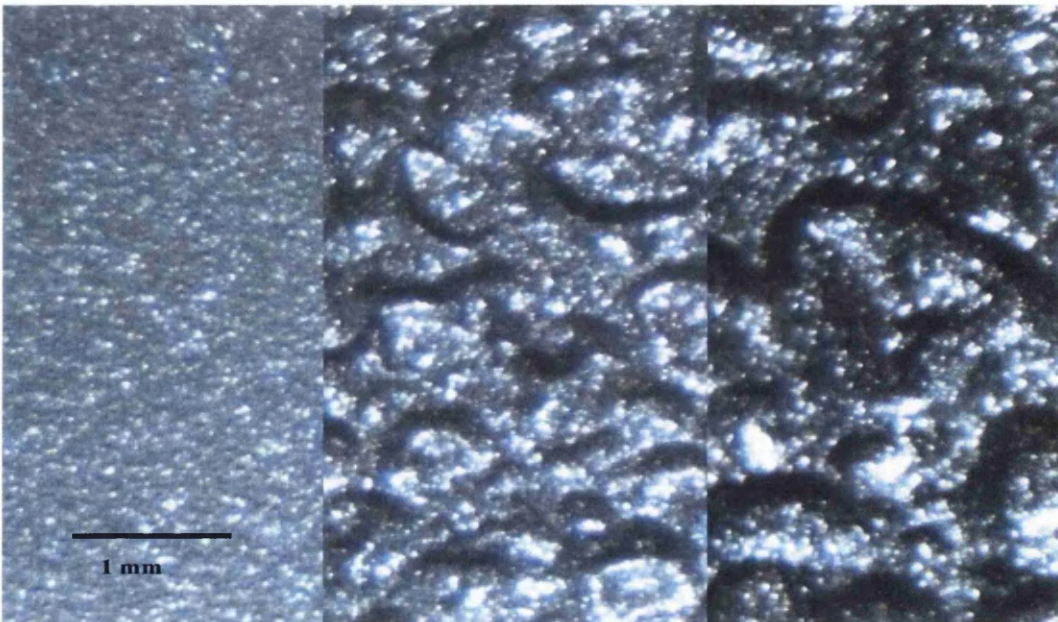


**Figure 6.29 - Comparison of Surface Finish: 7% Mica Pigment Coating (Left); 3.5% Aluminium Pigment/3.5% Mica Pigment Coating (Middle); 7% Aluminium Pigment Coating (Right) with 80% 0% 50% Lamp Power Settings**

Whilst the NIR transparency of a coating seems to be key to its ability to cure, there must be other factors involved as transparency alone does not explain the difference in curability between black and silver (aluminium flake) coatings.

Another physical property which will affect cure is emittance, the ability of a coating to re-emit absorbed radiation. The emittances of the aluminium, glass and mica flake coatings along with those for standard white and black polyester were measured with a Devices & Services AE1 emissometer and are shown in Figure 6.30. It can be seen that compared to all the other coatings, the silver (aluminium flake) coating has the lowest emittance of 0.68, i.e. it has the greatest ability to 'hold on' to the radiation that it has absorbed thus allowing a higher PMT to be reached during cure.

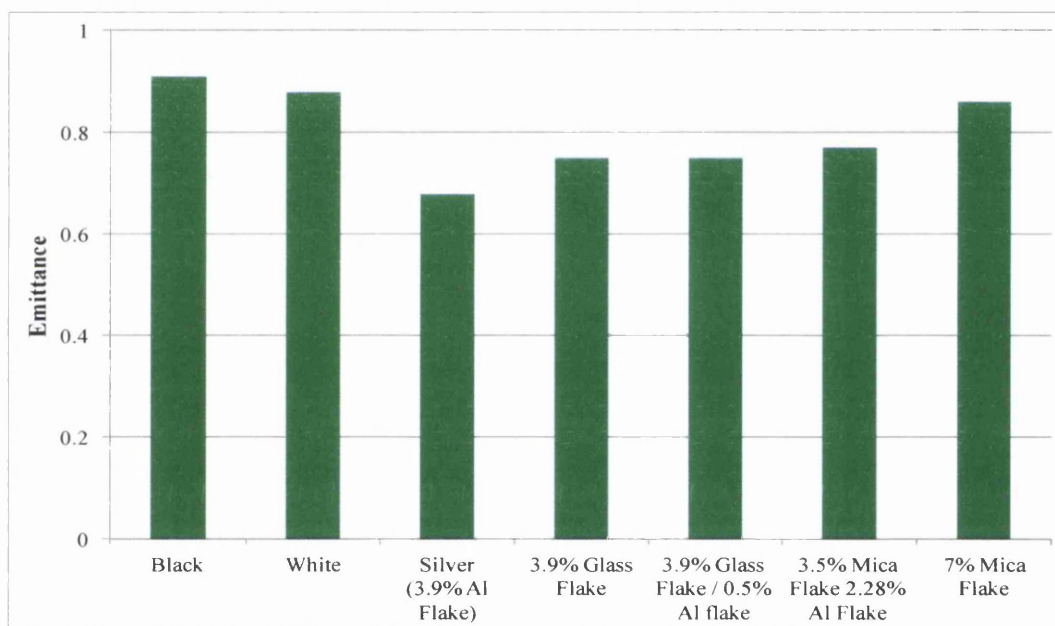


**Figure 6.30 – Emittance of Polyester Coatings**

## 6.4 Changes to Substrate

It was noted during NIR cure trials with MagiZinc substrate that in some of the cure trials using aluminium pigmented top coats, the microstructure of the galvanised substrate had changed, such as shown in Figure 6.31.

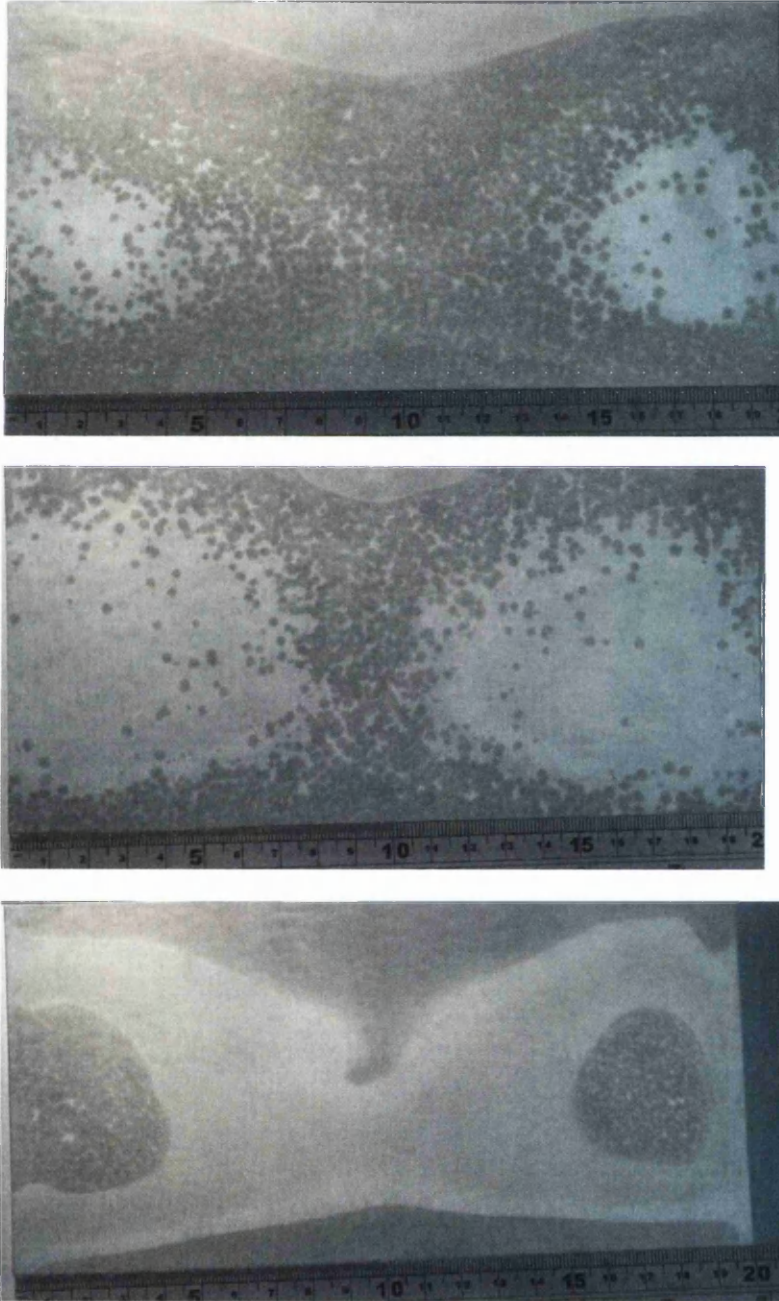


**Figure 6.31 – Changes to the Microstructure of the MagiZinc Substrate during NIR Cure**

This suggests that the galvanised surface has got hot enough to reflow the MagiZinc. Tin plate is often reflowed during production promoting the creation of an

iron-tin inter-metallic layer as this improves surface finish, and NIR has been demonstrated in this application [9].

The changes to the MagiZinc microstructure appear to correlate with temperature variation across the substrate panel during NIR cure caused by substrate holder heat sink effects and variation of air flow across the substrate due to oven geometry. It would be interesting to investigate this further using SEM and IR thermography.

## 6.5 Conclusions

This work has demonstrated the difficulty of NIR curing silver polyester coatings pigmented with aluminium flake. During the cure process both physical and chemical changes are taking place; the removal of solvents and the cross-linking of the polyester resin. With aluminium flake pigmented polyester coatings, it is very difficult to remove sufficient solvent before the polyester starts cross-linking and cured coatings result that are both soft (under cured) and blistered at the surface. Reformulation to remove some of the higher boiling solvents and a slower catalyst to delay the start of the polyester cross-linking reaction have been seen to improve the cure, but are unlikely to be adequate enough measures to allow industrial NIR cure of silver polyesters.

The assumption in this work was that a coating will cure most easily when it does not absorb a lot of NIR radiation but allows NIR that is not reflected at the surface to be transmitted through the coating to cure the coating from the bottom layer upwards. The aluminium flake was therefore replaced with less NIR absorbing coated mica flake or coated glass flake resulting in coatings that reached lower PMTs than an aluminium flake coating at the same NIR oven setting. These coatings however had a much lower hiding power; aluminium flake has a hiding power ca. 4.5 times that of glass flake.

Another physical property likely to affect the ability of a coating to NIR cure is emittance. Compared to black or white polyester coatings silver coatings have a lower emittance, and are thus less able to re-emit any NIR radiation absorbed. This will contribute to the propensity of silver polyesters to retain heat and visibly brown during curing.

Pigment morphology may also be playing a part. In contrast to other polyesters pigmented with organic or inorganic pigments where the pigments are less than the wavelength of NIR radiation in size, aluminium flakes have a lamellar geometry. The length of the flakes are approximately the thickness of the coating, so the flakes will end up orientating themselves in an over lapping manner as shown in Figure 6.32. This will lead to a longer more tortuous path being presented to the solvent for evaporation during cure. Indeed, aluminium flake is specifically used as a vapour barrier pigment in polymeric materials [10].

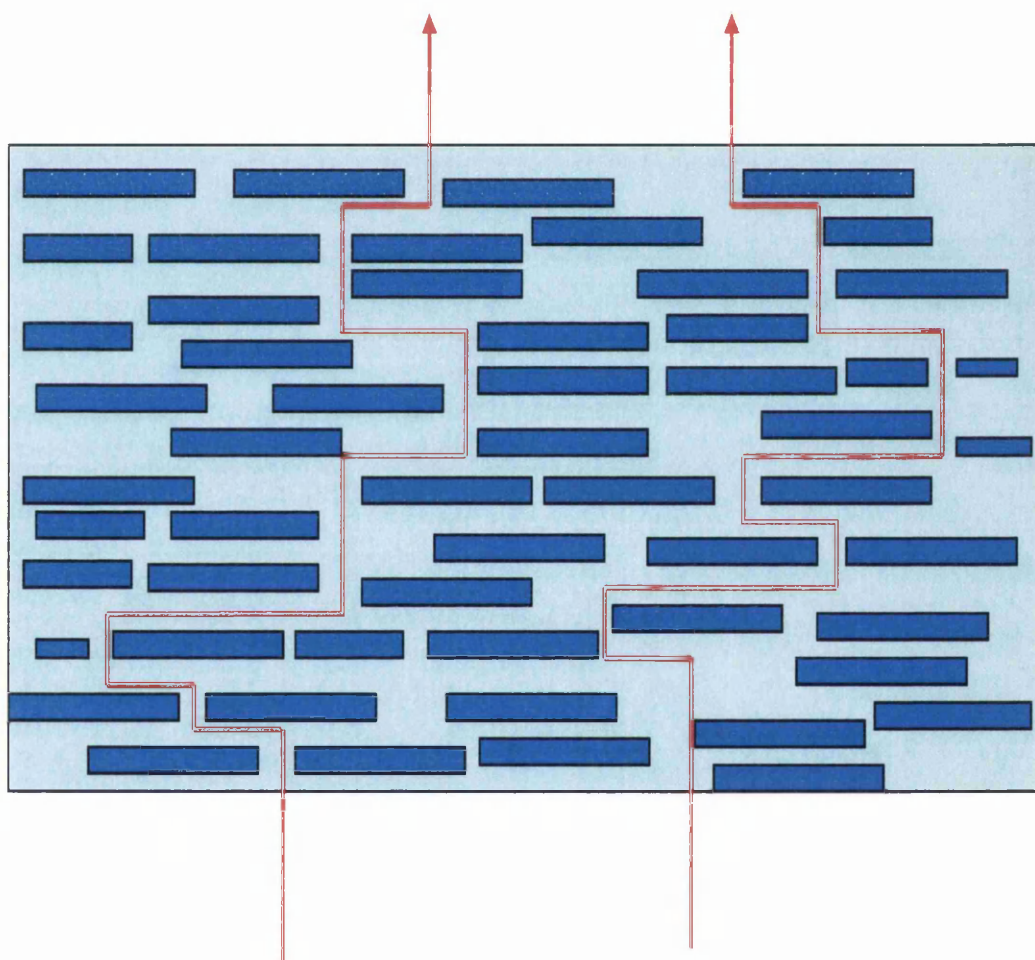


**Figure 6.32 – Lamellar Aluminium Flake Presenting a Barrier to Solvent Evaporation**

In conclusion, the best NIR formulation for silver polyesters may be one where the aluminium flake is replaced by mica flake, as it gives a coating with a higher emittance than glass flake. However, it should be remembered that the lamellar structure of mica flake could also act as a barrier to solvent evaporation during cure. Hiding

power of a mica flake coating could be increased by applying the coating over a primer tinted with small amounts of pigments such as carbon black. Mica flake size and size distribution range will affect the appearance of the coating, so a paint formulator will be able to use all these factors to formulate a coating with similar colour and appearance characteristics using a goniospectrophotometer to check colour difference. NIR curing trials can then be used to assess the cure window of this coating system.

## 6.6 References

1. Colorcoat, *Sustainable Building Envelope Centre*. (cited 13th Sept 2013). Available from: <http://www.colorcoat-online.com/blog/index.php/2012/05/sustainable-building-envelope-centre/>.
2. Personal communication with Broekhuis, R., Tata Steel. April 2011
3. Mabbett, I., *Applications of Near Infrared Heating of Interest to the Coil Coating Industry*. 2011, Eng. D., Swansea University
4. Kaupp, G., Schmidt, U., Schumacher, D., and Steinbach, K. *Effect pigments comprising a glass flake substrate*, EP1980594 A1 (2008)
5. Pfaff, G., *Special Effect Pigments*. 2nd ed. 2005: Vicentz Network.
6. Pfaff, G., *Special Effect Pigments: Technical Basics and Applications*. 2008: Vicentz Network.
7. Koleske, J.V., ed. *Paint & Coating Testing Manual*. 1995, ASTM.
8. Nadal, M.E. and Early, E.A., *Color measurements for pearlescent coatings*. Color Research and Application, 2004. **29**(1): p. 38-42.
9. Mabbett, I., Geary, S., Warren, D.J., Sullivan, J.H., Penney, D., Watson, T.M., and Worsley, D.A., *Near Infrared Heat Treatment to Flow Melt Tinplate Pore Formation and Characterization*. ECS Transactions, 2013. **50**(37): p. 155-164.
10. SpecialChem, *Aluminium Pigments*. (cited 17 Oct 2013). Available from: <http://www.specialchem4polymers.com/>.



**Chapter 7**  
**Investigation of Transpired Solar**  
**Collector Performance**

## 7.1 Introduction

Previous chapters have explored how NIR absorption and the locus of NIR absorbing pigments within the coating layers influence the NIR cure of polyester coating systems on galvanised steel substrates. Understanding from this research has been of use to Tata Steel in their industrial production of NIR cured polyester coil coating products.

Another Tata Steel product utilising the interaction of radiation with a coating system is the transpired solar collector Colorcoat Renew SC<sup>®</sup>, an example of which is shown in Figure 7.1.

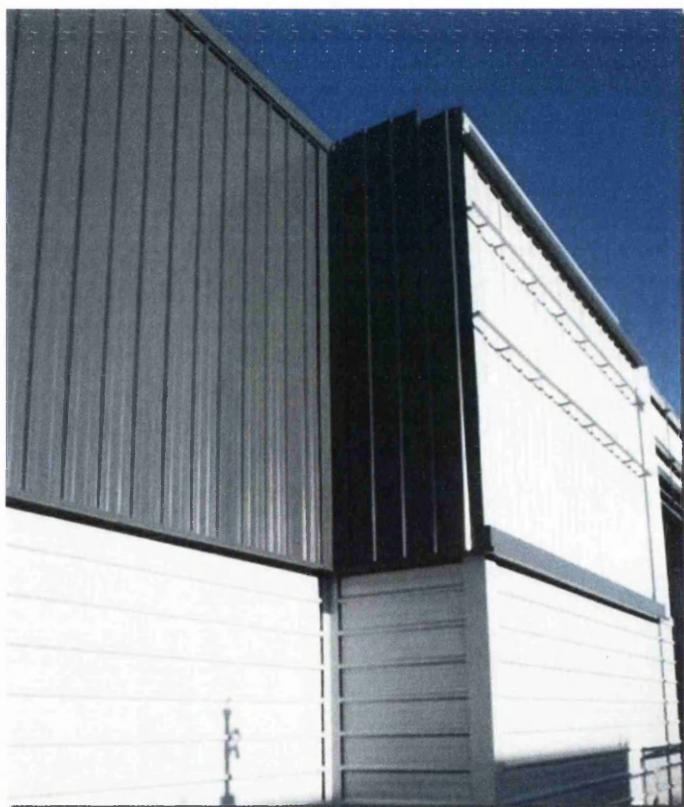


**Figure 7.1 – Jaguar Land Rover Deck 92 Project incorporating Colorcoat Renew SC<sup>®</sup>, a transpired solar collector [1]**

In contrast to the interaction of NIR with a polyester top coat during NIR cure, the aim with a transpired solar collector is for solar radiation (5% UV, 45% visible and 50% NIR) to interact with the coating system and produce a high heat gain. This heat is then transferred to the thin barrier layer of air in front of the collector which is drawn by

a fan through perforations in the collector surface into the plenum behind. The heated air is then carried on to supplement a building's heating system or to dry crops.

An ideal transpired solar collector will therefore have a surface with a low Total Solar Reflectance (TSR) and low emittance ; such surfaces are known as solar selective surfaces [2]. The ideal reflectance spectrum for such a surface is given in Figure 7.2.

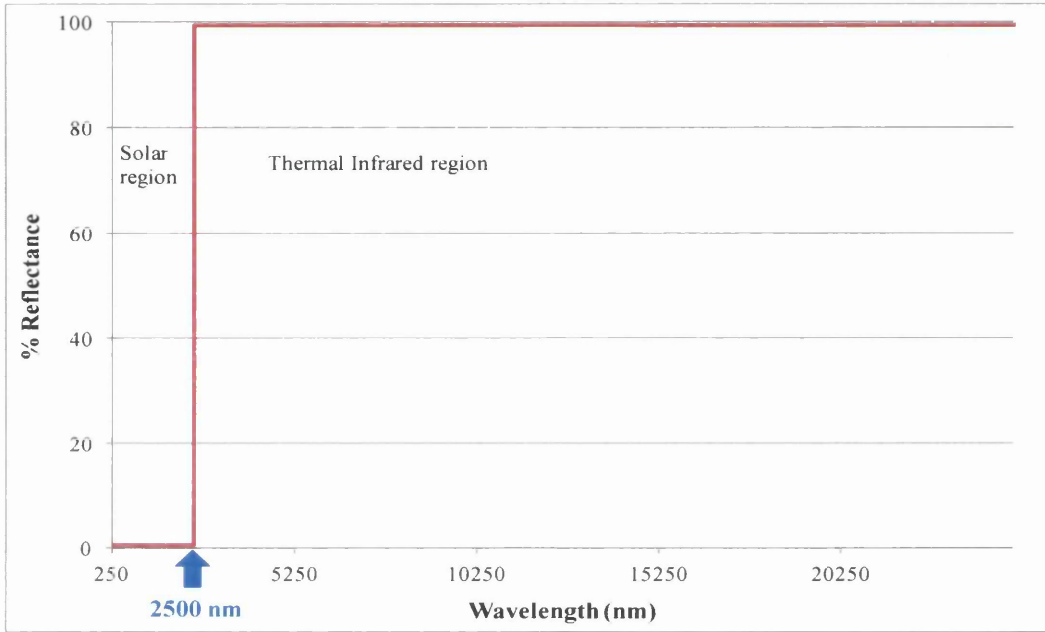


**Figure 7.2 – Ideal Reflectance Spectrum for a Solar Selective Surface**

Black coatings will obviously produce the lowest TSRs, but previous research suggests 85% of architects would prefer colours other than black, even if this incurs lower efficiencies [3]. Orel et al have produced coloured (red, blue and green) spectrally selective coatings whose spectral selectivity is independent of coating thickness, so called thickness insensitive spectrally selective (TISS) coatings [3, 4]. In these coatings, low emittance was achieved by the presence of aluminium flake, coloured aluminium flake or copper flake in the formulation whilst other inorganic pigments imparted colour with black pigment added to reduce TSR.

ASTM Standard E1980-11 defines the Solar Reflective Index (SRI) incorporating both TSR and emittance values to give a surface an index of ‘coolness’ and its associated Steady State Surface Temperature (SSST) [5, 6]. SRI is defined such that a standard black surface (reflectance = 0.05, emittance = 0.90) has a SRI of zero and a standard white surface (reflectance = 0.80, emittance = 0.90) a SRI of one.

For a surface exposed to the sun and when the conduction of the material is zero, its Steady State Surface Temperature (SSST) can be defined by:

**Equation 7.1** 
$$\alpha l = \varepsilon \sigma (T_s^4 - T_{sky}^4) + h_c (T_s - T_a)$$

where

$\alpha$  = solar absorbance = 1 - solar reflectance

$l$  = solar flux  $Wm^{-2}$

$\varepsilon$  = emittance

$\sigma$  = Stefan Boltzmann constant,  $5.66961 \times 10^{-8} W m^{-2} K^{-4}$

$T_s$  = steady state surface temperature, K

$T_{sky}$  = sky temperature, K

$h_c$  = convective coefficient,  $W m^{-2} K^{-1}$

$T_a$  = air temperature, K

If TSR, emittance and the convective coefficient are known, Equation 7.1 can be solved iteratively to obtain the steady state surface temperature. Alternatively, steady state surface temperature can be defined as follows:

**Equation 7.2** 
$$T_s = 309.7 + \frac{(1066.07\alpha - 31.98\varepsilon)}{(6.78\varepsilon + h_c)} - \frac{(890.94\alpha^2 + 2453.86\alpha\varepsilon)}{(6.78\varepsilon + h_c)^2}$$

Solar Reflective Index is defined as:

$$\text{Equation 7.3} \quad SRI = 100 \frac{(T_b - T_s)}{(T_w - T_s)}$$

where

$T_b$  = steady state temperature of black surface

$T_w$  = steady state temperature of white surface

Under standard solar and ambient conditions (solar flux =  $1000 \text{ Wm}^{-2}$ , ambient air temperature = 310 K, ambient sky temperature = 300 K), Equation 7.3 is reduced to:

$$\text{Equation 7.4} \quad SRI = 123.97 - 141.35\chi + 9.6555\chi^2$$

where

$$\text{Equation 7.5} \quad \chi = \frac{(\alpha - 0.029\varepsilon)(8.797 + h_c)}{(9.5205\varepsilon + h_c)}$$

An ideal transpired solar collector will therefore have a low SRI value. In this chapter the performance of transpired solar collectors were investigated. Two NIR absorbing pigments were assessed for their ability to improve transpired solar collector performance by increasing solar selectivity, and the outdoor performance of a transpired solar collector under UK weather conditions was investigated.

## 7.2 Experimental Techniques

### 7.2.1 Preparation of NIR Pigmented Coating Panels

Samples of Goosewing Grey (RAL 7038) polyester were prepared with a range of percentage weights of NIR absorbing pigment. Discussions with pigment manufacturers resulted in Iriotec 8840 (supplied by Merck) and IR202 (supplied by BASF) being used for this purpose. Iriotec 8840, formula  $\text{Cu}_3(\text{PO}_4)_2 \cdot \text{Cu}(\text{OH})_2$ , is a polymer laser marking additive for use with fibre, YAG and vanadate lasers from 1060 - 1070 nm. IR202 is a developmental research pigment of doped metal oxide nanoparticles, synthesised via a thermal plasma route. Goosewing Grey (RAL 7038) polyester was used as supplied by Tata Steel and dispersed with the NIR absorbing pigments with the aid of a high shear mixer.

Panels of 0.50 mm x 210 mm x 150 mm HDG steel substrate were coated with NIR pigmented GWG top coat (dft  $19 \pm 1 \mu\text{m}$ ) and cured in an AEW convection oven set at 340 °C with an oven dwell time of 30 secs.

### 7.2.2 Outdoor Testing of Transpired Solar Collector Panel

A unit of Solarduct® was used to investigate the outdoor performance of a transpired solar collector under typical UK weather conditions. Solarduct® is marketed by Conserva Engineering as a modular roof top transpired solar collector [7]. It was an ideal choice for this work as it is designed to be used in settings where a wall mounted collector is not feasible. Health and safety considerations at Swansea University campus meant that there was not a suitable location for a wall mounted collector study, so an open roof top location was chosen instead.

The Solarduct® unit used is shown in Figure 7.3 and had a solar collector plate of area  $0.79 \text{ m}^2$  and a porosity of 0.2%, where porosity is defined as the percentage of pores covering the collector area. The panel coating was GWG with no NIR absorbing pigment additions. A fan and variable voltage AC/DC adapter were fitted to the unit to best match the flow rate range ( $36 - 110 \text{ m}^3/\text{h}/\text{m}^2$ ) through the unit typical for transpired solar collectors given in the literature [8]. Hence a Bi-Sonic (BP802512H-03)12V DC fan with specification of  $75 \text{ m}^3/\text{h}$  flow rate was chosen, enabling a maximum flow rate of  $95 \text{ m}^3/\text{h}/\text{m}^2$ .



**Figure 7.3 – Unit of Solarduct® used for outdoor testing**

The unit was placed outdoors and orientated due south to maximize solar heat capture. K type thermocouples were connected to an Omega TC08 data logger and used to measure temperature at four locations on the unit, as shown in Figure 7.4.

The temperature of the collector panel was measured by a thermocouple taped to make contact with the underside of the panel. Ambient air temperature was measured at the back of the unit. The plenum (cavity) air temperature was measured by a thermocouple taped to the inside of the collector panel and dangling in the plenum air space. The final thermocouple was taped close to the fan outlet and measured fan outlet air temperature. Temperatures were logged at one second time intervals over a 45 minute time period.

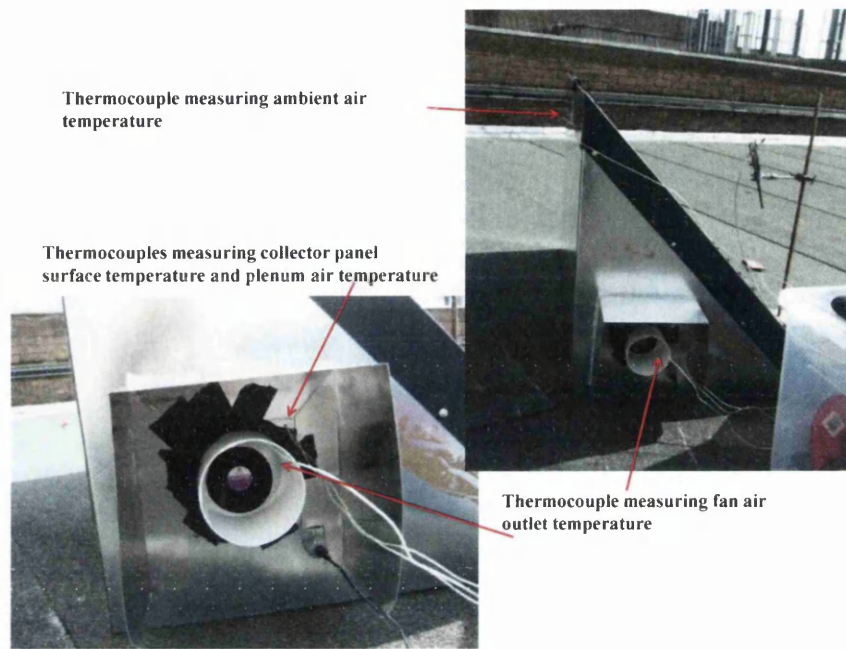


**Figure 7.4 – Side elevation of Solarduct® showing position of thermocouples**

A deuterium/tungsten halogen standard light source was used to make a radiometric calibration of the absolute spectral response of a portable Ocean Optics HR2000+ UV-visible-NIR spectrometer. The spectrometer was fitted with an optical fibre patch cable and cosine corrector, and used to measure solar irradiance during a 45 minute time period.

Measurements of solar irradiance ( $\text{Wm}^{-2}$ ) were taken at a distance of 400 mm from the collector panel surface with the spectrometer probe orientated at the same angle to the sun as the panel surface. Spectral acquisitions were made as an integral spectral range from 118 to 1106 nm, this range being limited by the range of the spectrometer's CCD detector. An acquisition was made as an average of every 10 scans and with a boxcar setting of 2. Box car width applies smoothing to spectral data acquisitions by averaging over a specified number of pixels to the left and right of a detector element.



## 7.3 Results and Discussion

### 7.3.1 Effect of NIR Absorbing Pigments on TSC Performance

UV-Vis-NIR spectra in reflectance mode were recorded of Goosewing Grey coated HDG panels with varying percentages of either Iriotec 8840 or IR202 added to the coating and typical spectra are shown in Figure 7.5 and Figure 7.6. Also superimposed in these Figures is the solar irradiation profile.

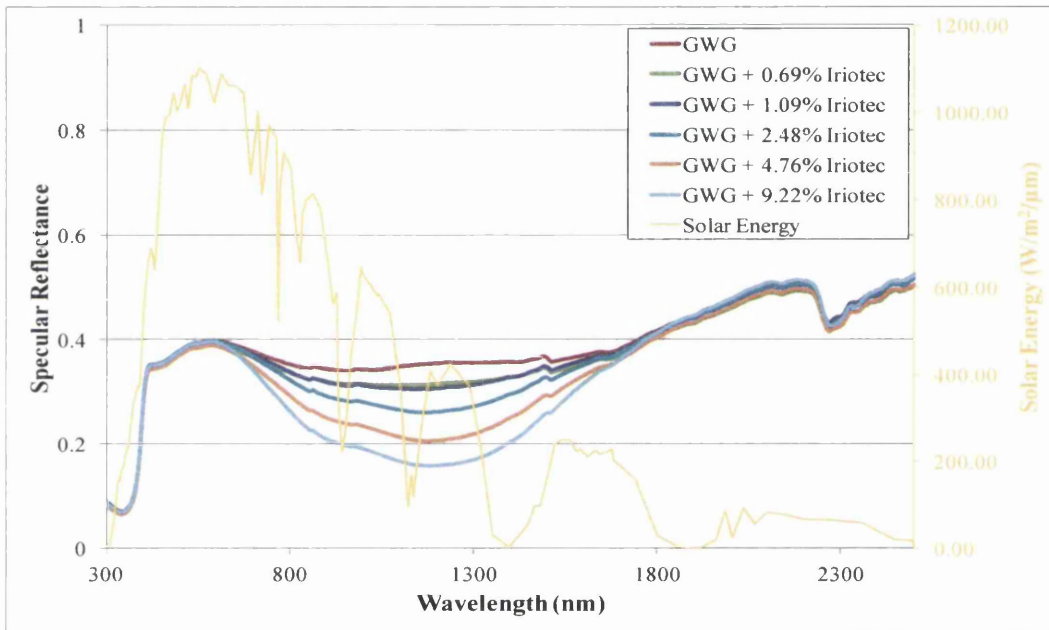
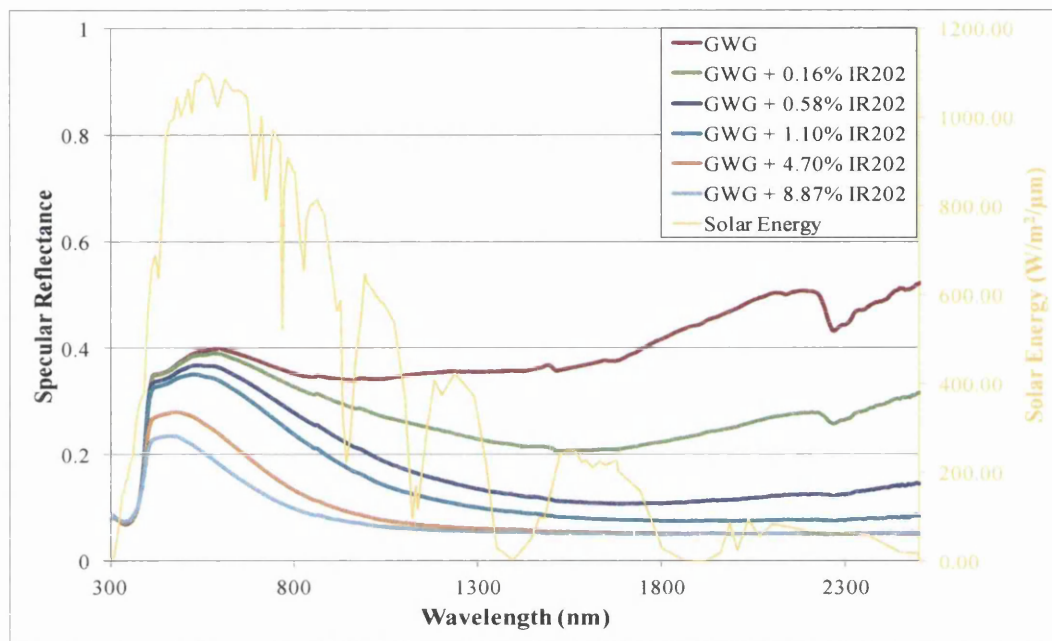


Figure 7.5 – UV-Vis-NIR Reflectance Spectra of GWG Polyester with additions of Iriotec 8840



**Figure 7.6 – UV-Vis-NIR Reflectance Spectra of GWG Polyester with additions of IR202**

Figure 7.5 and Figure 7.6 show that the presence of the NIR absorbing pigments decreases the reflectance of the coating. In the case of Iriotec 8840 the diminishing in reflectance is concentrated over a much narrower band of wavelengths than for IR202, with the maximum diminution occurring between 1180 -1190 nm. The IR202 pigment has a greater diminishing effect, and this effect also occurs over a far wider range of wavelengths. Decrease in reflectance for this pigment is however more pronounced in the visible range (380 - 700 nm) and this will have the disadvantage of affecting colour more. There is also more decrease at longer wavelengths (> 1800 nm); however solar irradiation levels are lower here too.

Addition of the NIR absorbing pigments has only a very small effect on the emittance of the coating surface, with 9% Iriotec 8840 increasing emittance by 0.02 and 9% IR202 increasing it by 0.05. This could be attributed to a slight increase in surface roughness on pigment addition.

TSR values were calculated from the UV-Vis-NIR reflectance spectra in Figure 7-5 and Figure 7.6, and together with emittance values were used to calculate the Steady State Surface Temperature using Equation 7.2. This equation requires a value for the

convective coefficient, which is a measure of heat transfer through convection due to wind and is specified in ASTM Standard E1980-11 as 5, 12 and 30  $\text{W m}^{-2} \text{K}^{-1}$  respectively for low, medium and high wind conditions.

The variation of Steady State Surface Temperature with NIR absorbing pigment content at low, medium and high convective coefficient values is shown in Figure 7.7, and highlights that as expected IR202 (red markers in Figure 7.7) has a greater effect on Steady State Surface Temperature than Iriotec 8840 (green markers in Figure 7.7). For example, a 5% pigment loading with medium wind conditions gives a  $5^\circ\text{C}$  lift in Steady State Surface Temperature with IR202 but less than  $2^\circ\text{C}$  lift with Iriotec 8840.

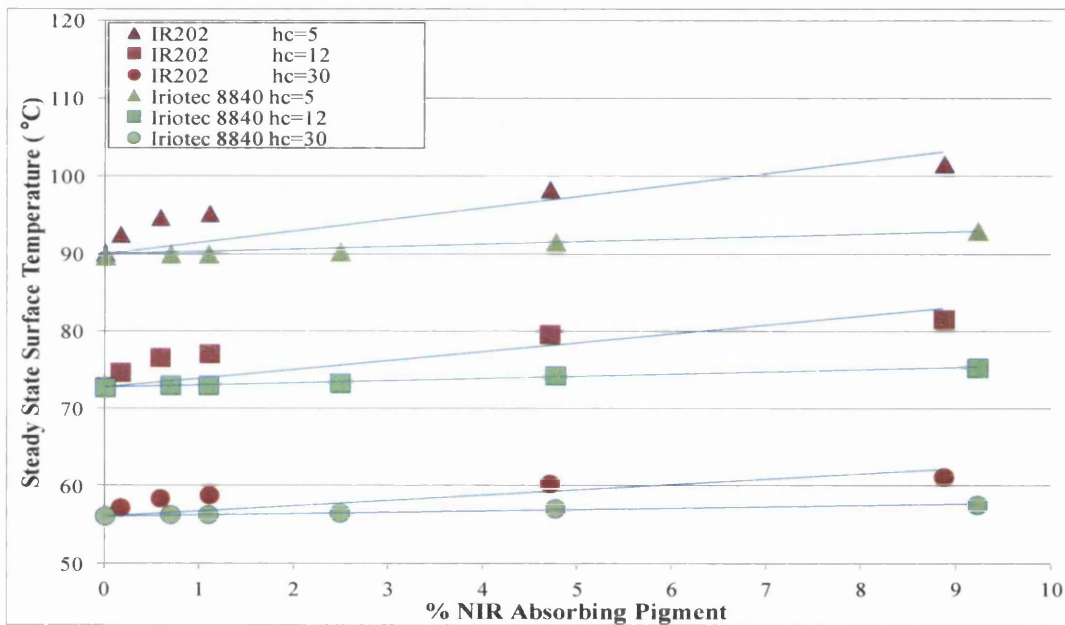


**Figure 7.7 – Variation of Steady State Surface Temperature with NIR absorbing pigment content, at low, medium and high convective coefficient ( $h_c$ ) values**

What is more interesting is the effect of wind speed on Steady State Surface Temperature, as shown for 1% pigmented coatings in Figure 7.8. Here, the effect of varying wind speed has a far greater effect than that shown by pigment addition in Figure 7.7. For example, by dropping from a high to a low wind speed ( $30$  to  $5 \text{ W m}^{-2} \text{K}^{-1}$ ), the Steady State Surface Temperature of the 1% pigmented IR202 coating increases by  $36^\circ\text{C}$  as the rate of convection off the surface decreases.

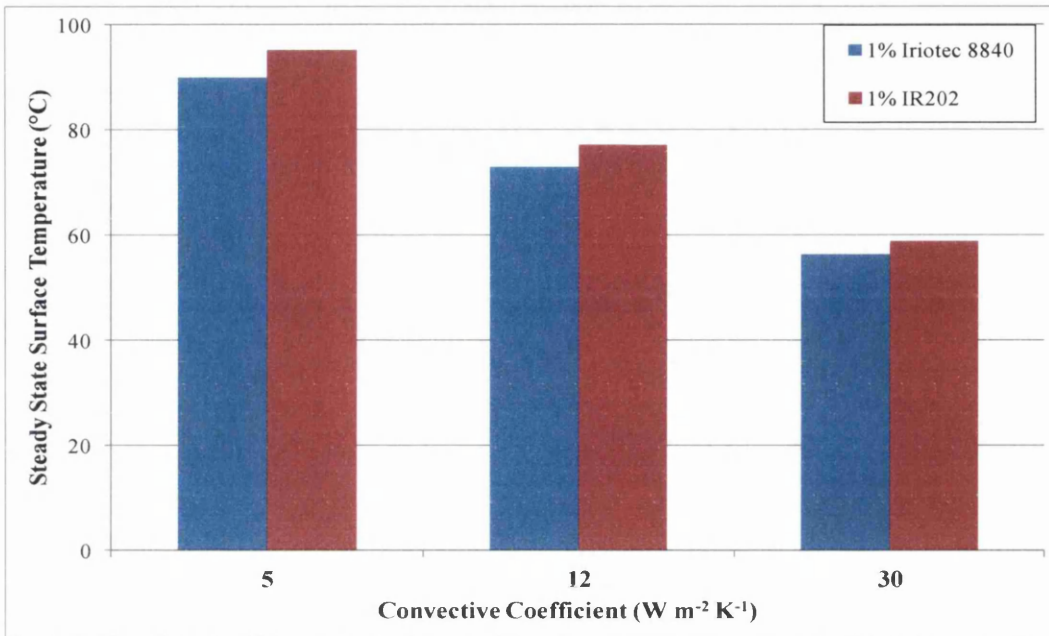
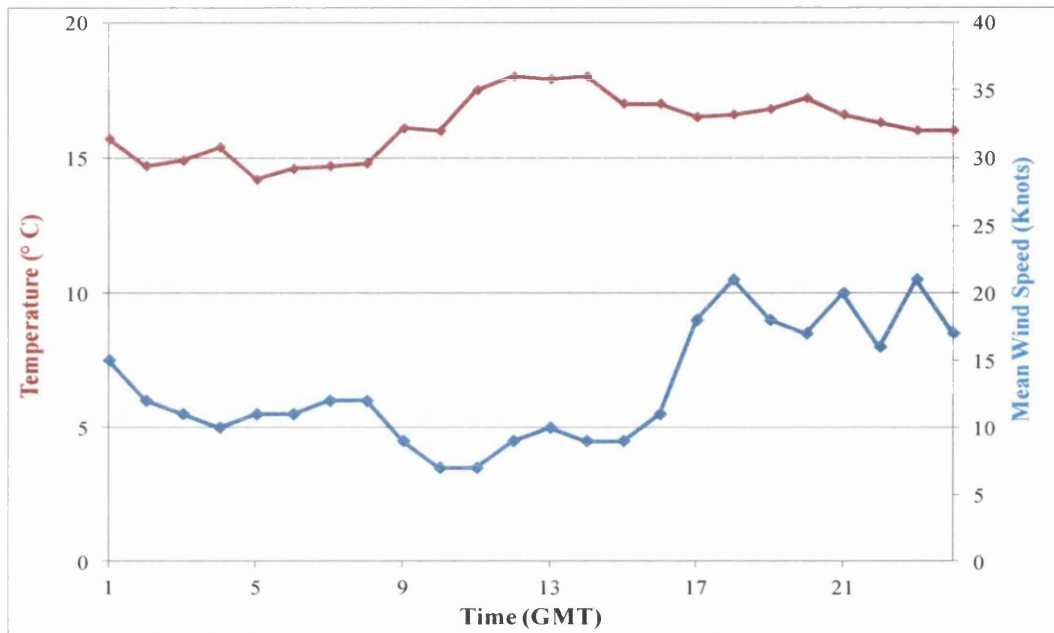


Figure 7.8 - Variation of Steady State Surface Temperature with convective coefficient (wind speed)

### 7.3.2 Outdoor Testing of Transpired Solar Collector Panel

Temperature and solar irradiance data was collected over 45 minute time intervals on 22 September 2010 at a Swansea University campus roof location. Meteorological Office data for this day from the nearest Meteorological station, Mumbles Head shows the variation in wind speed and temperature for that day is given in Figure 7.9 [9]. The maximum temperature for that day was 18 °C.



**Figure 7.9 – Mumbles Head Meteorological Station Weather Data for 22<sup>nd</sup> September 2010**

The solar collector was operated at three different flow rates by varying the voltage across the collector fan, and profiles for the collector surface temperature as well as the plenum air and fan air outlet temperature were measured against the ambient air temperature for each flow rate. The flow rate resulting from operation of the fan at its specified voltage of 12 V gave a flow rate of 95 m<sup>3</sup>/h/m<sup>2</sup> and was designated as the high flow rate. Designations of low and medium flow rate were given to the collector operating with 7.5 V and 3 V applied across the fan motor, although it was not possible to equate these voltages (applied using a variable voltage AC/DC adapter) to a numerical flow rate. Solar irradiance was measured over the experimental time period.

Temperature and solar irradiance profiles for the three flow rates are shown in Figure 7.10, Figure 7.11 and Figure 7.12. A clear lift in temperature is seen from ambient air temperature given by the purple plot, to the temperature at the back of the collector panel (blue plot). The temperature of the air inside the collector then drops as it makes its way through the collector unit due to heat transfer losses.

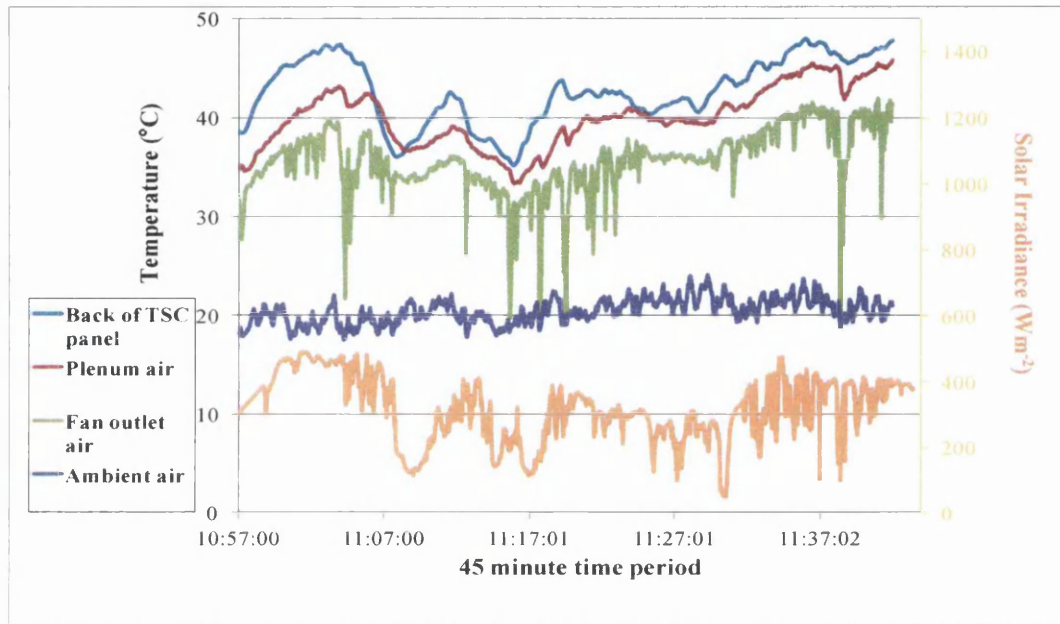


Figure 7.10 – TSC Temperature Profiles for Low Flow Rate Conditions

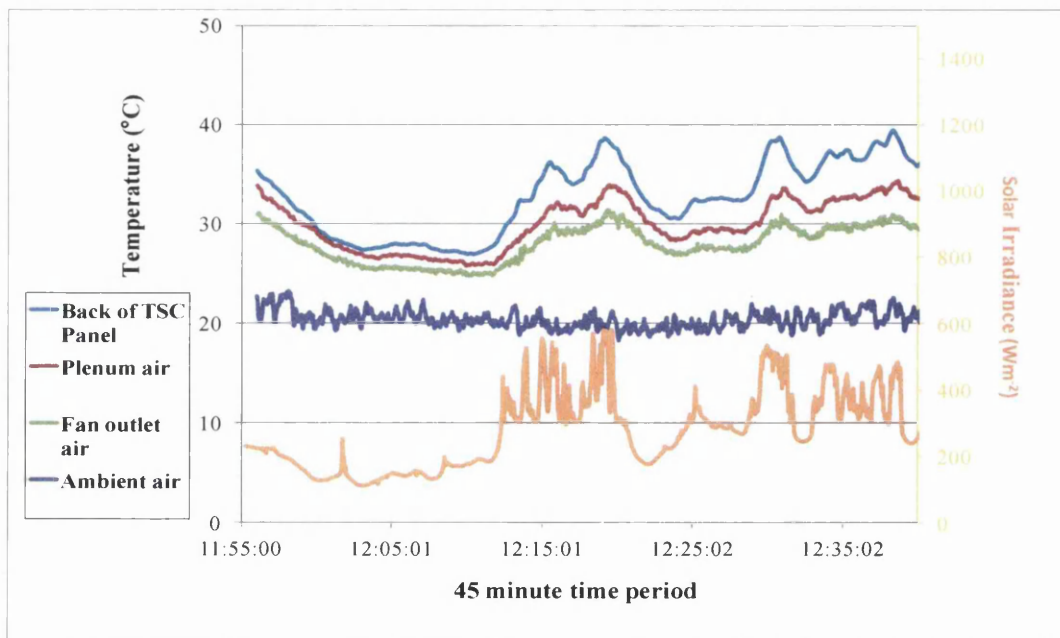
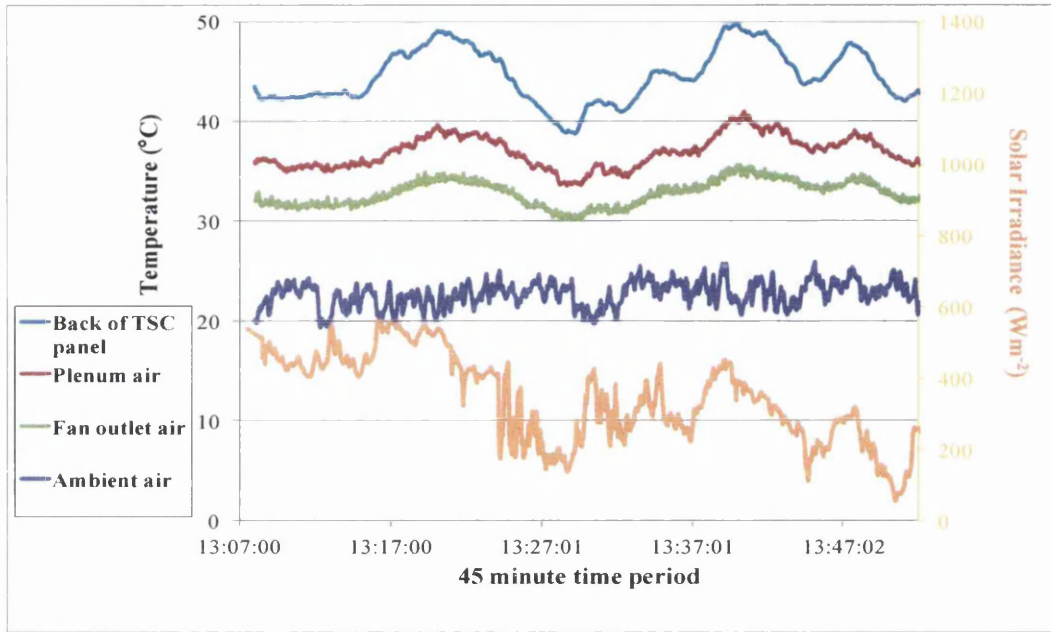


Figure 7.11 - TSC Temperature Profiles for Medium Flow Rate Conditions



**Figure 7.12 - TSC Temperature Profiles for High Flow Rate Conditions**

The fan outlet air temperature in Figure 7.10 shows a ‘noisy’ profile which can be attributed to electrical noise picked up by the thermocouple from the fan motor.

The mean ambient air temperatures from the above Figures are shown in Table 7.1 and are slightly higher than the mean meteorological station temperature of 16.2 °C. This can be attributed to passive solar gain; ambient air at the roof top location will be warmed via solar radiation absorbed by the asphalt roofing surface (asphalt emissivity = 0.93).

**Table 7.1 – Comparison of TSC Temperature Gain at Different Flow Rates**

	Low flow rate	Medium flow rate	High flow rate
Mean ambient air temperature (°C)	20	22	22
Mean back of panel temperature (°C)	43	37	42
Mean temperature gain (°C)	23	15	20
Mean Solar Irradiance (Wm <sup>-2</sup> )	327	267	284

The dynamic range of the spectrometer's charge-coupled device (CCD) detector is limited to the ultra violet, visible and near infrared wavelengths of the solar spectrum (up to wavelength 1106 nm); hence only 79% of the solar irradiance spectrum has been detected by the spectrometer's detector, with the longer infrared wavelengths unrecorded (Percentage derived from ASTM-G-173-03 data). Interestingly, despite this limitation the temperature profiles in Figure 7.10, Figure 7.11 and Figure 7.12 all mirror the solar irradiance profiles suggesting a clear link between solar irradiance and heat gain. This has occurred at all three flow rates, despite three very different patterns of solar irradiance within the experimental time periods, resulting from fluctuating cloud cover.

Table 7.1 also shows that the largest temperature gain of 23 °C is obtained with the collector operating at the lowest flow rate. Previous theoretical and empirical models have shown that collectors with lower flow rates give lower efficiencies and higher temperature rises, whilst higher flow rates give higher efficiency and lower temperature rises [8, 10-13]. However as solar irradiation and wind speed are also obviously fluctuating during these experiments and will affect temperature gain, these experiments cannot be used to draw conclusions about the effect of flow rate on temperature gain.



## 7.4 Conclusions

These experiments have shown that additions of NIR absorbing pigments to a transpired solar collector coating result in a modest increase in Steady State Surface temperature (ca. 5 °C lift for a 5% IR202 pigment loading), where Steady State Surface temperature is calculated via ASTM Standard E1980-1 using measured TSR and emittance values. Of the two NIR absorbing pigments investigated, IR202 has a greater effect on Steady State Surface temperature than Iriotec 8840 as its addition to the collector coating results in a more greatly reduced coating reflectance over a greater range of solar irradiance wavelengths, albeit with a more compromised coating colour.

In contrast to NIR pigment additions, convective heat transfer due to wind effects has a more significant effect on transpired solar collector surface temperature (ca. 36 °C decrease for 1% IR202 pigment loading on reduction from high to low wind speed). It can be concluded from this that decreasing the effect of wind from the surface of a transpired solar collector would be beneficial in increasing collector surface temperature. Possible ways of achieving this could be by the addition of baffles on the building to deflect wind, locating transpired solar collector panels on areas of a building where wind funnelling effects are minimised, or by the application of a transparent layer to the collector surface. A transparent layer over the collector surface would have the benefit of not only reducing convective losses due to wind, but also creating an artificial greenhouse effect. Sutton et al concluded that the introduction of a transparent layer on the surface of a transpired solar collector does improve performance but were unable to conclude whether this was due to the reduction of heat loss due to wind, the creation of an artificial greenhouse effect or to both [14].

These experiments have also shown that September UK weather conditions are capable of producing a temperature rise in excess of 20 °C across a transpired solar collector. These measured temperatures for the outdoor Solarduct® unit were lower than the Steady State Surface temperatures calculated from ASTM Standard E1980-11 due to the Standard's assumptions of standard solar conditions (solar flux = 1000 Wm<sup>-2</sup>, ambient air temperature = 310 K, ambient sky temperature = 300 K) and conditions of zero conductive heat transfer not being met in outdoor experimental conditions.

Outdoor experimental results showed that the temperature profile of the collector panel closely mirrored that of the solar irradiation profile falling on it, indicating a clear link between solar irradiation and heat gain.

Further work needs to be carried out in an outdoors experiment with a transpired solar collector, measuring the increase in temperature that could be realised with additions of IR202 pigment to the TSC coating. A carbon black tinted primer could be added to the coating system to increase absorption, and aluminium flake to the top coat to decrease emissivity. The experiments need to be run over longer time periods, and the University's recently acquired Kipp & Zonen pyranometer used to measure solar irradiance levels. A laboratory based experiment with a solar simulator source and a wind deflector to direct air onto the face of the collector panel would also provide complimentary results.

## 7.5 References

1. Colorcoat, *Jaguar Land Rover Deck 92*. (cited 30 August 2013). Available from: <http://www.colorcoat-online.com/blog/index.php/2012/05/jaguar-land-rover-deck-92/>.
2. Granqvist, C.G., *Solar energy materials*. *Advanced Materials*, 2003. **15**(21): p. 1789-1803.
3. Orel, B., Spreizer, H., Vuk, A.S., Fir, M., Merlini, D., Vodlan, M., and Kohl, M., *Selective paint coatings for coloured solar absorbers: Polyurethane thickness insensitive spectrally selective (TISS) paints (Part II)*. *Solar Energy Materials and Solar Cells*, 2007. **91**(2-3): p. 108-119.
4. Orel, B., Spreizer, H., Perse, L.S., Fir, M., Vuk, A.S., Merlini, D., Vodlan, M., and Kohl, M., *Silicone-based thickness insensitive spectrally selective (TISS) paints as selective paint coatings for coloured solar absorbers (Part I)*. *Solar Energy Materials and Solar Cells*, 2007. **91**(2-3): p. 93-107.
5. ASTM, *International Astm E1980 - 11 Standard Practice for Calculating Solar Reflectance Index of Horizontal and Low-Sloped Opaque Surfaces*. 1980.
6. Akbari, H., Levinson, R., and Berdahl, P., *ASTM Standards for Measuring Solar Reflectance and Infrared Emittance of Construction Materials and Comparing Their Steady-State Surface Temperatures*. 1996, Ernest Orlando Lawrence Berkeley National Laboratory.
7. Conserval Engineering Inc., *Solarduct Modular Rooftop Solar Air Heating System*. (cited 22 August 2013). Available from: <http://solarwall.com/en/products/solarwall-air-heating/solarduct.php>.
8. Brunger, A.P., *Low Cost, High Performance Solar Air-Heating Systems Using Perforated Absorbers*, in *IEA Report No. SHC.T14.Air.1*. 1999, IEA.
9. Met Office, (cited 30 August 2013). Available from: <http://data.gov.uk/metoffice-data-archive>.
10. Kutscher, C.F., Christensen, C., and Barker, G., *Unglazed transpired solar collectors: heat loss theory*. *ASME Journal of Solar Engineering*, 1993. **115**(3): p. 182-188.
11. Kutscher, C., Christensen, C., and Barker, G., *Unglazed transpired solar collectors - an analytical model and test results, 1991 Solar World Congress*,

*Vol 2 1245-1250*. 1991 Solar World Congress, Vol 1, Pts 1-2 ; Vol 2, Pts 1-2 ; Vol 3, Pts 1-2 ; Vol 4, ed. M.E. Arden, S.M.A. Burley, and M. Coleman. 1992. 1245-1250.

12. Van Decker, G.W.E., Hollands, K.G.T., and Brunger, A.P., *Heat-exchange relations for unglazed transpired solar collectors with circular holes on a square or triangular pitch*. Solar Energy, 2001. **71**(1): p. 33-45.
13. Leon, M.A. and Kumar, S., *Mathematical modeling and thermal performance analysis of unglazed transpired solar collectors*. Solar Energy, 2007. **81**(1): p. 62-75.
14. Sutton, R.J. and Ahmad, Q., *Developments in Building Integrated Transpired Solar Collectors*. 2011, Materials Engineering, Swansea University.

# **Chapter 8**

## **Conclusions and Future Work**

## 8.1 Conclusions and Future Work

Tata Steel Colors is an international manufacturer of pre-finished steel for the building envelope, domestic appliances and manufactured goods markets, with manufacturing bases in the UK (Shotton), Holland (IJmuiden), France (Myriad) and Turkey (Sakarya). Manufacture of pre-finished steel is commonly carried out by a coil coating process which has traditionally employed gas fired convection ovens for the coating cure. NIR curing is however of interest to coil coaters, due to the reduced cure time and oven length possible with this technology.

Tata Steel has a galvanising line at their IJmuiden site producing galvanised steel substrate for the building envelope market. In 2006 they installed a NIR coil coating section on the end of this line, with the coating section having potential to reach line speeds of 180m/min. At these line speeds the coating section of the line becomes more closely matched to the line speed capability of the galvanising section.

This Engineering Doctorate was sponsored by WEFO, Tata Steel Colors and BASF Coatings, and has looked at 25  $\mu\text{m}$  polyester coated galvanised steel products produced for the building envelope. It has built on the work of a prior Engineering Doctorate and further explored the NIR cure mechanism by looking at the effect on cure of changing the position of NIR absorbing pigments within the coating system. UV/Vis/NIR spectroscopy has been used to gain an understanding of where NIR absorption is likely to occur within the coating system and compared with laboratory based NIR curing trials showing ease of cure.

We have shown that white polyester coatings with titanium dioxide as their sole pigmenting agent cure with a wide cure window, whilst black coatings with carbon black as their sole pigmenting agent have a narrow cure window and are prone to solvent boil [1]. This can be attributed to the black coating system absorbing too much NIR radiation within the top coat. In the white coating system the top coat is much more transparent to NIR and substrate absorption plays an important part in the curing mechanism.

This thesis has shown that removing the carbon black content of red and brown polyester top coats widens their cure windows and makes them easier to cure, but this has a critical effect on their colour. Tinting the primer layer with carbon black in an attempt to restore the top coat colour is not successful, as the top coat is too opaque.

Further investigations with near infrared transparent black pigments such as Paliogen, replacing part or all of the carbon black pigment content of red and brown polyester formulations with Paliogen should be carried out, and a combination of UV/Vis/NIR spectroscopy, laboratory based cure trials and colour measurements used to assess the effect on NIR cure and any colour change. Potential problems with Paliogen are that unlike carbon black, it does not give a true black colour. Additionally the emissions from the Adphos NIR lamps spill over into the visible region, so this may limit the benefits of using Paliogen. Further work could therefore explore alternative methods to generate NIR radiation such as a laser source, where a narrow band of NIR wavelengths could be produced.

When a coating with a high degree of NIR transparency such as a coating solely pigmented with titanium dioxide is cured, absorption of NIR by the substrate will result in the coating being heated from the bottom upwards. Tinting the primer layer of such a coating system with carbon black, a pigment that absorbs strongly across the whole NIR region, results in the opportunity to reduce radiation intensity or increase line speed during NIR cure [2].

Chapter 4 showed that a small increase in efficiency can also be observed in the convection oven curing of white polyester coatings when a carbon black tinted primer is used. Here, the carbon black primer layer enables the residual IR black body emissions from the walls of the convection oven to be more efficiently absorbed [2, 3].

There was concern that inclusion of carbon black in the primer layer may have had a detrimental effect on the corrosion protection properties of the coating system, but in Chapter 4 in-situ scanning Kelvin probe studies showed that at additions of up to 3.5% wt. carbon black the coating delamination rate remained unchanged, whilst at 5% wt. addition the delamination rate was slowed down.

Outdoor weathering and accelerated QUV testing could be used to compare the durability performance of the same colour polyester coating cured by convection and NIR. A limited study of NIR cured coatings has already been carried out, and has concluded that NIR cure is not detrimental to performance [4].

PMTs recorded by thermocouples during laboratory based NIR cure trials in this thesis were often lower for a cured polyester coating, when compared to the target PMT range of 216 – 232 °C specified for polyester convection cure. Due to the short time of a NIR cure, it is likely that there is a temperature gradient across the coating system, with the coating probably reaching a temperature in excess of 232 °C for a short period of

time. In NIR cure, PMT cannot be taken as a good indication of coating temperature, as unlike in convection cure, there will not be enough time for thermal equilibrium between coating and metal substrate to be achieved. It would be interesting to use some depth profiling techniques to investigate whether the depth profile of NIR cured polyesters varies significantly from the depth profile of convection cured polyesters. Focussed ion beam-scanning electron microscopy could be used to image cross-sections of dried coating films to see if there is any difference in the 3D pigment dispersion of NIR cured coatings compared to convection cured coatings [5].

Chapter 5 showed that as well as increasing NIR absorption in the primer layer, adding NIR absorbing pigments to the backing coat is also beneficial to top coat cure, with the NIR absorbing pigment IR202 increasing the line speed of NIR cure by ca. 23% at 1% wt. addition to the backing coat.

Coatings pigmented with aluminium flake are particularly troublesome to cure with NIR. Although about half of incident radiation is reflected by these coatings, the coatings have a low transparency to NIR and absorb the remaining radiation. Aluminium pigment has a lamellar geometry with a high surface to volume ratio, so the path length of the radiation through the coating will be increased by undergoing multiple reflections and this will give it more chances of radiation being absorbed. Additionally, aluminium has a low emissivity, and lamellar pigment geometry will mean that solvents have to take a longer path length to escape during cure.

Further work could be undertaken to assess alternative ways of producing a silver metallic coating; one idea may be to explore the effect of pigmenting the primer layer with aluminium flake and over coating with a clear top coat. Grey metallic coatings can be formulated using silver-white mica pigments blended with carbon black, or by incorporating the carbon black into a  $\text{TiO}_2$ -mica structure to form a  $\text{TiO}_2$ -mica –carbon inclusion pigment [6]. The presence of carbon black in a top coat can lead to too much NIR absorption in the coating, so a coating system could be devised where the carbon black has been added to the primer layer instead. The high transparency of mica flake coatings could also be capitalised on to produce a new coating where a mica sparkly top layer is coated onto a coloured base layer.

Transpired solar collectors are another Tata Steel product where the interaction of radiation with a coating is applicable. Here, the aim is for an organic coating to have high absorption of solar radiation, enabling a high gain in air temperature as air flows through the collector. Chapter 7 identified that in an outdoor experiment the temperature



profile of a collector panel closely mirrored that of the solar irradiation falling on it. A model of steady state surface temperature showed that wind effects have a much more significant effect on collector surface temperature than weight additions of NIR absorbing pigment to the collector coating. For example, reducing the convective coefficient (wind speed) from 30 to 5 W m<sup>-2</sup> K<sup>-1</sup> increases the steady state surface temperature of the collector surface 9 times more than adding 1% wt. NIR absorbing pigment to the collector coating.

This thesis has shown that the NIR curing of polyester coil coatings is a complex process. Industrially, as wide a process window as possible is required and this necessitates a careful selection of pigments to provide colour and NIR absorption to the coating system, consideration of where in the coating system NIR absorbing pigments are placed (top coat, primer coat or backing coat), selection of solvents and catalyst used in the formulation, and consideration of the heating rate. It was noticed in this research that the Adphos Technicum ovens used at Deeside and IJmuiden required different lamp power settings to cure identical coatings, which is likely to be due to differences in the rate of forced air flow through the ovens. This leads to the idea that an oven with combined NIR and convection curing capability may be the most flexible option for curing coil coatings. Out of the two stages of the cure process the solvent removal stage is the one that can cope with the fastest heating rates so it would be more suitable to use NIR here. The cross-linking stage requires slower heat transfer to avoid problems with solvent boil, so convection cure could be used here.

Mathematical models have previously been used to quantify the curing of thermoset coatings (polyisocyanate/polyols) where solvent evaporation and cross-linking are taking place [7]. A similar approach could be applied to the cure of polyester coatings where both NIR and convection are used to transfer heat, and the model used to help optimise the cure process.

## 8.2 References

1. Mabbett, I., Elvins, J., Gowenlock, C., Jones, P., and Worsley, D., *Effects of highly absorbing pigments on near infrared cured polyester/melamine coil coatings*. Progress in Organic Coatings, 2013. **76**(9): p. 1184-1190.
2. Mabbett, I., Elvins, J., Gowenlock, C., Glover, C., Jones, P., Williams, G., and Worsley, D., *Addition of carbon black NIR absorber to galvanised steel primer systems: influence on NIR cure of polyester melamine topcoats and corrosion protection characteristics*. Progress in Organic Coatings, 2014. **76**: p. 1184-1190.
3. Gowenlock, C.E., Mabbett, I., and Worsley, D.A., *Optimization of near infrared cured polyester/melamine coil coatings by the use of near infrared absorbing primers*. GSTF Int J Eng Tech, 2013. **2**(2): p. 47-50.
4. Ireson, R., *Development of a 25 micron polyester coated product for the DVL2 line*. 2010, Tata Steel Research Development & Technology.
5. Lin, J.C., Heeschen, W., Reffner, J., and Hook, J., *Three-dimensional characterization of pigment dispersion in dried paint films using focused ion beam-scanning electron microscopy*. Microscopy and Microanalysis, 2012. **18**(2): p. 266-271.
6. Maisch, R., *New effect pigments from grey to black*. Progress in Organic Coatings, 1993. **22**(1-4): p. 261-272.
7. Kiil, S., *Quantification of simultaneous solvent evaporation and chemical curing in thermoset coatings*. Journal of Coatings Technology and Research, 2010. **7**(5): p. 569-586.